

QUANTUM FIELD THEORY OF TIME

The Weak Entanglement Symmetry Hypothesis
and Emergent Spacetime

Luca Casagrande

First Edition
January 24, 2026

Abstract

In canonical quantum gravity the Wheeler–DeWitt equation freezes evolution, while standard quantum theory treats time as an external parameter. The Weak Entanglement Symmetry Hypothesis (WESH) promotes entanglement as the carrier of statistical Lorentz-type symmetry and as an engine of endogenous dissipative dynamics. Lorentz symmetry is recovered in expectation over the Poissonian ensemble of *Eigentime* events (discrete stochastic localizations of the time-field operator $\hat{T}(x)$ within its continuous spectrum, induced by the quadratic WESH dissipators $\mathcal{D}[\hat{T}^2(x)]$ and $\mathcal{D}[L_{xy}]$ — mean spacing τ_{Eig}), whereas global conserved charges obey a stronger operator-level constraint (WESH–Noether, $\mathcal{L}^\dagger[\hat{Q}_a] = 0$). On this foundation, physical time becomes a local quantum field operator $\hat{T}(x)$, subject to superposition and objective collapse, with dynamics constructed from first principles. An open-system master equation in an auxiliary label s generates physical time through $dt/ds = \Gamma[\rho] \geq 0$. Complete positivity, no-signaling, and a pre-geometric WESH–Noether conservation principle single out a CPT-even Lindblad structure with quadratic local dissipators $\mathcal{D}[\hat{T}^2(x)]$ and a Rényi-2 weighted bilocal channel. In the infrared, spontaneous gradient alignment $\partial_\mu \langle \hat{T} \rangle = k \partial_\mu \Phi$ defines an emergent metric and reproduces the Einstein equations with Newton constant fixed by the same matching; no background geometry is assumed. The same eigentime statistics yields the cosmological constant as irreducible shot noise, with scaling $\delta\Lambda \sim H^2$. The framework predicts collective coherence scaling $\tau_{\text{coh}} \propto N^2$ and a robust $\cos^2\theta$ angular law for parity decay. Collision-model simulations ($N = 2–16$) and experiments on IBM Eagle and Rigetti Ankaa-3 show trends consistent with both signatures. A near-horizon analysis of the \hat{T}^2 channel and the emergent KMS structure yields

$$S_{\text{BH}} = \frac{A}{4L_P^2} + \gamma_{\text{BH}} \ln \frac{A}{L_P^2} + \dots$$

without thermal ansatz. The construction has no free dimensionless parameters; deviations from the $1/4$ prefactor, or the N^2 scaling would falsify the framework.

All resources are openly available.

Complete experimental data and analysis code are provided at

<https://github.com/Luca-Casagrande/QFTT-WESH>

*Sections 1, 5, 6 and Appendices A–D and F–J have been formally verified in
Lean 4/Mathlib.*

Box 1 — Logical Map

Motivation. Neither imposing an external time nor accepting a strictly timeless universe is satisfactory. QFTT–WESH derives physical time from quantum events weighted by entanglement, yielding a consistent route from the Wheeler–DeWitt constraint to general relativity and black–hole thermodynamics.

Primitives.

1. *Timeless constraint.* $\hat{H}_{\text{tot}} |\Psi\rangle = 0$ (WDW: no t , no metric).
2. *Quantum time field.* Local observable $\hat{T}(x)$ on an extended kinematical space, with mean eigentime profile $\tau(x) := \langle \hat{T}(x) \rangle_{\rho}$ in the effective (mean-field) description.
3. *Eigentimes & bootstrap.* $\frac{dt}{ds} = \Gamma[\rho] \geq 0$, $t(s) = \int_0^s \Gamma[\rho(u)] du$: eigentime events create the very flow that regulates their statistics.

Operational structure.

- *GKSL structure.* Locally GKSL (frozen-gate micro-steps), globally a CP/TP concatenation; causal generator \mathcal{L} with Hermitian channels $\hat{T}^2(x)$ and $L_{xy} = \hat{T}^2(x) - \hat{T}^2(y)$.
- *Covariant construction.* Once the emergent metric $g_{\mu\nu}^{(T)} = \zeta^{-1} \langle \partial_{\mu} \hat{T} \partial_{\nu} \hat{T} \rangle$ is defined, the master equation is made covariant by replacing $\partial \rightarrow \nabla$ and using a scalar causal kernel $K_{\xi}(\sigma(x, y))$ in the bilocal weight; WESH–Noether enforces conservation of global charges.
- *Finite-range Markov window.* Correlation time $\tau_{\text{corr}} \sim \xi/c$ with $\xi \simeq L_P$ and exponential-causal support.
- *Two-derivative IR truncation.* In $D=4$, diffeomorphism invariance together with a ≤ 2 -derivative truncation fixes the IR geometric sector to Einstein–Hilbert plus a cosmological constant; higher-derivative operators are treated as controlled EFT corrections.
- *No free parameters.* The normalization k is fixed by internal consistency via $k^2/(4\pi G) = \lambda_1 + 3\lambda_2$; no tunable dimensionless couplings remain.

Structure & Derived Laws.

1. *WESH–Noether conservation.* $\mathcal{L}^{\dagger}[\hat{Q}_a] = 0$: generator-level conservation on CPTP maps, path-independent global charges.
2. *Spacetime bootstrap dynamics.* WDW \Rightarrow continuous WESH evolution with instantaneous $C(\rho)$ feedback; eigentime events occur with propensity $\Gamma[\rho] \geq 0$ (> 0 under ND) and generate t via $dt/ds = \Gamma[\rho]$; the state is driven toward the swap-even (\mathbb{Z}_2) projected physical subset and maintains self-consistent equilibrium without introducing any discrete external time step. The bootstrap architecture $\rho \mapsto C[\rho] \mapsto \mathcal{L}_{C[\rho]} \mapsto \rho$ is the unique structure capable of representing chronogenesis; nonlinearity is its natural consequence.
3. *Fixed point and alignment.* The bootstrap map $\rho \mapsto \exp(\delta s \mathcal{L}_{C[\rho]}) \rho$ is nonlinear but continuous; by Schauder–Tychonoff a fixed point exists, and Dobrushin contraction ensures uniqueness. At equilibrium, $\partial_{\mu} \tau = k \partial_{\mu} \Phi$.

4. *Hidden-sector cancellation.* At the fixed point the hidden-sector stresses cancel in the continuum limit, $T_{\mu\nu}^{(T)} + T_{\mu\nu}^{(\text{nl})} = 0$ as $N \rightarrow \infty$, with controlled finite- N residual $\mathcal{O}(1/N)$; hence $G_{\mu\nu} + \Lambda g_{\mu\nu} = 8\pi G T_{\mu\nu}^{(m)} + \mathcal{O}(1/N)$.

Empirical targets (core vs. diagnostic).

- *Core: collective stability.* $\tau_{\text{coh}} \propto N^2$ — a structural discriminant of the N^{-2} bilocal weighting in the WESH channel.
- *Diagnostic: angular modulation.* Decoherence $\propto (1 + \varepsilon \cos^2 \theta)$, with a state- and geometry-dependent ε ; the expected W -state anti-modulation ($\varepsilon < 0$) provides a direct control for state dependence.
- *Core: BH sector (IR bridge).* A near-horizon KMS fixed point yields $S_{\text{BH}} = A/(4L_P^2) + \gamma_{\text{BH}} \ln(A/L_P^2) + \dots$ without imposing a thermal ansatz.

Scope & Controlled Approximations.

- *Domain.* IR continuum regime ($L \gg \xi$), $D=4$, swap-even projected physical subset.
- *Kernel & memory.* Exponential-causal kernel of range ξ , finite-memory Markov limit $\tau_{\text{corr}} \sim \xi/c$; curvature-induced deformations treated as EFT corrections.
- *Finite- N control.* $1/N$ residuals bounded via graph-to-manifold convergence.

Summary. A single CP/Markov pre-geometric dynamics (WESH), fixed by Noether consistency and without tuning, bootstraps spacetime from quantum events and yields both Einstein–Hilbert gravity and black-hole thermodynamics as its infrared manifestations in four dimensions.

QFTT-WESH — Graphical Synopsis

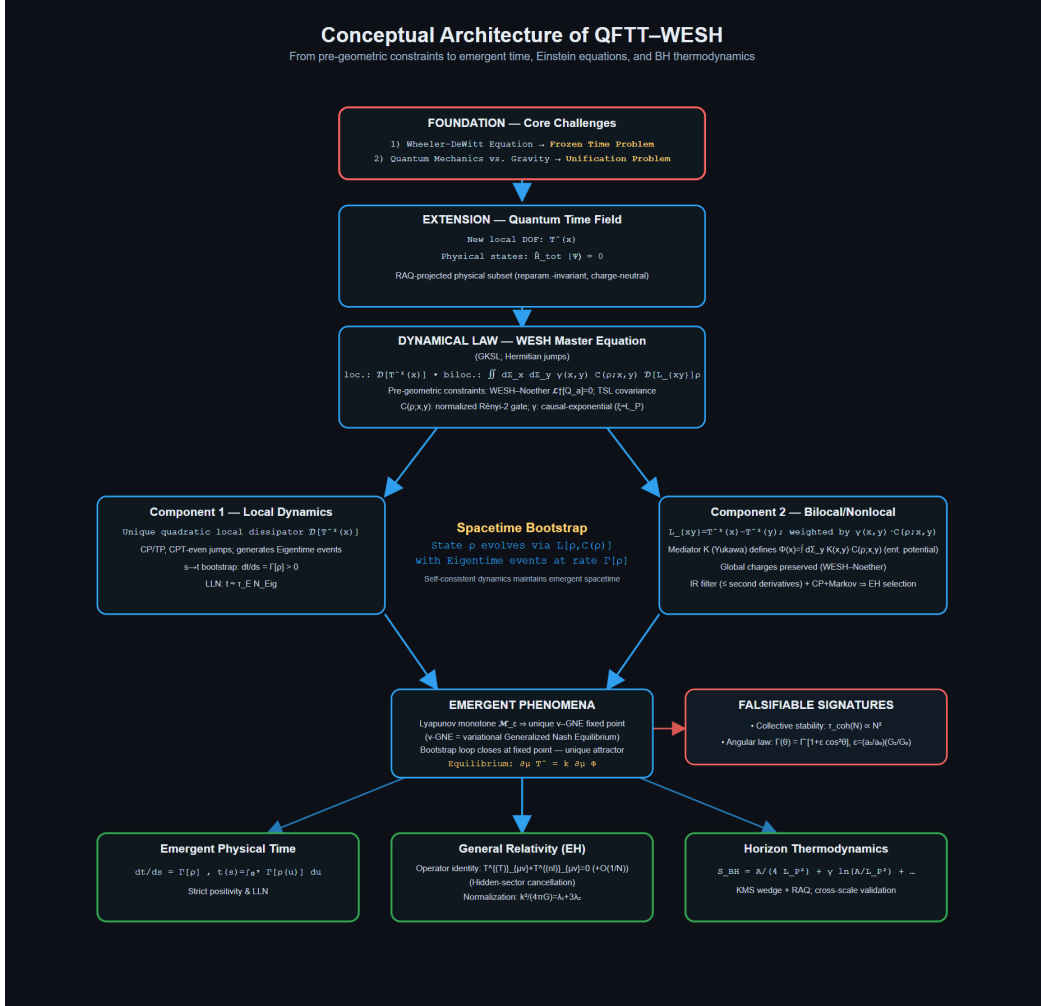


Figure 1: **Conceptual overview of the QFTT-WESH framework.** From the Wheeler–DeWitt constraint, the theory introduces a quantum time field evolving via the WESH master equation under pre-geometric charge conservation. Eigentime collapse events generate a spacetime bootstrap converging to emergent Einstein–Hilbert gravity and horizon thermodynamics.

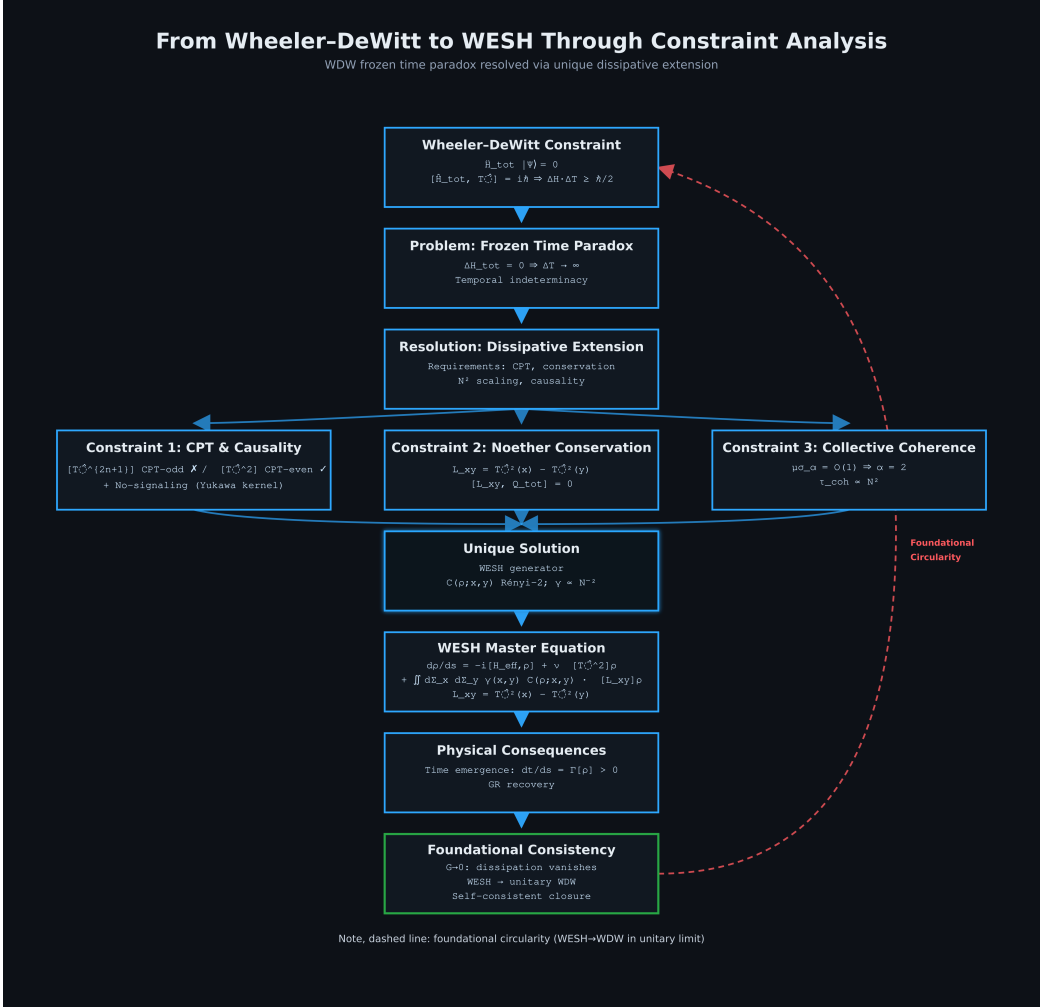


Figure 2: WESH as the unique dissipative extension of Wheeler-DeWitt.
The frozen time paradox ($\Delta H_{\text{tot}} = 0 \Rightarrow \Delta T \rightarrow \infty$) requires a GKSL dissipative structure. Three constraints—CPT symmetry with no-signaling causality, WESH–Noether charge conservation, and collective N^2 coherence scaling—uniquely determine the generator: a local channel $\mathcal{D}[\hat{T}^2(x)]$ plus a bilocal channel $\mathcal{D}[L_{xy}]$ weighted by Rényi–2 correlators. The dashed arrow indicates foundational closure: in the limit $G \rightarrow 0$, dissipation vanishes and WESH reduces to unitary Wheeler-DeWitt.

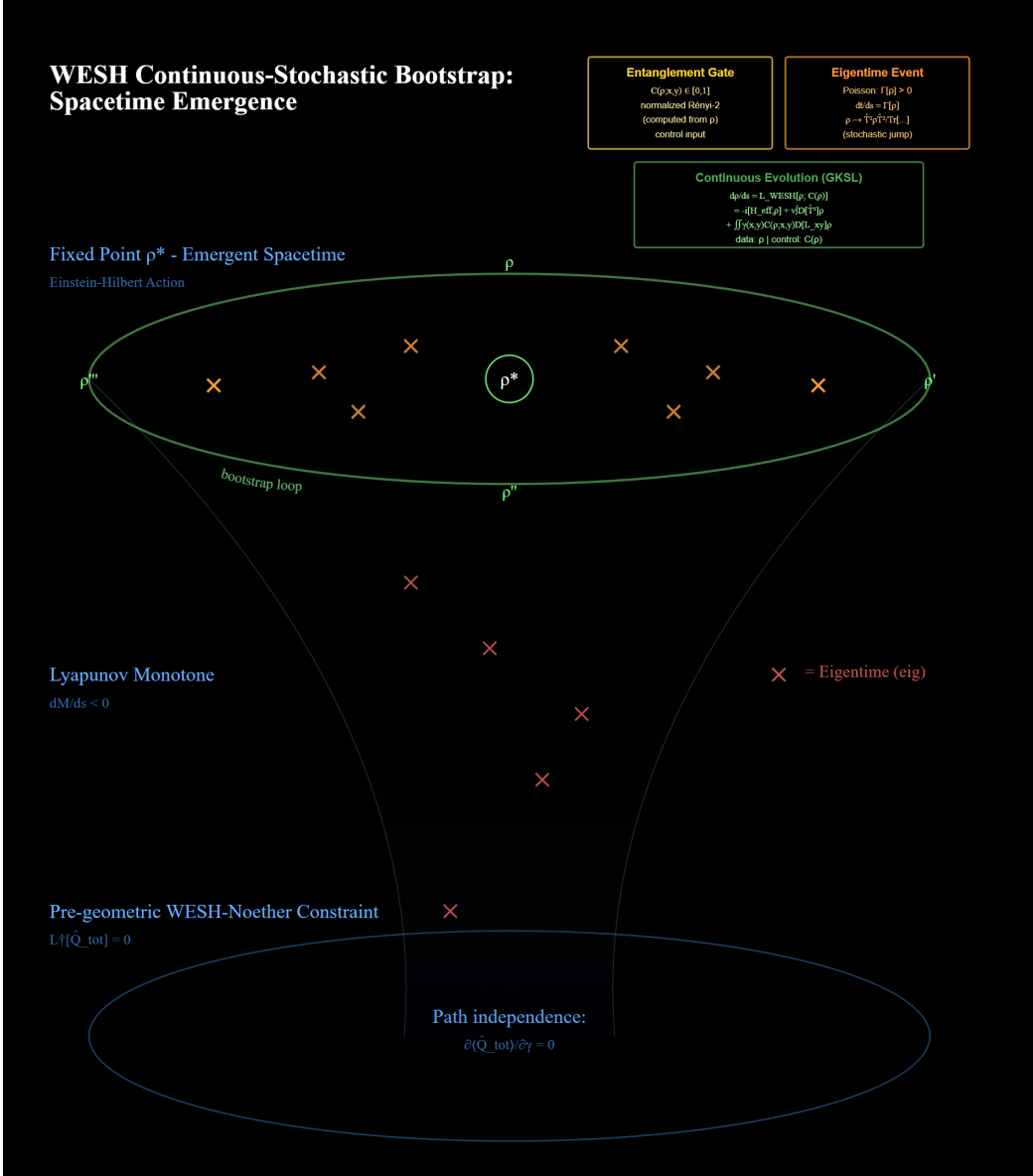


Figure 3: Spacetime bootstrap from pre-geometric dynamics. Starting from pre-geometric WESH constraints, the Lyapunov functional $\mathcal{M}_\epsilon[\rho]$ determines a unique fixed point on the emergent Einstein–Hilbert manifold. The global state $\rho(s)$ reaches this fixed point through continuous GKSL evolution punctuated by stochastic Poisson eigentime events ($\Gamma[\rho] \geq 0$ - red crosses), with the hybrid flow driving spacetime emergence from the pre-geometric sector (green annotations mark the self-consistent stationary state).

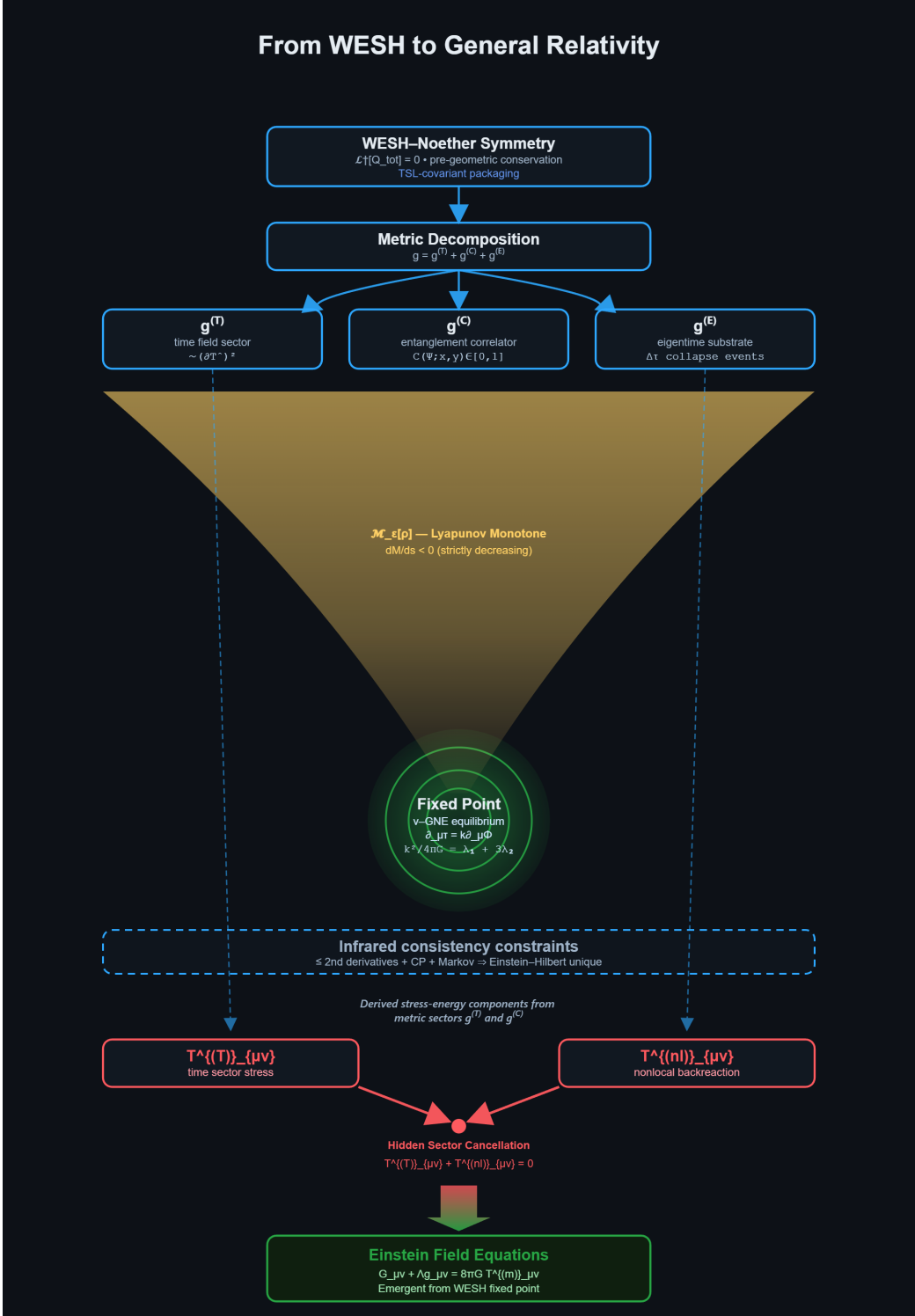


Figure 4: **Emergence of general relativity from WESH.** WESH–Noether symmetry and the stationary bootstrap fix the metric decomposition $g_{\mu\nu} = g_{\mu\nu}^{(T)} + g_{\mu\nu}^{(C)} + g_{\mu\nu}^{(E)}$ and determine the coupling matching. The Lyapunov flow converges to a unique stationary point characterized by gradient alignment $\partial_\mu \tau = k \partial_\mu \Phi$. At this point, hidden-sector cancellation reduces the infrared dynamics to the Einstein equations with cosmological constant and conserved matter stress–energy, up to $1/N$ corrections.

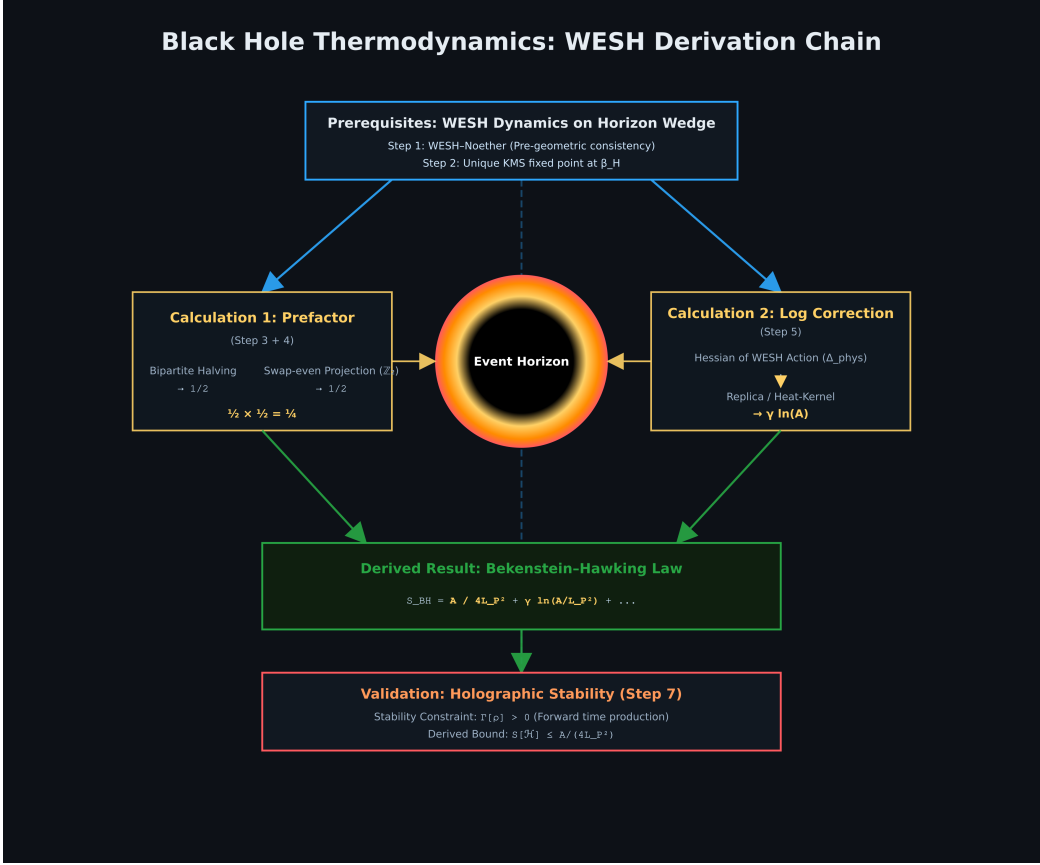


Figure 5: **Black-hole thermodynamics from WESH horizon dynamics.** WESH–Noether consistency and the unique KMS fixed point on the near–horizon wedge provide the entropy framework. Bipartite halving with swap-even (\mathbb{Z}_2) projection yields the $1/4$ prefactor; the WESH effective action Hessian with replica regularization produces logarithmic corrections. The condition $\Gamma[\rho] \geq 0$ implies the holographic bound $S[\mathcal{H}] \leq A/(4L_P^2) + \dots$.

Box 2: Foundational clarifications and core principles

For later reference we collect a few structural points that are easy to misread if one assumes standard Hamiltonian or semiclassical intuition. They follow from the constraints introduced in Sec. 1, rather than being added as independent postulates.

Auxiliary label s and emergence of physical time. The WESH master equation is written in an auxiliary ordering parameter s with dimensions of time, but s itself is never an observable. Physical time is reconstructed afterwards from eigentime events via $dt/ds = \Gamma[\rho(s)] \geq 0$ ($\Gamma > 0$ under nondegeneracy). Canonical commutators are imposed on an arbitrary kinematical Cauchy slice, so that the algebra does not depend on any prior choice of time coordinate; the distinction between s (ordering) and $t(s)$ (emergent physical time) removes the usual circularity of “time–evolution in time”.

Local time field and the scope of Pauli’s theorem. QFTT–WESH employs a local quantum time field $\hat{T}(x)$ on an extended kinematical space subject to the Wheeler–DeWitt constraint and open–system dynamics. Pauli’s no–go theorem concerns a single global self–adjoint time operator canonically conjugate to the Hamiltonian in a closed, unitary theory, which is not the setting considered here. Operational meaning is instead attached to $\hat{T}(x)$ through eigentime collapse events and the statistics of their rate.

Dissipator structure, entanglement gate, nonlinearity, and Markov window. CPT symmetry, WESH–Noether charge conservation, and the requirement of collective stability select Hermitian jumps $\hat{T}^2(x)$ and $L_{xy} = \hat{T}^2(x) - \hat{T}^2(y)$ (equivalently $\tilde{T}^2(x) - \tilde{T}^2(y)$ in dimensionless units with $\tilde{T} = \hat{T}/\tau_s$) and fix the N^{-2} bilocal scaling, rather than leaving a large family of GKSL terms. The Rényi-2 gate $C(\Psi; x, y)$ is a bounded scalar functional of the reduced state ρ_{xy} that weights the bilocal channel and couples only genuinely entangled subsystems. The resulting state-dependence $\rho \mapsto C[\rho] \mapsto \mathcal{L}_{C[\rho]} \mapsto \rho$ renders the evolution nonlinear; this is the necessary architecture of any chronogenetic theory where time emerges from the dynamics it regulates. For each frozen C the generator is of standard GKSL form, and the full evolution is a concatenation of positivity- and trace-preserving maps; the Schauder–Tychonoff theorem guarantees existence of a fixed point despite the nonlinearity. The interaction kernel has light–cone–restricted, exponential–causal support of range ξ , defining a finite–memory Markov window with $\tau_{\text{corr}} \sim \xi/c$ where memory effects are parametrically suppressed. In this regime the local rate ν is fixed by self–consistency with the bilocal sector on causal diamonds, so that Γ_{loc} and Γ_{bi} are not independently tunable and ν is *not* a free normalization parameter.

Hidden-sector cancellation as a dynamical outcome. The cancellation between time–sector and nonlocal stresses, $T_{\mu\nu}^{(T)} + T_{\mu\nu}^{(\text{nl})} = 0$ (in the $N \rightarrow \infty$ continuum limit), is not imposed by hand. It arises at the unique globally

attractive fixed point of the WESH flow, where the Lyapunov functional \mathcal{M}_ϵ enforces gradient alignment of the mean field $\partial_\mu \tau = k \partial_\mu \Phi$ (with $\tau := \langle \hat{T} \rangle_\rho$) and the matching relation between k and the WESH couplings fixes the relative normalization of the two sectors. In this regime the Einstein tensor is sourced only by ordinary matter, with residual $\mathcal{O}(1/N)$ corrections controlled by the continuum limit.

Black-hole entropy and the role of $(\kappa\xi)^2$. Near a stationary horizon, the same WESH dynamics leads to a Hartle–Hawking KMS state on the wedge and to a mean pair entropy $\bar{s} = 1 + \mathcal{O}((\kappa\xi)^2)$. Bipartite halving and swap-even projection then produce the universal area term $S_{\text{BH}} = A/(4L_P^2)$, while the Hessian of the WESH effective action yields the logarithmic correction. The combination $(\kappa\xi)^2$ is the natural small parameter of the calculation; for spherical horizons it reduces to the familiar $\mathcal{O}(L_P^2/A)$ scaling, but the more general form continues to apply to rotating or distorted horizons.

1 QFTT Framework & WESH

In this section we promote physical time to a local quantum field operator $\hat{T}(x)$ on an extended kinematical algebra and justify its operational meaning in constrained (Wheeler–DeWitt) cosmologies. From CPT symmetry, WESH–Noether conservation, and collective stability (bootstrap closure), within a completely positive and causal GKSL evolution, we derive a unique quadratic WESH Lindblad generator $\mathcal{D}[\hat{T}^2(x)]$, and couple it to entanglement through a normalized Rényi-2 correlator $C(\Psi; x, y)$. A self-consistent bootstrap driven by eigentime collapse events generates physical time and an entanglement-weighted dissipative flow, with a bilocal kernel $\gamma(x, y)$ enforcing causal support and collective N^{-2} scaling. The section concludes by fixing the fundamental scales in terms of Planck units and summarizing the resulting parameters and kernels in Table 1.

1.1 Problem of time and quantum gravity strategy

In canonical quantum cosmology, the Wheeler–DeWitt constraint $\hat{H}_{\text{tot}} |\Psi\rangle = 0$ freezes global evolution, while standard quantum theory still treats time as an external parameter. Most approaches to quantum gravity, loop quantum gravity (Ashtekar et al., 1995), string theory, and causal dynamical triangulations, either quantize an already geometric spacetime or work semiclassically on a fixed background, leaving the operational status of time itself unresolved. Alternative proposals such as the Page–Wootters mechanism (Page & Wootters, 1983) tie the emergence of time to entanglement between system and clock but do not derive dissipative dynamics or metric structure.

Here we address both issues at once: we promote physical time to a local quantum field operator $\hat{T}(x)$ on an extended kinematical algebra, evolve the state by a completely positive WESH master equation in an auxiliary ordering parameter s , and let physical time and metric relations emerge from eigentime events and entanglement-weighted dissipative flow. In the remainder of this section we derive quantitative pre-geometric predictions and show how general relativity and black-hole thermodynamics emerge in the infrared limit of the theory.

1.2 Time field and canonical structure

As mentioned, the resolution proposed here elevates physical time from an external parameter to a local quantum field operator $\hat{T}(x)$ defined on an extended kinematical Hilbert space. This extension follows from the canonical structure of constrained systems.

In the minisuperspace approximation, the Wheeler–DeWitt constraint decomposes as

$$\hat{H}_{\text{tot}} = \hat{H}_{\text{universe}} + \hat{P}_T \approx 0, \quad [\hat{T}, \hat{P}_T] = i\hbar, \quad (1.1)$$

where \hat{P}_T is the momentum conjugate to a global time variable. The constraint does not forbid dynamics; it enforces energy balance between the time sector and the remaining degrees of freedom. Passing to the local field-theoretic extension, we postulate canonical commutation relations on an arbitrary kinematical slice Σ (since the algebra is independent of the choice of coordinates prior to metric emergence):

$$[\hat{T}(\mathbf{x}), \hat{\Pi}_T(\mathbf{y})] = i\hbar \delta_{\Sigma}^{(3)}(\mathbf{x} - \mathbf{y}), \quad [\hat{T}, \hat{T}] = [\hat{\Pi}_T, \hat{\Pi}_T] = 0. \quad (1.2)$$

On the constraint surface, the conjugate momentum is identified with (minus) the local energy density,

$$\hat{\Pi}_T(\mathbf{x}) = -\hat{\mathcal{H}}(\mathbf{x}), \quad [\hat{\mathcal{H}}(\mathbf{x}), \hat{T}(\mathbf{y})] = i\hbar \delta_{\Sigma}^{(3)}(\mathbf{x} - \mathbf{y}), \quad (1.3)$$

so that the local Hamiltonian constraint $\hat{\mathcal{H}}(x) + \hat{\Pi}_T(x) \approx 0$ becomes the generator of local time translations. This identification transforms the Wheeler–DeWitt “frozen time” into a dynamical equilibrium condition: the constraint balances the quantum time frame against the local energy content.

The spectral decomposition

$$\hat{T}(x)|t\rangle_x = t|t\rangle_x, \quad \int_{-\infty}^{+\infty} dt |t\rangle_x \langle t| = \mathbb{1}_x \quad (1.4)$$

allows one to expand the global state as a superposition over temporal configurations:

$$|\Psi\rangle = \int \mathcal{D}t(x) \mathcal{D}\phi \Psi[t(x), \phi] \bigotimes_x |t(x)\rangle_x \otimes |\phi\rangle. \quad (1.5)$$

In the WDW sector, temporal indeterminacy is therefore physical, not artifactual: the universe exists in a quantum superposition of chronologies. Resolving this superposition requires a dynamical mechanism that cannot be unitary in the conventional sense, there is no external t to generate a Schrödinger flow, but must be dissipative. The structure of this dissipation is fixed by symmetry, as we now explain.

1.3 WESH–Noether conservation

The dissipative extension of Wheeler–DeWitt operates in a regime where no background metric exists: the constraint $\hat{H}_{\text{tot}}|\Psi\rangle = 0$ removes the generator of time translations, leaving only algebraic structure. In a closed universe there is no external bath to absorb conserved charges, so the generator must preserve them exactly:

$$\mathcal{L}^\dagger[\hat{Q}_a] = 0 \quad \forall a. \quad (1.6)$$

This *WESH–Noether conservation* is pre-geometric: it is formulated in the auxiliary parameter s , before physical time or spacetime have emerged, and guarantees path independence in state space, so that $\langle \hat{Q}_a \rangle$ does not depend on the particular trajectory $\rho(s)$.

Algebraic mechanism. The conservation law (1.6) translates into commutant conditions on the generator. For Hermitian Lindblad operators L , the adjoint dissipator acts on observables as

$$\mathcal{D}_L^\dagger[\hat{Q}] = -\frac{1}{2}[L, [L, \hat{Q}]]. \quad (1.7)$$

Under the WESH structure ($\nu > 0$, $\gamma(x, y) C(\Psi; x, y) \geq 0$, Hermitian jumps) and mild spectral regularity (Appendix G, Prop. G.2), $\mathcal{L}^\dagger[\hat{Q}_a] = 0$ is equivalent to

$$\begin{aligned} [H_{\text{eff}}, \hat{Q}_a] &= 0, & [\hat{T}^2(x), \hat{Q}_a] &= 0, \\ [L_{xy}, \hat{Q}_a] &= 0 \quad \text{for all } (x, y) \text{ with nonzero rate.} \end{aligned} \tag{1.8}$$

The double commutator (1.7) is the algebraic engine of conservation: it vanishes precisely when each Lindblad channel commutes with the charge.

Difference structure. For the bilocal channel, the commutant condition together with the requirement of pairwise-balanced redistribution (zero net injection) selects the difference form,

$$L_{xy} = \hat{T}^2(x) - \hat{T}^2(y). \tag{1.9}$$

This structure redistributes coherence between causally connected points without injecting or removing total charge: any increase at x is compensated by a decrease at y . The local channel $\mathcal{D}[\hat{T}^2(x)]$ satisfies the same commutant provided the time field is *T-neutral*,

$$[\hat{T}(x), \hat{Q}_{\text{tot}}] = 0 \quad \forall x. \tag{1.10}$$

T-neutrality is not imposed externally; it is the unique condition compatible with path independence, universal time emergence, and no-signaling (Appendix G, Remark G.4).

Theorem 1.1 (WESH–Noether). *Let \mathcal{L} be a GKSL generator with Hermitian jump operators $L_\alpha \in \{\hat{T}^2(x), L_{xy} = \hat{T}^2(x) - \hat{T}^2(y)\}$ and let \hat{Q}_a be any global charge. Then the following are equivalent:*

- (i) $\mathcal{L}^\dagger[\hat{Q}_a] = 0$ (generator-level conservation);
- (ii) $[H_{\text{eff}}, \hat{Q}_a] = 0$ and $[L_\alpha, \hat{Q}_a] = 0$ for all α (commutant conditions);
- (iii) for every trajectory $\rho(s)$ one has

$$\frac{d}{ds} \langle \hat{Q}_a \rangle_{\rho(s)} = \text{Tr}(\mathcal{L}^\dagger[\hat{Q}_a] \rho(s)) = 0, \tag{1.11}$$

(path independence in s).

Under T-neutrality (1.10), all three conditions hold for every conserved charge.

This theorem extends Noether’s result to dissipative quantum dynamics: constants of motion are identified with fixed points of the Heisenberg semigroup generated by \mathcal{L}^\dagger . The proof uses the double-commutator identity (1.7) together with mild spectral regularity assumptions.

Functional role in the present framework. In the remainder of this section, WESH–Noether is used as a selection principle: together with CPT symmetry and collective stability, it fixes the admissible form of the dissipative generator and singles out the quadratic WESH structure employed in Eq. (1.15). The same constraint plays a second role in the infrared analysis. There, its pre-geometric character becomes essential: the WESH flow admits a unique fixed point that minimizes a Lyapunov functional subject to the Noether constraints, and at this fixed point the gradients of the time field and of the entanglement potential align, $\partial_\mu \tau = k \partial_\mu \Phi$ (with $\tau := \langle \hat{T} \rangle_\rho$). The emergent Einstein–Hilbert dynamics and hidden-sector cancellation follow from this aligned fixed point. Both applications derive from the same algebraic condition; only the physical interpretation shifts from constraint selection to geometric emergence.

The complete operator-level derivation, including spectral regularity conditions and the bridge to alignment, is developed in Appendix G.

1.4 Focus on the Weak Entanglement Symmetry Hypothesis.

In this framework “weak” does not refer to a small coupling, but to the level at which Lorentz-type symmetry is enforced. Lorentz invariance is not required pointwise on each individual collapse trajectory, but is recovered in expectation over the Poissonian ensemble of eigentime events. Global conserved charges obey a stronger, operator-level constraint (Sec. 1.3). Entanglement correlations $C(\Psi; x, y)$ distribute the effect of a local collapse across all correlated regions, so that apparent local violations are globally compensated when averaged over the process. Such symmetry is therefore a property of the process measure rather than of individual realizations.

1.5 Constraint-driven selection of the WESH generator

We now address the mechanism by which a directed temporal order can emerge from within the Wheeler–DeWitt sector itself. Instead of coupling to an external bath, we model dissipation as *endogenous*: an effective redistribution of information among relational degrees of freedom in a closed universe, where the environment is internal to the WDW kinematics and no net charge or energy can be injected. This zero-sum condition, together with complete positivity, light-cone causality, WESH–Noether charge conservation, and collective stability at large

N , severely constrains the admissible GKSL generators. Under these requirements the space of allowed structures collapses to a single option: quadratic local channels $\mathcal{D}[\hat{T}^2(x)]$ and difference-form bilocal operators $L_{xy} = \hat{T}^2(x) - \hat{T}^2(y)$, modulated by the entanglement gate. The remainder of this subsection derives this uniqueness from first principles.

CPT symmetry. Under time reversal one has $\hat{T} \rightarrow -\hat{T}$, so any admissible local Lindblad operator must be an even function of the field. Writing $L_x = F(\hat{T}(x))$ with a power series $F(z) = \sum_{m \geq 1} a_{2m} z^{2m}$ excludes odd powers and confines the dynamics to CPT-even channels. The lowest non-trivial choice compatible with spontaneous collapse is the quadratic form $\mathcal{D}[\hat{T}^2(x)]$.

WESH–Noether conservation. Pre-geometric WESH–Noether conservation requires the generator to preserve all global charges exactly, $\mathcal{L}^\dagger[\hat{Q}_a] = 0$ for all a (Eq. (1.6)). For the WESH channels introduced in Sec. 1.3, this is implemented by the commutant conditions (1.8), which in particular fix the bilocal difference structure $L_{xy} = \hat{T}^2(x) - \hat{T}^2(y)$ (Eq. (1.9)) and ensure $[L_{xy}, \hat{Q}_{\text{tot}}] = 0$. Here we use these algebraic constraints as selection principles for the admissible GKSL generators.

Collective coherence scaling. The bilocal kernel must suppress pairwise coupling as the system size grows, keeping total collapse power bounded. Imposing $\gamma_{ij} \propto N^{-2}$ leads to a coherence time

$$\tau_{\text{coh}} \propto N^2, \quad (1.12)$$

a falsifiable prediction that distinguishes WESH from standard decoherence models, where τ_{coh} typically scales as N^{-1} or remains of order unity.

Proposition 1.1 (Quadratic dissipator from symmetry and stability). *Let the local Lindblad operators L_x be CPT-even, satisfy the WESH–Noether condition (1.6), and be coupled through a bilocal kernel $\gamma(x, y) \propto N^{-2}$ in such a way that the infrared coherence time obeys $\tau_{\text{coh}}(N) \propto N^2$ (Eq. 1.12 and Eq. 1.39). Then the only admissible local dissipator is $\mathcal{D}[\hat{T}^2(x)]$.*

Proof. CPT symmetry implies that L_x is an even function of $\hat{T}(x)$, $L_x \sim \hat{T}^{2n}(x)$ with $n \geq 1$. For a general even-power dissipator $\mathcal{D}[\hat{T}^{2n}]$ the combination of $\gamma \propto N^{-2}$ with dimensional analysis yields

$$\text{If } L_x \sim \hat{T}^{2n} \quad \Rightarrow \quad \tau_{\text{coh}}(N) \propto N^{2n}. \quad (1.13)$$

The collective stability requirement $\tau_{\text{coh}}(N) \propto N^2$ then fixes $n = 1$ uniquely, hence the local channel is $\mathcal{D}[\hat{T}^2(x)]$. \square

Remark 1.1 (Convergent IR rationale (ancillary)). *Independently of the collective-stability selection, a Wilsonian IR argument also singles out the quadratic operator: among CPT-even local monomials $F(\hat{T}) \sim \hat{T}^{2n}$, the lowest-dimension term dominates the long-wavelength fixed-regime, while higher even powers are irrelevant deformations. This IR minimality rationale is consistent with (and secondary to) the structural selection $n = 1$ enforced by $\tau_{\text{coh}}(N) \propto N^2$.*

Remark 1.2. *The role of $\alpha = 2$ is dynamical rather than kinematical: it emerges from bootstrap self-consistency (Eq. 1.39), not from an external constraint.*

1.6 The WESH master equation

The constraints derived above—CPT symmetry, WESH–Noether conservation, and collective N^2 stability—uniquely determine the structure of the generator. Before writing it explicitly, we fix the integration conventions.

Measure conventions. We use coarse-grained integration measures normalized to the correlation four-volume:

$$\int_x := \frac{1}{V_\xi} \int d^4x, \quad \int_{xy} := \frac{1}{V_\xi^2} \int d^4x d^4y, \quad V_\xi = \mathcal{O}(\xi^4). \quad (1.14)$$

With these conventions, ν carries dimensions of inverse time; Prop. 1.2 uses unnormalized integrals, so ν and $\int d^4y \gamma(x, y)$ scale as $\mathcal{O}(\gamma_0 V_\xi)$ and $\mathcal{O}(\gamma_0 V_\xi / N^2)$, respectively.

Generator. The unique GKSL generator compatible with the constraints takes the form

$$\boxed{\begin{aligned}\frac{d\rho}{ds} &= -i[\hat{H}_{\text{eff}}, \rho] + \nu \int \frac{d^4x}{V_\xi} \mathcal{D}[\tilde{T}^2(x)] \rho \\ &\quad + \iint \frac{d^4x d^4y}{V_\xi^2} \gamma(x, y) C(\Psi; x, y) \mathcal{D}[L_{xy}] \rho\end{aligned}} \quad (1.15)$$

where $\tilde{T} = \hat{T}/\tau_s$ is the dimensionless field and $V_\xi \sim \xi^4$ sets the coarse-graining four-volume. The effective Hamiltonian splits as

$$\hat{H}_{\text{eff}} = \hat{H}_{\text{local}} + \hat{H}_{\text{ent}}, \quad (1.16)$$

with \hat{H}_{local} collecting matter and time-field contributions and \hat{H}_{ent} the entanglement-mediated correction.

The dissipative part uses the standard Lindblad superoperator

$$\mathcal{D}[O] \rho \equiv O \rho O^\dagger - \frac{1}{2} \{O^\dagger O, \rho\}, \quad (1.17)$$

so that the local channel is generated by the Hermitian jump operator $\tilde{T}^2(x)$,

$$\mathcal{D}[\tilde{T}^2(x)] \rho = \tilde{T}^2(x) \rho \tilde{T}^2(x) - \frac{1}{2} \{\tilde{T}^4(x), \rho\}, \quad (1.18)$$

and can be interpreted as the continuous counterpart of the conditional update

$$\rho \longrightarrow \frac{\hat{T}^2(x) \rho \hat{T}^2(x)}{\text{Tr}[\hat{T}^2(x) \rho \hat{T}^2(x)]} \quad (1.19)$$

at the point x .

Causal kernel. The bilocal weight combines exponential falloff, causal support, and collective suppression:

$$\gamma(x, y) = \frac{\gamma_0}{N^2} K_\xi(x - y) \Theta[\text{causal}(x, y)], \quad (1.20)$$

with $K_\xi(z)$ a short-range profile of range $\xi \simeq L_P$ (e.g. $K_\xi(z) = e^{-d(z)/\xi}$), $\gamma_0 > 0$ a rate scale, and Θ the causal step function vanishing for spacelike separation. The N^{-2} prefactor ensures that the sum over all pairs yields a total rate of order γ_0 , independent of system size.

Terminological note. Two kernels appear with distinct roles. The function $\gamma(x, y)$ in Eq. (1.20) is the exponential-causal dissipative weight entering the generator (1.15). A Yukawa-type kernel $K(x - y)$, introduced in Appendix A, defines an entanglement potential $\Phi(x) = \int d^4y K(x - y) C(\Psi; x, y)$ and enters the metric-emergence analysis of Sec. 4. Both kernels have the same short range $\xi \simeq L_P$, but γ weights collapse rates whereas K averages correlations for the emergent geometry.

Entanglement gate. The bilocal channel is modulated by a normalized Rényi-2 correlator,

$$C(\Psi; x, y) = \frac{[\text{Tr } \rho_{xy}^2 - \text{Tr } \rho_x^2 \text{ Tr } \rho_y^2]_+}{1 - \text{Tr } \rho_x^2 \text{ Tr } \rho_y^2} \in [0, 1], \quad [u]_+ := \max(u, 0). \quad (1.21)$$

When $\text{Tr } \rho_x^2 \text{ Tr } \rho_y^2 = 1$ (pure product marginals), we set $C = 0$ by convention (no synchronization channel for uncorrelated pure states).

For comparison with standard connected correlators, one may also define

$$C_{\text{loc}}(\Psi; x, y) = \langle \hat{f}(x) \hat{f}(y) \rangle_\Psi - \langle \hat{f}(x) \rangle_\Psi \langle \hat{f}(y) \rangle_\Psi, \quad (1.22)$$

for a local observable $\hat{f}(x)$. This quantity is used only as a diagnostic; it never appears in the weights of Eq. (1.15). When $\text{Tr } \rho_{xy}^2 \geq \text{Tr } \rho_x^2 \text{ Tr } \rho_y^2$, the complement takes the normalized deficit form

$$1 - C(\Psi; x, y) = \frac{1 - \text{Tr } \rho_{xy}^2}{1 - \text{Tr } \rho_x^2 \text{ Tr } \rho_y^2}. \quad (1.23)$$

The $[.]_+$ construction ensures $0 \leq C \leq 1$ in all cases and yields $C = 1$ whenever ρ_{xy} is pure (non-factorized). When x and y are maximally entangled, $C \rightarrow 1$ and the synchronization channel operates at full strength; for product states, $C = 0$ and the points evolve independently. This state-dependent weighting is the core of the Weak Entanglement Symmetry Hypothesis: geometry emerges from the entanglement structure, not the reverse.

Difference form. The bilocal Lindblad operator

$$L_{xy} = \tilde{T}^2(x) - \tilde{T}^2(y) \quad (1.24)$$

is simply the rescaled version of the difference form $L_{xy} = \hat{T}^2(x) - \hat{T}^2(y)$ of Eq. (1.9), using the dimensionless field $\tilde{T}(x) = \hat{T}(x)/\tau_s$. It penalizes temporal desynchronization between causally connected points. Its difference structure guarantees that no net charge is introduced or removed by the bilocal channel, a property that will later underpin the pre-geometric conservation principle.

No-signaling. Because $\gamma(x, y)$ vanishes for spacelike pairs, the bilocal generator has causal support only. For any region $A \subset \Sigma$ with complement A^c , the reduced state obeys

$$\frac{d}{ds} \rho_A(s) = \text{Tr}_{A^c} (\mathcal{L}_{J(A)}[\rho(s)]), \quad (1.25)$$

where $\mathcal{L}_{J(A)}$ denotes the restriction of the generator to operators supported in the causal domain $J(A)$. Hence spacelike operations on A^c cannot instantaneously affect ρ_A (Appendix H).

Causality is thus built into the generator itself. Here ‘causal’ denotes pre-geometric admissibility of pairs enforced by the WESH kernel; at the alignment fixed point it coincides with metric causal separation.

Remark 1.3 (Nonlinearity, CP/TP, and no-signaling). *Under the structural assumptions in Box 2, freezing the state-dependent gate $C(\Psi; x, y)$ on each micro-interval yields a standard GKSL generator with Hermitian jumps and nonnegative rates, so that each step of the WESH evolution is completely positive, trace preserving, and causal (McCauley et al., 2020). The state dependence of C can then be viewed as inducing a time-dependent generator; complete positivity and trace preservation for the resulting non-autonomous dynamics follow from product-integral constructions for time-dependent GKSL evolutions (Rivas & Huelga, 2012). Appendix H provides the full operator-level proof of CP/TP and no-signaling for Eq. (1.15).*

1.7 Bootstrap, Eigentimes, and the Emergence of Spacetime

In this subsection we analyse how a directed temporal ordering, and subsequently spacetime geometry, may emerge once time is promoted to a local quantum field operator $\hat{T}(x)$ in the Wheeler–DeWitt sector. Spatial geometry, though not quantized directly, emerges from the alignment dynamics governed by entanglement correlations and the causal kernel, as developed in the Einstein–Hilbert derivation of Sec. 5. The construction must generate temporal order and geometric structure without reintroducing an external time parameter or any pre-assigned causal layering.

Throughout this subsection $\langle \cdot \rangle_{\rho(s)}$ denotes expectation in the state $\rho(s)$, $\Delta\hat{T}(x) := \hat{T}(x) - \langle \hat{T}(x) \rangle_{\rho(s)}$, and we set $\hbar = c = 1$.

Architectural necessity. Once time is encoded by the operator $\hat{T}(x)$, it cannot simultaneously act as an external evolution parameter; introducing a separate clock would restart the hyper-time regress. Any emergent temporal order must therefore arise *endogenously*, from the statistics and structure of collapse events of $\hat{T}(x)$ itself.

A theory that aims to generate spacetime from a setting that, by necessity, lies *prior to* geometric structure—and simultaneously excludes any external evolution parameter—must satisfy strict architectural constraints tied to the endogenous handling of information. We may therefore identify the following prohibitions:

- *Sequential* constructions presuppose a pre-existing temporal ordering;
- *Hierarchical* constructions presuppose layered or stratified causality;
- *Iterative* algorithms presuppose discrete temporal steps.

The bootstrap is not a modeling choice but the *only self-sufficient mathematical architecture* compatible with these constraints. This places our construction in continuity with earlier self-consistency programmes—Chew’s *S*-matrix bootstrap (Chew, 1961) and the conformal bootstrap of Rattazzi, Rychkov, Tonni, and Vichi (2008), where physical quantities are fixed by global consistency rather than external inputs. Here, the same philosophy governs *chronogenesis* and the induced emergence of spacetime structure. In short, the bootstrap provides a self-consistent, atemporal configuration in which the Markovian dynamics and Poissonian stochasticity conspire to generate temporal order and geometric structure without any external temporal input or historical memory.

Bootstrap as an atemporal configuration. In WESH, the bootstrap is *not* a temporal sequence. It is an atemporal, non-hierarchical configuration in which multiple elements co-determine one another, closer to a Nash-type equilibrium than to a causal chain. To illustrate (as *mutual constraints*, not chronological stages): the quantum state fixes entanglement correlations $C(\Psi; x, y)$; these correlations weight dissipative channels; stochastic eigentime events realize localized outcomes of the time field; the concentration of such events constitutes the emergent spacetime arena in which the state is defined. No element is “first”; each requires the others for consistency.

This dissolves apparent circularities. As in the Page–Wootters mechanism (Page & Wootters, 1983), where a timeless global state encodes relational temporal correlations, and as in Wheeler–DeWitt, which admits no “before” once time emerges, here there is no “before the first eigentime” because eigentimes *constitute* the temporal structure. Questions that presuppose a pre-existing sequence are simply ill-posed. Combined with truly stochastic localization (which carries no

temporal memory) and with the causal kernel $\gamma(x, y)$ enforcing a finite memory window $\tau_{\text{corr}} \ll \tau_{\text{Eig}}$, this yields the *minimal sufficient* pre-geometric framework: the bootstrap eliminates external temporal scaffolding; Poissonian statistics eliminate dynamical memory; the short-range causal kernel coordinates the process without long-term history dependence.

Eigentimes as time quanta and geometric seeds. The basic quanta of this construction are *Eigentimes*: stochastic localizations of the time field at definite outcomes of the spectral measure of $\hat{T}(x)$. Let $E_x(dt)$ be the spectral measure of $\hat{T}(x)$, so that

$$\hat{T}(x) = \int_{\mathbb{R}} t E_x(dt), \quad \mathbb{1}_x = \int_{\mathbb{R}} E_x(dt). \quad (1.26)$$

For a local time-sector state $|\psi_T(x)\rangle$, the spectral expansion reads

$$|\psi_T(x)\rangle = \int_{\mathbb{R}} E_x(dt) |\psi_T(x)\rangle, \quad (1.27)$$

and an eigentime event in a Borel window $\Delta \subset \mathbb{R}$ is modeled operationally by the localization

$$|\psi_T(x)\rangle \longrightarrow \frac{E_x(\Delta) |\psi_T(x)\rangle}{\sqrt{\langle \psi_T(x) | E_x(\Delta) | \psi_T(x) \rangle}}, \quad p_x(\Delta) = \langle \psi_T(x) | E_x(\Delta) | \psi_T(x) \rangle. \quad (1.28)$$

Eigentimes are therefore *time quanta*: discrete stochastic realizations of the continuous spectrum of $\hat{T}(x)$, not quanta of space. Spatial geometry is induced indirectly: the pattern of eigentime events, weighted by entanglement via $C(\Psi; x, y)$ and correlated by the causal kernel $\gamma(x, y)$, seeds the smooth spacetime geometry reconstructed in Sec. 5. Regions where eigentimes concentrate densely support a well-defined geometric structure; sparsity leaves geometry weakly defined.

The mean production rate of eigentimes along the auxiliary flow is

$$\begin{aligned} \left\langle \frac{dN_{\text{Eig}}}{ds} \right\rangle &= \frac{\Gamma[\Psi(s)]}{\tau_{\text{Eig}}} \\ &= \nu \int \frac{d^4x}{V_\xi} \text{Tr} [\tilde{T}^2(x) \rho(s) \tilde{T}^2(x)] \\ &\quad + \iint \frac{d^4x d^4y}{V_\xi^2} \gamma(x, y) C(\Psi; x, y) \text{Tr} [L_{xy}^\dagger L_{xy} \rho(s)], \end{aligned} \quad (1.29)$$

with $\nu > 0$ a state-independent intensity scale. The local hazard—the instantaneous propensity at point x —satisfies

$$\lambda(x) = \nu \text{Tr} [\tilde{T}^2(x) \rho \tilde{T}^2(x)] \geq \nu (\text{Var}_\rho[\tilde{T}(x)])^2, \quad (1.30)$$

(Cauchy–Schwarz). Since $\tilde{T}(x) = \hat{T}(x)/\tau_s$ shares the same spectral projectors as $\hat{T}(x)$, the activation condition can equivalently be expressed in terms of the physical variance of $\tilde{T}(x)$:

$$\langle (\Delta \hat{T}(x_0))^2 \rangle_{\rho(s)} > \tau_{\text{thr}}^2 \implies \text{eigentime at } x_0. \quad (1.31)$$

Two scales control the statistics:

$$\tau_{\text{Eig}} \equiv \nu^{-1}, \quad \tau_{\text{ref}}(x) \sim \frac{1}{\nu} \frac{1}{(\text{Var}_{\rho}[\tilde{T}(x)])^2}. \quad (1.32)$$

Here τ_{Eig} is the mean spacing in the homogeneous limit, whereas $\tau_{\text{ref}}(x)$ acts as a local refractory period after strong localization.

Time-production functional. The relation between the auxiliary coordinate s (a reparametrization-invariant bookkeeping parameter; see Appendix B) and emergent time t is fixed by

$$\frac{dt}{ds} = \Gamma[\Psi], \quad t(s) = \int_0^s \Gamma[\Psi(s')] ds', \quad (1.33)$$

The lower integration bound is a convention fixing the origin of the auxiliary parameter s ; physical statements depend only on differences $t(s_2) - t(s_1) = \int_{s_1}^{s_2} \Gamma[\Psi(s')] ds'$ and are invariant under s -translations.

The functional $\Gamma[\Psi]$ is given by

$$\begin{aligned} \Gamma[\Psi] = \tau_{\text{Eig}} & \left[\nu \int \frac{d^4x}{V_{\xi}} \text{Tr}[\tilde{T}^2(x) \rho \tilde{T}^2(x)] \right. \\ & \left. + \iint \frac{d^4x d^4y}{V_{\xi}^2} \gamma(x, y) C(\Psi; x, y) \text{Tr}[L_{xy}^\dagger L_{xy} \rho] \right]. \end{aligned} \quad (1.34)$$

The prefactor $\tau_{\text{Eig}} = \nu^{-1}$ renders Γ dimensionless; by the law of large numbers, $t(s) \approx \tau_{\text{Eig}} N_{\text{Eig}}(s)$. For later use we isolate the bilocal term:

$$\Gamma_{\text{bi}}[\Psi(s)] = \iint \frac{d^4x d^4y}{V_{\xi}^2} \gamma(x, y) C(\Psi; x, y) \langle (\tilde{T}^2(x) - \tilde{T}^2(y))^2 \rangle_{\rho(s)}. \quad (1.35)$$

Lemma 1.1 (Monotonicity of t). *Let $\rho(s) \geq 0$ with $\text{Tr } \rho(s) = 1$. Assume time-sector nondegeneracy (ND): either $\exists x_0$ with $\text{Tr}[\tilde{T}^2(x_0) \rho(s) \tilde{T}^2(x_0)] > 0$, or $\exists (x, y)$ with $C[\rho(s); x, y] > 0$ and $\text{Tr}[\rho(s) (\tilde{T}^2(x) - \tilde{T}^2(y))^2] > 0$. With $\nu > 0$, $\gamma(x, y) \geq 0$, and $0 \leq C[\rho(s); x, y] \leq 1$, one has $\Gamma[\rho(s)] \geq 0$, with $\Gamma > 0$ under (ND); hence $dt/ds = \Gamma[\rho(s)] \geq 0$ and $t(s)$ is strictly increasing under (ND).*

Lemma 1.2 (Eigentime activation on chronogenetic segments). *Under the standing integrability assumptions on $\hat{T}(x)$ (finite fourth moments), assume nondegeneracy (ND) holds along a segment of the s -flow, so that $\Gamma[\rho(s)] > 0$ on that segment (Lemma 1.1). Define the survival probability of having no eigentime event on a segment of length $\delta > 0$ by*

$$S_{s_0}(\delta) := \exp\left(-\int_{s_0}^{s_0+\delta} \frac{\Gamma[\rho(s')]}{\tau_{\text{Eig}}} ds'\right).$$

Then $S_{s_0}(\delta) < 1$ on any chronogenetic segment (equivalently: eigentime events have non-zero intensity on every such segment). No segment is privileged: the statement is s -translation invariant.

Lemma 1.3 (Contraction to equilibrium and $\alpha = 2$). *Let $\Phi_{s,\delta s}$ be the update-mix map over $[s, s + \delta s]$. In the Markov regime $\mu = \tau_{\text{corr}}/\tau_{\text{Eig}} \ll 1$ there exist $L \gg \xi$ and $\varepsilon = \Theta(\mu) > 0$ such that*

$$\|\Phi_{s,\delta s}(\rho) - \Phi_{s,\delta s}(\sigma)\|_1 \leq (1 - \varepsilon) \|\rho - \sigma\|_1, \quad \forall \rho, \sigma.$$

(Uniqueness and mixing) *Since the state space is complete in trace norm, the strict contraction above implies (by the Banach fixed-point theorem) a unique fixed point ρ_∞ of $\Phi_{s,\delta s}$, and exponential convergence of iterates:*

$$\|\Phi_{s,\delta s}^n(\rho) - \rho_\infty\|_1 \leq (1 - \varepsilon)^n \|\rho - \rho_\infty\|_1, \quad \|\Phi_{s,\delta s}^n(\rho) - \Phi_{s,\delta s}^n(\sigma)\|_1 \leq (1 - \varepsilon)^n \|\rho - \sigma\|_1.$$

This uniqueness/mixing mechanism is purely Markovian (Dobrushin-type) and does not rely on any KMS/detailed-balance/thermal structure. Appendix D provides an existence proof via Schauder–Tychonoff under constraints even without a contraction estimate; Sec. 6.2 gives an independent (specialized) uniqueness route via primitivity and KMS spectral gap. With $\varepsilon = \Theta(\mu)$ and the collective-stability law $\tau_{\text{coh}}(N) \propto N^\alpha$, the fixed-point balance $\mu \sigma_\alpha = \mathcal{O}(1)$ uniquely selects $\alpha = 2$.

Sketch. Finite interaction range ξ and the N^{-2} normalization imply bounded per-site influence $\mathcal{O}(\mu)$ on blocks $L \gg \xi$. Standard Dobrushin-type arguments for finite-range Markov mixing then yield trace-norm contraction with $\varepsilon = \Theta(\mu)$, and the Banach fixed-point theorem gives uniqueness and exponential mixing. An independent uniqueness proof in the KMS/detailed-balance specialization is given in Sec. 6.2. \square

Self-consistent closure. Lemma 1.1 ensures $\Gamma[\rho] \geq 0$, with $\Gamma > 0$ under non-degeneracy (ND), so $t(s)$ is non-decreasing in general and strictly increasing under (ND), defining an intrinsic arrow of time. No external clock is introduced at

any stage: the statistics of eigentimes, constrained by WESH–Noether conservation and collective stability in the Markov window, fully determine the emergent temporal order. Markovianity, Poissonian statistics, and the atemporal bootstrap architecture thus form a single logical package: the evolution depends only on the present state, carries no temporal memory, and is closed under self-consistency. The foundational circularity (WESH derived from Wheeler–DeWitt by constraints, and the WESH dynamics contracting back to the frozen Wheeler–DeWitt constraint in the $G \rightarrow 0$ limit) is not a defect but a signature of self-consistency in a pre-geometric theory: time, geometry, and dynamics co-emerge from the same WESH completion of the timeless constraint.

1.8 Foundational consistency and parameter fixing

A necessary check on any dissipative extension of Wheeler–DeWitt is the behavior of the theory in two limiting regimes: the decoupling of gravitational effects and the thermodynamic scaling at horizons.

Finite memory (Born–Markov).

$$\int_0^\infty dt \|\langle \mathcal{C}(t)\mathcal{C}(0) \rangle\| < \infty, \quad \tau_{\text{corr}} = \xi/c \ll \tau_{\text{Eig}} \equiv 1/\nu. \quad (1.36)$$

Note. We use $\mathcal{C}(t)$ for the memory kernel to avoid clashes with the entanglement gate $C(\Psi; x, y)$.

Compatibility with N^2 stability (ratio scaling).

$$\frac{\tau_{\text{corr}}}{\tau_{\text{Eig}}^{(\text{eff})}} \sim N^{-2} \quad (\text{bilocal } \gamma \propto N^{-2}, \quad \tau_{\text{Eig}}^{(\text{eff})} \propto N^2). \quad (1.37)$$

Fundamental scales. The fundamental scales of the theory are anchored to Planck units:

$$\xi = \frac{\hbar}{m_T c} \simeq L_P, \quad \gamma_0 \simeq t_P^{-1}. \quad (1.38)$$

Terminology. m_T fixes the range ξ of the kernel used in $\gamma(x, y)$; it is not an on-shell degree of freedom.

Proposition 1.2 (Decoupling in the $G \rightarrow 0$ limit). *Let $\xi \simeq L_P \propto \sqrt{G}$ and $\gamma_0 \simeq t_P^{-1} \propto G^{-1/2}$, and write*

$$\gamma(x, y) = \frac{\gamma_0}{N^2} K_\xi(x-y) \Theta[\text{causal}(x, y)], \quad K_\xi \geq 0, \quad \|K_\xi\|_{L^1(\mathbb{R}^{1,3})} \sim V_\xi = \mathcal{O}(\xi^4).$$

Define the shorthand

$$\int \gamma \equiv \int d^4y \gamma(x, y).$$

Then

$$\nu \propto \gamma_0 V_\xi \rightarrow 0, \quad \int \gamma = \frac{\gamma_0}{N^2} \|K_\xi\|_{L^1} \sim \frac{\gamma_0}{N^2} V_\xi \rightarrow 0,$$

so for any bounded operator A ,

$$\left\| \frac{d}{ds} \text{Tr}(A\rho) \right\|_{\text{diss}} \leq C_A (\nu + \int \gamma) \rightarrow 0.$$

Proof sketch. $\|K_\xi\|_{L^1} \sim c\xi^4$ yields $\nu, \int \gamma = \mathcal{O}(\gamma_0 \xi^4) \rightarrow 0$; standard Lindblad bounds give $\|\mathcal{D}\| \leq \text{const} \cdot (\nu + \int \gamma) \rightarrow 0$, hence strong convergence to the unitary group.

Constraint continuity (The Frozen Limit). Since the fundamental scales satisfy $\xi \sim L_P \propto \sqrt{G}$ and $\gamma_0 \sim t_P^{-1}$, taking the formal limit $G \rightarrow 0$ implies $\nu \rightarrow 0$ and $\int \gamma \rightarrow 0$. In this limit, the dynamics undergoes a structural contraction:

- (i) **Vanishing dissipation.** The non-unitary terms in the master equation scale to zero, leaving a unitary flow generated solely by \hat{H}_{eff} .
- (ii) **Halting of temporal flow.** Crucially, the eigentime event rate $\langle dN_{\text{Eig}}/ds \rangle$ (Eq. 1.29) vanishes as $\nu \rightarrow 0$ and $\int \gamma \rightarrow 0$ (Prop. 1.2): no eigentimes occur, and the arrow of time ceases to emerge.

Physical interpretation. The limit $G \rightarrow 0$ enables us to recognize WESH and Wheeler–DeWitt as two regimes of the same fundamental constraint. When gravitational coupling is active, the constraint unfolds into a dissipative, dynamical structure that generates temporal flow; when gravity is turned off, both the production of time and the emergence of spacetime geometry halt simultaneously, and the theory continuously contracts back to the frozen, timeless sector $\hat{H}_{\text{tot}}|\Psi\rangle = 0$.

Physical time and Einstein gravity emerge as complementary aspects of a single dissipative resolution of the Wheeler–DeWitt constraint: time arises through the eigentime bootstrap ($dt/ds = \Gamma > 0$), while spacetime geometry crystallizes

through gradient alignment and hidden-sector cancellation, which together constitute the unique infrared attractor of the WESH flow (Sec. 5). Neither structure is logically prior; both derive from the same pre-geometric algebraic constraints—CPT invariance, WESH–Noether charge conservation, and collective stability—without postulating a background arena.

Fixed-regime summary. Combining the N^{-2} kernel scaling with the Markov condition $\tau_{\text{corr}} \ll \tau_{\text{Eig}}$ yields a self-consistent fixed point:

$$(\tau_{\text{coh}}(N) \propto N^2) \& (\mu := \frac{\tau_{\text{corr}}}{\tau_{\text{Eig}}} \ll 1) \iff \alpha = 2 \quad (1.39)$$

The bootstrap mechanism should be understood as a self-consistency requirement that constrains the dynamics of the theory, analogous to closure conditions successfully employed in conformal field theory to fix operator dimensions (Rattazzi et al., 2008). It is not a circular definition, but rather a dynamical equilibrium condition: the parameters that govern dissipation (γ_0 , ξ) and the resulting statistical properties of eigentime events (ν , τ_{coh}) must mutually adjust to maintain Markovian memory within a collective N^2 stability window.

Remark 1.4. *The scaling statement in Eq. (1.39) is encoded by the bilocal part of the WESH generator (1.15) with causal kernel (1.20): the N^{-2} prefactor provides collective protection (per-site rate $\Gamma_i \sim \gamma_0/N$), while the finite correlation length ξ fixes a state-independent correlation time $\tau_{\text{corr}} \sim \xi/c$. Together these imply the Markov window $\mu := \tau_{\text{corr}}/\tau_{\text{Eig}} \ll 1$ in the large- N regime (see the heuristics in Appendix E).*

Preview: thermodynamic validation. The same dissipative structure, applied to the near-horizon region of a black hole, reproduces the Bekenstein–Hawking entropy $S = A/4L_P^2$ with calculable logarithmic corrections (Sec. 6). This cross-scale consistency—from Planck-scale dynamics to macroscopic thermodynamics—provides a non-trivial validation of the framework.

1.9 Foundational Considerations

We conclude this foundational exposition by highlighting the strict parsimony of the construction. The transition from the static Wheeler–DeWitt constraint to the dynamic WESH evolution is not an ad hoc extension, but establishes a rigorous

lineage from the first principles of the quantum universe: the WESH dynamics is derived directly from the Wheeler–DeWitt constraint as its necessary dissipative realization. This unfolding into a causal history is achieved without expanding the fundamental physics: the theory posits no extra spatial dimensions, no supersymmetric partners, no discrete spacetime atoms, nor ad hoc "chronon" particles. Instead, the framework relies exclusively on established theoretical components: the kinematics of quantum theory, the canonical constraints of General Relativity, and the structure of quantum entanglement. The novelty resides entirely in the architectural synthesis, which rests on two non-trivial structural keystones:

- The pre-geometric algebraic foundation of conservation, where WESH–Noether symmetry is enforced at the operator level prior to the emergence of any background metric (essential for deriving the Einstein tensor in Sec. 5 and the Bekenstein–Hawking law in Sec. 6.2);
- The bootstrap closure, which replaces linear evolution with a self-consistent cycle where the geometry necessary to define the field \hat{T} is generated by the field's own dissipative activity.

In this architecture, entanglement plays a dual, constitutive role: it acts simultaneously as the carrier of statistical symmetry and as the engine of Poissonian stochastic dissipation. The parameters appearing in the final structure (ν, k, α) are therefore not free couplings, but structural constants locked by the stability of this interdependence. In this sense, QFTT–WESH represents a *minimal sufficiency* approach to quantum gravity: it demonstrates that the ingredients necessary to resolve the frozen-time paradox are already present in quantum mechanics and relativity, but their consistent integration demands a methodological shift, from unitary linearity to a bootstrap-closed, algebraic dissipative dynamics, capable of accessing solutions (chronogenesis, hidden-sector cancellation) that remain invisible to standard background-dependent approaches.

Box 3: Beyond Detailed Balance – Pre-geometric Consistency

In standard open quantum systems, convergence to a stationary state is often tied to *Detailed Balance* (DB) with respect to a fixed thermal state, a condition that presupposes a background time and an externally given equilibrium ensemble. In QFTT–WESH we are in a pre-temporal, pre-geometric regime: such structures are not available, and DB cannot be imposed as an input.

Pre-temporal constraints (in s). The fundamental constraints are algebraic, not thermal. (i) *WESH–Noether*: the generator exactly preserves all global charges at the operator level (path independence; App. G). In particular,

$$\mathcal{L}^\dagger[\hat{Q}_a] = 0 \quad \forall a. \quad (1.40)$$

(ii) *Causal support*: the bilocal kernel has light-cone support and forbids superluminal signaling (Eq. (4.35)). (iii) *Positivity/trace preservation & finite memory*: the flow preserves positivity and unit trace (stepwise CPTP) within a finite Markov window (Eq. (1.36)).

Emergence. Under (i)–(iii) and mixing (contraction of the WESH update–mix map on coarse-grained windows; App. D), the pre-temporal GKSL flow admits a unique stationary state. Detailed Balance is not assumed at this level: it reappears later as a KMS/detailed-balance property of the emergent near-horizon equilibrium (Sec. 6.2), once physical time and geometry have formed.

Implication. Placing algebraic conservation first, and thermodynamic notions only at the emergent level, removes circularity and keeps the pre-geometric generator (1.15) free of thermal priors.

Table 1: Summary of fundamental parameters and scales in the QFTT–WESH formalism. All quantities use natural units with $\hbar = c = 1$ where applicable.

Symbol	Meaning	Dimensions	Scale / Definition	Eq.
ξ	Corr. length	[length]	Planck ($\simeq L_P$)	(1.38), (1.20)
γ_0	WESH rate scale	[time] $^{-1}$	$\simeq t_P^{-1} \times \Theta_0$	(1.38), (A.6)
N_{Eig}	eigentime count	—	via Eq. (1.29)	(1.29), (1.33)
τ_{Eig}	Mean eigentime spacing	[time]	$1/\nu$	(1.32)
ν	Local eigentime rate	[time] $^{-1}$	matched (no explicit N)	(1.29), (A.5)
τ_{corr}	Correlation time	[time]	ξ/c	(1.36)
τ_{coh}	Coherence time	[time]	$\propto N^2$	(1.39)
α	Stability exponent	—	2	(1.39)
$\Gamma[\Psi]$	Time-production functional	—	≥ 0	(1.33), (1.34)
$C(\Psi; x, y)$	Entanglement corr.	—	$[0, 1]$	(1.21)
L_{xy}	Bilocal jump operator	—	$\tilde{T}^2(x) - \tilde{T}^2(y)$	(1.9), (1.24)
m_T	Kernel mass scale	[mass]	$\propto 1/\xi$	(1.38)
k	Alignment factor	[time]	via $\lambda_{1,2}$ matching	(4.2), (4.8)

Units Note. With $\tilde{T} = \hat{T}/\tau_s$ and normalized measures $\int \frac{d^4x}{V_\xi}$ and $\iint \frac{d^4x d^4y}{V_\xi^2}$, each additive term in the generator carries units of inverse time. With $\|K_\xi\|_{L^1(\mathbb{R}^{1,3})} \sim V_\xi = \mathcal{O}(\xi^4)$, the integrated bilocal weight scales as

$$\int \gamma = \frac{\gamma_0}{N^2} \|K_\xi\|_{L^1} \sim \frac{\gamma_0}{N^2} V_\xi.$$

Using the normalized measures ensures consistent dimensions in Eq. (1.15). The time-production functional $\Gamma[\Psi]$ is rendered dimensionless by the prefactor $\tau_{\text{Eig}} = 1/\nu$ in Eq. (1.34), ensuring that the map $dt/ds = \Gamma[\Psi]$ is dimensionally consistent.

2 Key Theoretical Predictions

Overview. Building on the WESH–Noether structure developed in Sec. 1, we now isolate two quantitative signatures of the framework: (i) collective stability, expressed by the N –scaling of coherence, which acts as a structural discriminant of the bilocal WESH channel; and (ii) a $\cos^2 \theta$ angular modulation in parity decay, which provides a diagnostic test of state/geometry factorization and causal connectivity. Both follow from the WESH master equation and its causal kernel, and

they provide quantitative targets for the simulations and hardware tests of Sec. 3.

2.1 Collective stability and N -scaling

The fundamental signature of WESH dynamics is the suppression of pairwise dissipative couplings as the system size grows. Unlike standard decoherence, where independent local errors accumulate linearly, the WESH interaction strength scales inversely with the square of the number of constituents:

$$\gamma_{ij}(N) = \frac{\gamma_0}{N^2}, \quad i \neq j. \quad (2.1)$$

This N^{-2} scaling is not arbitrary but required to maintain the total collapse power finite in the thermodynamic limit ($\sum \gamma_{ij} \sim \mathcal{O}(\gamma_0)$), ensuring that the effective rate per subsystem decreases as $\Gamma_i \sim 1/N$.

Consequently, we predict a **collective enhancement of coherence time** that defies standard local noise models:

$$\tau_{\text{coh}}(N) \propto N^2. \quad (2.2)$$

This quadratic protection is valid in the Markovian regime where the correlation time τ_{corr} is small compared to the eigentime scale τ_{Eig} (see Appendix E for the heuristic derivation).

2.2 Angular dependence: projection → geometry → state

A second, diagnostic signature connects the detector geometry to the prepared quantum state. The decay rate of parity oscillations is predicted to follow a robust angular modulation:

$$\Gamma_{\text{dec}}(\theta) = \bar{\Gamma}(1 + \varepsilon \cos^2 \theta), \quad \varepsilon = \frac{a_2}{a_0} \frac{G_2}{G_0}. \quad (2.3)$$

Here, ε factorizes into an intrinsic state anisotropy (a_2/a_0) and a device-specific geometric factor (G_2/G_0). Intuitively, the rotated-parity measurement projects two-body contributions onto the $\cos^2 \theta$ harmonic; the bilocal WESH channel then aggregates these pairwise projections over the chip geometry, while the prepared state supplies the intrinsic quadrupolar bias. Importantly, this allows us to distinguish WESH effects from isotropic background noise:

- **GHZ states:** exhibit positive modulation ($\varepsilon > 0$).
- **W-states:** are expected to show anti-modulation ($\varepsilon < 0$), providing a crucial control for state dependence.

2.3 Discrimination from conventional decoherence models

The predictions of Sec. 2.1–2.2 are informative only insofar as they can be *discriminated* from conventional (non-WESH) decoherence mechanisms. Here we (i) state an explicit null class of models, (ii) isolate the two WESH-specific discriminants already derived in the framework (collective N -scaling and state–geometry factorization of the angular law), and (iii) summarize falsification criteria and the minimal control program needed to exclude device-driven explanations.

Null class of models (non-WESH). We take as baseline any model in which decoherence is fully accounted for by *state-independent hardware noise* (possibly including spatial correlations) plus control imperfections. Concretely, this includes: (i) independent local Markovian channels (dephasing, depolarizing, amplitude damping) with per-qubit rates not decreasing with system size, and (ii) device-level correlated noise that may be anisotropic in space but remains *independent of the prepared entanglement class* (GHZ vs W vs product), once gate depth and readout are matched. Under this null class, any observed advantage of an entangled preparation must be attributable either to circuit-level differences or to geometry-only correlations, not to a bilocal, state-gated channel.

Structural discriminant: inverse pair scaling and collective stability. Within the WESH master-equation structure used in Sec. 2.1, the suppression of pairwise dissipative couplings,

$$\gamma_{ij}(N) = \gamma_0/N^2, \quad i \neq j$$

(Eq. (2.1)) is not a fit choice but the condition that keeps the total bilocal collapse power finite when the number of pairs grows with N . In the regime in which the reduced description applies (Markov window as specified in the framework), this yields the collective coherence enhancement

$$\tau_{\text{coh}}(N) \propto N^2,$$

(Eq. (2.2)). By contrast, in the null class above, increasing N does not generically increase coherence time for genuinely entangled states beyond trivial control effects: independent local error accumulation is constant at best and typically degrades with N , and correlated noise can at most change the *rate of degradation* unless one engineers a symmetry-protected subspace (addressed below). Therefore, observing sustained superlinear enhancement in entangled coherence with growing N is a *structural* rejection of the baseline class, while the absence of any superlinear trend across accessible N places a quantitative upper bound on the WESH coupling and, if persistent, would falsify the collective-stability prediction as stated.

Diagnostic discriminant: factorized, state-dependent angular modulation.

The angular law

$$\Gamma_{\text{dec}}(\theta) = \bar{\Gamma}(1 + \varepsilon \cos^2 \theta), \quad \varepsilon = \frac{a_2}{a_0} \frac{G_2}{G_0},$$

(Eq. (2.3)) is derived in Appendix F from (i) rotated-parity projection, (ii) lattice-weighted geometry, and (iii) weak even gate anisotropy. Importantly, the framework predicts not merely a $\cos^2 \theta$ harmonic, but a *factorization*: G_2/G_0 is device/layout-specific and state-independent, while a_2/a_0 is an intrinsic state-class parameter controlling the *sign* and magnitude of ε . A purely device-driven anisotropy can indeed generate a $\cos^2 \theta$ modulation in parity decay, so the harmonic *alone* is not sufficient for discrimination. The diagnostic power arises from the *state-coupled* structure: when geometry and readout are held fixed, the framework predicts a sign reversal of the modulation between GHZ-type preparations ($\varepsilon > 0$) and W-type controls ($\varepsilon < 0$), as already used as a control in Sec. 3.

Minimal control set implied by the framework. Discrimination requires treating the WESH signature as a *joint constraint* rather than a single effect:

1. **Gate-matched entanglement control (Sec. 3).** The fake-GHZ procedure isolates entanglement from gate depth: if the observed protection were a circuit artifact, fake-GHZ would reproduce it; instead, the separation between GHZ and product-like controls is used as the operational discriminator.
2. **State swap at fixed geometry (Sec. 3).** Replacing GHZ by a W-state while keeping the same device subset and readout targets the state-coupled nature of ε .
3. **Cross-platform reproducibility (Sec. 3).** Reproducing the angular signature across distinct hardware stacks (IBM Eagle vs Rigetti Ankaa-3)

reduces the plausibility of vendor-specific correlated noise as a complete explanation.

4. **Sequence/band robustness (Sec. 3).** Protection that persists across the spectroscopy band and across CPMG depths constrains interpretations in which the effect is primarily a dynamical-decoupling filter artifact.

Appendix F further clarifies that an angle-independent baseline (hardware noise) can coexist with the modulation without generating it; hence, controls must target the *state dependence* of the modulation amplitude rather than the existence of a baseline rate.

Signature	WESH (this work)	State-independent hardware noise (null class)	Standard alternatives
Angular modulation	$\cos^2 \theta$ with factorization and GHZ/W sign flip	possible device-tied anisotropy, no state-class sign reversal	fixed pattern from bath / layout
Scaling with N	$\tau_{\text{coh}} \propto N^2$ (collective stability)	$\tau_{\text{coh}} = \mathcal{O}(1)$ or degrading with N	model-dependent, typically sub-quadratic
Gate-matched GHZ vs fake-GHZ	protection persists under gate-matched control	differences attributable to overhead only	depends on encoding/implementation
GHZ vs W modulation sign	$\varepsilon_{\text{GHZ}} > 0$, $\varepsilon_W < 0$ at fixed geometry	no systematic dependence on entanglement class	no generic sign flip at fixed layout

Table 2: Schematic discrimination logic. The WESH framework is constrained by a *joint* signature set: collective N -scaling, factorized angular modulation, and state-dependent sign reversal at fixed geometry. Conventional noise mechanisms may reproduce individual rows but must account for the full pattern simultaneously.

Alternative explanations and what they must reproduce. The following conventional mechanisms can mimic *parts* of the observed phenomenology, but are constrained by the full signature set above:

1. **Spatially correlated Markovian noise (device anisotropy).** This can generate a $\cos^2 \theta$ harmonic if correlations define a preferred direction.

To explain the WESH pattern it must additionally reproduce (at fixed geometry) the GHZ/W sign reversal and the gate-matched GHZ vs fake-GHZ separation, rather than producing a modulation that tracks only device orientation.

2. **Non-Markovian (colored) noise under dynamical decoupling.** Such noise can produce strong sequence-dependent changes in apparent decay rates. To mimic the WESH claims it must yield a state-class dependent modulation (including sign reversal) that remains consistent across CPMG depths and across the tested frequency band.
3. **Decoherence-free subspace / collective-noise protection.** DFS effects require an approximate permutation-symmetric coupling structure not naturally realized on fixed-geometry superconducting chips with inhomogeneous couplings. Moreover, DFS protection is highly state-selective; to replace the WESH explanation it must account simultaneously for the entanglement-specific protection (gate-matched control) *and* the state-coupled angular signature derived in Appendix F.

Status of the collision model. The collision model used in Sec. 3 is a deliberately reduced *surrogate*: it does not attempt to simulate the full WESH master equation (e.g. the full causal-kernel structure or the pre-geometric WESH–Noether constraint), but isolates the specific ingredient tested there—inverse scaling of the effective couplings implied by Eq. (2.1)—in a tractable Markovian dynamics with an explicit local benchmark. In this controlled setting, extracting effective decay rates yields a clear pre-asymptotic power law $\gamma(N) \propto N^{\alpha_\gamma}$ with $\alpha_\gamma \simeq -1.80$ over $N = 2\text{--}16$ (while the matched local benchmark returns $\alpha_\gamma = -1$), i.e. trending toward the WESH asymptote $\alpha_\gamma = -2$ and already cleanly separated from local scaling. The collision model therefore serves as a *quantitative consistency check* (numerical proof-of-concept) for the collective-stability mechanism and for the scaling-inference pipeline; it is not, by itself, standalone empirical evidence. Empirical support is instead sought in the hardware signatures of Sec. 3, where the angular modulation and the entanglement-linked protection are observed under gate-matched controls on real processors.

Falsification criteria. Within the present formulation, the framework is constrained or ruled out by any of the following:

1. **No collective enhancement:** entangled coherence does not show a superlinear improvement with N under gate-matched conditions as hardware capabilities extend to larger multipartite registers.

2. **No state-coupled angular signature:** the $\cos^2 \theta$ modulation is absent on entangled states, or appears identically on product/fake-GHZ controls (indicating a device artifact rather than a state-coupled effect).
3. **No GHZ/W sign reversal:** the modulation amplitude does not change sign under a GHZ \leftrightarrow W state swap at fixed geometry and readout.
4. **Protection compatible with overhead only:** the observed protection ratio remains consistent with gate-depth/readout overhead alone in the gate-matched control protocol.

Current data (Sec. 3) are consistent with the angular and protection signatures for $N = 3, 4$ and show degradation for $N \geq 5$, defining the present sensitivity frontier on NISQ processors. Decisive tests of the collective-stability discriminant require higher-fidelity multipartite entanglement at larger N . A natural next step is to repeat the same control stack (state swap, geometry control, gate-matched fake-GHZ) on platforms with cleaner and more characterizable noise models and reconfigurable connectivity (e.g., trapped-ion or neutral-atom architectures), where scaling regimes beyond current superconducting hardware become experimentally accessible.

3 Experimental Validation

We test these predictions through a dual approach combining controlled classical simulations and quantum hardware experiments.

First, we employ a pre-asymptotic collision model on CPUs to isolate the collective stability mechanism. This model deliberately implements inverse couplings in a tractable regime ($N \leq 16$) to verify the scaling laws without the overhead of full quantum simulation.

Second, we execute production runs on superconducting quantum processors (IBM Eagle and Rigetti Ankaa-3). These experiments probe the angular dependence and protection gaps in a physical setting, leveraging large-scale statistics ($\sim 3 \times 10^6$ shots) to extract signals from the NISQ noise floor.

All datasets and analysis scripts are available in the companion repository:
<https://github.com/Luca-Casagrande/QFTT-WESH>.

3.1 Numerical Evidence: Collective Stability

The collision model simulations are consistent with the non-standard scaling predicted by Eq. (2.1). As shown in Figure 3.1, the coherence time for the WESH model grows with system size ($\alpha_{coh} \approx 2.5$), in stark contrast to the standard local decoherence model where coherence remains flat or degrades ($\alpha_{coh} \approx 0$).

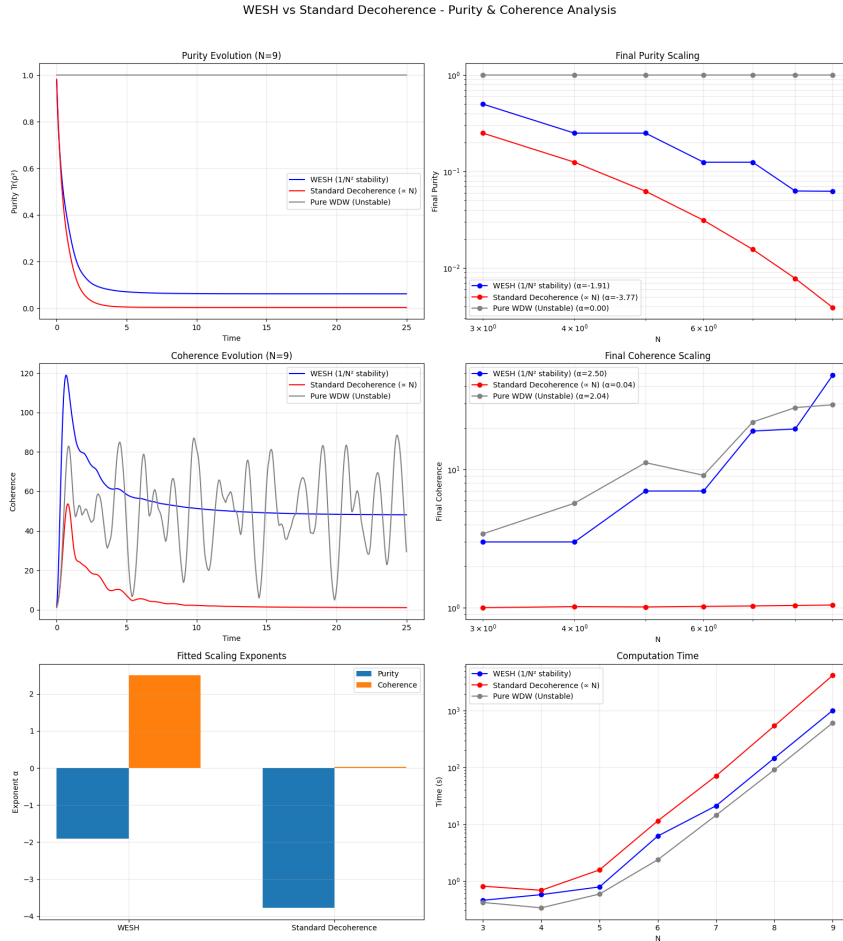


Figure 3.1: Purity and coherence scaling ($N = 3–9$). Comparison of WESH (collective jump $L \propto T/N$), Standard (local jumps σ_x), and Pure WDW baselines. **Left:** Time traces at $N = 9$. WESH maintains significantly higher purity and coherence. **Right:** Log-log scaling. WESH coherence grows super-linearly ($\alpha \approx 2.5$), supporting the collective stability hypothesis. Standard decoherence shows no such enhancement.

The robustness of this scaling is further tested under different coupling profiles

(Figure 3.2). Only inverse-scaling profiles ($1/N$, $1/N^2$) yield a negative loss exponent b , confirming that collective suppression is necessary for stability.

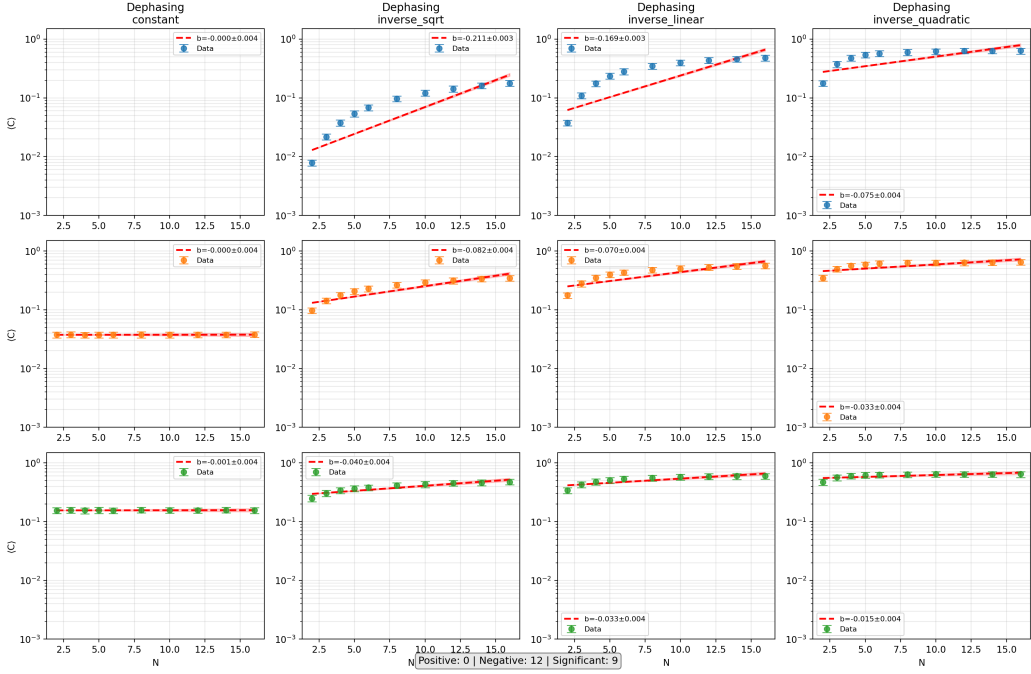


Figure 3.2: **Robustness of protection.** Final coherence $C(N)$ for various noise channels and coupling profiles. Only inverse scaling ($1/N^k$) enables coherence preservation (rising trends), whereas constant coupling leads to rapid decay (flat-/dropping trends).

Extending the analysis to $N = 16$ (Figure 3.3), we extract a rate scaling exponent $\alpha \approx -1.80$. This value approaches the theoretical prediction of -2 and is clearly distinguishable from the $\alpha = -1$ scaling of standard local control models (Figure 3.4).

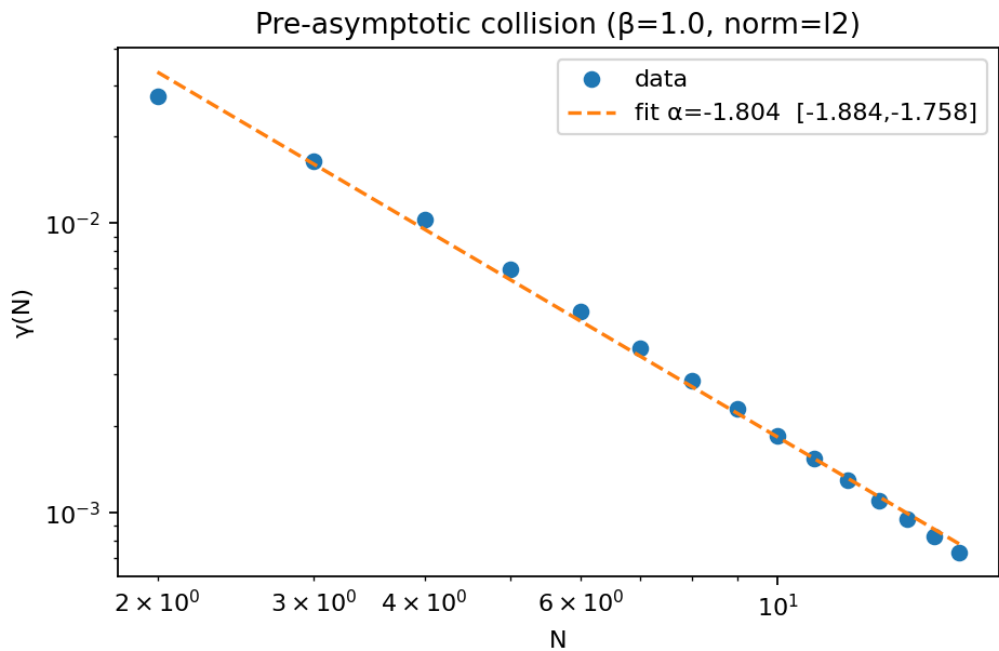


Figure 3.3: **Pre-asymptotic rate scaling.** Log-log regression yields $\gamma(N) \propto N^{-1.80}$, consistent with an approach to the asymptotic N^{-2} WESH prediction.

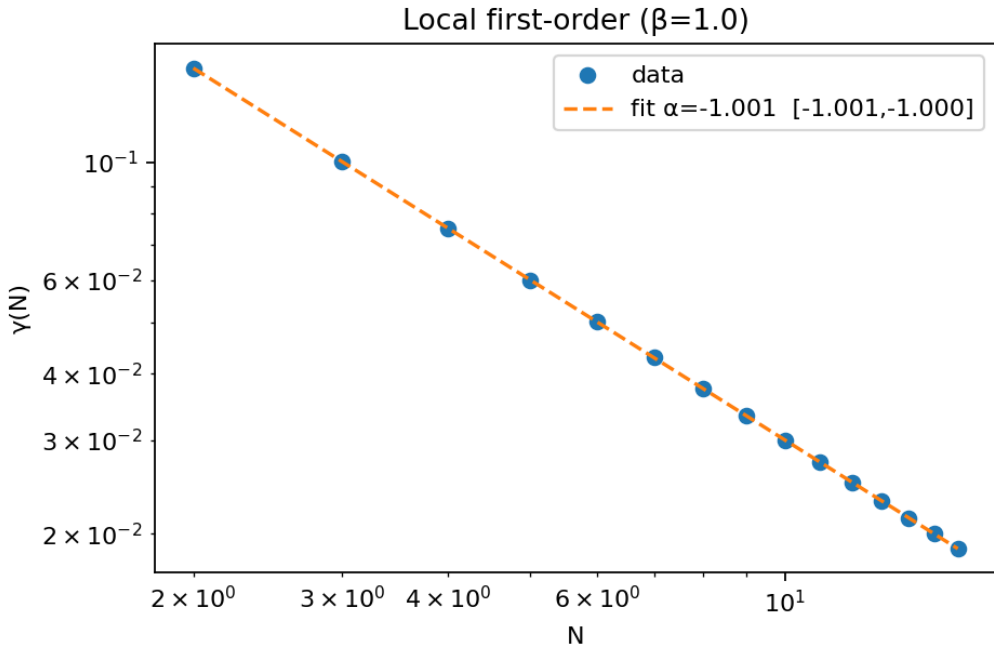


Figure 3.4: **Local baseline check.** The same analysis on a local first-order model yields $\alpha = -1.00$, validating the sensitivity of the metric.

3.2 Hardware Evidence: Angular Law and Protection

On quantum hardware, we focus on the angular signature (Eq. (2.3)). Experiments on IBM Eagle ($N = 3, 4$) reveal a clear $\cos^2 \theta$ modulation of the parity decay rate. Figure 3.5 shows a high-quality fit ($R^2 = 0.947$) with modulation amplitude $\varepsilon \approx 0.31$. Crucially, preparing a W-state reverses the sign of the effect (anti-modulation), confirming the state-dependence predicted by the theory.

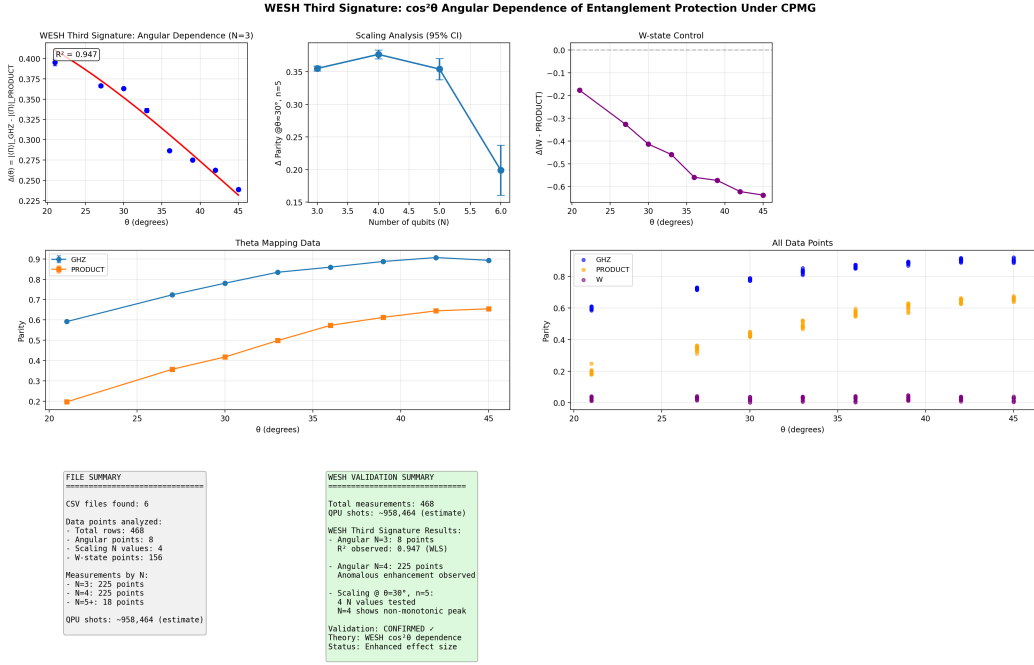


Figure 3.5: **Angular dependence on IBM Eagle.** **Top Left:** Decay rate modulation follows the predicted $\cos^2 \theta$ law ($R^2 = 0.947$). **Top Right:** W-state control shows the predicted sign reversal (anti-modulation).

To rule out gate-overhead artifacts, we performed a controlled comparison (Figure 3.6) between GHZ states and "fake-GHZ" states (entanglement created and immediately undone). The GHZ state retains significantly higher parity, with a decay rate ratio $\Gamma_{\text{PROD}}/\Gamma_{\text{GHZ}} \approx 2.6$, far exceeding the factor attributable to gate depth alone (~ 1.2).

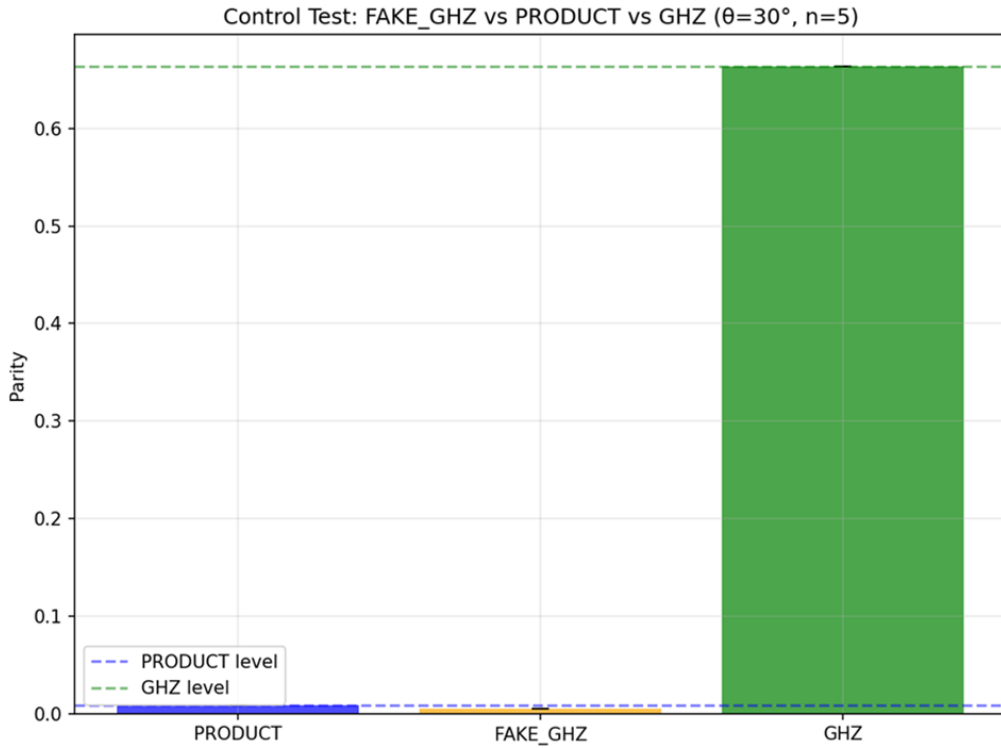


Figure 3.6: **Gate-matched control.** The "Fake-GHZ" (disentangled) behaves like the product state, while the true GHZ state maintains high parity. This isolates entanglement as the protective resource.

Comprehensive data from 1.9M shots (Figure 3.7) confirms this separation across the frequency spectrum. The distribution of parity outcomes for GHZ states is bimodally separated from product states (Figure 3.8), providing model-independent evidence of entanglement-enhanced stability.

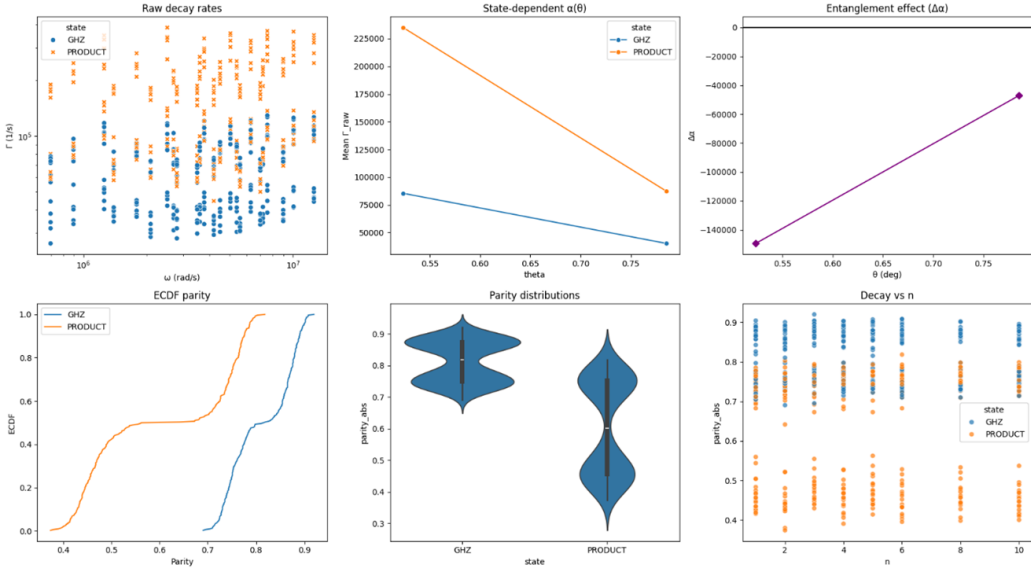


Figure 3.7: Spectral consistency. (a) Raw decay rates show GHZ (blue) consistently lower than product states (orange) across the 0.1–2.0 MHz band. (d) Protection persists across varying CPMG depths.

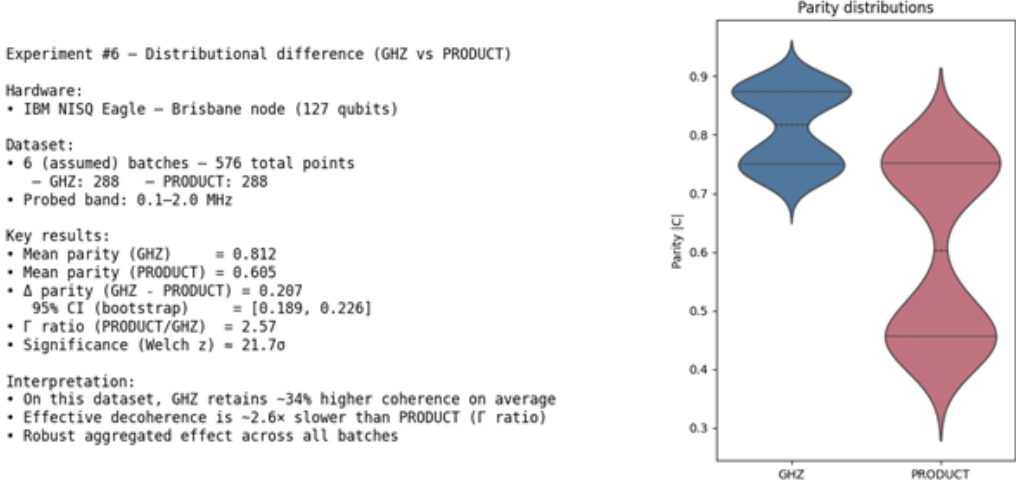


Figure 3.8: Distributional separation. Violin plots of parity outcomes ($N = 576$) show a statistically significant gap (21σ) between GHZ (blue, protected) and product states (red, decaying).

Note. In this dataset, multipartite entanglement is observed to suppress decoherence, as quantified by the $\sim 2.6\times$ slower decay of the GHZ state. This protective effect, measured on a 127-qubit superconducting processor, highlights entan-

glement not only as a computational resource but also as a potential stabilizing mechanism for quantum information in near-term hardware, and merits further investigation independently of any specific theoretical framework.

Experiment 7, Counter-proof - Rigetti Ankaa-3

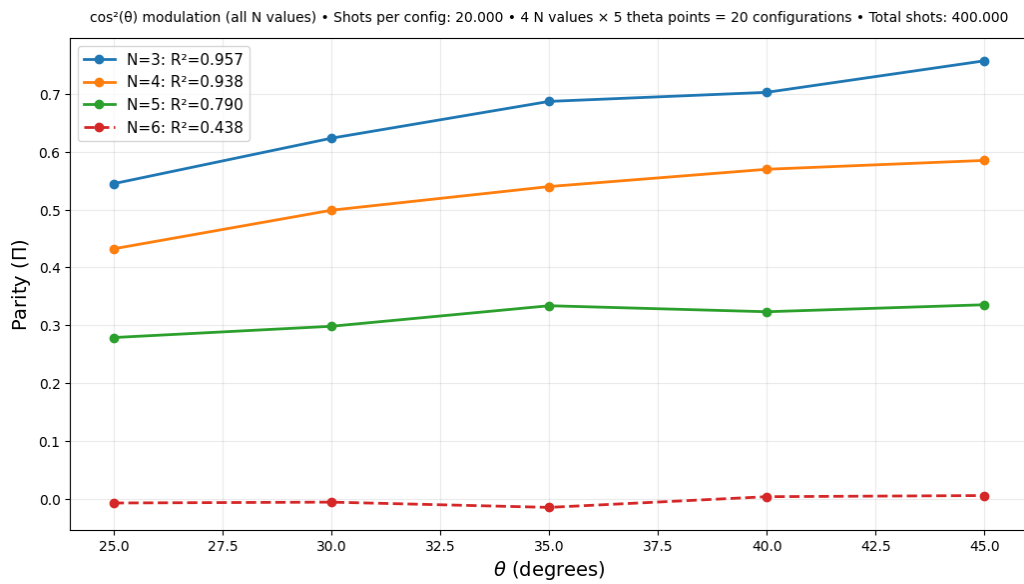


Figure 3.9: **Cross-platform check (Rigetti Ankaa-3).** The angular law is reproduced for $N = 3, 4$. Signal-to-noise ratio degrades for $N \geq 5$, defining the current hardware sensitivity limit.

Box 4: Experimental Summary

The combined numerical and experimental evidence supports the two pillars of WESH phenomenology:

1. **Collective stability:** simulations are consistent with $\tau_{\text{coh}} \propto N^\alpha$ with $\alpha \approx 2$, driven by inverse-scaling couplings.
2. **Geometric structure:** hardware data are consistent with the specific $\cos^2 \theta$ modulation and its dependence on the quantum state (GHZ vs W), distinguishing it from isotropic noise.

Metric	WESH (Collision Model)	Standard Noise	Pure WDW
Coherence Scaling (α_C)	+2.498 (protected)	+0.036 (flat)	—
Rate Scaling (α_γ)	-1.804 (N^{-2} trend)	-1.001 (local)	—
Purity Scaling (α_{pur})	-1.909	-3.772	~ 0
Thermodynamic Arrow	Yes	Yes	No

Table 3: Scaling metric comparison. The WESH model uniquely combines a thermodynamic arrow of time with collective protection of coherence, distinct from both unitary evolution (Pure WDW) and standard local decoherence.

4 General Relativity, part I: Emergence from QFTT-WESH

Overview: This section and Section 5 offer two complementary perspectives on the emergence of gravity within QFTT-WESH. Here we adopt a consistency-check approach: we introduce the Einstein–Hilbert term in S_{eff} (Eq. (4.9)) and verify its compatibility with WESH through hidden-sector cancellation, recovering $G_{\mu\nu} + \Lambda g_{\mu\nu} = 8\pi G T_{\mu\nu}^{(m)} + O(1/N)$ (Eqs. (4.19)–(4.21)). Here and below, Λ denotes the effective IR cosmological constant (i.e. $\Lambda \equiv \Lambda_{\text{eff}}$); its IR interpretation and stochastic width are discussed in the subsection “ Λ as entanglement IR imprint” and Appendix J. Section 5 complements this by deriving the EH term dynamically, without postulating it. Together, these routes can be viewed

as a microscopic realization of Sakharov's induced-gravity scenario (Sakharov, 1967), where spacetime curvature emerges from quantum vacuum fluctuations rather than being assumed from the outset.

4.1 Stationary alignment: the bridge from time to geometry

We now discuss the emergence of spacetime. The WESH dynamics induce a stationary alignment between the time field and the entanglement potential; this alignment underlies the subsequent metric reconstruction.

Lemma 4.1 (Bootstrap alignment — stationary condition).

Entanglement potential and its functional variation. In the present effective description we treat the local eigentime profile $\tau(x) := \langle \hat{T}(x) \rangle_\rho$ as the relevant variational degree of freedom. Accordingly, the functional derivative $\delta C / \delta \hat{T}(z)$ in Eq. (4.1) is to be understood as taken with respect to local shifts of the mean field $\tau(z)$ (mean-field limit of the operator variation).

$$\begin{aligned} \Phi(x) &= \int d^4y K(x-y) C(\Psi; x, y), \\ \delta\Phi(x) &= \int d^4y K(x-y) \int d^4z \frac{\delta C(\Psi; x, y)}{\delta \hat{T}(z)} \delta \hat{T}(z). \end{aligned} \tag{4.1}$$

Stationary alignment.

$$\text{Assume (stationary, mean-field): } \quad \partial_\mu \tau(x) = k \partial_\mu \Phi(x), \quad \tau(x) := \langle \hat{T}(x) \rangle_\rho. \tag{4.2}$$

Proof (sketch). In the Markovian regime ($\tau_{\text{corr}} \ll \tau_{\text{Eig}}$), stationarity of the CP–TP flow is equivalent to vanishing first variation of a WESH monotone ($\delta \mathcal{M}_\epsilon = 0$). The variation produces a mixed term $\mathcal{J}^\mu(x) \partial_\mu \tau(x)$ with $\mathcal{J}^\mu \propto \partial^\mu \Phi(x)$ (cf. Part II, Thm. 5.2). Here \mathcal{J}^μ denotes this variational mixed-term current and should not be confused with the entanglement current J^μ introduced in Lemma 4.2. The stationarity condition thus requires $\partial_\mu \tau \parallel \partial_\mu \Phi$; the proportionality constant k is fixed by the linear matching (Eq. (4.8)). \square

4.2 Emergent metric decomposition (uniqueness)

Complete metric: time + entanglement + eigentime substrate.

The emergence of Einstein's equations requires the physical metric $g_{\mu\nu}$ to be a composite field, reconstructed from three distinct sectors: the time-field contribution $g_{\mu\nu}^{(T)}$ (set by gradients of \hat{T}), the entanglement contribution $g_{\mu\nu}^{(C)}$ (encoded by the nonlocal potential Φ), and the discrete eigentime substrate $g_{\mu\nu}^{(E)}$ (the inertial seed). This decomposition is minimal and dictated by the WESH architecture:

$$g_{\mu\nu}(x) = g_{\mu\nu}^{(T)}(x) + g_{\mu\nu}^{(C)}(x) + g_{\mu\nu}^{(E)}(x). \quad (4.3)$$

Definitions of $g^{(T)}$ and $g^{(C)}$.

$$\begin{aligned} g_{\mu\nu}^{(T)} &= \zeta^{-1} \langle \partial_\mu \hat{T} \partial_\nu \hat{T} \rangle, \\ g_{\mu\nu}^{(C)}(x) &= \beta_G V_\xi \int d^4y K(x-y) \partial_\mu^{(x)} \partial_\nu^{(x)} \ln C(\Psi; x, y), \end{aligned} \quad (4.4)$$

where $\beta_G = \frac{1}{4\pi G}$ (see Eq. (4.38)). In the geometric regime where the metric is well-defined, $C(\Psi; x, y) \geq C_{\min} > 0$ throughout the domain of interest; the logarithm is thus well-defined.

Eigentime contribution (mollified; smooth continuum limit).

$$g_{\mu\nu,\varepsilon}^{(E)}(x) = \frac{V_\xi}{N} \sum_{i=1}^N \eta_{\mu\nu} w_i K_\varepsilon(x - x_i), \quad \lim_{\substack{N \rightarrow \infty \\ \varepsilon \rightarrow 0}} g_{\mu\nu,\varepsilon}^{(E)} = g_{\mu\nu}^{(E)} \text{ (smooth)}. \quad (4.5)$$

Weights. We assume bounded weights with $\sup_i |w_i| = \mathcal{O}(1)$ and normalization $\sum_i w_i = \mathcal{O}(N)$, consistent with the coarse-grained estimator.

Seed inertial structure. The tensor $\eta_{\mu\nu}$ in $g^{(E)}$ is the local inertial seed (Lorentz signature) on the pre-geometric label space; the event mesh then dresses it into a smooth, macroscopic background.

Derivatives. All ∂_μ are taken with respect to the Minkowski label coordinates. In the emergent geometric regime they may be covariantized $\partial_\mu \rightarrow \nabla_\mu$ with respect to $g_{\mu\nu}$, with differences suppressed on coarse-graining windows $L \gg \xi$.

Emergent metric (concise statement).

$$g_{\mu\nu}(x) = g_{\mu\nu}^{(T)}(x) + g_{\mu\nu}^{(C)}(x) + g_{\mu\nu}^{(E)}(x) \quad (4.6)$$

Theorem 4.1 (Uniqueness). *Under the constraints Emergence, Physicality and Dynamic Consistency, the decomposition (4.6) is unique among functionals built from the QFTT–WESH primitives \hat{T} , $C(\Psi; x, y)$ and the eigentime substrate $\{x_i\}$.*

Sketch (metric decomposition uniqueness). With gradient alignment $\partial_\mu \tau = k \partial_\mu \Phi$ (Eq. (4.2)) and the cancellation matching (4.18), the $(\partial\Phi)^2$ terms in $T_{\mu\nu}^{(T)}$ cancel those in the nonlocal sector at continuum, leaving Einstein with matter up to $\mathcal{O}(1/N)$ (Eqs. (4.11)–(4.21)). A formal proof of this uniqueness theorem is given in Sec. 5.4.

Example 1 (CPT as an atemporal symmetry). *Let \mathcal{G}_{CPT} act on observables as the antiunitary CPT transformation. Since $\mathcal{D}[\hat{T}^2(x)]$ and $\mathcal{D}[L_{xy}]$ are CPT-even (cf. Eqs. (1.18), (1.24)), one has $\mathcal{G}_{\text{CPT}} \circ \Phi_{s \rightarrow s'} = \Phi_{s \rightarrow s'} \circ \mathcal{G}_{\text{CPT}}$ for the CP-TP maps generated by Eq. (1.15) with frozen coefficients on each micro-interval. Therefore, CPT parity is exactly preserved along s : $\frac{d}{ds} \langle \hat{\Pi}_{\text{CPT}} \rangle = 0$. Via $dt/ds = \Gamma[\Psi]$ (Eq. (1.33)), this implies preservation in t as well, up to $\mathcal{O}(1/N)$ corrections when feedback is restored.*

4.3 Connection induced by $\nabla\Phi$ and linear curvature

To determine the dynamics, we examine how the emergent geometry responds to the entanglement potential Φ . Since Φ is a nonlocal entanglement potential, the curvature tensor arises as a linear response to its gradients.

In the IR regime ($L \gg \xi$) and for $C \geq C_{\min} > 0$, the functional $\ln C$ admits a controlled derivative expansion; the potential Φ then provides the closed nonlocal variable controlling the leading curvature response.

Linearized Ricci response to the entanglement potential.

Let λ_1 and λ_2 denote the effective IR response coefficients characterizing the non-local entanglement backreaction (see $g^{(C)}$ in Eq. (4.4)). At linear order in the entanglement potential Φ the curvature response can be written as

$$\delta R_{\mu\nu} = (\lambda_1 + 3\lambda_2) (\nabla_\mu \nabla_\nu \Phi - g_{\mu\nu} \square \Phi) + \mathcal{O}(\Phi^2). \quad (4.7)$$

Coefficient matching, yielding GR normalization.

$$\frac{k^2}{4\pi G} = \lambda_1 + 3\lambda_2. \quad (4.8)$$

4.4 Effective action and variation

The field equations are derived from a variational principle. In the stationary regime, the alignment conditions can be expressed as Euler–Lagrange equations of an effective action $S_{\text{eff}}[g, \Psi]$. By IR closure at ≤ 2 derivatives, S_{eff} reduces to the Einstein–Hilbert form plus matter and WESH-sector terms.

Effective action: EH + matter + WESH sector terms.

$$S_{\text{eff}}[g, \Psi] = \frac{1}{16\pi G} \int d^4x \sqrt{-g} (R - 2\Lambda) + S_{\text{mat}}[\Psi, g] + S_T[g^{(T)}] + S_C[g^{(C)}] + S_E[g^{(E)}]. \quad (4.9)$$

Field equations from variation of S_{eff} .

$$G_{\mu\nu} + \Lambda g_{\mu\nu} = 8\pi G \left(T_{\mu\nu}^{(m)} + T_{\mu\nu}^{(T)} + T_{\mu\nu}^{(nl)} \right). \quad (4.10)$$

Stress energy of the time sector.

$$T_{\mu\nu}^{(T)} = \zeta^{-1} \left(\langle \partial_\mu \hat{T} \partial_\nu \hat{T} \rangle - \tfrac{1}{2} g_{\mu\nu} \langle \partial_\lambda \hat{T} \partial^\lambda \hat{T} \rangle \right). \quad (4.11)$$

Nonlocal stress from entanglement and eigentime sectors.

$$T_{\mu\nu}^{(nl)} = -\frac{2}{\sqrt{-g}} \frac{\delta}{\delta g^{\mu\nu}} \left[S_C[g^{(C)}] + S_E[g^{(E)}] \right]. \quad (4.12)$$

Lemma 4.2 (WESH–Noether (field form), continuity and closure). *With the finite-range Yukawa mediator K and the normalized Rényi-2 gate $C \in [0, 1]$, the entanglement current reads*

$$J^\mu(x) = \int d^4y K(x-y) C(\Psi; x, y) \hat{I}^\mu(x, y), \quad (4.13)$$

where the bilocal information-flow operator $\hat{I}^\mu(x, y)$ satisfies

$$\hat{I}^\mu(x, y) = -\hat{I}^\mu(y, x), \quad \partial_\mu^{(x)} \hat{I}^\mu(x, y) = \delta^{(4)}(x-y) \hat{S}(x),$$

with $\hat{S}(x)$ a local source operator (neutral in the mean). Taking expectations one obtains the continuity law with neutral source:

$$\partial_\mu \langle J^\mu(x) \rangle = \langle \hat{S}(x) \rangle, \quad \int d^4x \langle \hat{S}(x) \rangle = 0. \quad (4.14)$$

Since $K(x-y)$ (and $\gamma(x, y)$) has finite range $\sim \xi$, coarse graining over any window $L \gg \xi$ yields

$$\nabla_\mu \langle J^\mu \rangle \approx 0 \quad (L \gg \xi), \quad (4.15)$$

consistent with the $\mathcal{O}(1/N)$ control of global sources used in Sec. 5.2.

4.5 Hidden-sector cancellation and the emergent Einstein equations

With the effective action framework and the metric decomposition $g_{\mu\nu} = g_{\mu\nu}^{(T)} + g_{\mu\nu}^{(C)} + g_{\mu\nu}^{(E)}$ in place, we turn to the dynamical consequence of WESH at the level of the field equations: the cancellation of the hidden-sector stresses $T_{\mu\nu}^{(T)}$ and $T_{\mu\nu}^{(nl)}$. This cancellation is not assumed but follows from three ingredients:

- (i) **Stationary gradient alignment** $\partial_\mu \tau = k \partial_\mu \Phi$,
- (ii) **WESH–Noether continuity (neutral source)** (Lemma 4.2, Eq. (4.14)),

- (iii) **Cancellation matching** $\frac{k^2}{\zeta} = \lambda_1 + 3\lambda_2$ (Eq. (4.18)).

This leads to Einstein's equations with matter only, up to controlled $\mathcal{O}(1/N)$ corrections.

Linear response of $T^{(nl)}$ and dominant structure. For IR kernels and the normalizations introduced in Sec. 1, the variation of $S_C + S_E$ gives

$$T_{\mu\nu}^{(nl)}(x) = - \int d^4y K(x-y) \nabla_\mu \nabla_\nu \ln C(\Psi; x, y) + (\text{lower-order covariant terms}). \quad (4.16)$$

IR tensorial closure. Finite-range Markov locality (kernel support $\sim \xi$) ensures that on coarse-grained windows $L \gg \xi$ the entanglement functional admits a local derivative expansion in Φ . Under stationary alignment, diffeomorphism invariance and the ≤ 2 -derivative truncation then force the dominant contribution of $T_{\mu\nu}^{(nl)}$ into the universal scalar-kinetic form quadratic in first derivatives of Φ (Part II, Lemma 5.5, Eq. (5.5)); subleading terms are suppressed by ξ/L .

Key cancellation mechanism. Under the stationary gradient alignment

$$\partial_\alpha \hat{T} = k \partial_\alpha \Phi, \quad \Phi(x) = \int d^4y K(x-y) C(\Psi; x, y), \quad (4.17)$$

the leading quadratic contributions are

$$T_{\mu\nu}^{(T)} \sim \frac{k^2}{\zeta} \partial_\mu \Phi \partial_\nu \Phi + \dots, \quad T_{\mu\nu}^{(nl)} \sim -(\lambda_1 + 3\lambda_2) \partial_\mu \Phi \partial_\nu \Phi + \dots.$$

The unique WESH *cancellation matching* condition

$$\frac{k^2}{\zeta} = \lambda_1 + 3\lambda_2 \quad (4.18)$$

ensures exact cancellation of the $(\partial\Phi)^2$ terms at continuum.

Theorem 4.2 (Hidden-sector cancellation yields Einstein equations). *Assume stationarity with gradient alignment (4.2), the cancellation matching (4.18), and the self-consistency matching for the local rate (Eq. (A.5)). Then:*

- (i) *In the continuum limit ($N \rightarrow \infty$),*

$$T_{\mu\nu}^{(T)} + T_{\mu\nu}^{(nl)} = 0. \quad (4.19)$$

(ii) At finite N , the residual satisfies

$$\| T_{\mu\nu}^{(T)} + T_{\mu\nu}^{(nl)} \|_{L^\infty(B_L)} = \mathcal{O}(1/N) \quad (L \gg \xi), \quad (4.20)$$

consistently with the graph-to-manifold convergence bounds (Eqs. (4.31)–(4.32)).

(iii) Consequently, the emergent field equations are

$$G_{\mu\nu} + \Lambda g_{\mu\nu} = 8\pi G T_{\mu\nu}^{(m)} + \mathcal{O}(1/N). \quad (4.21)$$

Physical interpretation. The time-field stress $T_{\mu\nu}^{(T)}$ sources curvature, while the entanglement backreaction $T_{\mu\nu}^{(nl)}$ provides the precise counter-stress required by Wheeler–DeWitt consistency. This cancellation is *not* a fine-tuning: it follows uniquely from the WESH bootstrap, gradient alignment, and the cancellation matching (4.18).

Link to matter conservation. The cancellation (4.19) ensures that the full field equations reduce to Einstein’s equations with matter stress only. Matter conservation follows from the contracted Bianchi identity (see below for the detailed derivation).

Dimensional consistency. We work in the dimensionless normalization used throughout QFTT–WESH (natural units $\hbar = c = 1$, with lengths expressed in units of the microscopic scale $\xi \simeq L_P$). With this convention the matchings (4.18) and (4.8) are dimensionally consistent, and at the GR fixed point they identify the time-sector normalization as $\zeta = 4\pi G$. A complete unit-restoration (including the role of V_ξ and ξ -scaling) is given in Appendix J.

4.6 Bianchi Identity and Matter Conservation

The geometric consistency of the emergent Einstein equations requires the total stress-energy tensor to be covariantly conserved. In the stationary regime where the metric is well-defined, the contracted Bianchi identity enforces this constraint.

Total conservation from Bianchi.

With $G_{\mu\nu} + \Lambda g_{\mu\nu} = 8\pi G T_{\text{tot}}^{\mu\nu}$ and

$$T_{\text{tot}}^{\mu\nu} = T^{(m)\mu\nu} + T^{(T)\mu\nu} + T^{(nl)\mu\nu},$$

the identity $\nabla_\mu G^{\mu\nu} \equiv 0$ implies

$$\nabla_\mu T_{\text{tot}}^{\mu\nu} = \nabla_\mu \left(T^{(m)\mu\nu} + T^{(T)\mu\nu} + T^{(nl)\mu\nu} \right) = 0. \quad (4.22)$$

Emergence of matter conservation.

At the stationary point, the hidden-sector stresses cancel to leading order (Eqs. (4.19)–(4.20)):

$$\nabla_\mu \left(T^{(T)\mu\nu} + T^{(nl)\mu\nu} \right) = \mathcal{O}(1/N). \quad (4.23)$$

Substituting into (4.22) isolates the visible sector:

$$\nabla_\mu T^{(m)\mu\nu} = \mathcal{O}(1/N), \quad (4.24)$$

recovering standard matter conservation and geodesic motion in the continuum limit.

4.7 Λ as entanglement IR imprint

IR status: the unique zero-derivative coupling.

By IR uniqueness at ≤ 2 derivatives, the coarse-grained gravitational sector closes on the Einstein–Hilbert class. The only diffeomorphism-invariant contribution at *zero derivatives* is the volume operator, whose coefficient defines the effective cosmological constant:

$$S_{\text{eff}}^{\text{IR}}[g] \supset \frac{1}{16\pi G} \int d^4x \sqrt{-g} \left(-2\Lambda_{\text{eff}} \right). \quad (4.25)$$

Dynamical origin: intrinsic shot noise.

While the hidden-sector cancellation constrains the gradient terms (the tensor sector), it does not eliminate the global scalar residue of the GKSL process. Since eigentime production is a stochastic counting process, the vacuum term acquires an *irreducible shot-noise width* on any finite four-volume V_4 . Consistent with the Central Limit (martingale) scaling derived in Appendix J, the typical amplitude is:

$$\delta\Lambda_{\text{typ}}(V_4) \sim \frac{\alpha_\Lambda}{\sqrt{V_4}}, \quad \alpha_\Lambda = \mathcal{O}(1), \quad (4.26)$$

yielding the cosmological scaling $\delta\Lambda_{\text{typ}} \sim H^2$ for $V_4 \sim H^{-4}$. This estimate concerns the typical fluctuation amplitude; the instantaneous sign remains stochastic.

4.8 Linearized limit and Newtonian recovery

Following the hidden-sector cancellation (Theorem 4.2), the visible matter sector remains as the sole macroscopic source at $\mathcal{O}(1/N)$. We now verify that this residual dynamics correctly recovers standard General Relativity in the weak-field regime (here we temporarily restore factors of c for clarity).

Linearized Einstein in Lorentz gauge.

$$g_{\mu\nu} = \eta_{\mu\nu} + h_{\mu\nu}, \quad \bar{h}_{\mu\nu} = h_{\mu\nu} - \frac{1}{2}\eta_{\mu\nu}h, \quad \partial^\mu \bar{h}_{\mu\nu} = 0 \Rightarrow \square \bar{h}_{\mu\nu} = -16\pi G T_{\mu\nu}^{(m)}. \quad (4.27)$$

Newtonian limit and Poisson equation.

Here ρ_m denotes the nonrelativistic mass density.

$$\text{Newtonian: } \nabla^2 \phi_N = 4\pi G \rho_m, \quad \bar{h}_{00} = -\frac{4\phi_N}{c^2}. \quad (4.28)$$

4.9 Example (vacuum, spherically symmetric): Schwarzschild

Since the emergent equations reduce to the standard GR vacuum form (and to $R_{\mu\nu} = 0$ when Λ_{eff} is neglected on the scales considered), the theory admits the usual vacuum solutions of General Relativity.

Schwarzschild line element (vacuum).

$$ds^2 = -\left(1 - \frac{2GM}{rc^2}\right)c^2 dt^2 + \left(1 - \frac{2GM}{rc^2}\right)^{-1} dr^2 + r^2 d\Omega^2, \quad R_{\mu\nu} = 0. \quad (4.29)$$

Kretschmann scalar.

$$\text{Kretschmann: } R_{\mu\nu\rho\sigma}R^{\mu\nu\rho\sigma} = \frac{48 G^2 M^2}{c^4 r^6}. \quad (4.30)$$

4.10 Eigentime substrate: convergence to continuum

Discrete-to-continuum bounds for $g^{(E)}$.

Assumptions (A1)–(A3) for the convergence bound $\mathcal{O}(N^{-1/4})$. (A1) Local correlation with length ξ ; (A2) coarse-grained sampling of eigentimes within causal diamonds; (A3) bounded curvature and mollifier with compact support. Under (A1)–(A3) the kernel estimator achieves $\|g_{\mu\nu,\varepsilon}^{(E)} - g_{\mu\nu}^{(E)}\|_\infty = \mathcal{O}(N^{-1/4})$.

Let $n_{\text{Eig}} := N/V_4$ denote the eigentime event density, where V_4 is the four-volume of the coarse-graining window $L \gg \xi$; in the quasi-uniform regime $n_{\text{Eig}} \sim \bar{\lambda}_{\text{Eig}}$ (see Proposition below).

$$\ell_{\text{Eig}} \sim n_{\text{Eig}}^{-1/4}, \quad \|g_{\mu\nu,\varepsilon}^{(E)} - g_{\mu\nu}^{(E)}\|_\infty = \mathcal{O}(N^{-1/4}). \quad (4.31)$$

Proposition 4.1 (smoothing and optimal convergence).

Let

$$\lambda_{\text{Eig}}(x) = \nu \text{Tr}[\rho \hat{T}^4(x)] + \iint d^4y \gamma(x, y) C(\Psi; x, y) \text{Tr}[\rho (\hat{T}^2(x) - \hat{T}^2(y))^2],$$

be the hazard rate governing eigentime events (so that it contributes to $dt/ds = \Gamma[\Psi(s)]$). For any ball B_L with $L \gg \xi$ there exists a constant $\kappa = \mathcal{O}(1)$, depending only on $\|\gamma\|_{L^1(B_L)}$, the variance $\text{Var}_\rho(\hat{T}^2)$, and the geometry of B_L , such that

$$\frac{\sup_{B_L} \lambda_{\text{Eig}}}{\inf_{B_L} \lambda_{\text{Eig}}} \leq 1 + \kappa e^{-L/\xi}.$$

Hence eigentime events form a quasi-uniform inhomogeneous-Poisson mesh on scales $\gg \xi$, with characteristic spacing $\ell_{\text{Eig}} \sim \lambda_{\text{Eig}}^{-1/4}$ in four dimensions and fill distance $h_N = \mathcal{O}(N^{-1/4})$ for N events in B_L .

With the kernel regularization of Eq. (4.5), the relevant fields entering the continuum limit are Lipschitz on B_L ; therefore the sampling error obeys

$$\|\mathcal{F}_{\text{disc}} - \mathcal{F}_{\text{cont}}\|_{L^\infty(B_L)} \leq \text{Lip}(\mathcal{F}) h_N = \mathcal{O}(N^{-1/4}),$$

which yields the convergence rate $\mathcal{O}(N^{-1/4})$ in Eq. (4.31). (Without smoothing one only obtains $\mathcal{O}(N^{-1/4+\varepsilon})$ for any $\varepsilon > 0$.)

Box 5: Assumptions leading to $\mathcal{O}(N^{-1/4})$ convergence

(A1) Short-range clustering: the kernel with correlation length ξ enforces the rapid decay of connected correlators beyond $\mathcal{O}(\xi)$.

(A2) Quasi-uniform sampling: eigentime events provide a mesh with bounded hole size and aspect ratio in the emergent 3+1 geometry.

(A3) Regular mollifier: the kernel estimator uses a C^2 mollifier with bounded moments and curvature-controlled bandwidth.

Under (A1)–(A3) the graph-to-manifold estimator achieves $\|g_{\mu\nu,\varepsilon}^{(E)} - g_{\mu\nu}^{(E)}\|_\infty = \mathcal{O}(N^{-1/4})$, faster than i.i.d. kernel rates due to correlated sampling induced by WESH dynamics.

Curvature convergence and Hausdorff dimension.

$$\|R_{\mu\nu}^{(\text{disc})} - R_{\mu\nu}\| = \mathcal{O}(\ell_{\text{Eig}}^2), \quad \lim_{N \rightarrow \infty} d_H(\mathcal{G}_N) = 4. \quad (4.32)$$

Remark 4.1 (Scaling of the finite- N hidden-sector residual). *The hidden-sector cancellation $T_{\mu\nu}^{(T)} + T_{\mu\nu}^{(\text{nl})} = 0$ holds exactly in the continuum limit $N \rightarrow \infty$. At finite N , potential sources of residual error are:*

- (i) geometric discretization errors, bounded by $O(N^{-1/2})$ at the level of curvature (Eq. (4.32));
- (ii) finite- N corrections to the variational alignment and matching, controlled by the N^{-2} prefactor of the bilocal WESH channel.

Crucially, the errors in (i) enter $T_{\mu\nu}^{(T)}$ and $T_{\mu\nu}^{(\text{nl})}$ through the same functional dependence on Φ and its derivatives; since the cancellation matching (4.18) (and, at

the GR fixed point, (4.8)) is algebraic and N -independent, these geometric errors cancel at leading order in the sum $T^{(T)} + T^{(\text{nl})}$, leaving only alignment deviations as the dominant finite- N residual. On coarse-grained windows B_L with $L \gg \xi$, spatial averaging further suppresses local fluctuations. The bound

$$\| T_{\mu\nu}^{(T)} + T_{\mu\nu}^{(\text{nl})} \|_{B_L} = O(1/N) \quad (4.33)$$

is therefore controlled by the N^{-2} dissipative scaling and is consistent with the collective-stability law $\tau_{\text{coh}}(N) \propto N^2$.

4.11 Markovianity, causality, no-signaling

The finite range ξ of the WESH kernel ensures that the dynamics is effectively Markovian on coarse-grained timescales and respects relativistic causality in the emergent spacetime.

Finite memory time from ξ ; Markovian regime.

$$\tau_{\text{corr}} \sim \xi/c \Rightarrow \text{finite memory; Markov for } \Delta t \gg \tau_{\text{corr}}. \quad (4.34)$$

No-signaling. The causal structure of the WESH kernel ensures

$$(x - y)^2 > 0 \Rightarrow \gamma(x, y) K(x - y) = 0 \quad (\text{exponential-causal; no-signaling}). \quad (4.35)$$

4.12 Collective stability: N^2 scaling

A key prediction of the WESH channel is the suppression of decoherence rates for large entangled systems. The quadratic scaling $\tau_{\text{coh}} \sim N^2$ reflects the collective protection mechanism underlying the semiclassical limit.

Quadratic stability law for coherence lifetime.

$$\gamma(N) \sim \frac{1}{N^2}, \quad \tau_{\text{coh}}(N) \sim N^2. \quad (4.36)$$

collision model: $\gamma \propto N^{-2}$.

$$\text{Collision model: } \theta_i = \sqrt{\kappa dt} N^{-1} w_i, \quad \sum_i w_i^2 = 1 \Rightarrow \gamma \propto N^{-2}. \quad (4.37)$$

4.13 Normalizations and matching to GR

The free coefficients in the metric decomposition are fixed by consistency with the GR normalization of Newton's constant.

β normalization and explicit $g^{(C)}$.

$$\beta_G = \frac{1}{4\pi G}, \quad g_{\mu\nu}^{(C)}(x) = \beta_G V_\xi \int d^4y K(x-y) \partial_\mu^{(x)} \partial_\nu^{(x)} \ln C(\Psi; x, y). \quad (4.38)$$

ζ normalization from GR matching.

The time-sector normalization is fixed at the GR fixed point by the cancellation matching (4.18) together with the GR response normalization (4.8), yielding $\zeta = 4\pi G$. The Minkowski vacuum corresponds to the state where the composite metric reduces to $\eta_{\mu\nu}$ in the absence of sources:

$$\zeta = 4\pi G, \quad g_{\mu\nu}^{(T)} = \zeta^{-1} \langle \partial_\mu \hat{T} \partial_\nu \hat{T} \rangle. \quad (4.39)$$

Parameter relations (k, λ) and alignment.

$$\frac{k^2}{4\pi G} = \lambda_1 + 3\lambda_2, \quad \partial_\mu \tau = k \partial_\mu \Phi$$

(4.40)

Box 6: Two roles of G — microscopic scale vs. macroscopic coupling

The symbol G enters the theory in two *a priori* distinct ways:

- **Microscopic scale anchor.** In Eqs. (1.38), (A.3), G appears only through Planck units, $L_P = \sqrt{\hbar G/c^3}$ and $t_P = \sqrt{\hbar G/c^5}$, which fix the correlation length ξ and the kernel scale γ_0 . Here, G acts as a *dimensional* parameter setting the discreteness scale, not a classical coupling.
- **Macroscopic gravitational coupling.** In Eqs. (4.8), (4.21), (4.38), G is the Newton constant in Einstein's equations, with $\beta_G = 1/(4\pi G)$ fixing the normalization of the entanglement-metric sector.

The theory does *not* assume these two appearances coincide. Rather, consistency of the hidden-sector cancellation matching (Eq. (4.18)) with the GR normalization (Eq. (4.8)) *identifies* them as a consequence of internal consistency between microphysics (eigentimes, entanglement) and macro-physics (metric, curvature). Consistency via the cancellation matching (4.18) *enforces* a relation between the microscopic correlation length (set by L_P through G) and the macroscopic coupling measured in Einstein's equations. The identification emerges from hidden-sector cancellation, not as an external input.

4.14 Summary of the emergence scheme

Metric decomposition ($T + C + E$).

$$g_{\mu\nu} = g_{\mu\nu}^{(T)} + g_{\mu\nu}^{(C)} + g_{\mu\nu}^{(E)} \quad (4.41)$$

Einstein equations from hidden-sector cancellation.

$$T_{\mu\nu}^{(T)} + T_{\mu\nu}^{(nl)} = 0 \implies G_{\mu\nu} + \Lambda g_{\mu\nu} = 8\pi G T_{\mu\nu}^{(m)} + \mathcal{O}(1/N) \quad (4.42)$$

Conservation, Λ , and Planck-scale parameters.

$$\boxed{\nabla_\mu T^{(m)\mu\nu} = \mathcal{O}(1/N), \quad \Lambda_{\text{eff}} \text{ (IR parameter; see App. J)}, \quad \xi \simeq L_P, \gamma_0 \simeq t_P^{-1}} \quad (4.43)$$

5 General Relativity, part II: Dynamic derivation

Overview.

This section derives Einstein–Hilbert gravity *dynamically* from the WESH evolution in a fully covariant Tomonaga–Schwinger–Lindblad (TSL) representation that preserves locality, CP/TP, and no-signaling. A pre-geometric condition (operator level path independence of global charges; App. H) constrains the generator. On this basis we establish three results.

(1) Variational fixed point (alignment). There exists a Lyapunov monotone for the WESH flow with a unique globally attractive fixed point characterized by the gradient-alignment relation

$$\partial_\mu \tau = k \partial_\mu \Phi,$$

with k fixed by internal consistency (Eq. (4.8)). Existence, uniqueness and global attractivity follow from mixing/primitivity (reversible spectral gap) in the KMS geometry (Thm. 5.2, App. D).

(2) Hidden-sector cancellation \Rightarrow Einstein equations. At the fixed point the time-sector and nonlocal stresses cancel as a tensor identity,

$$T_{\mu\nu}^{(T)} + T_{\mu\nu}^{(\text{nl})} = 0 \quad (\text{Eq. (4.19)}),$$

yielding the matter-only field equations up to controlled corrections,

$$G_{\mu\nu} + \Lambda g_{\mu\nu} = 8\pi G T_{\mu\nu}^{(m)} + \mathcal{O}(1/N) \quad (\text{Eq. (4.21)}).$$

(3) IR uniqueness of the gravitational sector. Among diffeomorphism-invariant local completions compatible with CP/Markov and causal support and truncated at second derivative order, the gravitational action is uniquely Einstein–Hilbert with Λ . This identification is consistent with the normalization fixed by Eq. (4.8).

The section first introduces the TSL packaging, then establishes the alignment fixed point, and uses it to derive the hidden-sector cancellation and IR uniqueness, closing the $\text{WDW} \rightarrow \text{WESH} \rightarrow (s \rightarrow t)$ bootstrap in a covariant route to GR. In Sec. 5.7 we also reformulate the cancellation as a *variational generalized Nash equilibrium* ($v\text{-GNE}$). In that formulation, the standard equivalence between generalized Nash problems and variational inequalities (Facchinei & Pang, 2003) appears as a strongly monotone VI/KKT stationarity condition on the feasible set \mathcal{Z} , whose unique solution reproduces Einstein's equations.

Notation consistency. We use the GKSL convention $\mathcal{D}[O]\rho = O\rho O^\dagger - \frac{1}{2}\{O^\dagger O, \rho\}$ as in Sec. 1.

5.1 Atemporal symmetry on CP–TP evolution and emergent conservation

Definition 5.1 (Atemporal symmetry of the evolution). *Let $\{\Phi_{s \rightarrow s'}\}_{s \leq s'}$ be the positivity- and trace-preserving (stepwise CPTP) family solving the (possibly nonlinear) WESH master equation. A $*$ -automorphism $\mathcal{G} : \mathfrak{A} \rightarrow \mathfrak{A}$ is an atemporal symmetry if $\mathcal{G} \circ \Phi_{s \rightarrow s'} = \Phi_{s \rightarrow s'} \circ \mathcal{G}$ for all $s \leq s'$.*

Theorem 5.1 (Extended WESH–Noether atemporal (map-based)). *If \mathcal{G} is an atemporal symmetry, the associated charge $\hat{Q}_\mathcal{G}$ (in the GNS representation) obeys*

$$\frac{d}{ds} \langle \hat{Q}_\mathcal{G} \rangle = 0, \quad \frac{d}{dt} \langle \hat{Q}_\mathcal{G} \rangle = 0, \quad \frac{dt}{ds} = \Gamma[\Psi] > 0. \quad (5.1)$$

Discrete symmetries (e.g. CPT-evenness of the dissipator) produce exact s -conservations (hence exact t -conservations when $dt/ds = \Gamma > 0$); deformed continuous symmetries (scale/rotations tied to N^{-2} weights and support) are only effective at finite N and yield drifts suppressed as $\mathcal{O}(1/N)$ in the emergent description.

Example 2 (CPT as atemporal symmetry). *Since $\mathcal{D}[\hat{T}^2(x)]$ and $L_{xy} = \hat{T}^2(x) - \hat{T}^2(y)$ are CPT-even, the CPT transform \mathcal{G}_{CPT} satisfies $\mathcal{G}_{\text{CPT}} \circ \Phi_{s \rightarrow s'} = \Phi_{s \rightarrow s'} \circ \mathcal{G}_{\text{CPT}}$, hence $d\langle \hat{Q}_{\text{CPT}} \rangle/ds = 0$ and $d\langle \hat{Q}_{\text{CPT}} \rangle/dt = 0$.*

5.2 Covariant packaging: Tomonaga–Schwinger–Lindblad and IR Ward–Takahashi/Bianchi

Lemma 5.1 (Tomonaga–Schwinger–Lindblad evolution and WESH current).

Define a Tomonaga–Schwinger–Lindblad (TSL) evolution for a foliation $\{\Sigma_\Lambda\}$ (label Λ is a foliation parameter, not the cosmological constant) with unit normal n^μ and induced determinant h by

$$\frac{d\rho}{d\Lambda} = \mathcal{L}[\rho] = \mathcal{L}_{\text{unitary}}[\rho] + \int_{\Sigma_\Lambda} d^3x \sqrt{h} n^\mu J_\mu[\rho],$$

with the WESH-compatible current (with $\nu > 0$)

$$J_\mu[\rho](x) = -\nu \mathcal{D}[\hat{T}^2(x)] \rho n_\mu(x) - \int d^4y \gamma(x, y) C(\Psi; x, y) \mathcal{D}[L_{xy}] \rho n_\mu(x).$$

Here ν and $\gamma(x, y)$ are understood as rate densities per unit proper time and per unit three-volume on the leaf Σ_Λ , so that the contraction $n^\mu J_\mu$ defines a proper current density and the integral over Σ_Λ in the TSL generator is dimensionally consistent.

Let $S(x) := \nabla_\mu J^\mu(x)$. On coarse-grained windows $L \gg \xi$ one has $\nabla_\mu \langle J^\mu \rangle \approx 0$. This follows from the WESH–Noether continuity law (G.1), which guarantees global neutrality of the source term $\int d^4x \langle S(x) \rangle = 0$, combined with the finite-range (exponential-causal) support of $\gamma(x, y)$. This TSL evolution reproduces the WESH dissipator in the IR, is foliation-independent, and preserves no-signaling.

Bilocal covariance. The bilocal term is weighted by the normal at the insertion point x , so $J_\mu(x)$ is manifestly leaf-local. Since $\gamma(x, y)$ has finite range ξ , one has $n_\mu(y) = n_\mu(x) + \mathcal{O}(\xi/L)$ on coarse-graining windows $L \gg \xi$; thus the difference between a symmetric prescription and the leaf-local choice is IR-suppressed, while $\nabla_\mu \langle J^\mu \rangle \approx 0$ remains the correct large-scale statement.

$$\mathcal{K}(t-t') = 0 \quad \text{for } |t-t'| > \tau_{\text{corr}} \sim \xi/c, \quad \|K_\xi\|_{L^1(\text{causal LC})} = O(V_\xi) = O(\xi^4). \quad (5.2)$$

(The L^1 norm refers to the unnormalized kernel $K_\xi^{\text{unnorm}} = V_\xi K_\xi$; see App. A. Used in Lemma 5.3 as the finite-memory hypothesis.)

Proposition 5.1 (IR Ward–Takahashi \Rightarrow Bianchi). *If the coarse-grained TSL is diffeomorphism-invariant on scales $L \gg \xi$ (i.e. invariant under normal deformations of Σ_Λ up to boundary terms), then the associated generating functional is diffeomorphism-invariant and the Ward–Takahashi identities imply*

$$\nabla_\mu \langle T_{\text{tot}}^{\mu\nu} \rangle = 0$$

in the IR (cf. Eqs. (??)–(4.24)).

Definition 5.2 (Total stress tensor from the TSL-effective action). *Let $S_{\text{eff}}[\rho; g]$ be the coarse-grained effective action that reproduces the TSL generator on a foliation $\{\Sigma_\Lambda\}$, in the sense that its first functional variation in the metric yields the local/bilocal GKSL currents when pulled back to each leaf. We define the total stress tensor by*

$$T_{\text{tot}}^{\mu\nu}[\rho] := \frac{2}{\sqrt{-g}} \frac{\delta S_{\text{eff}}[\rho; g]}{\delta g_{\mu\nu}}. \quad (5.3)$$

Remark 5.1 (Foliation covariance and Noether content). *Under WESH–Noether and TSL covariance, the definition (5.3) is foliation independent up to boundary terms: normal deformations of Σ_Λ generate the same local currents that appear in the TSL evolution, so that Ward–Takahashi identities for diffeomorphisms imply the Bianchi-type closure $\nabla_\mu \langle T_{\text{tot}}^{\mu\nu} \rangle = 0$ on scales $L \gg \xi$ (Prop. 5.1). Thus $T_{\text{tot}}^{\mu\nu}$ is the Noether current of normal deformations encoded variationally in S_{eff} , not an ad hoc object.*

5.3 Alignment as a unique stationary fixed point of the WESH flow

Definition 5.3 (Regularized WESH monotone (dimensionless form)). *Define*

$$\mathcal{M}[\rho] = \int d^4x \left(\langle \tilde{T}^4(x) \rangle - \langle \tilde{T}^2(x) \rangle^2 \right) + \iint d^4x d^4y \gamma(x, y) C(\Psi; x, y) \langle L_{xy}^2 \rangle,$$

and the technical regularization

$$\mathcal{M}_\epsilon[\rho] = \mathcal{M}[\rho] + \epsilon S_2[\rho], \quad S_2[\rho] := \text{Tr } \rho^2, \quad \epsilon > 0.$$

Here $\tilde{T} = \hat{T}/\tau_s$ and $L_{xy} = \tilde{T}^2(x) - \tilde{T}^2(y)$.

Remark 5.2. All terms are dimensionless by construction (via $\tilde{T} = \hat{T}/\tau_s$). This dimensionless normalization matches Appendix D (see Def. 5.3). In dissipative many-body dynamics, Lyapunov functionals arise naturally as generalized free energies driving relaxation toward equilibrium (Spohn, 1991). Here \mathcal{M}_ϵ can be interpreted as playing that role in the WESH setting, driving the flow toward the GR fixed point.

Remark 5.3 (Gradient flow structure). The WESH dynamics admits a gradient-flow-like interpretation in quantum state space, reminiscent of the structures developed for quantum Markov semigroups with detailed balance (Carlen & Maas, 2017), where the relative entropy to the fixed point plays the role of Lyapunov functional.

Lemma 5.2 (First variation of the WESH monotone). Let \mathcal{M}_ϵ be as in Def. 5.3. Then

$$\frac{\delta \mathcal{M}_\epsilon}{\delta \tilde{T}(x)} = 4 \left(\langle \tilde{T}^3(x) \rangle - \langle \tilde{T}(x) \rangle \langle \tilde{T}^2(x) \rangle \right) + \mathcal{J}^\mu(x) \partial_\mu \tilde{T}(x) + \dots,$$

with $\mathcal{J}^\mu \propto \partial^\mu \Phi$ and $\Phi(x) = \int d^4y K(x-y) C(\Psi; x, y)$ (Eq. (4.1)). Stationarity entails $\partial_\mu \tilde{\tau} = (k/\tau_s) \partial_\mu \Phi$, hence $\partial_\mu \tau = k \partial_\mu \Phi$ (Eqs. (4.2), (4.8)).

Theorem 5.2 (Variational alignment via a WESH monotone). Statement. In the Markov window $\Delta t \gg \tau_{\text{corr}}$, the WESH flow with the regularized Lyapunov functional \mathcal{M}_ϵ admits a unique stationary point and it is characterized by the alignment

$$\partial_\mu \tau = k \partial_\mu \Phi,$$

with k fixed by Eq. (4.8). This stationary point is globally attractive. Full proof and strengthened form (monotonicity, uniqueness, global attractivity and error control) are given in Appendix D.

Uniqueness mechanism. Uniqueness and global attractivity follow from mixing/primitivity (reversible spectral gap) of the WESH semigroup in the KMS geometry on the Markov window, as established in Appendix D.

Orthogonal suppression. Decompose the gradient of the time field into components parallel and orthogonal to the entanglement potential,

$$\partial_\mu \tilde{T} = \alpha \partial_\mu \Phi + \partial_\mu \tilde{T}^\perp, \quad \partial_\mu \tilde{T}^\perp \partial^\mu \Phi = 0.$$

Mixing/primitivity (reversible spectral gap) implies exponential suppression of the orthogonal component $\partial_\mu \tilde{T}^\perp$ by the contractive WESH semigroup (Appendix D). The only stationary direction is therefore $\partial_\mu \tilde{T} \parallel \partial_\mu \Phi$, with the proportionality constant k fixed by the matching condition (4.8).

5.4 IR uniqueness at ≤ 2 derivatives (EH selection)

Noether input. We use WESH–Noether (Appendix H; pre-geometric path independence) together with the TSL covariant packaging (Lemma 5.1) as symmetry constraints for the IR selection. Combined with causality/no-signaling and the Markov window (see Lemma 5.1 and Eq. (5.2)), these constraints restrict the admissible local completion at ≤ 2 derivatives to the Einstein–Hilbert sector.

Lemma 5.3 (CP/Markov IR filter: only EH+ Λ survives in $D = 4$). *Consider a TSL-covariant Markovian evolution whose generator is GKSL with exponential-causal kernels of range ξ (Sec. 5.2). Let $\tau_{\text{corr}} \sim \xi/c$ be the memory time and suppose the finite-memory condition (5.2) holds on the wedge for the coarse-grained kernel \mathcal{K} . Then:*

- (i) *Any effective gravitational action whose linearized metric equations, about an IR background, require time derivatives of order > 2 for the metric alone either (a) can be rewritten as a second-order system at the price of introducing additional propagating fields, or (b) propagates ghost-like degrees of freedom with indefinite kinetic energy (Ostrogradsky instabilities). Case (b) is incompatible with complete positivity and with the contractive decay of the WESH Lyapunov functional \mathcal{M}_ϵ (App. F); in case (a) the extra modes are not part of the WESH gravitational sector (exhausted by \hat{T} , C and the eigentime substrate) and must instead be treated as matter. In both situations such terms cannot define the IR gravitational dynamics generated by the WESH GKSL semigroup on the metric sector.*

- (ii) In $D = 4$, among local diffeomorphism-invariant actions whose metric equations are second order and propagate only the two massless spin-2 polarizations, Lovelock's theorem reduces the admissible class to Einstein–Hilbert plus cosmological constant ($\text{EH} + \Lambda$). Curvature-squared pieces ($R^2, R_{\mu\nu}R^{\mu\nu}$, Weyl 2) enter only as radiative counterterms renormalizing couplings and/or introducing extra propagating modes as in (i), and therefore do not define the deterministic IR equations of motion under the CP/Markov WESH constraints.

Proof sketch. Generic curvature-squared corrections such as $R_{\mu\nu}R^{\mu\nu}$ or Weyl 2 yield fourth-order-in-time metric equations whose linearized spectrum contains, besides the massless graviton, a massive spin-2 mode with negative norm (the standard higher-derivative spin-2 ghost). Recasting such dynamics as a first-order system exhibits an unbounded-from-below Hamiltonian and exponentially growing solutions, incompatible with the contractivity of completely positive quantum Markov semigroups and with the monotone decay of \mathcal{M}_ϵ .

When higher derivatives are cured by introducing additional healthy auxiliary fields (as in $f(R)$ models with $f''(R) > 0$, dynamically equivalent to GR plus a scalaron), the extra propagating modes lie outside the WESH gravitational sector and are absorbed into matter. In either case, the metric equations relevant for the GKSL/TSL WESH generator must be second order and propagate only the two GR polarizations. In $D=4$ Lovelock's theorem then selects $\text{EH} + \Lambda$ as the unique local, diffeomorphism-invariant, second-order metric action. Curvature-squared pieces reduce to perturbative counterterms that renormalize couplings without altering the IR classical equations subject to the CP/Markov constraints. Note: pure conformal gravity (Weyl 2 in $D = 4$) is a paradigmatic example of case (ii); Its fourth-order Bach equations propagate a massless spin-2 ghost, so that no finite-memory GKSL representation with positive energy exists.

□

Example: $R_{\mu\nu}R^{\mu\nu}$ and a massive spin-2 ghost

Consider

$$S_g = \frac{1}{16\pi G} \int d^4x \sqrt{-g} (R + \beta R_{\mu\nu}R^{\mu\nu}), \quad \beta \neq 0.$$

Linearizing around Minkowski and decomposing into spin components shows that, besides the massless graviton, the spectrum contains a massive spin-2 excitation with negative residue in the propagator (a spin-2 ghost). The associated mode admits exponentially growing solutions for suitable initial data and an unbounded-from-below energy density. Such behaviour cannot be generated by a completely

positive, trace-preserving semigroup with finite memory, whose norm is contractive in any KMS geometry; hence this type of higher-derivative correction is excluded by Lemma 5.3.

Lemma 5.4 (Ghost instabilities vs GKSL semigroups). *Let $x(t)$ denote a linearized gravitational mode evolving under a GKSL semigroup $e^{t\mathcal{L}}$: in any KMS norm one has $\|e^{t\mathcal{L}}\| \leq 1$ for all $t \geq 0$. A mode generated by a higher-derivative ghost, with solutions containing factors $e^{+\gamma t}$ for some $\gamma > 0$, cannot be represented in this way. Therefore any metric theory whose linearized spectrum contains ghost modes (as in the $R_{\mu\nu}R^{\mu\nu}$ example above) is incompatible with the CP/Markov WESH dynamics on the gravitational sector.*

Remark 5.4 (Higher dimensions). *In $D > 4$, the Lovelock tower may contribute additional second-order terms; the same CP/Markov filter selects the Lovelock class and excludes genuine higher-time-derivative dynamics. Our derivation in $D = 4$ thus matches the standard uniqueness of EH+ Λ .*

Theorem 5.3 (EH as the unique IR covariant option under WESH constraints). *Assuming locality for $L \gg \xi$, CP–TP and complete positivity, Markovianity (Eq. (5.2)), no-signaling (Eq. (4.35)), and TSL covariance (Lemma 5.1), the only IR covariant metric functional with ≤ 2 derivatives and positive energy is the Einstein–Hilbert form (up to boundary/ Λ), with normalization*

$$\frac{k^2}{4\pi G} = \lambda_1 + 3\lambda_2 \quad (\text{Eq. (4.8)}).$$

Corollary 5.1 (IR selection at ≤ 2 derivatives). *Within the Markov window ($\tau_{\text{corr}} \sim \xi/c$) and under CP, the causal kernel and no-signaling, together with Markovianity (Eq. (5.2)), exclude any diffeomorphism-invariant local completion beyond the Einstein–Hilbert sector at ≤ 2 derivatives at leading order. In particular, R^2 , $R_{\mu\nu}R^{\mu\nu}$, and Weyl² terms either violate the Markov locality (invoke higher-derivative memory), or require fine-tuned ghost-avoidance inconsistent with the cutoff ξ .*

Corollary 5.2 (“Quantum Lovelock” under CP/Markov: exclusions and reasons). *In $D = 4$ the following are excluded under WESH constraints:*

- R^2 : for $f(R) = R + \alpha R^2$ with $f''(R) > 0$ the theory is dynamically equiv-

alent to GR plus a healthy massive scalaron ϕ with $(\square - m_\phi^2)\phi = 0$ and positive kinetic energy. In the WESH setting such an extra degree of freedom belongs to the matter sector and must be encoded in $T_{\mu\nu}^{(m)}$, not in the purely geometric IR functional singled out by the CP/Markov filter. Hence R^2 does not define an independent gravitational completion at ≤ 2 derivatives, but a scalar-matter contribution that is already accounted for in $T_{\mu\nu}^{(m)}$.

- $R_{\mu\nu}R^{\mu\nu}$: in the generic quadratic action $R + \alpha R^2 + \beta R_{\mu\nu}R^{\mu\nu}$ the $R_{\mu\nu}R^{\mu\nu}$ term produces a massive spin-2 mode with negative norm (Stelle-type ghost) and fourth-order equations of motion. This is an Ostrogradsky-unstable sector with an energy functional unbounded from below, incompatible with complete positivity and with the contractivity of the GKSL/WESH semigroup on the Markov window $\Delta t \gg \tau_{\text{corr}}$.
- Weyl²: in pure conformal gravity (Weyl² in $D = 4$) the Bach equations are fourth order and propagate additional spin-2 ghost degrees of freedom. This again realizes an Ostrogradsky-unstable spin-2 sector (a massless ghost in the conformal limit), which falls under case (ii) of Lemma 5.3 and is excluded by the CP/Markov IR filter.

Thus, the admissible class reduces to $R - 2\Lambda$ with normalization fixed by Eq. (4.8).

5.5 Quantum features and falsifiability: connection to gravitational wave squeezing

Recent analyses in the effective field theory (EFT) of gravity have highlighted that nonlinear self-interactions of the Einstein–Hilbert action can act as sources of genuinely nonclassical gravitational-wave states. In particular, Guerreiro (2025) shows that high-frequency gravitational waves propagating on weakly curved backgrounds undergo a three-wave mixing process where cubic GR self-interactions generate squeezed and entangled states, with squeezed variances below the vacuum level ($V_{\text{sq}} < 1$) and logarithmic-negativity oscillations between coupled modes. These results clarify that nonlinear general relativity can both *produce* and *detect* quantum correlations among gravitational degrees of freedom, even in the geometric-optics limit.

The QFTT–WESH framework arrives at closely related structures from the opposite direction. Rather than quantizing perturbations on a pre-given metric,

WESH begins with pre-geometric quantum correlations and reconstructs space-time through eigentime production and hidden-sector cancellation. Yet, the quantum signatures that emerge in the two approaches display notable parallels. The $\cos^2 \theta$ angular modulation that appears in WESH collective decoherence protection (Sec. 3) plays a role similar to the angular dependence of Guerreiro’s three-mode couplings, where polarization tensors mediate the redistribution of quantum fluctuations across interacting frequency bands. In both cases, the angular structure encodes how gravitational dynamics select phase-sensitive quantum correlations.

Moreover, the quadratic Hermitian dissipator $\mathcal{D}[\hat{T}^2]$ that drives eigentime localization in WESH naturally builds non-Gaussian correlations between modes. After the continuum limit, where the same composite operator contributes to the cubic Einstein–Hilbert vertex, this structure inherits exactly the ingredients required to generate squeezed and entangled states of the type identified in the EFT treatment. In other words, the microscopic WESH mechanism and the macroscopic EFT analysis isolate the same operational cause: nonlinear graviton couplings acting as parametric amplifiers.

This comparison yields a sharp falsifiability requirement. Any emergent-gravity framework claiming to reproduce general relativity in the infrared must also accommodate the quantum features generated by nonlinear gravitational dynamics, squeezing, multipartite entanglement, and state-dependent mode-coupling, as demonstrated in the EFT regime. Structurally, QFTT–WESH satisfies this requirement: its pre-geometric correlations, dissipative generator, and continuum limit contain the requisite non-Gaussianity to support such states. A full quantitative comparison, matching WESH spectral weights to Guerreiro’s squeezed-state parameters, is a natural next step.

5.6 Hidden-sector cancellation as an operator identity

Theorem 5.4 (Operator-level hidden-sector cancellation at the fixed point). *Let $\mathfrak{A}_{\text{wedge}}$ be the von Neumann algebra of the near-horizon wedge. Assume:*

- (i) *The stationary state is the unique wedge KMS state $\sigma_{\text{KMS}} \propto e^{-\beta_H H_R}$ (Sec. 6.2, Thm. 6.2), and $\mathfrak{A}_{\text{wedge}}$ is a Type III₁ factor.*
- (ii) *The WESH wedge semigroup is primitive (irreducible) and detailed-balanced with respect to σ_{KMS} (Sec. 6.2), so that the GNS vector Ω_{KMS} is cyclic and separating for $\mathfrak{A}_{\text{wedge}}$, as required by Tomita–Takesaki theory. Modular*

theory (Takesaki, 1970) provides the operator-algebraic foundation for this structure and its KMS implementation.

- (iii) *Variational alignment holds at the global attractor (Thm. 6.1 / Thm. 5.2), and the cancellation matching (4.18) is satisfied. In the geometric IR, together with (4.8) this identifies $\zeta = 4\pi G$ (i.e. $\beta_G = \zeta^{-1}$).*

Then, in the sense of quadratic forms on a common core,

$$T_{\mu\nu}^{(T)} + T_{\mu\nu}^{(\text{nl})} = 0 \quad \text{on } \mathfrak{A}_{\text{wedge}}. \quad (5.4)$$

At finite N , one has $\| T^{(T)} + T^{(\text{nl})} \| = \mathcal{O}(1/N)$ on coarse-grained windows $L \gg \xi$, hence

$$G_{\mu\nu} + \Lambda g_{\mu\nu} = 8\pi G T_{\mu\nu}^{(m)} + \mathcal{O}(1/N).$$

Proof sketch. By Sec. 6.2 the wedge KMS state is unique and the WESH semigroup is primitive/detailed-balanced; thus the GNS representation is standard and Ω_{KMS} is cyclic and separating for $\mathfrak{A}_{\text{wedge}}$. Using Thm. 6.1 (variational alignment) and the cancellation matching (4.18), one shows that for all local polynomials \mathcal{O} with support in the wedge (which generate a σ -weakly dense $*$ -subalgebra of $\mathfrak{A}_{\text{wedge}}$),

$$\langle \Omega_{\text{KMS}}, (T_{\mu\nu}^{(T)} + T_{\mu\nu}^{(\text{nl})}) \mathcal{O} \rangle = 0.$$

Cyclicity and separability then imply $(T_{\mu\nu}^{(T)} + T_{\mu\nu}^{(\text{nl})}) = 0$ as a quadratic form on a common core (Tomita–Takesaki), i.e. an operator identity on the wedge. \square

Example 3 (Cancellation of $(\partial\Phi)^2$ terms (schematic)). *In a local frame, the quadratic time-sector contribution reads $T_{00}^{(T)} \sim \zeta^{-1} (\partial_0 \hat{T})^2 = \frac{k^2}{\zeta} (\partial_0 \Phi)^2$ under alignment, while the nonlocal backreaction yields $T_{00}^{(\text{nl})} \sim -\beta_G \delta_{g^{00}}[S_{\text{ent}}] \sim -\frac{k^2}{\zeta} (\partial_0 \Phi)^2$. At the fixed point, combining the cancellation matching (4.18) with the GR normalization (4.8) identifies $\beta_G = \zeta^{-1}$ (equivalently, $\zeta = 4\pi G$). Hence $T_{00}^{(T)} + T_{00}^{(\text{nl})} = 0$ at continuum, and similarly for spatial components.*

Symmetry protection. The cancellation is protected by the atemporal symmetry (WESH–Noether, Eq. (G.1)): any deformation that breaks the commutant constraints or the alignment $\partial_\mu \tau \propto \partial_\mu \Phi$ violates conservation and spoils the emergent Einstein equation.

Tensorial closure (IR uniqueness under alignment). The cancellation established above is not restricted to a single component (e.g. 00): at two-derivative order, the

WESH primitives admit only one admissible *gradient-sector* stress-tensor structure.

Lemma 5.5 (Tensorial closure of the gradient sector). *Work on a coarse-grained window $L \gg \xi$ in the Markov/IR regime, and adopt the ≤ 2 -derivative truncation used in the IR completion. Assume stationary gradient alignment $\nabla_\mu \tau = k \nabla_\mu \Phi$ (Eq. (4.2)). Then the derivative-dependent parts of the hidden-sector stresses are forced to share the universal scalar-kinetic tensor:*

$$\begin{aligned} T_{\mu\nu}^{(T)}|_{\nabla\Phi} &= \frac{k^2}{\zeta} \left(\nabla_\mu \Phi \nabla_\nu \Phi - \frac{1}{2} g_{\mu\nu} (\nabla \Phi)^2 \right), \\ T_{\mu\nu}^{(\text{nl})}|_{\nabla\Phi} &= -(\lambda_1 + 3\lambda_2) \left(\nabla_\mu \Phi \nabla_\nu \Phi - \frac{1}{2} g_{\mu\nu} (\nabla \Phi)^2 \right), \end{aligned} \quad (5.5)$$

up to higher-derivative corrections suppressed by ξ/L and finite- N corrections (collectively denoted $O(\xi/L) + O(1/N)$). Any remaining zero-derivative contribution is proportional to $g_{\mu\nu}$ and is therefore absorbed into Λ_{eff} (Appendix J).

Sketch. Alignment makes the time sector depend on the system only through the scalar field Φ at first-derivative order, since $\nabla \tau = k \nabla \Phi$; inserting this into the definition of $T_{\mu\nu}^{(T)}$ yields the first identity in Eq. (5.5). For the nonlocal sector, finite-range Markov locality (kernel support $\sim \xi$) implies that on $L \gg \xi$ the IR contribution of $S_C + S_E$ admits a *local* derivative expansion in the single scalar $\Phi(x) = \int d^4y K(x-y) C(\Psi; x, y)$. Diffeomorphism invariance together with the ≤ 2 -derivative truncation leaves a unique nontrivial kinetic term proportional to $(\nabla \Phi)^2$; its metric variation is fixed and produces exactly the canonical tensor $\nabla_\mu \Phi \nabla_\nu \Phi - \frac{1}{2} g_{\mu\nu} (\nabla \Phi)^2$. The coefficient of this term is the IR response combination $\lambda_1 + 3\lambda_2$ (cf. Eq. (4.8)), giving the second identity in Eq. (5.5). \square

Consequently, once the cancellation matching $\frac{k^2}{\zeta} = \lambda_1 + 3\lambda_2$ is imposed (Eq. (4.18)), the entire gradient-sector tensor cancels, not just a particular component; residuals are controlled by $O(\xi/L) + O(1/N)$ as claimed.

Discrete-to-continuum control. On scales $L \gg \xi$, eigentime events form a quasi-uniform inhomogeneous Poisson mesh with spacing $\ell_{\text{Eig}} \sim \lambda_{\text{Eig}}^{-1/4}$ and fill distance $h_N = \mathcal{O}(N^{-1/4})$. With kernel regularization the fields entering the limit are Lipschitz, so that discrete-to-continuum errors satisfy $\|\mathcal{F}_{\text{disc}} - \mathcal{F}_{\text{cont}}\|_{L^\infty} = \mathcal{O}(N^{-1/4})$, and curvature errors scale as $\mathcal{O}(\ell_{\text{Eig}}^2)$. These bounds yield the stated $\mathcal{O}(1/N)$ precision for the hidden-sector cancellation on coarse-grained windows.

5.7 Variational GNE formulation of the hidden-sector cancellation

Motivation. Up to now, hidden-sector cancellation has been shown as a dynamical consequence of alignment and matching. Here we repackage it as a *variational fixed point*: the WESH flow minimizes a regularized Lyapunov functional \mathcal{M}_ϵ under WESH–Noether/TSL constraints, so that cancellation is the *unique* stationary solution of a strongly monotone VI—equivalently, a variational generalized Nash equilibrium (v–GNE). Strong monotonicity is guaranteed by mixing/primitivity (reversible spectral gap) in the KMS geometry (Appendix D).

Definition 5.4 (Feasible set, operator, and VI/KKT). *Let the feasible set be*

$$\begin{aligned} \mathcal{Z} := \Big\{ z = (\rho, \hat{T}) : & \rho \geq 0, \operatorname{Tr} \rho = 1, \\ & \text{WESH–Noether (App. H, Eq. (G.1)),} \\ & \text{TSL covariance (Sec. 5.2)} \Big\}, \end{aligned} \quad (5.6)$$

a closed subset of the natural state/field space. For any $z = (\rho, \hat{T}) \in \mathcal{Z}$ we define the entanglement potential $\Phi[\rho, \hat{T}]$ by the finite-range Yukawa mediator K and the normalized Rényi-2 gate $C \in [0, 1]$ (Sec. 4.1, Eq. (4.1), App. F). Define the operator

$$F(z) := \nabla \mathcal{M}_\epsilon(\rho, \hat{T}, \Phi[\rho, \hat{T}])|_{\mathcal{Z}}, \quad z := (\rho, \hat{T}) \in \mathcal{Z}, \quad (5.7)$$

where \mathcal{M}_ϵ is the regularized WESH Lyapunov functional of Appendix D. Endow the wedge algebra with the reversible KMS inner product

$$\langle A, B \rangle_* := \operatorname{Tr}(\sigma_{\text{KMS}}^{1/2} A^\dagger \sigma_{\text{KMS}}^{1/2} B), \quad (5.8)$$

the GNS/KMS inner product on the wedge algebra (Sec. 6.2). The VI problem $\text{VI}(F, \mathcal{Z})$ is: find $z^* \in \mathcal{Z}$ such that

$$\langle F(z^*), z - z^* \rangle_* \geq 0 \quad \forall z \in \mathcal{Z}, \quad (5.9)$$

equivalently the KKT stationarity for the constrained minimization of \mathcal{M}_ϵ on \mathcal{Z} .

Lemma 5.6 (Strong monotonicity and contraction). *Under CP–TP and complete positivity, finite–memory/Markov locality (Eq. (5.2)) and mixing/primitivity (reversible spectral gap) in the KMS geometry, the operator $F = \nabla \mathcal{M}_\epsilon$ is (strongly) monotone on \mathcal{Z} , i.e.*

$$\langle F(z) - F(w), z - w \rangle_* \geq \mu \|z - w\|_*^2 \quad (\mu > 0). \quad (5.10)$$

Moreover, the wedge-restricted GKSL semigroup is contractive in the KMS geometry, and detailed balance (Sec. 6.2) implies a positive spectral gap on the orthogonal complement of the fixed point.

Theorem 5.5 (Unique v-GNE and hidden-sector cancellation). *Let \mathcal{Z} and $F = \nabla \mathcal{M}_\epsilon$ be as above. Then:*

1. *The VI (5.9) admits a unique solution $z^* \in \mathcal{Z}$. Existence follows from the compactness of the sublevel sets of \mathcal{M}_ϵ in the KMS topology and the continuity of F . Uniqueness follows from the strong monotonicity (5.10) of F on \mathcal{Z} , induced by mixing/primitivity (reversible spectral gap) in the KMS geometry.*
2. *The KKT stationarity at z^* enforces the gradient alignment $\partial_\mu \tau = k \partial_\mu \Phi$ (Thm. 6.1, Appendix D), and, substituting this relation in the stress tensors (Eqs. (4.11)–(4.12)), one obtains, at continuum and with the cancellation matching (4.18), the operator identity*

$$T_{\mu\nu}^{(T)}(x) + T_{\mu\nu}^{(\text{nl})}(x) = 0$$

in the sense of local quadratic forms on the wedge algebra (Sec. 5.6).

3. *The semigroup $e^{s\mathcal{L}}$ converges exponentially to z^* in the KMS geometry, with mixing rate set by the reversible spectral gap (Sec. 6.2).*

Corollary 5.3 (Robustness and coarse-grained stability). *For any fixed $\epsilon > 0$, the solution $z^*(\epsilon)$ of VI(F, \mathcal{Z}) is Lyapunov-stable; as $\epsilon \downarrow 0$, $z^*(\epsilon) \rightarrow z^*$ by Γ -convergence (Appendix D). Hence the cancellation persists under coarse-graining/noise regularization, and the Einstein–Hilbert phase is the unique, robust IR fixed point under WESH constraints.*

Remark 5.5 (Quantum-coordinated equilibrium and Araki/KMS). *On the wedge, Araki’s relative entropy w.r.t. the KMS state is a Lyapunov; its first-law variation yields the same VI stationarity near equilibrium. Null-plane Markov saturation (Sec. 6.2) means that conditional relative entropy vanishes only on scalars, as characterized by the Petz recovery map (Petz, 1986), enforcing the uniqueness of the fixed point. Entanglement thus acts as the coordination resource that allows the local (time) and nonlocal (backreaction) sectors to reach the unique v-GNE: the operator cancellation is the quantum-coordinated equilibrium on the wedge.*

Box 7: The WESH Bridge – From Timeless Constraint to Spacetime and Holography

Start (timeless): Wheeler–DeWitt constraint

$$\hat{H}_{\text{tot}} |\Psi\rangle = 0 \quad (\text{no time, no evolution})$$

Unique extension (pre-geometric dynamics): WESH master equation (Eq. (1.15))

$$\begin{aligned} \partial_s \rho &= \mathcal{L}[\rho], \\ \mathcal{L} &= \int d^4x \mathcal{D}_{\hat{T}^2(x)}[\rho] + \iint d^4x d^4y \gamma(x, y) C(\Psi; x, y) \mathcal{D}_{L_{xy}}[\rho], \end{aligned}$$

with Hermitian jumps $\hat{T}^2(x)$, $L_{xy} = \hat{T}^2(x) - \hat{T}^2(y)$, and satisfying the fundamental constraints (Sec. 1): (i) global charge neutrality, (ii) pre-geometric Noether conservation, and (iii) CPT-causality with collective coherence (CS). This uniquely fixes the WESH dissipative completion and yields emergent physical time.

Emergent chain:

$$\begin{aligned} dt/ds &= \Gamma[\Psi] > 0 && (\text{physical time emerges}) \\ \partial_\mu \tau &= k \partial_\mu \Phi && (\text{unique attractor: gradient alignment}) \\ T_{\mu\nu}^{(T)} + T_{\mu\nu}^{(\text{nl})} &= 0 && (\text{hidden-sector cancellation, operator level}) \\ \Downarrow & & & (\text{IR CP/Markov filter in } D=4) \\ G_{\mu\nu} + \Lambda g_{\mu\nu} &= 8\pi G T_{\mu\nu}^{(m)} && (\text{Einstein eq.; matching } k \text{ via Eq. (4.8)}) \\ \Downarrow & & & (\text{Rindler wedge + KMS + RAQ}) \\ S_{\text{BH}} &= \frac{A}{4L_P^2} + c_{\log} \ln \frac{A}{L_P^2} + \dots && (\text{Bekenstein–Hawking law}) \end{aligned}$$

Interpretation. General Relativity and black hole thermodynamics are not independent inputs. They arise as dual macroscopic consequences of resolving the timeless Wheeler–DeWitt constraint through WESH: the same pre-geometric, CP/Markov, entanglement-driven dynamics yields both the Einstein–Hilbert action and the Bekenstein–Hawking area law.

6 Black Hole Thermodynamics: a Cross-Scale Validation of WESH

Overview

If WESH is a fundamental description of quantum spacetime, its microscopic structure—Planck-scale correlation length $\xi \simeq L_P$, bilocal dissipator $L_{xy} = \hat{T}^2(x) - \hat{T}^2(y)$, and pre-geometric charge conservation via WESH–Noether—must remain consistent across all gravitational scales. Black-hole horizons provide the decisive test: quantum information, geometry, and thermodynamics converge in regimes separated by 45–50 orders of magnitude from the Planck length.

This section proves that black-hole thermodynamics is not an external input but a necessary consequence of the same dynamical principles that govern Planckian eigentimes. The Bekenstein–Hawking entropy

$$S_{\text{BH}} = \frac{A}{4L_P^2} + \gamma \ln \frac{A}{L_P^2} + \dots \quad (6.1)$$

emerges **uniquely**, without additional free parameters and without ad hoc projections. The derivation requires no thermal ansatz and no fine-tuning. Unlike Euclidean path-integral approaches, which target equilibrium, the present Lorentzian treatment describes dynamical relaxation toward equilibrium, including slowly evolving horizons. The argument proceeds as follows.

1. **Pre-geometric consistency.** WESH–Noether enforces path independence of global charges in the auxiliary s -flow. This pre-geometric constraint, formulated at Planck scale, must hold universally if WESH is fundamental.
2. **Thermal emergence.** In a Rindler wedge, the same GKSL dynamics admits a unique KMS fixed point at $\beta_H = 2\pi/\kappa$. This is precisely the Kubo–Martin–Schwinger characterization of equilibrium for quantum statistical mechanics on operator algebras (Haag, Hugenholtz, & Winnink, 1967). No thermal prior is imposed; KMS emerges from modular covariance of the \hat{T}^2 -channel.
3. **Universal prefactor.** The $1/4$ coefficient arises from bipartite halving across the horizon ($1/2$) combined with RAQ projection, continuous + discrete \mathbb{Z}_2 , onto the horizon-even physical subspace (another $1/2$), both inherited from constraint structure.

4. **Robustness and EFT control.** Spectral concentration bounds yield $\bar{s} = 1 + \mathcal{O}(L_P^2/A)$. Curvature-induced kernel deformations are suppressed by $(L_P/M)^4$ for macroscopic horizons, confirming $\xi \simeq L_P$ as a controlled approximation. Here ξ is the correlation length of Table 1 (Sec. 1), understood as its infrared fixed-point value; possible ultraviolet running can be absorbed into the renormalization of G , leaving the Bekenstein–Hawking combination $A/(4G)$ invariant.
5. **Subleading structure.** Logarithmic corrections $\gamma \ln(A/L_P^2)$ are fixed by the heat-kernel expansion of the gauge-fixed quadratic form Δ_{phys} , tied to the variational alignment (Thm. 5.2, Appendix D). For regular horizons, $\gamma = \sigma_{\text{phys}}\chi(\mathcal{H})$ with $\chi(S^2) = 2$.
6. **Extension to rotating horizons.** The framework extends to Kerr via co-rotating KMS structure ($\chi = \partial_t + \Omega_H \partial_\phi$) and hidden-symmetry covariance. The leading $A/(4L_P^2)$ is universal; spin dependence enters only through extrinsic-curvature terms in $\gamma(J)$.
7. **Holography as chronogenetic stability.** The bound $S[\mathcal{H}] \leq A/(4L_P^2) + \dots$ is *derived* as a stability condition: the chronogenetic requirement $\Gamma[\Psi] > 0$ (forward time production) implies the holographic entropy bound. This aligns with the covariant formulation of the entropy bound (Bousso, 1999), where entropy on light-sheets cannot exceed the area of the boundary surface.

Logical status. This is not a “WESH model of black holes.” It is a **cross-scale consistency theorem**: if WESH is fundamental at L_P , then black hole thermodynamics must hold as observed, with the numerical coefficients derived above. Any deviation, in the leading $1/4$, in the KMS temperature $\beta_H = 2\pi/\kappa$, in the logarithmic coefficient γ , or in the holographic bound, would falsify the framework. Conversely, its reproduction on a macro scale constitutes a non-trivial validation of WESH as a candidate theory of quantum spacetime.

Assumptions and falsifiability. The derivation requires: (i) Hartle–Hawking KMS regularity in the near-horizon window; (ii) exponential-causal support of the WESH kernel with $\xi \simeq L_P$ undeformed to leading order; (iii) gauge-invariant bipartite splitting implemented via RAQ projection. These are not fine-tunings but *consistency requirements* for the scaling hypothesis. Curvature-induced deformations are treated within effective field theory and shown to be negligible ($\mathcal{O}((L_P/M)^4)$) for macroscopic horizons, while providing falsifiable signatures,

deviations in γ , shifts in spectral weights, breakdown of KMS balance, for near-Planckian or rapidly rotating black holes.

Roadmap. The section proceeds from pre-geometric conservation (Sec. 1.3) through wedge KMS structure (Sec. 6.2) to RAQ projection (Sec. 6.3) and spectral analysis (Sec. 6.4), yielding the entropy law and its holographic interpretation.

Step	Fundamental input / tool	Output / consequence
1	Pre-geometric coherence: WESH–Noether ($\mathcal{L}^\dagger[\hat{Q}_a] = 0$)	Athermal GKSL class commuting with charges; path-independence in s .
2	Modular covariance in a Rindler wedge; null-plane Markov property	Unique KMS fixed point at $\beta_H = 2\pi/\kappa$.
3	Bipartite pairing + RAQ even projection (\mathbb{Z}_2 swap)	Universal prefactor $1/4$ in $S_{\text{BH}} = A/(4L_P^2) + \dots$
4	One-loop Hessian Δ_{phys} + replica/heat kernel	Logarithmic correction $\gamma \ln(A/L_P^2)$.
5	Chronogenetic split $\Gamma = \Gamma_{\text{loc}} + \Gamma_{\text{bi}}$ + KMS calibration	Holographic bound as stability condition; saturation at HH.

6.1 Pre-geometric foundation: the WESH–Noether principle (path independence)

Overview. This subsection fixes the pre-geometric conservation law that selects the physically admissible s –dynamics in QFTT–WESH before the emergence of physical time t . The law is imposed directly on the GKSL generator and expresses *path independence* of global currents (no vorticity) in the auxiliary flow. It is formulated as an algebraic necessity—on par with the closure of a constraint algebra—rather than as a thermodynamic prior. Near-horizon thermality (KMS) and detailed balance are *not* assumed here; they will follow as stationary properties of the wedge dynamics once the pre-geometric generator is constrained by this principle and locality/causality.

GKSL generator and Heisenberg dual. The s –evolution of the state $\rho(s)$ is generated by

$$\partial_s \rho = \mathcal{L}[\rho] = -i [H_{\text{eff}}, \rho] + \sum_{\alpha} \left(L_{\alpha} \rho L_{\alpha}^{\dagger} - \frac{1}{2} \{ L_{\alpha}^{\dagger} L_{\alpha}, \rho \} \right). \quad (6.2)$$

where local and bilocal channels are admitted (e.g. $L_x \sim \hat{T}^2(x)$ and $L_{xy} \sim \hat{T}^2(x) - \hat{T}^2(y)$) with exponential-causal kernel K_{ξ} (Sec. 1), and H_{eff} collects coherent terms and gauge contributions (Sec. 4). The Heisenberg dual acts as

$$\mathcal{L}^{\dagger}[\hat{O}] = i [H_{\text{eff}}, \hat{O}] + \sum_{\alpha} \left(L_{\alpha}^{\dagger} \hat{O} L_{\alpha} - \frac{1}{2} \{ L_{\alpha}^{\dagger} L_{\alpha}, \hat{O} \} \right). \quad (6.3)$$

Axiom 1 (WESH–Noether: pre-geometric conservation/path independence). *Let $\{\hat{Q}_a\}$ be the set of global first-class charges (total energy/momentum, total T-charge, Hamiltonian/diffeomorphism constraints, etc.). The physical pre-geometric dynamics is the maximal subclass of GKSL generators that annihilates every charge in the adjoint:*

$$\mathcal{L}^{\dagger}[\hat{Q}_a] = 0 \quad \text{for all } a. \quad (6.4)$$

Lemma 6.1 (Equivalent formulations). *The following are equivalent to (G.1):*

1. **Conservation in mean:** $\frac{d}{ds} \text{Tr}(\rho \hat{Q}_a) = \text{Tr}(\rho \mathcal{L}^{\dagger}[\hat{Q}_a]) = 0$ for every state ρ .
2. **Path independence (no vorticity):** the functional one-form $\omega_a[\rho] := \text{Tr}(\hat{Q}_a \mathcal{L}[\rho]) ds$ vanishes identically, hence $\oint \omega_a = 0$ on any closed loop in state space.
3. **Structural constraint:** in canonical (minimal) GKSL form, a sufficient condition is

$$[H_{\text{eff}}, \hat{Q}_a] = 0, \quad [L_{\alpha}, \hat{Q}_a] = 0 \quad \forall \alpha. \quad (6.5)$$

Under standard linear-independence/minimality assumptions for the channel set, (6.5) is also necessary up to unitary mixing within the Lindblad span.

Remark 6.1 (Geometric content). *Equation (G.1) enforces the absence of circulation of global charges along the s -flow: the auxiliary evolution is path indepen-*

dent with respect to $\{\hat{Q}_a\}$. This elevates conservation to an internal consistency requirement of the pre-geometric generator (cf. the role of first-class constraints).

Proposition 6.1 (Closedness and monotonicity). *Let $\mathfrak{G}_{\text{phys}} := \{\mathcal{L} : \mathcal{L}^\dagger[\hat{Q}_a] = 0 \forall a\}$. Then:*

1. $\mathfrak{G}_{\text{phys}}$ is convex and stable under unitary conjugation; it preserves the level sets of $\{\text{Tr}(\rho \hat{Q}_a)\}$.
2. For any $\mathcal{L} \in \mathfrak{G}_{\text{phys}}$, the CPTP semigroup $e^{s\mathcal{L}}$ admits a Lyapunov functional $\mathcal{M}[\rho]$ (e.g. a relative entropy with respect to the fixed-point manifold) such that $\partial_s \mathcal{M} \leq 0$, with equality iff ρ is stationary (LaSalle invariance in quantum state space).

Sketch. (1) follows from linearity of (G.1). For (2), contractivity of CPTP maps ensures monotonicity of suitable f -divergences; invariance of $\{\hat{Q}_a\}$ forbids coherent drift along constrained directions, so fixed points are precisely the zero-derivative locus. \square

Lemma 6.2 (Charge-preserving descent of relative entropy). *Let σ be any stationary state of the pre-geometric flow on \mathfrak{A} , with the same global charges as ρ_0 . If $\mathcal{L}^\dagger[\hat{Q}_a] = 0$ for all a (WESH–Noether), then along $\rho(s) = e^{s\mathcal{L}^*}[\rho_0]$ the relative entropy $S_{\mathfrak{A}}(\rho(s)\|\sigma)$ is non-increasing, with trajectories confined to the charge level sets. Stationarity conditions $\delta S_{\mathfrak{A}}(\rho\|\sigma) = 0$ under local variations reduce to the gradient-alignment equations of Theorem 6.1.*

Sketch. Noether conservation fixes the admissible directions in state space; contractivity of $S(\cdot\|\sigma)$ under the CPTP semigroup yields monotonic descent. First-order optimality on the constrained manifold enforces collinearity of functional gradients, reproducing (6.6). \square

Theorem 6.1 (Gradient alignment as the attracting fixed manifold). *Assume locality/causality of the mediator (K_ξ exponential-causal, Sec. 1) and impose (G.1) for energetic and gauge charges. Then the attracting stationary manifold of the s -flow is characterized by the gradient alignment*

$$\partial_\mu \tau = k \partial_\mu \Phi, \tag{6.6}$$

with k fixed by the normalizations used in Sec. 4. On this manifold, hidden-sector cancellation yields the effective action reproducing Einstein dynamics.

Sketch. This theorem is a direct corollary of the global alignment result proved in Appendix D (Thm. 5.2). There, a WESH monotone \mathcal{M}_ϵ is constructed and one shows that the stationarity condition $\delta\mathcal{M}_\epsilon/\delta\tilde{T} = 0$ forces collinearity of the functional gradients of \tilde{T} and the geometric potential Φ . Imposing the WESH–Noether constraint (G.1) eliminates forbidden drift directions and pins the stationary manifold to the solutions of (6.6). The proportionality constant k is uniquely fixed by the normalizations in Sec. 4, where the emergent Einstein sector is matched. \square

Remark 6.2 (Role of RAQ vs swap projection). *When some \hat{Q}_a are first-class (Hamiltonian/diffeomorphisms), (G.1) ensures compatibility of the generator with the constrained subspace, and the RAQ/group-averaging map $\eta = \int_{\mathcal{G}_{\text{cont}}} d\mu(g) U(g)$ implements the continuous constraint surface in the usual way. This continuous RAQ projector $\hat{\mathcal{P}}_{\text{RAQ}}$ does not halve the mode count at leading order: it projects out gauge orbits of measure zero and ensures that the determinants are well defined, while preserving the $\mathcal{O}(A/\xi^2)$ scaling.*

The additional factor 1/2 relevant for black-hole entropy arises from selecting the swap-even superselection sector (state-level projection $P_+ = \frac{1}{2}(\mathbf{1} + G_{xy})$). At the observable level this is conveniently expressed via the conditional expectation $\mathbb{E}_{\text{even}}(X) = \frac{1}{2}(X + G_{xy}XG_{xy})$, which block-diagonalizes the swap decomposition. This is a boundary superselection associated with the modular/CPT structure of the wedge, not a first-class constraint. Combined with the bipartite halving (1/2 from pairing out/in modes), the swap-even projection yields the universal 1/4 prefactor of the Bekenstein–Hawking law.

EFT normalization of the kernel. The mediator scale ξ is identified with the fundamental short distance of the WESH sector (naturally $\xi \sim L_P$). In curved backgrounds, $m_T = \xi^{-1}$ receives curvature corrections of effective-field-theory type (e.g. from the Kretschmann scalar), but for macroscopic black holes the relative shift is suppressed by powers of (L_P/M) ; thus $\xi = L_P$ is a controlled leading-order approximation.

Prelude to horizon thermodynamics. Equation (G.1) is athermal; it imposes algebraic coherence of the pre-geometric flow. In a near-horizon (Rindler) wedge, the same coherence singles out, as the normal stationary state on the wedge algebra, a KMS state with respect to boosts. Uniqueness follows from the structure

of GKSL semigroups with quantum detailed balance on the wedge algebra. This provides the thermal fixed point needed for the entropy analysis without assuming thermality *a priori*.

Definition 6.1 (Araki relative entropy and basic properties). *Let ρ, σ be normal states on a von Neumann algebra \mathfrak{A} . The Araki relative entropy (Araki, 1976) $S_{\mathfrak{A}}(\rho\|\sigma)$ is the algebraic extension of $\text{Tr } \rho(\log \rho - \log \sigma)$ that is well-defined also for type-III local algebras. It obeys:*

- **Positivity and faithfulness:** $S_{\mathfrak{A}}(\rho\|\sigma) \geq 0$, with equality iff $\rho = \sigma$.
- **Monotonicity (data processing):** for any inclusion of von Neumann algebras $\mathfrak{A} \subset \mathfrak{B}$ and normal states ρ, σ on \mathfrak{B} ,

$$S_{\mathfrak{A}}(\rho|_{\mathfrak{A}}\|\sigma|_{\mathfrak{A}}) \leq S_{\mathfrak{B}}(\rho\|\sigma)$$

(restriction to subsystems does not increase relative entropy).

For bipartite algebras, the mutual information is a relative entropy,

$$I(A:B)_\rho = S(\rho_{AB}\|\rho_A \otimes \rho_B).$$

Remark. In algebraic quantum field theory (AQFT; Haag, 1996), local algebras are typically type-III, so von Neumann entropies of subregions may diverge; Araki's $S(\rho\|\sigma)$ is the correct, regulator-independent quantity for all local statements used below.

Definition 6.2. (Modular-KMS spectral regularity of \hat{T}^2 on the wedge)

Let $\mathfrak{A}(\mathcal{W}_R)$ be the right-Rindler wedge algebra and H_R its boost generator. We say that the composite channel density \hat{T}^2 enjoys modular-KMS spectral regularity on \mathcal{W}_R if:

- (i) **Tempered KMS two-point structure.** The KMS two-point Wightman distributions of $O := \hat{T}^2$ are tempered and satisfy the standard strip analyticity with respect to the modular flow generated by H_R ; equivalently, their boost-frequency spectra obey the KMS reflection relations on the strip $\text{Im } t \in (0, \beta_H)$.
- (ii) **Finite null-second moment for the even four-point.** On any null generator (affine parameter u) of the horizon cut, consider the connected four-point function of $O = \hat{T}^2$,

$$G_c(u_1, u_2, u_3, u_4) := \langle O(u_1)O(u_2)O(u_3)O(u_4) \rangle_c.$$

We define its even part under the swap (u_1, u_3) as

$$G_c^{\text{even}}(u_1, u_2, u_3, u_4) := \frac{1}{2} \left(G_c(u_1, u_2, u_3, u_4) + G_c(u_3, u_2, u_1, u_4) \right),$$

and require that, for coincident pairs $(u_1, u_3) = (u, u)$ and $(u_2, u_4) = (0, 0)$, the null-second moment

$$\int_{\mathbb{R}} du u^2 \|G_c^{\text{even}}(u, 0, u, 0)\|$$

is finite. This guarantees that the even modular spectral form factor of O admits a \mathcal{C}^1 Taylor expansion at $\omega = 0$.

- (iii) **Absolutely continuous modular spectrum near $\omega = 0$.** The modular spectral measure of O (with respect to H_R) is absolutely continuous in a neighborhood of $\omega = 0$ with locally bounded density.

Lemma 6.3 (Spectral regularity implies charge–commutant equivalence). *Let \mathcal{L} be the WESH generator with Hermitian channels $\{\hat{T}^2(x), L_{xy} = \hat{T}^2(x) - \hat{T}^2(y)\}$ on the near-horizon Rindler wedge \mathcal{W}_R . Under the above spectral regularity conditions, the charge–commutant equivalence of Appendix G (Prop. G.2) applies: for any global charge \hat{Q} ,*

$$\mathcal{L}^\dagger[\hat{Q}] = 0 \iff [H_{\text{eff}}, \hat{Q}] = 0 \text{ and } [L_\alpha, \hat{Q}] = 0 \text{ for all channels } L_\alpha. \quad (6.7)$$

Proof. The Modular–KMS spectral regularity conditions (Definition 6.2) — specifically: (i) tempered two-point KMS correlator, (ii) finite null second moment for the even connected four-point function, and (iii) absolutely continuous modular spectrum near $\omega = 0$ — together provide the mild spectral regularity hypothesis required by Proposition G.2 (Appendix G).

In detail: conditions (ii) and (iii) ensure that the operator \hat{T}^2 possesses a non-degenerate spectral resolution in the measure-theoretic sense on the wedge. This nondegeneracy allows the transition from the double-commutator identity $\mathcal{D}_L^\dagger[\hat{Q}] = -\frac{1}{2}[L, [L, \hat{Q}]] = 0$ (implied by $\mathcal{L}^\dagger[\hat{Q}] = 0$) to the single-commutator condition $[L, \hat{Q}] = 0$ for each Hermitian Lindblad operator $L \in \{\hat{T}^2(x), L_{xy}\}$.

Therefore, Proposition G.2 applies in the wedge geometry, establishing the stated equivalence. \square

Remark. The near-horizon KMS regime is a concrete physical realization where the general algebraic framework applies. The equivalence is not re-derived here

but follows from verifying that the wedge satisfies the regularity conditions of Proposition G.2.

6.2 Emergence of thermality: the KMS state as the unique stationary solution in a Rindler frame

Overview. This subsection derives, rather than assumes, the near-horizon KMS structure by solving the WESH master equation in a uniformly accelerated (Rindler) frame. In the Rindler wedge, the WESH generator is KMS-symmetric with respect to the boost modular flow; consequently, the unique normal stationary state on the wedge algebra is a KMS state at inverse temperature $\beta_H = 2\pi/\kappa$, where κ is the surface gravity. Detailed balance for the \hat{T}^2 -channel and the horizon thermodynamic relations follow as corollaries. No thermodynamic prior is used; the result is anchored in pre-geometric conservation (Sec. 1.3), locality/causality of the mediator, and modular covariance on the wedge.

Rindler wedge, boost modular flow, and β_H

Fix a regular, non-extremal Killing horizon with surface gravity $\kappa > 0$ and introduce Rindler coordinates $(\eta, \rho, \mathbf{x}_\perp)$ so that, in leading order,

$$ds^2 = -\kappa^2 \rho^2 d\eta^2 + d\rho^2 + d\mathbf{x}_\perp^2, \quad \rho > 0. \quad (6.8)$$

The right wedge $\mathcal{W}_R = \{\rho > 0\}$ carries the boost Killing field ∂_η with wedge Hamiltonian H_R generating η -translations on the wedge algebra $\mathfrak{A}(\mathcal{W}_R)$. The Unruh/Hawking inverse temperature is

$$\beta_H = \frac{2\pi}{\kappa}. \quad (6.9)$$

On $\mathfrak{A}(\mathcal{W}_R)$, the restriction of the Minkowski (or Hartle–Hawking) vacuum is a KMS state with respect to the modular flow generated by H_R ; on null cuts of the wedge boundary, the modular Hamiltonian admits a local expression in terms of null stress components, supplying the near-horizon template for what follows.

WESH generator in a uniformly accelerated frame

The pre-geometric s -evolution is governed by the GKSL generator in Eq. (6.2). Its wedge-restricted form reads

$$\mathcal{D}_{\text{loc}}[\rho] = \int_{\mathcal{W}_R} d\Sigma_x \gamma(x) \left(\hat{T}^2(x) \rho \hat{T}^2(x) - \frac{1}{2} \{ \hat{T}^2(x)^2, \rho \} \right), \quad (6.10)$$

$$\mathcal{D}_{\text{bi}}[\rho] = \iint_{\mathcal{W}_R \times \mathcal{W}_R} d\Sigma_x d\Sigma_y \Gamma(x, y) \left(L_{xy} \rho L_{xy}^\dagger - \frac{1}{2} \{ L_{xy}^\dagger L_{xy}, \rho \} \right), \quad (6.11)$$

where γ, Γ are smooth, exponentially causal kernels with correlation length ξ , and H_{eff} commutes with the global charges by WESH–Noether (Sec. 1.3). The algebra of accessible observables is $\mathfrak{A}(\mathcal{W}_R)$, and all integrals are understood in the sense of operator-valued distributions on wedge Cauchy sections.

Boost spectral decomposition. Let $\text{ad}_{H_R}(A) := [H_R, A]$. Any $A \in \mathfrak{A}(\mathcal{W}_R)$ admits the Bohr (boost-frequency) decomposition

$$A = \int_{\mathbb{R}} d\omega A(\omega), \quad \text{ad}_{H_R}(A(\omega)) = \omega A(\omega), \quad (6.12)$$

which diagonalizes the action of the modular flow and isolates frequency-resolved rate densities in (6.10)–(6.11).

KMS symmetry (quantum detailed balance) on the wedge

For a faithful, normal state σ on $\mathfrak{A}(\mathcal{W}_R)$, define the GNS inner product

$$\langle A, B \rangle_\sigma := \langle \Omega_\sigma, A^\dagger B \Omega_\sigma \rangle \quad (\text{in a } \xi\text{-regulated/type-I representation: } \text{Tr}(\sigma^{1/2} A^\dagger \sigma^{1/2} B)). \quad (6.13)$$

A GKSL generator \mathcal{L} satisfies σ -detailed balance (KMS symmetry) iff $\langle A, \mathcal{L}[B] \rangle_\sigma = \langle \mathcal{L}[A], B \rangle_\sigma$ for all A, B , in which case σ is stationary, $\mathcal{L}^*[\sigma] = 0$.

Lemma 6.4 (KMS symmetry of the wedge-restricted WESH generator). *Let $\sigma_{\text{KMS}} \propto e^{-\beta_H H_R}$ be the KMS state on $\mathfrak{A}(\mathcal{W}_R)$ at inverse temperature β_H . Suppose the \hat{T}^2 -correlators in σ_{KMS} enjoy standard KMS analyticity and that $\Gamma(x, y)$ is boost-covariant and decays exponentially on scales $\gtrsim \xi$. Then the frequency-resolved rates from (6.10)–(6.11) obey*

$$\Gamma(+\omega) = e^{-\beta_H \omega} \Gamma(-\omega), \quad (6.14)$$

and $\mathcal{L}_{\text{WESH}}$ is σ_{KMS} -detailed balanced, hence $\mathcal{L}_{\text{WESH}}^*[\sigma_{\text{KMS}}] = 0$.

Sketch. Insert (6.12) into (6.10)–(6.11) and express the Golden rule rate densities as Fourier transforms of connected four-point functions of \hat{T} in σ_{KMS} . KMS analyticity yields (6.14). With jump operators $A(\omega)$ and $A^\dagger(\omega)$ organized by ω , one verifies σ -self-adjointness of $\mathcal{L}_{\text{WESH}}$ relative to (6.13), implying stationarity. Boost covariance of Γ ensures closure on $\mathfrak{A}(\mathcal{W}_R)$. \square

Proposition 6.2 (Relative-entropy Lyapunov functional). *Let $\mathcal{L}_{\text{WESH}}$ be σ_{KMS} -detailed balanced on $\mathfrak{A}(\mathcal{W}_R)$, and let $\rho(s) = e^{s\mathcal{L}_{\text{WESH}}^*}[\rho_0]$. Then the Araki relative entropy to the KMS state,*

$$\mathcal{S}(s) := S_{\mathfrak{A}(\mathcal{W}_R)}(\rho(s) \parallel \sigma_{\text{KMS}}),$$

is non-increasing in s and strictly decreasing unless $\rho(s) = \sigma_{\text{KMS}}$. Hence \mathcal{S} is a Lyapunov functional for the wedge semigroup; combined with primitivity, it implies uniqueness of the stationary state.

Sketch. Detailed balance makes $\mathcal{L}_{\text{WESH}}$ self-adjoint in the σ_{KMS} inner product, so the generator is a gradient flow for a convex functional; contractivity of CPTP maps entails the data-processing inequality for $S(\cdot \parallel \sigma_{\text{KMS}})$, ensuring $\partial_s \mathcal{S} \leq 0$ with equality only at the fixed point. \square

Fixed point and uniqueness

Proposition 6.3. (Irreducibility from null-plane Markovity). *Let $\mathfrak{A}(\mathcal{W}_R)$ be the wedge algebra and let the WESH generator on the wedge be*

$$\begin{aligned} \mathcal{L}_{\text{WESH}}[\rho] &= -i[H_{\text{eff}}, \rho] + \int_{\mathcal{W}_R} d\Sigma_x \gamma(x) \mathcal{D}_{\hat{T}^2(x)}[\rho] \\ &\quad + \iint_{\mathcal{W}_R \times \mathcal{W}_R} d\Sigma_x d\Sigma_y \Gamma(x, y) \mathcal{D}_{L_{xy}}[\rho], \end{aligned} \quad L_{xy} := \hat{T}^2(x) - \hat{T}^2(y).$$

with Hermitian jumps and kernels as in Sec. 6.2 (Eqs. (6.10)–(6.11)). Assume:

- (K1) Spectral regularity (Definition 6.2). *The quadratic channel \hat{T}^2 enjoys modular-KMS spectral regularity on the wedge (tempered KMS two-point, finite second moment of the even connected four-point on null cuts, absolutely continuous modular spectral measure near $\omega=0$).*

- (K2) Cross–horizon support. *$\Gamma(x, y)$ has exponentially causal support of range ξ and is non–vanishing for a set of (x, y) of positive measure with x outside and y inside the horizon neighborhood (Planck–thickened cross–sections), i.e. the bilocal channel truly couples the two sides.*
- (K3) Null–plane Markov property. *The vacuum restricted to $\mathfrak{A}(\mathcal{W}_R)$ is Markov on nested null intervals (saturation of strong subadditivity / conditional independence along null generators). This ensures that the modular flow is local and generated by a horizon–local integral of the stress tensor (Casini, Testé, & Torroba, 2017).*

Then the quantum Markov semigroup $\{e^{s\mathcal{L}_{\text{WESH}}}\}_{s \geq 0}$ is primitive (irreducible) on $\mathfrak{A}(\mathcal{W}_R)$: it admits a unique faithful normal stationary state. Since $\mathcal{L}_{\text{WESH}}$ satisfies $\sigma_{\text{KMS}}\text{--detailed balance}$ at $\beta_H = 2\pi/\kappa$, that unique stationary state is the $\chi\text{--KMS}$ state at Hawking temperature,

$$\rho_{\text{st}} = \sigma_{\text{KMS}} \propto e^{-\beta_H H_R}.$$

Remark 6.3 (On the uniqueness hypotheses). Assumptions (K1)–(K3) play disjoint roles. (K1) guarantees that Hermitian jumps generated by \hat{T}^2 admit a non-degenerate modular spectral resolution; this collapses invariant corners to scalars via $\mathcal{D}_L^\dagger[Q] = -\frac{1}{2}[L, [L, Q]]$. (K2) ensures cross-horizon connectivity (no decoupled components) at range ξ . (K3) (null-plane Markov property) rules out “shielded” subalgebras on nested null intervals by saturating strong subadditivity along the generators. Together with detailed balance, these imply primitivity and thus uniqueness of the KMS fixed point.

Proof sketch.

Step 1 (Trivial commutant under spectral regularity). By Hermiticity of the jumps and Definition 6.2, the double-commutator identity $\mathcal{D}_L^\dagger[Q] = -\frac{1}{2}[L, [L, Q]]$ holds on the relevant domain. If a von Neumann subalgebra $\mathcal{N} \subset \mathfrak{A}(\mathcal{W}_R)$ were invariant under the semigroup, then for every $Q \in \mathcal{N}$ one would have $\mathcal{D}_L^\dagger[Q] \in \mathcal{N}$ for all $L \in \{\hat{T}^2(x), L_{xy}\}$. Spectral regularity (non-degenerate modular spectral measure for the local polynomials of \hat{T}) implies that $[Q, \hat{T}^2(x)] = [Q, L_{xy}] = 0$ almost everywhere forces Q to lie in the commutant of the local quadratic field algebra, hence Q is scalar. Thus any invariant von Neumann subalgebra is trivial. (Appendix G, Prop. G.2 gives the same conclusion for global charges from $\mathcal{L}^\dagger[Q] = 0$.)

Step 2 (Connectivity from the bilocal kernel). Coarse-grain the horizon into Planck-thickened null cells $\{C_i\}$ of diameter $\sim \xi$ along each generator. By (K2), the weighted adjacency matrix $A_{ij} := \int_{C_i \times C_j} \Gamma(x, y) d\Sigma_x d\Sigma_y$ is irreducible (one giant connected component): every cell on the “out” side is coupled to the “in” side within $\mathcal{O}(\xi)$ along the null direction. Therefore, the $*$ -algebra generated by the set $\{\hat{T}^2(C_i), \hat{T}^2(C_i) - \hat{T}^2(C_j)\}$ acts cyclically on the wedge algebra: there is no nontrivial decomposition preserved by all jumps.

Step 3 (Null-plane Markovity kills hidden corners). Assumption (K3) states that along any nested null intervals $I_1 \subset I_2 \subset I_3$ on a generator the vacuum (and its χ -KMS deformations) is Markov, $I(I_1 : I_3 | I_2) = 0$. Equivalently, there exists a Petz recovery map $\mathbb{E}_{I_2} : \mathfrak{A}(I_1 \cup I_3) \rightarrow \mathfrak{A}(I_2)$ saturating strong subadditivity. Suppose now that $\mathcal{N} \subset \mathfrak{A}(\mathcal{W}_R)$ were a nontrivial von Neumann subalgebra invariant under the WESH semigroup. By Step 2, \mathcal{N} must contain operators with support on both sides of the horizon. Pick $N \in \mathcal{N} \cap \mathfrak{A}(I_1)$ with nonzero projection onto $\mathfrak{A}(I_3)$. Invariance of \mathcal{N} under the dynamics and locality of the bilocal kernel then imply that $\mathbb{E}_{I_2}(N)$ carries nontrivial correlations between I_1 and I_3 . But Markov saturation forces any such operator to have vanishing conditional mutual information unless it is proportional to the identity: $I(I_1 : I_3 | I_2) = 0$ together with data processing implies $N \propto \mathbf{1}$ in the GNS space of σ_{KMS} . By translating this argument along the generators and using cross-horizon connectivity (Step 2), one concludes that $\mathcal{N} = \mathbb{C} \mathbf{1}$. Hence the semigroup is primitive.

Step 4 (Detailed balance \Rightarrow uniqueness). Under Sec. 6.2, $\mathcal{L}_{\text{WESH}}$ satisfies σ_{KMS} detailed balance; hence it is self-adjoint in the $\langle A, B \rangle_{\sigma_{\text{KMS}}} = \text{Tr}(\sigma_{\text{KMS}}^{1/2} A^\dagger \sigma_{\text{KMS}}^{1/2} B)$ inner product. By Steps 1–3 the kernel of $\mathcal{L}_{\text{WESH}}$ is one-dimensional (scalars), and the orthogonal complement has strictly positive spectrum. Standard results for detailed-balance quantum Markov semigroups therefore give a unique faithful stationary state and mixing $e^{s\mathcal{L}_{\text{WESH}}^*}[\rho] \rightarrow \sigma_{\text{KMS}}$ for all normal ρ . \square

Remarks.

1. *What could fail?* If the cross-horizon gate vanished on a set of nonzero measure (no Rényi-2 correlations across some pairs), one could engineer a nontrivial invariant corner. Assumption (K3) excludes this near the horizon: the vacuum is Markov on null cuts and the modular Hamiltonian is local, so two-point (and controlled four-point) data extend across arbitrarily small null separations.
2. *Alignment with the pre-geometric structure.* Appendix D–H provide the Lyapunov functional \mathcal{M} and the Noether-level commutant arguments used

implicitly in Step 1; they ensure that no global charge generates hidden invariant directions for the wedge semigroup.

3. *Spectral gap.* In the detailed–balance geometry the primitive property implies a strictly positive spectral gap on the orthogonal complement of the scalars in the σ_{KMS} –GNS space. This gap sets the wedge mixing time and coincides with the width of the low–frequency peak entering the spectral weight estimates in Sec. 6.4.

Remark 6.4 (Null-plane Markovity and relative entropy). *On nested null intervals $I_1 \subset I_2 \subset I_3$, the vacuum (and its χ –KMS deformations) satisfies $I(I_1 : I_3 | I_2) = 0$, i.e. saturation of strong subadditivity. Equivalently, the conditional mutual information equals a conditional relative entropy that vanishes, and a Petz recovery map exists localized on I_2 . This formulation makes precise why no “screened” invariant corner survives on the wedge: data processing along the null inclusion chain collapses relative entropy to zero only on scalars, which enforces primitivity once cross-horizon connectivity is present.*

Remark 6.5 (Ergodicity from cross-horizon coupling). *The uniqueness of the KMS fixed point relies on primitivity, not merely on energy conservation. While $[L_{xy}, H_R] = 0$ ensures stationarity, the cross-horizon support of the bilocal kernel (Assumption K2) prevents the formation of decoupled sectors that would otherwise relax to non-thermal Generalized Gibbs Ensembles. Combined with the null-plane Markov property (K3), this guarantees that the only invariant subalgebra is trivial, forcing unique relaxation to the χ -KMS state.*

Theorem 6.2 (Uniqueness of the KMS stationary state). *Assume the hypotheses of Lemma 6.4, exponential clustering of connected cumulants of \hat{T} with range ξ , and primitivity (irreducibility) of the dissipative representation generated by $\{\hat{T}^2(x), L_{xy}\}$ on $\mathfrak{A}(\mathcal{W}_R)$. Then the semigroup $e^{s\mathcal{L}_{\text{WESH}}}$ admits a unique normal stationary state on $\mathfrak{A}(\mathcal{W}_R)$,*

$$\rho_{\text{staz}} = \sigma_{\text{KMS}} \quad (\chi\text{-KMS state at } \beta_H = \frac{2\pi}{\kappa}), \quad (6.15)$$

(in a ξ -regulated/type-I model: $\sigma_{\text{KMS}} \propto e^{-\beta_H H_R}$)

and $e^{s\mathcal{L}_{\text{WESH}}^*}[\rho_0] \rightarrow \sigma_{\text{KMS}}$ for any normal ρ_0 (weak*), with mixing rate governed by the spectral gap of $\mathcal{L}_{\text{WESH}}$ in the $\langle \cdot, \cdot \rangle_{\sigma_{\text{KMS}}}$ geometry.

Sketch. By Lemma 6.4, σ_{KMS} is stationary. Exponential clustering and finite-

range kernels imply (quasi-)compactness of the dissipator on frequency sectors; primitivity excludes invariant subalgebras other than scalars. Standard results for detailed-balance quantum Markov semigroups then give uniqueness and convergence with a strictly positive gap. \square

Corollary 6.1 (Hawking/Unruh detailed balance). *For the \hat{T}^2 -channel, the upward/downward transition rates obey*

$$\frac{\Gamma_{\uparrow}(\omega)}{\Gamma_{\downarrow}(\omega)} = e^{-\beta_H \omega}, \quad \beta_H = \frac{2\pi}{\kappa}, \quad (6.16)$$

providing the near-horizon detailed balance used in the thermodynamic analysis.

Spectral weights and the horizon pair entropy

Combining Corollary 6.1 with the Golden-rule rate densities yields the WESH–HH spectral weight

$$W_{\text{HH}}(\omega) = \Gamma_{\text{WESH}}(\omega) \rho(\omega) \frac{e^{-\beta_H \omega}}{1 - e^{-\beta_H \omega}}, \quad (6.17)$$

where $\Gamma_{\text{WESH}}(\omega)$ is the \hat{T}^2 spectral response and $\rho(\omega)$ the smooth near-horizon density of states on $\mathfrak{A}(\mathcal{W}_R)$. Equation (6.17) governs the KMS-weighted pair-entropy average that fixes the leading area coefficient in the entropy law (Sec. 6.3), and it appears here as a consequence of the KMS fixed point rather than a modeling choice.

Emergent thermality: s versus t

KMS symmetry and detailed balance are emergent properties of the wedge-restricted dynamics *after* bootstrapping to physical time via $dt/ds = \Gamma[\Psi]$. The WESH–Noether constraint (Sec. 1.3) remains the athermal, pre-geometric input selecting admissible generators; thermality is a stationary property induced by boost modular flow in the near-horizon regime.

Domain of validity and controlled deformations

The derivation holds in the Rindler window where (i) boost covariance and wedge modular structure are accurate; (ii) kernels are undeformed up to curvature-suppressed corrections $\mathcal{O}((\kappa\xi)^n)$; and (iii) clustering at range ξ persists. Curvature-induced renormalizations of kernel parameters are treated within EFT and are parametrically suppressed for macroscopic horizons; they do not alter the existence or

temperature of the KMS fixed point, but only dress approach-to-equilibrium rates and higher cumulants that feed subleading (logarithmic/power-law) corrections.

Outlook: rotating horizons

For stationary rotating black holes, replace H_R with the co-rotating generator $H_R - \Omega_H J$ on the wedge algebra adapted to Kerr (or NHEK). The fixed point becomes $\sigma_{\text{KMS}} \propto e^{-\beta_H(H_R - \Omega_H J)}$, i.e. a KMS state with an angular momentum chemical potential; the modular picture on null generators remains the organizing principle. Hidden symmetries (Killing–Yano tower) ensure separability and allow a covariant spectral decomposition of the \hat{T}^2 channel, paving the way to the analysis of superradiant channels and logarithmic corrections in the rotating case.

6.3 Physical projection via RAQ and the universal $\frac{1}{4}$ prefactor

Overview. This subsection replaces the heuristic ‘physical projector’ with a mathematically well-defined construction based on canonical first-class constraints and group averaging (Refined Algebraic Quantization, RAQ; Ashtekar et al., 1995). The near-horizon bipartite Hilbert space factors as $\mathcal{H}_{\text{kin}} \simeq \mathcal{H}_{\text{out}} \otimes \mathcal{H}_{\text{in}}$ with entanglement-effective dimension D on a regulator window set by the correlation length ξ . WESH–Noether guarantees that the constraints commute with the adjoint pre-geometric generator, so the RAQ projection is dynamically consistent. We show that the gauge average including the discrete horizon swap \mathbb{Z}_2 yields an even-sector projection whose normalized trace is asymptotically $1/2$; combined with bipartite halving, this produces the universal $\frac{1}{4}$ prefactor of the Bekenstein–Hawking law. From the wedge point of view, the $\mathbb{Z}_2^{(\text{swap})}$ factor implements the discrete CPT reflection associated with the modular structure of the Rindler algebra; imposing invariance under the swap thus enforces that physical states respect the fundamental CPT symmetry of the vacuum, rather than introducing an *ad hoc* gauge choice. Edge/center modes and RAQ measure issues affect only $\mathcal{O}(1)$ terms.

Constraints and gauge group. Collect the constraints

$$\hat{\mathcal{C}} = \left\{ \begin{array}{l} \hat{H}_{\text{tot}}(x) \approx 0 \text{ (Wheeler–DeWitt/Hamiltonian),} \\ \hat{\mathcal{H}}_a(x) \approx 0 \text{ (spatial diffeomorphisms),} \\ \hat{Q}_T \approx 0 \text{ (global } T\text{-charge neutrality)} \end{array} \right\}, \quad (6.18)$$

with \hat{Q}_T fixed by WESH-Noether. In the near-horizon (Rindler) window the wedge modular flow (boosts) commutes with the constraint set on the regulated algebra (domain subtleties understood), so that the physical gauge group can be taken as the (semi-)direct product

$$\mathcal{G}_{\text{cont}} = \exp(i\alpha^A \hat{\mathcal{C}}_A), \quad \hat{\mathcal{C}}_A \in \hat{\mathcal{C}}. \quad (6.19)$$

The trans-horizon swap G_{xy} is implemented *separately* as the horizon-even conditional expectation \mathbb{E}_{even} (Eq. (6.25)), i.e. a boundary superselection compatible with the wedge modular/KMS structure.

RAQ (group averaging) and the physical projector. In RAQ the rigging map $\eta : \mathcal{D} \subset \mathcal{H}_{\text{kin}} \rightarrow \mathcal{D}^*$ averages kinematical vectors over \mathcal{G} ,

$$\eta(|\psi\rangle)[|\phi\rangle] := \int_{\mathcal{G}_{\text{cont}}} d\mu_{\text{cont}}(\alpha) \langle \phi | e^{i\alpha^A \hat{\mathcal{C}}_A} |\psi\rangle, \quad |\phi\rangle, |\psi\rangle \in \mathcal{D}. \quad (6.20)$$

Here $d\mu_{\text{cont}}(\alpha)$ is the (generalized) Haar measure on $\mathcal{G}_{\text{cont}}$. The induced (formal) projector is

$$\begin{aligned} \hat{\mathcal{P}}_{\text{RAQ}} &\propto \int_{\mathcal{G}_{\text{cont}}} d\mu_{\text{cont}}(\alpha) e^{i\alpha^A \hat{\mathcal{C}}_A}, \\ \hat{\mathcal{P}}_{\text{phys}} &:= \mathbb{E}_{\text{even}} \circ \hat{\mathcal{P}}_{\text{RAQ}}, \quad \mathbb{E}_{\text{even}}(X) = \tfrac{1}{2}(X + G_{xy} X G_{xy}). \end{aligned} \quad (6.21)$$

Standard RAQ technology (choice of dense domain \mathcal{D} , distributional completion, gauge–volume normalization for non–compact groups) ensures well–posedness; for linear constraints on free fields the continuous average implements $\prod_A \delta(\hat{\mathcal{C}}_A)$ as a sesquilinear form, while interactions are handled by adiabatic/regularized averages before taking the physical limit.

Horizon bipartition, modular flow, and swap symmetry. On the Rindler wedge algebra the modular Hamiltonian equals the boost generator; locality on null cuts renders it quasi-local, so the swap action G_{xy} and the modular flow commute

on the algebra generated by trans–horizon pairs (up to edge–mode centers). This validates the evaluation of (6.21) directly on $\mathcal{H}_{\text{out}} \otimes \mathcal{H}_{\text{in}}$ using the symmetric/antisymmetric decomposition.

Theorem 6.3 (Asymptotic halving under RAQ gauge projection). *Let $\mathcal{H}_{\text{kin}} = \mathcal{H}_{\text{out}} \otimes \mathcal{H}_{\text{in}}$ with $\dim \mathcal{H}_{\text{out}} = \dim \mathcal{H}_{\text{in}} = D < \infty$. Assume: (i) the continuous constraints in (6.18) act reducibly with equal multiplicities across out/in factors on the near–horizon regulated algebra; (ii) the swap G_{xy} exchanges the factors and commutes with the continuous average; (iii) the Hartle–Hawking/KMS sector is invariant under the diagonal action of G_{xy} . Then the projector (6.21) induces an even projection on \mathcal{H}_{kin} with normalized trace*

$$\frac{\text{Tr}_{\mathcal{H}_{\text{kin}}}[\hat{\mathcal{P}}_{\text{phys}}]}{\text{Tr}_{\mathcal{H}_{\text{kin}}}[\mathbf{1}]} = \frac{D(D \pm 1)/2}{D^2} = \frac{1}{2} \pm \frac{1}{2D} \xrightarrow[D \rightarrow \infty]{} \frac{1}{2}, \quad (6.22)$$

where \pm select the even/odd sector; the physical sector is even. Hence the gauge projection contributes a universal factor $1/2$ to the leading area term.

Sketch. The continuous average restricts to the joint kernel of $\widehat{\mathcal{C}}$ with equal multiplicities on out/in (assumption (i)), so the residual multiplicity factorizes. The discrete average splits $\mathcal{H}_{\text{out}} \otimes \mathcal{H}_{\text{in}}$ into the symmetric/antisymmetric \mathbb{Z}_2 representations of dimensions $D(D \pm 1)/2$, giving (6.22). Invariance of the HH/KMS sector under G_{xy} and its commutation with modular flow single out the even (orientation–preserving) sector as physical. The $1/(2D)$ correction is subleading and vanishes in the thermodynamic ($D \rightarrow \infty$) limit. \square

Proposition 6.4 (Edge/center modes and robustness). *Gauge centers localized at the entangling surface induce superselection sectors (edge modes). The RAQ projection implements the gauge–invariant algebra; center degrees contribute only additive $\mathcal{O}(1)$ terms to the entropy and do not modify the A –proportional leading coefficient. Measure–normalization ambiguities in RAQ likewise shift only the constant part of S .*

Corollary 6.2 (The universal $\frac{1}{4}$ prefactor). *Let $N_{\text{naive}} = A/\xi^2$ be the UV mode count at correlation length ξ (Sec. 5). Bipartite pairing across the horizon yields $N_{\text{bi}} = \frac{1}{2} A/\xi^2$. The RAQ gauge projection (Theorem 6.3) contributes another*

factor $\frac{1}{2}$, so the number of physical horizon modes is

$$N_{\text{phys}} = \frac{1}{4} \frac{A}{\xi^2}.$$

With the KMS-weighted mean pair entropy $\bar{s} = \mathcal{O}(1)$ (cf. Prop. 6.6), the entropy is

$$S_{\text{BH}} = N_{\text{phys}} \bar{s} = \frac{A}{4\xi^2} \left(1 + \mathcal{O}(\xi^2/A) \right) \xrightarrow{\xi=L_P} \frac{A}{4L_P^2} + \mathcal{O}(1). \quad (6.23)$$

The $\mathcal{O}(1)$ and further subleading terms collect edge/center contributions, RAQ measure choices, and curvature-sensitive one-loop (heat-kernel) corrections, to be quantified in subsequent sections.

Consistency with WESH–Noether and modular structure. WESH–Noether enforces $\mathcal{L}^\dagger[\hat{\mathcal{C}}_A] = 0$, ensuring that the constraint surface is invariant under the pre-geometric flow (path independence). Thus the RAQ projector is not an external device but the representation-theoretic implementation of the very conservation principle encoded in the generator. On the wedge algebra, the modular Hamiltonian (boost) commutes with G_{xy} , so thermality (Sec. 6.2) and RAQ projection are compatible. The resulting chain,

WESH–Noether \Rightarrow RAQ-consistent constraints \Rightarrow even projection \Rightarrow universal $1/2$, combined with bipartite halving and $\bar{s} \simeq 1$, yields the $\frac{1}{4}$ law from first principles.

RAQ constraints vs. horizon superselection: a clean factorization

Definition 6.3 (Two-step physical projection). Let $\hat{\mathcal{C}}_A$ denote the first-class constraints (WDW Hamiltonian and spatial diffeomorphisms, including possible global T-charge) acting on the regulated bipartite Hilbert space $\mathcal{H}_{\text{kin}} \simeq \mathcal{H}_{\text{out}} \otimes \mathcal{H}_{\text{in}}$, and let G_{xy} be the unitary implementing the trans-horizon swap. Define:

(i) **RAQ / constraint average.**

$$\hat{\mathcal{P}}_{\text{RAQ}} := \int_{G_{\text{cont}}} d\mu(\alpha) e^{i\alpha^A \hat{\mathcal{C}}_A}, \quad (6.24)$$

When acting on operators $X \in \mathcal{B}(\mathcal{H}_{\text{kin}})$, the average is understood via the adjoint action, $X \mapsto \int d\mu(\alpha) e^{i\alpha^A \hat{\mathcal{C}}_A} X e^{-i\alpha^A \hat{\mathcal{C}}_A}$.

(ii) **Horizon even-sector expectation.**

$$\mathbb{E}_{\text{even}}(X) = \frac{1}{2} (X + G_{xy} X G_{xy}), \quad (6.25a)$$

$$X \in \mathcal{B}(\mathcal{H}_{\text{kin}}). \quad (6.25b)$$

Swap projectors. On the regulated bipartite space, the swap satisfies $G_{xy}^\dagger = G_{xy}$ and $G_{xy}^2 = \mathbf{1}$. Let $P_\pm := \frac{1}{2}(\mathbf{1} \pm G_{xy})$. Then $\mathbb{E}_{\text{even}}(X) = \frac{1}{2}(X + G_{xy} X G_{xy}) = P_+ X P_+ + P_- X P_-$.

The physical superselection sector is the + block (swap-even states), so the halving in the mode count uses P_+ : $\text{Tr}(P_+)/\text{Tr}(\mathbf{1}) = D(D+1)/(2D^2) = \frac{1}{2} + \frac{1}{2D}$.

The physical map factorizes as

$$\boxed{\hat{\mathcal{P}}_{\text{phys}} = \mathbb{E}_{\text{even}} \circ \hat{\mathcal{P}}_{\text{RAQ}}.} \quad (6.26)$$

Remark 6.6 (Swap–even is not a gauge average). The second factor \mathbb{E}_{even} is a normal, completely positive idempotent (a conditional expectation) onto the even subalgebra fixed by G_{xy} ; it implements a boundary superselection tied to edge–mode coherence at the entangling surface (horizon), rather than a quotient by a first–class gauge constraint. In gravitational and gauge theories, the correct localization of degrees of freedom on boundaries requires an extended phase space with edge modes; horizon “soft” charges provide precisely such boundary data and organize physical sectors. The even sector singled out by modular covariance/KMS on the wedge coincides with the sector compatible with these boundary symmetries (soft hair / edge–mode literature).

Proposition 6.5 (Commutation, trace factorization, and halving). Suppose (a) the constraint set $\{\hat{\mathcal{C}}_A\}$ and the swap G_{xy} commute on the regulated wedge algebra (modulo standard domain issues), which is ensured when the adjoint WESH generator conserves the global charges (WESH–Noether) and the wedge modular flow respects the bipartition; (b) $\dim \mathcal{H}_{\text{out}} = \dim \mathcal{H}_{\text{in}} = D < \infty$ at fixed regulator. Then:

1. \mathbb{E}_{even} and $\hat{\mathcal{P}}_{\text{RAQ}}$ commute on $\mathcal{B}(\mathcal{H}_{\text{kin}})$, hence (6.26) is well–defined and independent of order.

2. The swap-even subspace $P_+(\mathcal{H}_{\text{out}} \otimes \mathcal{H}_{\text{in}})$ has dimension $\text{Tr}(P_+) = D(D+1)/2$. Consequently,

$$\frac{\text{Tr}_{\mathcal{H}_{\text{kin}}}[P_+]}{\text{Tr}_{\mathcal{H}_{\text{kin}}}[\mathbf{1}]} = \frac{D(D+1)/2}{D^2} = \frac{1}{2} + \frac{1}{2D} \xrightarrow[D \rightarrow \infty]{} \frac{1}{2}. \quad (6.27)$$

Proof sketch. (1) WESH–Noether at generator level implies constraint charges commute with the Lindblad set and with the effective Hamiltonian; modular covariance on the wedge makes G_{xy} a symmetry of the near-horizon algebra. These properties imply $[\hat{\mathcal{C}}_A, G_{xy}] = 0$ on the regulated domain, hence $\hat{\mathcal{P}}_{\text{RAQ}}\mathbb{E}_{\text{even}} = \mathbb{E}_{\text{even}}\hat{\mathcal{P}}_{\text{RAQ}}$. (2) The swap decomposition into symmetric/antisymmetric tensors has dimensions $D(D\pm 1)/2$. Traces factorize at fixed regulator because $\hat{\mathcal{P}}_{\text{RAQ}}$ acts diagonally on the joint kernel of the constraints, while \mathbb{E}_{even} is block-diagonal in the swap basis; (6.27) follows. \square

Note. Generator-level conservation is established in Appendix G, Prop. G.2. Modular compatibility follows from the pre-geometric path independence detailed in Appendix C.2. Edge-mode/soft-symmetry structures justify the boundary superselection through the horizon-even conditional expectation.

Corollary 6.3 (From two-step projection to the $\frac{1}{4}$ law). At leading order, the physical mode count is $N_{\text{phys}} = (A/\xi^2) \times \underbrace{\frac{1}{2}}_{\text{bipartite halving}} \times \underbrace{\frac{1}{2}}_{\text{swap-even}} = A/(4\xi^2)$,

and with $\xi \simeq L_P$ and $\bar{s} = \mathcal{O}(1)$ (cf. Prop. 6.6 and Remark 6.9) one obtains $S_{\text{BH}} = A/(4L_P^2) + \mathcal{O}(\ln A, 1)$. The swap-even factor originates from boundary superselection (not gauge fixing) and is therefore robust under the inclusion of gravitational edge modes/soft charges.

Remark 6.7 (Independence of the two halving factors). The prefactor $1/4$ in the Bekenstein–Hawking law arises from two independent reductions acting at distinct levels:

1. **Bipartite pairing (geometric/combinatorial).** The bilocal mediator $L_{xy} = \hat{T}^2(x) - \hat{T}^2(y)$ couples trans-horizon modes within the correlation length ξ . As a consequence, the A/ξ^2 horizon cells organize into approximately $A/(2\xi^2)$ entangled pairs $(\text{out}_i, \text{in}_i)$. The entanglement entropy is, by definition, the von Neumann entropy of the reduced state on \mathcal{H}_{out} (partial trace over \mathcal{H}_{in}), but the leading extensive factor is set by how many independent pairs exist. In the regime where each pair contributes on average

$\bar{s} = \mathcal{O}(1)$ (cf. Prop. 6.6) to the entropy (Sec. 6.4), this geometric/combinatorial pairing yields the first factor $1/2$.

2. **Modular superselection (algebraic/boundary).** On top of this pairing structure, the conditional expectation \mathbb{E}_{even} onto the swap-symmetric sector implements the modular/CPT structure of the KMS state on the horizon edge algebra. This is a boundary superselection rule—not a gauge constraint—which removes antisymmetric configurations incompatible with the modular horizon algebra. As shown in Proposition 6.5, \mathbb{E}_{even} reduces the normalized trace ratio by an additional factor $1/2$ in the large-area limit.

These reductions are logically independent: the first concerns how many entangled units exist (geometric/combinatorial pairing), the second concerns which states are physically admissible on the horizon edge (algebraic/modular superselection). Their product, combined with the spectral concentration $\bar{s} = \mathcal{O}(1)$ (Prop. 6.6), yields

$$S_{\text{BH}} = \frac{A}{4L_P^2} + \gamma \ln \frac{A}{L_P^2} + k_0 + \mathcal{O}\left(\frac{L_P^2}{A}\right)$$

without any double counting of trans-horizon degrees of freedom.

Context note (internal consistency). The separation (6.26) is compatible with the pre-geometric WESH–Noether constraint algebra at generator level (no–vorticity/path–independence) and with wedge modular structure on null surfaces, ensuring that RAQ and horizon superselection can be implemented without logical overlap.

6.4 Leading order and robustness: spectral control and EFT stability of the kernel

Overview. We place the leading Bekenstein–Hawking law on firm ground by controlling the near-horizon spectral weight that enters the mean pair-entropy and by promoting the undeformed-kernel choice $\xi \simeq L_P$ to a controlled effective-field-theory (EFT) approximation in curved backgrounds. The first part derives the low-frequency structure of the WESH–HH weight and a quantitative concentration bound for the spectral average \bar{s} ; the second part quantifies curvature-induced deformations of

the mediator scale ξ and shows that they are parametrically suppressed on macroscopic horizons.

Spectral structure at low frequency and concentration of the entropy average. With the KMS fixed point on the wedge (Sec. 6.2) and the physical projection (Sec. 6.3), the mean pair-entropy is

$$\bar{s} = \frac{\int_0^\infty \frac{d\omega}{2\pi} W_{\text{HH}}(\omega) s(\beta_H \omega)}{\int_0^\infty \frac{d\omega}{2\pi} W_{\text{HH}}(\omega)}, \quad s(x) = \frac{x}{e^x - 1} - \ln(1 - e^{-x}), \quad \beta_H = \frac{2\pi}{\kappa}. \quad (6.28)$$

Here

$$W_{\text{HH}}(\omega) = \Gamma_{\text{WESH}}(\omega) \varrho(\omega) \frac{e^{-\beta_H \omega}}{1 - e^{-\beta_H \omega}} = \omega^{2+p} F(\omega \xi) \frac{e^{-\beta_H \omega}}{1 - e^{-\beta_H \omega}}, \quad (6.29)$$

where $p \geq 0$ parametrizes the near-horizon density of states and F is smooth, positive and single-peaked with $F(0) = 1$ and UV suppression for $\omega \gtrsim \xi^{-1}$. For a minimally coupled scalar field on a Schwarzschild background one has

$$p = 0,$$

corresponding to an essentially flat density in tortoise coordinates. For higher spins or in Kerr backgrounds, p receives $\mathcal{O}(1)$ corrections (e.g. of order $(a/M)^2$ in the slow-rotation regime), but remains bounded and does not alter the conclusion that $\bar{s} = \mathcal{O}(1)$ independently of A . Let $x = \beta_H \omega$ and write $\tilde{W}(x) := x^n \tilde{F}(x) e^{-x} (1 - e^{-x})^{-1}$ with $n = 2 + p$ and $\tilde{F}(x) = F(x \xi / \beta_H)$. The peak x_* satisfies

$$\frac{d}{dx} \ln \tilde{W}(x) \Big|_{x_*} = 0 \iff \frac{n}{x_*} - 1 - \frac{1}{e^{x_*} - 1} = -\frac{d}{dx} \ln \tilde{F}(x) \Big|_{x_*} = \mathcal{O}(\kappa \xi), \quad (6.30)$$

so $x_* = \mathcal{O}(1)$ and, for slowly varying \tilde{F} , $x_* = x_n + \mathcal{O}(\kappa \xi)$, where x_n is the $\mathcal{O}(1)$ solution of $\frac{n}{x} - 1 - \frac{1}{e^{x-1}} = 0$.

Proposition 6.6 (Concentration of the spectral average). *If \tilde{W} is positive, smooth, single-peaked with thermal width $\Delta x = \mathcal{O}(1)$, then*

$$\bar{s} = s(x_*) + \delta s, \quad |\delta s| \leq \sup_{x \in I} |s'(x)| \sqrt{\text{Var}_{\tilde{W}}(x)} + \frac{1}{2} \sup_{x \in I} |s''(x)| \text{Var}_{\tilde{W}}(x),$$

where $\text{Var}_{\tilde{W}}(x) := \mathbb{E}_{\tilde{W}}[(x - x_*)^2]$ denotes the second moment around the mode, for any compact interval $I = [\varepsilon, \Lambda]$ with $0 < \varepsilon < x_* < \Lambda$ covering the bulk of \tilde{W} . The tail $x > \Lambda$ is exponentially suppressed by the thermal factor (and further suppressed by F); the tail $x < \varepsilon$ is power-law suppressed ($\tilde{W} \sim x^{n-1}$) and has total weight $\mathcal{O}(\varepsilon^n)$ (hence a negligible contribution to \bar{s} , at worst logarithmically enhanced). Since $\text{Var}_{\tilde{W}}(x) = \mathcal{O}(1)$ (thermal) and s', s'' are bounded on I ,

$$\bar{s} = s(x_*) + \delta s. \quad (6.31)$$

In particular, \bar{s} remains an $\mathcal{O}(1)$ quantity fixed by the KMS weight (no hidden A -dependence).

Sketch. Normalize \tilde{W} to a probability density on \mathbb{R}_+ and expand s to second order around x_* and use $\mathbb{E}|x - x_*| \leq \sqrt{\text{Var}_{\tilde{W}}(x)}$. The thermal width $\Delta x = \mathcal{O}(1)$ gives $\text{Var}_{\tilde{W}}(x) = \mathcal{O}(1)$; with s', s'' bounded on the bulk interval $I = [\varepsilon, \Lambda]$, the correction δs is $\mathcal{O}(1)$ but A -independent. The tail $x < \varepsilon$ has weight $\mathcal{O}(\varepsilon^n)$ by the x^{n-1} behavior near zero, hence its contribution to \bar{s} is negligible (at worst logarithmically enhanced); the tail $x > \Lambda$ is exponentially suppressed by the thermal factor (and further suppressed by F). \square

Remark 6.8 (Origin of $\bar{s} = \mathcal{O}(1)$). *The result $\bar{s} = s(x_*) + \delta s$ with $x_* = \mathcal{O}(1)$ is a structural consequence of the KMS spectral weight, not a numerical coincidence. The bosonic pair-entropy function $s(x) = x/(e^x - 1) - \ln(1 - e^{-x})$ is of order unity for $x = \mathcal{O}(1)$; since the KMS weight peaks at $x_* = \mathcal{O}(1)$, the spectral average \bar{s} is automatically of order unity. The value of \bar{s} is fixed by the KMS spectral structure (not by A); it is not a tunable parameter but a consequence of the microscopic physics encoded in p and the WESH kernel.*

Remark 6.9 (Role of the single-pair entropy in the $\frac{1}{4}$ law). *The $1/4$ prefactor is fixed by the two structural $1/2$ reductions (bipartite pairing and swap-even boundary superselection, Sec. 6.3). The spectral average $\bar{s} = \mathcal{O}(1)$ (Prop. 6.6) multiplies N_{phys} as an overall A -independent constant and only affects the identification of the microscopic cutoff ξ with the phenomenological Planck scale in the matching to the emergent gravitational coupling.*

EFT stability of the kernel: curvature-induced deformations and domain of validity. Interpreting the mediator scale as $m_T = \xi^{-1}$, curvature renormalizes the quadratic kernel via diffeomorphism-invariant local terms:

$$m_{\text{eff}}^2 = m_T^2 + \alpha_1 R + \alpha_2 R_{\mu\nu} R^{\mu\nu} + \alpha_3 R_{\mu\nu\rho\sigma} R^{\mu\nu\rho\sigma} + \dots, \quad (6.32)$$

with Wilson coefficients α_i set at the Planck scale. For Schwarzschild, $R = 0$ while $K := R_{\mu\nu\rho\sigma} R^{\mu\nu\rho\sigma} \Big|_{r \sim r_H} \sim r_H^{-4}$. Naturalness suggests $\alpha_3 = \mathcal{O}(L_P^2)$, giving

$$\begin{aligned} \delta m_T^2 &\sim \alpha_3 K \sim L_P^2 K, \\ \frac{\delta m_T^2}{m_T^2} &\sim K L_P^4 = \mathcal{O}\left((L_P/r_H)^4\right), \\ \frac{\delta\xi}{\xi} &\simeq -\frac{1}{2} \frac{\delta m_T^2}{m_T^2}. \end{aligned} \quad (6.33)$$

Extrinsic-curvature deformations at the horizon affect subleading coefficients (e.g. the logarithmic term) at order κL_P but do not alter the leading area law.

Proposition 6.7 (Controlled kernel approximation and leading law). *For macroscopic Schwarzschild horizons ($r_H \gg L_P$) one has*

$$\kappa\xi = \mathcal{O}(L_P/r_H) \ll 1, \quad \frac{\delta\xi}{\xi} = \mathcal{O}\left((L_P/r_H)^4\right).$$

Consequently:

- (i) $x_\star = x_n + \mathcal{O}(\kappa\xi)$, where $x_n = \mathcal{O}(1)$ solves $\frac{n}{x} - 1 - \frac{1}{e^x - 1} = 0$ (cf. Prop. 6.6);
- (ii) $\text{Var}_{\tilde{W}}(x) = \mathcal{O}(1)$ (thermal width, cf. Prop. 6.6);
- (iii) $\bar{s} = \mathcal{O}(1)$ (no hidden A -dependence). Therefore the leading Bekenstein–Hawking term derived in Secs. 6.2–6.3 is stable under the EFT kernel deformations controlled here, and one retains

$$S_{\text{BH}} = \frac{A}{4L_P^2} + \gamma \ln \frac{A}{L_P^2} + k_0 + \mathcal{O}\left(\frac{L_P^2}{A}\right), \quad (6.34)$$

where the subleading terms are controlled within the EFT expansion.

Sketch. Use $\kappa \sim r_H^{-1}$ and $\xi \sim L_P$ to obtain $\kappa\xi \sim L_P/r_H$. Item (i) follows from (6.30); item (ii) from Prop. 6.6. For (iii), $\bar{s} = \mathcal{O}(1)$ (Remark 6.8) guarantees that the spectral integral cannot generate any hidden A -dependent prefactor; hence it cannot renormalize the leading coefficient fixed by the two $1/2$ factors (pairing and swap—even boundary superselection) in Secs. 6.2–6.3. Kernel deformations are suppressed by (6.33), so only subleading terms are affected at this order. \square

Remark 6.10 (Thermal width vs. coarse-graining error). *The estimate $\text{Var}_{\tilde{W}}(x) = \mathcal{O}(1)$ refers to the thermal width of the KMS weight in the dimensionless variable $x = \beta_H \omega$. The $\mathcal{O}((\kappa\xi)^2)$ terms appearing in Lemma 6.5 arise instead from ξ -scale null-buffer coarse-graining on the modular length κ^{-1} , and are logically independent of the thermal variance.*

Remark 6.11 (Domain of validity). *For astrophysical black holes $r_H/L_P \gg 1$, the deformation $\delta\xi/\xi$ is negligible at leading order. For primordial or near-Planckian horizons the expansion in L_P/r_H must be resummed; shifts of x_* and dressing of subleading coefficients then provide a concrete arena for beyond-leading-order predictions within the same formalism.*

6.5 Subleading corrections and unification with GR: Δ_{phys} as Hessian and the logarithmic term via replicas

Overview. Quantum corrections to black-hole entropy in QFTT–WESH are controlled by the same effective action whose first variation yields the emergent Einstein sector. At one loop, the physical fluctuation operator is the Hessian of the gauge–fixed WESH effective action evaluated on a black–hole background. The logarithmic coefficient is then obtained from the replica (or conical) variation of the horizon–local heat–kernel coefficient. This subsection formalizes these statements and makes the connection to the pre-geometric and modular structures developed in Secs. 1.3, 6.2 and 6.3 explicit.

Physical fluctuation operator. Let $S_{\text{eff}}[\Phi]$ denote the (gauge-fixed) WESH effective action whose stationary points reproduce the GR limit (Sec. 4). For a stationary black-hole background $\bar{\Phi}$ (metric, time-field, mediator, gauge-fixing and ghost data), write $\varphi = \Phi - \bar{\Phi}$. The quadratic expansion is

$$S_{\text{eff}}[\bar{\Phi} + \varphi] = S_{\text{eff}}[\bar{\Phi}] + \frac{1}{2} \langle \varphi, \Delta_{\text{phys}} \varphi \rangle + \mathcal{O}(\varphi^3), \quad (6.35)$$

where

$$\Delta_{\text{phys}} \equiv \left. \frac{\delta^2 S_{\text{eff}}}{\delta \Phi \delta \Phi} \right|_{\bar{\Phi}}. \quad (6.36)$$

Blockwise,

$$\Delta_{\text{phys}} = \begin{bmatrix} \Delta_g & \Delta_{gT} & \cdots \\ \Delta_{Tg} & \Delta_T & \cdots \\ \vdots & \vdots & \ddots \end{bmatrix} \oplus \Delta_{\text{gh}}, \quad (6.37)$$

where Δ_{gh} arises from Faddeev–Popov ghosts and gauge fixing. The refined constraint projection (RAQ/group averaging, Sec. 6.3) implements the physical subspace at quadratic order: null directions associated with first-class constraints are quotiented before taking determinants, so that only gauge-inequivalent modes contribute.

Theorem 6.4 (One-loop generator of subleading entropy). *Let S_{eff} be the WESH effective action whose classical limit yields GR. Then the one-loop correction to black-hole entropy is governed by the quadratic form defined by $\Delta_{\text{phys}} = \delta^2 S_{\text{eff}} / \delta \Phi^2 |_{\bar{\Phi}}$ on the RAQ-projected fluctuation space. In particular, the logarithmic coefficient γ is determined by the horizon-local Seeley–DeWitt density of Δ_{phys} on the replica/conical geometry.*

Box 8: Logarithmic Corrections via the WESH Hessian

Setup. Let $\mathcal{M}^{(\alpha)}$ be the α -replicated Euclidean manifold with angular periodicity $2\pi\alpha$ around the smooth horizon cross-section \mathcal{H} . Define the gauge-fixed WESH effective action pulled back to $\mathcal{M}^{(\alpha)}$ as $S_{\text{eff}}^{(\alpha)}[\Phi]$, with background $\bar{\Phi}$ solving the classical equations away from the conical locus (and regular at $\alpha = 1$), with the standard conical/brane prescription at the tip. Writing $\Phi = \bar{\Phi} + \varphi$ and expanding to quadratic order,

$$S_{\text{eff}}^{(\alpha)}[\bar{\Phi} + \varphi] = S_{\text{eff}}^{(\alpha)}[\bar{\Phi}] + \frac{1}{2} \langle \varphi, \Delta_{\text{phys}}^{(\alpha)} \varphi \rangle + \mathcal{O}(\varphi^3),$$

$$\Delta_{\text{phys}}^{(\alpha)} := \left. \frac{\delta^2 S_{\text{eff}}^{(\alpha)}}{\delta \Phi \delta \Phi} \right|_{\bar{\Phi}}.$$

Here $\Delta_{\text{phys}}^{(\alpha)}$ is the *projected* quadratic operator on the physical fluctuation space: it includes Faddeev-Popov ghosts, gauge-fixing, and the RAQ/constraint projection (Sec. 6.3), so that pure-gauge/constraint zero-modes are removed at the outset (cf. App. F-H).

Gaussian path integral and zeta regularization. The one-loop partition function on $\mathcal{M}^{(\alpha)}$ is Gaussian,

$$Z_{\text{1-loop}}(\alpha) \propto (\text{sdet } \Delta_{\text{phys}}^{(\alpha)})^{-1/2}, \quad W_1(\alpha) := -\ln Z_{\text{1-loop}}(\alpha) = \frac{1}{2} \ln \text{sdet } \Delta_{\text{phys}}^{(\alpha)}.$$

Using zeta-function regularization,

$$\begin{aligned} \ln \det_{\zeta} \Delta &= - \left. \frac{d}{dz} \right|_{z=0} \frac{1}{\Gamma(z)} \int_0^{\infty} d\tau \tau^{z-1} \text{Tr}(e^{-\tau \Delta}) \\ &= - \int_{0^+} \frac{d\tau}{\tau} \text{Tr}(e^{-\tau \Delta}) + \dots, \end{aligned}$$

and in $d = 4$ the heat-kernel expansion $\text{Tr}(e^{-\tau \Delta}) \sim (4\pi\tau)^{-2} \sum_{k \geq 0} a_k(\Delta) \tau^k$ shows that the *logarithmic* sensitivity comes entirely from a_2 .

Replica extraction of the logarithmic coefficient. The von Neumann entropy follows from $S_{\text{1-loop}} = (\alpha \partial_{\alpha} - 1) W_1(\alpha)|_{\alpha=1}$. Isolating the log term in $d = 4$:

$$\gamma = \frac{1}{2} \partial_{\alpha} \left[a_2 \left(\Delta_{\text{phys}}^{(\alpha)} \right) - \alpha a_2 \left(\Delta_{\text{phys}}^{(1)} \right) \right]_{\alpha=1},$$

$$S_{\text{BH}} = \frac{A}{4L_P^2} + \gamma \ln \frac{A}{L_P^2} + \dots$$

(6.38)

Equation (6.38) is the precise Hessian→replica link used in Sec. 6.5.

Horizon-local form. On smooth sections \mathcal{H} , the conical variation localizes on \mathcal{H} :

$$a_2(\Delta_{\text{phys}}^{(\alpha)}) - \alpha a_2(\Delta_{\text{phys}}^{(1)}) = \int_{\mathcal{H}} dA \left[b_1(\alpha)R_{\mathcal{H}} + b_2(\alpha)K_{ab}K^{ab} + b_3(\alpha)\text{Tr } E + b_4(\alpha)\text{Tr}(\Omega_{ab}\Omega^{ab}) \right],$$

where the coefficient functions $b_i(\alpha)$ encode the purely conical contribution and satisfy $b_i(1) = 0$.

so that for bifurcation surfaces of stationary Killing horizons (in particular Schwarzschild, where $K_{ab} = 0$) one gets $\gamma = \sigma_{\text{phys}} \chi(\mathcal{H})$ with $\chi(\mathcal{H}) = \frac{1}{4\pi} \int_{\mathcal{H}} R_{\mathcal{H}} dA$; for non-minimal/deformed horizon sections the extrinsic piece $\propto \partial_\alpha b_2(\alpha)|_{\alpha=1} \int_{\mathcal{H}} K_{ab}K^{ab} dA$ yields a calculable shift. For stationary Kerr, rotation dependence is encoded in the full horizon-local invariants of Δ_{phys} (in particular through the E and Ω sectors), with extrinsic terms contributing only when the chosen section is not minimal.

Remarks.

1. *Same S_{eff} on and off the cone.* $\Delta_{\text{phys}}^{(\alpha)}$ is the Hessian of the same S_{eff} that yields GR at tree level (Sec. 4); RAQ/constraint projection ensures gauge-invariant determinants.
2. *Consistency with gravitational replica / cosmic branes.* For $S_{\text{eff}} \rightarrow S_{\text{EH}}$, (6.38) reproduces Lewkowycz-Maldacena/Dong; extra WESH fields modify a_2 in the standard way.
3. *Boundary terms and edge modes.* GHY/Hayward and edge modes enter via gauge-fixing and physical projection: they shift a_2 with local functions on the horizon without affecting the leading $A/(4L_P^2)$.
4. *Scheme independence.* Power divergences renormalize the couplings (e.g., $1/G_N$); the log coefficient γ is universal.

Replica/cone evaluation and the log coefficient. On the Euclidean α -replica ($2\pi\alpha$ periodicity around the horizon), the one-loop generating functional is

$$W_1(\alpha) = -\ln Z_{\text{1-loop}}(\alpha) = \frac{1}{2} \ln \det(\Delta_{\text{phys}}^{(\alpha)}), \quad (6.39)$$

with $\Delta_{\text{phys}}^{(\alpha)}$ the lifted operator (including ghosts and the physical projection). The von Neumann entropy follows from

$$S_{\text{1-loop}} = (\alpha \partial_\alpha - 1) W_1(\alpha)|_{\alpha=1} \quad (6.40)$$

Using the heat-kernel representation and the small- s expansion in $d = 4$,

$$\begin{aligned} \ln \det \Delta &= - \int_0^\infty \frac{d\tau}{\tau} \text{Tr } e^{-\tau\Delta}, \\ \text{Tr } e^{-\tau\Delta_{\text{phys}}^{(\alpha)}} &\sim \frac{1}{(4\pi\tau)^2} \sum_{k \geq 0} a_k [\Delta_{\text{phys}}^{(\alpha)}] \tau^k, \end{aligned}$$

the ln-sensitive piece is controlled by a_2 . Varying with respect to α yields

$$\gamma = \frac{1}{2} \partial_\alpha \Big|_{\alpha=1} \left(a_2 [\Delta_{\text{phys}}^{(\alpha)}] - \alpha a_2 [\Delta_{\text{phys}}^{(1)}] \right), \quad S_{\text{BH}} = \frac{A}{4L_P^2} + \gamma \ln \frac{A}{L_P^2} + \dots \quad (6.41)$$

Horizon-local structure. The coefficient a_2 on a smooth horizon cross-section \mathcal{H} decomposes into intrinsic/extrinsic invariants:

$$\begin{aligned} a_2 [\Delta_{\text{phys}}^{(\alpha)}] - \alpha a_2 [\Delta_{\text{phys}}^{(1)}] &= \int_{\mathcal{H}} dA \left[b_1(\alpha) R_{\mathcal{H}} + b_2(\alpha) K_{ab} K^{ab} \right. \\ &\quad \left. + b_3(\alpha) \text{Tr } E + b_4(\alpha) \text{Tr } \Omega_{ab} \Omega^{ab} \right], \end{aligned} \quad (6.42)$$

where the coefficient functions $b_i(\alpha)$ encode the purely conical contribution and satisfy $b_i(1) = 0$.

where $R_{\mathcal{H}}$ is the intrinsic scalar curvature of \mathcal{H} , K_{ab} its extrinsic curvature, E the endomorphism term in the second-order operator, and Ω the field-strength of

the relevant bundle connection after gauge fixing. The sector decomposition inherited from Δ_{phys} naturally splits a time-field contribution and a constraint/ghost (projection) contribution. For regular spherical horizons ($K_{ab} = 0$),

$$\boxed{\begin{aligned}\gamma &= \sigma_{\text{phys}} \chi(\mathcal{H}), & \sigma_{\text{phys}} &= \sigma_T + \sigma_{\text{proj}}, \\ \chi(\mathcal{H}) &= \frac{1}{4\pi} \int_{\mathcal{H}} R_{\mathcal{H}} dA,\end{aligned}} \quad (6.43)$$

while for deformed horizons (e.g. rotating cases) the extrinsic term produces a calculable shift

$$\Delta\gamma = \frac{1}{2} \partial_\alpha b_2(\alpha) \Big|_{\alpha=1} \int_{\mathcal{H}} K_{ab} K^{ab} dA, \quad (6.44)$$

encoding spin-dependent corrections.

Remark 6.12 (Numerical value of σ_{phys}). *The coefficient σ_{phys} is fixed by the horizon-local Seeley–DeWitt density of the physical Hessian Δ_{phys} on the replica/conical geometry. Its explicit evaluation requires the full mode decomposition of Δ_{phys} , including time-field, metric, ghost and constraint sectors, and will be carried out in a dedicated follow-up. Here we only use the structural decomposition*

$$\gamma = \sigma_{\text{phys}} \chi(\mathcal{H}) + \Delta\gamma(J),$$

which is the falsifiable prediction of the WESH framework: different microscopic realizations give different σ_{phys} and $\Delta\gamma(J)$, but must respect this horizon-local form.

Renormalization and universality. The one-loop functional $\frac{1}{2} \ln \det(\Delta_{\text{phys}}/\mu^2)$ contains a renormalization scale μ . Area-divergent pieces renormalize $1/G_N$ and are absorbed by the classical $A/(4L_P^2)$ term; the remaining finite \ln -piece is universal and fixed by a_2 . Matching to the microscopic WESH scale $\xi^{-1} \sim L_P^{-1}$ ensures $\gamma = \mathcal{O}(1)$ with no dependence on long-distance details. Because Δ_{phys} is the Hessian of the same S_{eff} that yields GR at leading order, the field content, normalizations and gauge choices entering γ are not tunable inputs but are already fixed by the emergent sector and by the RAQ projection (Sec. 6.3).

Example: smooth S^2 and deformations. For a regular S^2 cross-section, $\chi(S^2) = 2$ and $K_{ab} = 0$, hence

$$\gamma_{S^2} = 2\sigma_{\text{phys}} \quad (\sigma_{\text{phys}} = \sigma_T + \sigma_{\text{proj}}).$$

For Kerr-type horizons, $K_{ab}K^{ab} \neq 0$ on generic sections and the b_2 -term in (6.42) generates a spin-dependent $\Delta\gamma[J]$. The same framework applies in NHEK limits and admits checks via null-surface modular Hamiltonians and Rényi continuations.

Synthesis. Equations (6.35)–(6.41) close the logical chain: the pre-geometric WESH–Noether constraint (Sec. 1.3) selects admissible generators; modular/KMS analysis on the wedge (Sec. 6.2) fixes the thermal structure; RAQ implements the physical projection (Sec. 6.3); and the same S_{eff} that yields the Einstein sector at leading order provides, through its Hessian Δ_{phys} , the universal logarithmic correction via the replica/cone method. The subleading structure is thus a horizon-local prediction tied to the very mechanism that produces the classical gravitational dynamics.

6.6 Kerr horizons: rotating KMS, hidden symmetries, and WESH thermodynamics

Overview. The WESH near-horizon thermodynamics extends from static to stationary rotating (Kerr) black holes once (i) the thermal flow is generated by the horizon Killing field $\chi^\mu = \partial_t^\mu + \Omega_H \partial_\phi^\mu$, so that KMS relations involve the corotating frequency $\tilde{\omega} \equiv \omega - m\Omega_H$, and (ii) the \hat{T}^2 channel is organized covariantly under the hidden symmetry tower generated by the principal conformal Killing–Yano tensor. With these replacements, the fixed-point/KMS derivation, the bipartite halving plus swap–even projection, and the Hessian/replica evaluation of logarithmic corrections carry over verbatim: the leading $A/4L_P^2$ law is universal, while subleading terms acquire Kerr-specific (spin-dependent) structure through the horizon-local invariants of Δ_{phys} (in particular the E and Ω sectors) and superradiant shifts in the spectral weights, with extrinsic terms contributing only for non-minimal/deformed sections.

Assumptions and notation. Work on a four-dimensional stationary axisymmetric Kerr spacetime with mass M and angular momentum $J = aM$. All KMS statements are understood on the near-horizon corotating wedge algebra (a local

statement). A global χ -KMS/Hartle–Hawking completion in asymptotically flat Kerr requires suitable boundary conditions to control superradiance, but is not needed for the wedge analysis used here. The outer horizon has surface gravity κ and angular velocity Ω_H . Frequencies decompose in azimuthal modes (ω, m) ; the corotating combination is $\tilde{\omega} = \omega - m\Omega_H$. Units $\hbar = c = k_B = G = 1$ are used. The WESH short-range scale remains $\xi \simeq L_P$ to leading order; curvature-induced renormalizations are treated in EFT and are suppressed by powers of L_P/M for macroscopic horizons.

Rotating KMS and detailed balance. Let $\mathcal{A}_{\text{wedge}}$ be the algebra of observables in the exterior corotating wedge adapted to χ^μ . A state $\sigma_{\chi\text{KMS}}$ is χ -KMS at $\beta_H = 2\pi/\kappa$ if for all $A, B \in \mathcal{A}_{\text{wedge}}$, $F_{A,B}(t) = \langle A \alpha_t^\chi(B) \rangle$ analytically extends to $0 < \text{Im } t < \beta_H$ and obeys $F_{A,B}(t + i\beta_H) = \langle \alpha_t^\chi(B) A \rangle$, where α_t^χ is the Heisenberg evolution generated by $K_\chi = i\mathcal{L}_\chi$. In Fourier modes,

$$\tilde{C}_\chi(-\omega, -m) = e^{-\beta_H(\omega - m\Omega_H)} \tilde{C}_\chi(\omega, m), \quad \beta_H = \frac{2\pi}{\kappa}. \quad (6.45)$$

Theorem 6.5 (Rotating KMS fixed point). *Under the pre-geometric WESH–Noether constraint (Sec. 1.3), locality/causality of the kernels, and wedge modular covariance, and assuming the Kerr analogue of the primitivity hypotheses used in the static wedge case (spectral regularity, cross-horizon support, null-plane Markovity), the WESH generator reduced to $\mathcal{A}_{\text{wedge}}$ is $\sigma_{\chi\text{KMS}}$ -detailed balanced, and $\sigma_{\chi\text{KMS}}$ is the unique faithful normal stationary state on $\mathcal{A}_{\text{wedge}}$. Consequently, the frequency-resolved up/down rates for the \hat{T}^2 channel satisfy*

$$\frac{\Gamma_\uparrow(\omega, m)}{\Gamma_\downarrow(\omega, m)} = \exp \left[-\beta_H(\omega - m\Omega_H) \right], \quad (6.46)$$

and the Kerr horizon weight entering spectral averages is

$$W_{\text{Kerr}}(\omega, m) = \Gamma_{\text{WESH}}(\omega, m) \rho_{\text{Kerr}}(\omega, m) \frac{e^{-\beta_H(\omega - m\Omega_H)}}{1 - e^{-\beta_H(\omega - m\Omega_H)}}. \quad (6.47)$$

Superradiance and positivity. Spectral averages (e.g. (6.49)) are understood over the corotating positive-frequency sector $\tilde{\omega} = \omega - m\Omega_H > 0$. The $\tilde{\omega} < 0$ (superradiant) contributions are accounted for by the KMS/detailed-balance pairing of modes, i.e. by mapping $(\omega, m) \leftrightarrow (-\omega, -m)$ using (6.45)–(6.46), so that the effective weight entering the averages is positive. Greybody factors/boundary conditions enter only through the positive response $\Gamma_{\text{WESH}} \rho_{\text{Kerr}}$. The bilocal WESH channel and the RAQ physical projection maintain complete positivity of the reduced dynamics as in the static case, with modular flow generated by K_χ .

Hidden-symmetry covariance of the dissipator. Kerr admits a principal CKY 2-form $h_{\mu\nu}$; its square yields the Killing tensor $K_{\mu\nu}$ that organizes separability. To align dissipation with this structure, define quadratic densities

$$\mathcal{O}_q(x) = \hat{T}_{\mu\nu}(x) (\mathcal{Q}^{\mu\nu})_{\alpha\beta} \hat{T}^{\alpha\beta}(x), \quad (\mathcal{Q})_q \in \text{Alg}[g_{\mu\nu}, K_{\mu\nu}, h_{\mu\nu}, \nabla], \quad (6.48)$$

and select the scalar in the hidden-symmetry decomposition as the dominant dissipative component. Near the horizon, Cauchy sections degenerate to null sheets generated by χ^μ ; the modular Hamiltonian is local along such null generators for weakly-coupled sectors, matching the corotating KMS structure (6.45).

Box 9: Kerr Dissipator Selection Principle

Set-up. Let (\mathcal{M}, g) be a Kerr (or NHEK) background with horizon Killing field $\chi^\mu = \partial_t^\mu + \Omega_H \partial_\phi^\mu$, principal conformal Killing–Yano form $h_{\mu\nu}$ and associated Killing tensor $K_{\mu\nu}$. Denote by $K_\chi \equiv i\mathcal{L}_\chi$ the corotating modular generator and by $\sigma_{\chi\text{KMS}} \propto e^{-\beta_H K_\chi}$ the χ –KMS state at $\beta_H = 2\pi/\kappa$. On the wedge algebra $\mathfrak{A}(\mathcal{W}_\chi)$, equip observables with the reversible inner product $\langle A, B \rangle_\chi := \text{Tr}(\sigma_{\chi\text{KMS}}^{1/2} A^\dagger \sigma_{\chi\text{KMS}}^{1/2} B)$. Consider admissible quadratic densities for the WESH dissipator of the form

$$\mathcal{O}_q(x) = T_{\mu\nu}(x) (\mathcal{Q}^{\mu\nu})_{\alpha\beta} T^{\alpha\beta}(x), \quad (\mathcal{Q})_q \in \text{Alg}[g_{..}, K_{..}, h_{..}, \nabla.],$$

with exponentially causal kernel of range ξ as in Sec. 6.2, and subject to the WESH–Noether commutant constraints $[H_{\text{eff}}, \hat{Q}_a] = [\mathcal{O}_q(x), \hat{Q}_a] = 0$ for all global charges \hat{Q}_a (Appendix H).

Dirichlet form and spectral gap. For a GKSL generator \mathcal{L}_q built from \mathcal{O}_q and its bilocal difference $L_{xy}^{(q)}$, reversibility with respect to $\sigma_{\chi\text{KMS}}$ (detailed balance) implies that \mathcal{L}_q is self-adjoint in $\langle \cdot, \cdot \rangle_\chi$ and defines the non-negative Dirichlet form

$$\mathcal{E}_\chi^{(q)}[A] := -\langle A, \mathcal{L}_q[A] \rangle_\chi, \quad \lambda_{\text{gap}}(\mathcal{L}_q) := \inf_{\substack{A=A^\dagger \\ \langle A, \mathbf{1} \rangle_\chi = 0}} \frac{\mathcal{E}_\chi^{(q)}[A]}{\langle A, A \rangle_\chi},$$

which governs the mixing rate $\|e^{s\mathcal{L}_q}[A] - \langle A \rangle_\sigma \mathbf{1}\|_\chi \leq e^{-\lambda_{\text{gap}} s} \|A - \langle A \rangle_\sigma \mathbf{1}\|_\chi$.

Principle 6.1 (Hidden-symmetry alignment). *Among all admissible quadratic densities $\{\mathcal{O}_q\}$ built from the hidden-symmetry tower, choose \mathcal{O}_{q^*} to maximize the reversible spectral gap:*

$$q^* \in \arg \max_q \lambda_{\text{gap}}(\mathcal{L}_q),$$

subject to (i) WESH–Noether commutant constraints, (ii) χ –KMS detailed balance, and (iii) exponential–causal kernel of range ξ . The maximizer is the K_χ –invariant scalar in the hidden–symmetry decomposition, i.e. the scalar constructed from the principal tensor tower that commutes with K_χ and the axial $U(1)$, thereby yielding the fastest mixing to the χ –KMS fixed point.

Proof sketch. (1) By axial and corotating invariance, $\mathfrak{A}(\mathcal{W}_\chi)$ decomposes into Fourier modules labelled by (ω, m) for K_χ and ∂_ϕ . Reversibility block-diagonalizes \mathcal{L}_q across these modules.

(2) Within each block, the WESH–Noether commutant condition suppresses directions that transform nontrivially under the hidden–symmetry algebra generated by $\{K_{\mu\nu}, h_{\mu\nu}\}$. By Schur’s lemma, the *only* choice whose jump set has trivial commutant on every (ω, m) block is the scalar component of the hidden–symmetry tower. Any vector/tensor choice leaves a nontrivial commutant, creating \mathcal{L}_q –invariant subalgebras and strictly reducing the Rayleigh quotient that defines λ_{gap} .

(3) Because the bilocal channel furnishes cross-horizon connectivity and the vacuum is Markov on null cuts, each (ω, m) block is ergodic once the dissipator is K_χ –invariant and scalar; detailed balance then identifies the unique fixed point with the χ –KMS state and the corresponding gap is maximal among admissible choices. Finally, the scalar constructed from the principal tensor tower is the unique such K_χ –invariant. \square

Consequences. (i) *Uniqueness and fastest mixing.* The selected dissipator ensures primitivity and maximizes the reversible spectral gap, giving the fastest approach to χ –KMS at $\beta_H = 2\pi/\kappa$ (Sec. 6.2). (ii) *Continuity to Schwarzschild.* In the limit $\Omega_H \rightarrow 0$ the principle reproduces the static scalar channel used in Sec. 6.2. (iii) *Kerr/CFT compatibility.* K_χ –invariance aligns the dissipative weights with the corotating Virasoro zero–mode used in the Kerr/CFT literature, ensuring that subleading data (e.g. $\gamma(J)$) can be cross–checked against horizon symmetry charges. This principle leverages that structure for the variational selection of the dissipator.

Link to the WESH monotone. In the reversible geometry $\langle \cdot, \cdot \rangle_\chi$, the Dirichlet form $\mathcal{E}_\chi^{(q)}$ is the quadratic dissipation rate of the WESH Lyapunov functional (Appendix D); hence maximizing λ_{gap} is equivalent to *minimizing* the relaxation time of the WESH monotone under the constraints above, i.e. an

optimal-control selection consistent with the Phase–F variational framework.

Status. The Hidden–Symmetry Alignment principle is *not* derived from the core WESH axioms. It is introduced as an additional selection criterion for the Kerr extension, motivated by: (i) uniqueness and fastest mixing to the χ –KMS state; (ii) smooth reduction to the static case as $\Omega_H \rightarrow 0$; and (iii) compatibility with Kerr/CFT structures. The argument in Box 9 should therefore be read as: *given* this principle, the admissible dissipator is uniquely fixed to the scalar hidden–symmetry channel aligned with K_χ ; it does not constitute a derivation of the principle itself from WESH–Noether.

Remark 6.13 (Physical rationale). *The reversible spectral gap λ_{gap} controls the mixing time $s_{\text{mix}} \sim \lambda_{\text{gap}}^{-1}$ and quantifies the positivity-improving power of the semigroup on each Fourier block (ω, m) . Any jump set leaving a non-trivial commutant—i.e. hidden-symmetry components not invariant under K_χ —necessarily yields a smaller Rayleigh quotient and hence slower relaxation. The scalar component aligned with the principal Killing–Yano tower is the unique choice whose commutant is trivial, making the semigroup primitive and “fastest” under all symmetry constraints. This variational criterion is the rotating analogue of the static local quadratic channel selected in Sec. 6.2.*

Leading area law and pair entropy in Kerr. Let $x = \beta_H(\omega - m\Omega_H)$. With the pair-entropy functional $s(x) = x/(e^x - 1) - \ln(1 - e^{-x})$, the Kerr average reads

$$\bar{s}_{\text{Kerr}} = \frac{\sum_m \int_0^\infty \frac{d\omega}{2\pi} \Theta(\omega - m\Omega_H) W_{\text{Kerr}}(\omega, m) s(\beta_H(\omega - m\Omega_H))}{\sum_m \int_0^\infty \frac{d\omega}{2\pi} \Theta(\omega - m\Omega_H) W_{\text{Kerr}}(\omega, m)}. \quad (6.49)$$

Assuming the low-frequency scalings justified in Sec. 6.4 (Kerr wedge density $\rho_{\text{Kerr}} \sim \tilde{\omega}^p$ and response $\Gamma_{\text{WESH}} \sim \tilde{\omega}^k \tilde{F}(\tilde{\omega}\xi)$ with smooth UV cutoff at ξ^{-1}), the weight $\tilde{W}(x) \propto x^n e^{-x} (1 - e^{-x})^{-1} \tilde{F}(x)$ is single-peaked with $x_* = x_n + \mathcal{O}(\kappa\xi)$ (cf. Prop. 6.6), hence

$$\bar{s}_{\text{Kerr}} = \mathcal{O}(1) \quad (\text{no hidden } A\text{-dependence, cf. Remark 6.8}). \quad (6.50)$$

Short-range mode counting gives $N \sim A/\xi^2$; bipartite halving yields $A/(2\xi^2)$; swap-even boundary superselection (Sec. 6.3) contributes an additional factor $1/2$ in the χ -adapted even sector. Therefore,

$$S_{\text{BH}}^{\text{Kerr}} = \frac{A}{4L_P^2} + \gamma_{\text{Kerr}} \ln \frac{A}{L_P^2} + c_{\text{Kerr}} + \mathcal{O}\left(\frac{L_P^2}{A}\right), \quad (6.51)$$

with the same universal leading coefficient.

Logarithmic corrections from the Hessian. Let Δ_{phys} be the Hessian of the WESH effective action evaluated on the Kerr background (Sec. 6.5). On the Euclidean replica/conical geometry, the log coefficient is

$$\begin{aligned} \gamma_{\text{Kerr}} &= \frac{1}{2} \partial_\alpha \Big|_{\alpha=1} \left(a_2 \left[\Delta_{\text{phys}}^{(\alpha)} \right] - \alpha a_2 \left[\Delta_{\text{phys}}^{(1)} \right] \right) \\ &= \sigma_{\text{phys}} \chi(\mathcal{H}) + \frac{1}{2} \partial_\alpha b_2(\alpha) \Big|_{\alpha=1} \int_{\mathcal{H}} K_{ab} K^{ab} dA + \dots, \end{aligned} \quad (6.52)$$

where \mathcal{H} is a smooth horizon section (topologically S^2), $\chi(\mathcal{H}) = 2$, and the ellipsis denotes additional gauge/ghost terms fixed by the RAQ projection. Rotation dependence is encoded in the Kerr-sensitive horizon-local invariants of Δ_{phys} (notably the E and Ω sectors); extrinsic terms contribute only when the chosen horizon section is non-minimal/deformed. The resulting $\Delta\gamma(J)$ vanishes smoothly as $J \rightarrow 0$.

Extremal (NHEK) limit and Kerr/CFT interface. In the NHEK limit ($\kappa \rightarrow 0$) the corotating KMS structure reduces to a zero-temperature (ground-state) KMS with respect to K_χ . Hidden-symmetry covariance dovetails with the integrable mode structure and offers a natural interface to Kerr/CFT tools (e.g., emergent Virasoro) for organizing subleading corrections and boundary data in the throat region.

EFT control of kernel deformations. Treating WESH as an EFT, the mediator mass $m_T = \xi^{-1}$ receives curvature-dependent renormalizations $m_{\text{eff}}^2 = m_T^2 +$

$c_1 R + c_2 R_{\mu\nu\rho\sigma} R^{\mu\nu\rho\sigma} + \dots$. For Kerr, $R = 0$ while the Kretschmann scalar is nonzero; thus $\delta\xi/\xi = \mathcal{O}((L_P/M)^4)$ on macroscopic horizons. Leading area scaling is unaffected; Kerr-specific shifts enter only subleading coefficients (γ_{Kerr} , c_{Kerr}).

Corollary 6.4 (Leading law and Kerr log shift). *With $\xi \simeq L_P$ and hidden-symmetry-covariant dissipation,*

$$\bar{s}_{\text{Kerr}} = \mathcal{O}(1) \quad \text{and} \quad S_{\text{BH}}^{\text{Kerr}} = \frac{A}{4L_P^2} + \dots$$

as in Eq. (6.51). The logarithmic coefficient splits as

$$\gamma_{\text{Kerr}} = 2\sigma_{\text{phys}} + \Delta\gamma(J), \quad (6.53)$$

with $\Delta\gamma(J)$ determined by the Kerr-sensitive horizon-local invariants of Δ_{phys} (in particular the E and Ω sectors, and extrinsic terms only for non-minimal sections),

$$\Delta\gamma \rightarrow 0 \quad \text{for } J \rightarrow 0.$$

Synthesis. The rotating extension shows that once the correct modular flow (K_χ) is used, WESH thermodynamics reproduces the universal leading area law and encodes rotation through controlled subleading structures governed by horizon-local invariants and hidden symmetries. Together with Secs. 1.3, 6.2, 6.3 and 6.5, this yields a unified chain: pre-geometric conservation \Rightarrow rotating KMS fixed point \Rightarrow physical projection $\Rightarrow A/4L_P^2$ universality + Kerr-specific logarithmic corrections.

6.7 The holographic bound from WESH stationarity

Guiding claim. In QFTT–WESH the very existence of a well-defined emergent time map $t(s)$ with non-negative production rate,

$$\frac{dt}{ds} = \Gamma[\Psi] \geq 0, \quad (6.54)$$

with $\Gamma > 0$ for forward-time production and $\Gamma = 0$ at the stationary HH/BH fixed point, imposes an information-geometric *stability* constraint that *upper-bounds* the admissible cross-sectional entanglement on codimension-two boundaries. In a near-horizon window this becomes a holographic inequality

$$S[\mathcal{H}] \leq \frac{A(\mathcal{H})}{4L_P^2} + \text{subleading}, \quad (6.55)$$

with saturation at the Hartle–Hawking/KMS fixed point. The bound is *derived* from $\Gamma[\Psi] \geq 0$ together with the WESH–Noether conservation principle (Sec. 1.3) and the wedge–modular structure underpinning the KMS fixed point (Sec. 6.2); the normalization of the bound is fixed by the bipartite halving \times swap–even superselection (Sec. 6.3) and the KMS spectral calibration (Sec. 6.4).

Local/bilocal split of the chronogenesis rate. The emergent-time production functional admits a canonical decomposition

$$\Gamma[\Psi] = \Gamma_{\text{loc}}[\Psi] - \Gamma_{\text{cost}}[\Psi], \quad \Gamma_{\text{loc}} \geq 0, \quad \Gamma_{\text{cost}} \geq 0, \quad (6.56)$$

where Γ_{loc} collects strictly local GKSL contributions, fixed in sign by complete positivity and constrained by WESH–Noether, while Γ_{cost} encodes bilocal, entanglement–driven channels weighted by the mediator kernel K_ξ (exponential–causal support with range $\xi \simeq L_P$). The sign convention emphasizes that cross–boundary correlations *consume* chronogenetic capacity.

Here Γ_{cost} denotes the information-theoretic cost of maintaining trans-horizon correlations; it is controlled by the bilocal channel and enters with a minus sign because cross-boundary entanglement *consumes* chronogenetic capacity.

Remark 6.14 (Physical interpretation of the split). *Local channels act independently on each side of the horizon and generate temporal order by aligning gradients (cf. Theorem 6.1); their contribution $\Gamma_{\text{loc}} \geq 0$ measures the intrinsic rate of time production inside each wedge. The bilocal channel, instead, couples trans-horizon pairs within a Planck-thick layer and must expend part of this order to maintain cross-cut correlations. The associated information cost—proportional to the average mutual information of the pairs—appears with a minus sign as Γ_{cost} . At the Hartle–Hawking/KMS fixed point the two effects balance ($\Gamma = 0$): the horizon saturates the maximal sustainable cross-horizon correlation compatible with stationarity. For $\Gamma > 0$, forward chronogenesis requires a sub-holographic correlation content, leading to the entropy bound derived below.*

Near-horizon modular control. Restricting to a Rindler wedge, the modular Hamiltonian generates boosts and admits a local, null-surface expression for suitable QFT sectors. This supplies sharp null-plane inequalities (relative entropy, Markov property) that relate modular energy to mutual information and provide area-type control of cross-horizon entanglement on \mathcal{H} .

Kernel geometry and area scaling. Boundary-crossing pairs are localized within a Planck-thick layer ($\sim \xi$) around \mathcal{H} . The same geometry that controls the mode count ($\sim A/\xi^2$, reduced by halving+projection) also bounds the bilocal subtraction in (6.56) through an L^1 kernel norm times an information density per pair:

$$\Gamma_{\text{cost}}[\Psi] \lesssim \tilde{c} \frac{A}{\xi^2} \bar{\mathcal{I}}_\Psi, \quad \tilde{c} := \|K_\xi\|_{L^1} \xi^{-4} = \mathcal{O}(1), \quad (6.57)$$

with $\bar{\mathcal{I}}_\Psi$ a KMS-weighted pair-information functional (defined below).

Lemma 6.5 (Pair-information control on null wedges). *Let $\mathfrak{A}(\mathcal{W}_R)$ be the right-Rindler wedge algebra and consider three contiguous intervals (A, B, C) along a fixed null generator with B a buffer of thickness $\gtrsim \xi$ around the bifurcation surface. For the vacuum (or any χ -KMS deformation with $\beta_H = 2\pi/\kappa$), the null-plane Markov property implies $I(A : C | B) = 0$ (saturation of strong subadditivity). For trans-horizon pairs $(x \in A, y \in C)$ drawn with kernel density K_ξ and weighted by the horizon modular spectrum, the KMS-weighted pair information*

$$\bar{\mathcal{I}}_\Psi := \frac{\int_0^\infty \frac{d\omega}{2\pi} W_{\text{HH}}(\omega) \mathbb{E}_{(x,y) \sim K_\xi} [\mathcal{I}_\Psi(x : y)]}{\int_0^\infty \frac{d\omega}{2\pi} W_{\text{HH}}(\omega)} \quad \left(\mathcal{I}_\Psi(x : y) = \frac{1}{2} S_{\mathfrak{A}_{xy}}(\rho_{xy} \| \rho_x \otimes \rho_y) \right)$$

obeys the bound

$$\bar{\mathcal{I}}_\Psi \leq \bar{s} + \mathcal{O}((\kappa\xi)^2), \quad (6.58)$$

where \bar{s} is the KMS-weighted pair-entropy average (Sec. 6.4) and the error term is controlled by ξ -scale null-buffer coarse-graining on the modular length κ^{-1} (hence by $\kappa\xi$), and is A -independent.

Sketch. Markov saturation $I(A : C | B) = 0$ on null triads gives a chain-rule identity $I(A : C) = I(A : BC) - I(A : B)$; with a buffer B of size $\gtrsim \xi$, the long-range part of $I(A : C)$ is exhausted by local null contributions near the cut. Express $2\mathcal{I}_\Psi(x : y)$ as a relative entropy, $2\mathcal{I}_\Psi(x : y) = D(\rho_{xy} \| \rho_x \otimes \rho_y)$,

and decompose fields in boost modes with weight $W_{\text{HH}}(\omega)$ (Sec. 6.2). By the entanglement first law around the χ -KMS state, the leading variation of D is set by the modular-energy variation and coincides with the bosonic pair-entropy functional $s(x)$ at $x = \beta_H \omega$, up to $\mathcal{O}((\kappa\xi)^2)$ corrections controlled by ξ -scale null-buffer coarse-graining on the modular length κ^{-1} (and independent of A). Averaging over ω and the kernel K_ξ gives (6.58), with \bar{s} defined in Eq. (6.28). The entanglement first-law step and modular-energy variation follow Casini, Testé, & Torroba (2017), while the null-plane Markov property and relative-entropy control build on Blanco, Casini, Hung, & Myers (2013); see Appendix G for a detailed discussion.

□

Corollary 6.5 (Calibrated chronogenetic threshold). *With the chronogenetic split $\Gamma = \Gamma_{\text{loc}} - \Gamma_{\text{cost}}$, $\Gamma_{\text{loc}} \geq 0$ and*

$$\Gamma_{\text{cost}} \lesssim \tilde{c} \frac{A}{\xi^2} \bar{\mathcal{I}}_\Psi, \quad \tilde{c} = \mathcal{O}(1), \quad (6.59)$$

At the Hartle–Hawking state, detailed balance enforces $\Gamma_{\text{loc}} = \Gamma_{\text{cost}}$, and the bound saturates at the Bekenstein–Hawking value derived independently in Sec. 6.4; in particular the leading coefficient is the same universal $1/4$ fixed by pairing \times swap–even projection. Consequently,

$$\boxed{\Gamma > 0 \implies S[\mathcal{H}] \leq \frac{A(\mathcal{H})}{4L_P^2} + \gamma \ln \frac{A}{L_P^2} + k_0 + \mathcal{O}\left(\frac{L_P^2}{A}\right)}, \quad (6.60)$$

with γ and k_0 the one-loop/log and constant terms computed from the physical Hessian on the cone (Sec. 6.5).

Remark 6.15 (Non-circularity of the calibration). *The value $A/(4L_P^2)$ is not assumed here as an ansatz for the chronogenetic bound. It has already been obtained independently in Secs. 6.2–6.4 from WESH–Noether, uniqueness of the KMS fixed point, spectral concentration $\bar{s} = \mathcal{O}(1)$ and the bipartite+swap projection yielding the universal $1/4$ prefactor. The chronogenetic argument of this subsection provides a second, dynamical route to the same threshold by demanding $\Gamma = 0$ at the Hartle–Hawking fixed point. The calibration at $A/(4L_P^2)$ is therefore a consistency requirement between two logically independent derivations, not a circular assumption.*

Sketch. Use (6.57) with Lemma 6.5: $\Gamma_{\text{cost}} \lesssim \tilde{c} \frac{A}{\xi^2} [\bar{s} + \mathcal{O}((\kappa\xi)^2)]$. From Sec. 6.4, $\bar{s} = \mathcal{O}(1)$ (no hidden A -dependence, cf. Remark 6.8), and from Sec. 6.3 the physical mode count carries the universal factor $1/4$ (bipartite halving \times even-sector projection). At the HH point, detailed balance yields $\Gamma_{\text{loc}} = \Gamma_{\text{cost}}$; this calibrates the threshold at $S_{\text{BH}} = A/(4L_P^2) + \gamma \ln(A/L_P^2) + \dots$. Therefore $\Gamma > 0$ forces S below that calibrated value, establishing (6.60). *Refs:* modular Markov and KMS weights; Appendix D–H for Γ , the RAQ/constraint average, and the swap-even projector. \square

Proposition 6.8 (Relative-entropy formulation of the chronogenetic bound). *For trans-horizon pairs (x, y) distributed by the mediator kernel K_ξ , the pair information used in Eq. (6.57) satisfies $2\mathcal{I}_\Psi(x : y) = S(\rho_{xy} \| \rho_x \otimes \rho_y)$. By monotonicity under inclusions adapted to the null wedge and by the KMS calibration at the HH point,*

$$\Gamma_{\text{cost}} \lesssim \tilde{c} \frac{A}{\xi^2} \overline{S(\rho_{xy} \| \rho_x \otimes \rho_y)} \quad (\tilde{c} = \mathcal{O}(1)).$$

Hence the forward-time condition $\Gamma > 0$ enforces $S[\mathcal{H}] \leq \frac{A}{4L_P^2} + \gamma \ln(A/L_P^2) + k_0 + \mathcal{O}(L_P^2/A)$, with equality at the HH fixed point where the relative-entropy "budget" is exhausted.

Theorem 6.6 (Holographic bound from chronogenetic stability). *Assume:*

- (i) **WESH–Noether conservation:** Pre-geometric path independence (Sec. 1.3, Eq. (G.1));
- (ii) **GKSL structure:** Quadratic channels $\{\hat{T}^2(x), L_{xy}\}$ with exponential-causal mediator K_ξ of range $\xi \simeq L_P$ (Sec. 1, Eqs. (1.15)–(1.20));
- (iii) **Near-horizon KMS:** Wedge-modular control with thermal fixed point at $\beta_H = 2\pi/\kappa$ (Sec. 6.2, Thm. 6.5);
- (iv) **Physical projection:** Bipartite halving \times swap-even boundary superselection yields factor $1/4$ (Sec. 6.3, Thm. 6.3).

Then the chronogenetic condition $\Gamma[\Psi] \geq 0$ in a near-horizon window implies

$$S[\mathcal{H}] \leq \frac{A(\mathcal{H})}{4L_P^2} + \gamma \ln \frac{A}{L_P^2} + k_0 + \mathcal{O}\left(\frac{L_P^2}{A}\right), \quad (6.61)$$

with sharp saturation at the Hartle–Hawking/KMS fixed point, i.e., at the Bekenstein–Hawking equilibrium. The coefficient of the leading term is universally $1/4$.

Sketch of proof.

- (1) **Local positivity.** By complete positivity and WESH–Noether, $\Gamma_{\text{loc}} \geq 0$ with strict positivity on any wedge of finite modular energy: local channels *produce* t (no conservative drift along forbidden directions).
- (2) **Bilocal subtraction and area control.** Using (6.57) and null–plane modular inequalities, the pair–information density obeys $\bar{\mathcal{I}}_\Psi \leq \bar{s} + \mathcal{O}((\kappa\xi)^2)$, where \bar{s} is the KMS–weighted pair entropy. Secs. 6.2 and 6.4 give $\bar{s} = \mathcal{O}(1)$ (no hidden A -dependence) with $\xi \simeq L_P$. Hence $\Gamma_{\text{cost}} \lesssim \tilde{c} \frac{A}{\xi^2} [1 + \mathcal{O}((\kappa\xi)^2)]$, with \tilde{c} fixed by WESH normalization and $\|K_\xi\|_{L^1}$.
- (3) **Calibration at the fixed point.** At the HH fixed point detailed balance enforces pairwise cancellation in frequency space, so $\Gamma_{\text{loc}} = \Gamma_{\text{cost}}$ and $\Gamma = 0$. The threshold value of the cross-horizon entropy at which equality holds is precisely the BH value: the factor $1/4$ is fixed by bipartite halving \times swap–even superselection (Sec. 6.3) together with $\bar{s} = \mathcal{O}(1)$ (Sec. 6.4). Therefore $\Gamma > 0$ implies $S[\mathcal{H}] \leq A/(4L_P^2) + \dots$, while S above that value would force $\Gamma \leq 0$.
- (4) **Subleading structure.** The \ln and A^{-1} terms come from the one–loop determinant of the physical quadratic form (Sec. 6.5) and from the finite width of the KMS weight, respectively; they do not shift the leading coefficient.

Operational domain and “WESH stability cone”. Equation (6.61) identifies the *WESH stability cone*

$$\mathcal{C}_{\text{WESH}} = \left\{ (\mathcal{H}, \Psi) : \Gamma[\Psi] \geq 0, \quad S[\mathcal{H}] \leq \frac{A(\mathcal{H})}{4L_P^2} + \gamma \ln(A/L_P^2) + k_0 + \mathcal{O}(L_P^2/A) \right\}. \quad (6.62)$$

States attempting $S > A/(4L_P^2)$ would overload the bilocal channel and stall t –fabrication, rendering them dynamically inadmissible for forward–oriented emergent time in the near–horizon wedge.

Corollaries. (i) *BH saturation.* Stationary horizons saturate (6.61): $\Gamma = 0$ at HH; deformations into the exterior wedge satisfy the entropy–area flux identity $\dot{S}_{\text{rad}} = -\dot{A}/(4L_P^2) \geq 0$. (ii) *Kerr generality.* The argument extends to rotating horizons by replacing ∂_t with $\chi^\mu = \partial_t + \Omega_H \partial_\phi$ (Sec. 6.6); the leading threshold remains $1/4$, while spin enters only through subleading coefficients (e.g., $\gamma(J)$) via horizon-local invariants. (iii) *EFT stability.* Buffer/coarse-graining corrections

scale as $\mathcal{O}((\kappa\xi)^2) = \mathcal{O}((L_P/M)^2)$, while curvature-induced renormalizations of the kernel scale ξ enter at $\mathcal{O}((L_P/M)^4)$ (cf. Sec. 6.4); for macroscopic holes both effects leave the leading threshold intact, with controlled deviations predicted only near the Planckian regime.

Pair-information functional (definition). Let \mathcal{A}_{out} and \mathcal{A}_{in} be the von Neumann algebras on the two sides of \mathcal{H} . For Planck-thickened surface elements (x, y) with $x \in \text{out}$, $y \in \text{in}$, define

$$\mathcal{I}_\Psi(x : y) = \frac{1}{2} S_{\mathfrak{A}_{xy}}(\rho_{xy} \| \rho_x \otimes \rho_y), \quad \bar{\mathcal{I}}_\Psi = \frac{\int_0^\infty \frac{d\omega}{2\pi} W_{\text{HH}}(\omega) \mathbb{E}_{(x,y)}[\mathcal{I}_\Psi(x : y)]}{\int_0^\infty \frac{d\omega}{2\pi} W_{\text{HH}}(\omega)}. \quad (6.63)$$

Here $W_{\text{HH}}(\omega)$ is the near-horizon KMS weight (Sec. 6.2), and $\mathbb{E}_{(x,y)}$ averages over trans-horizon pairs drawn with kernel density K_ξ . On the HH fixed point, $\bar{\mathcal{I}}_\Psi = \bar{s}$; near it, $\bar{\mathcal{I}}_\Psi \leq \bar{s} + \mathcal{O}((\kappa\xi)^2)$ by null-plane relative-entropy inequalities.

Remark 6.16 (Per-side information cost). *The factor $\frac{1}{2}$ in the definition of \mathcal{I}_Ψ reflects the bipartite structure of near-horizon entanglement. For thermofield-double-like states, the full mutual information satisfies $I(x : y) = 2S(\rho_x)$: the correlation "bridge" is supported equally by both sides. Since the Bekenstein-Hawking entropy $S_{\text{BH}} = N_{\text{phys}}\bar{s}$ counts the information cost per exterior mode, the budget entering Γ_{cost} must likewise be the per-side share, $\mathcal{I}_\Psi = \frac{1}{2}I(x : y)$. This ensures $\bar{\mathcal{I}}_\Psi = \bar{s}$ at the HH fixed point in the regulated thermofield-double (two-sided) realization, without extraneous factors.*

Remark 6.17 (Operational Bound (WESH Holography)). *For any near-horizon wedge where WESH dynamics admits a Rindler modular description and the mediator has range $\xi \simeq L_P$,*

$$S[\mathcal{H}] \leq \frac{A(\mathcal{H})}{4L_P^2} + \gamma \ln \frac{A}{L_P^2} + k_0 + \mathcal{O}\left(\frac{L_P^2}{A}\right),$$

with equality at the HH/BH fixed point.

(6.64)

The coefficients γ and k_0 are determined by the one-loop Hessian of the WESH effective action (Sec. 6.5).

Interpretation. Equation (6.64) reframes black-hole holography as a *spacetime-emergence stability bound*. The area term sets the maximal sustainable cross-horizon information compatible with forward t -production; saturation pins Γ to zero (stationarity), while sub-holographic configurations yield $\Gamma > 0$ and obey the entropy-area flux identity. Above the threshold the bilocal channel would dominate and stall chronogenesis. Thus an information-theoretic “holographic censorship” follows directly from pre-geometric conservation and wedge modular KMS structure, completing the chain:

WESH–Noether \implies KMS fixed point \implies physical projection (RAQ + swap-even)

$$\implies S_{\text{BH}} = \frac{A}{4L_P^2} + \gamma \ln \frac{A}{L_P^2} + \dots,$$

with the inequality (6.64) as the dynamical stability envelope of the BH sector.

Epilogue

This work has pursued a specific goal: to resolve the Wheeler–DeWitt frozen-time problem through its unique dissipative completion. The WESH master equation is not an alternative to Wheeler–DeWitt, but its dynamical extension: the minimal GKSL structure that unfreezes the constraint $\hat{H}_{\text{tot}}|\Psi\rangle = 0$ while preserving CPT symmetry, Noether charges, and complete positivity. From this completion, both the Einstein–Hilbert action and black hole thermodynamics emerge without assuming spacetime as a background structure.

The technical path connected several domains not usually placed in contact: GKSL dissipation in a timeless Wheeler–DeWitt sector, Noether-type constraints at the generator level, variational alignment as a dynamical fixed point, and near-horizon KMS structure as the bridge to thermodynamics. At each step, we required internal consistency and falsifiability rather than formal elegance alone. The result is a framework where spacetime emergence and thermodynamic equilibrium coincide: competing tendencies—loss of coherence, gradient flows, global conservation—self-organize into a stable configuration that satisfies Einstein’s equations up to controlled corrections.

The framework offers concrete, testable predictions: collective coherence scaling as $\tau_{\text{coh}}(N) \propto N^2$, angular modulation of decoherence rates following $1 + \varepsilon \cos^2 \theta$, and holographic consistency across ~ 50 orders of magnitude from the Planck scale to macroscopic horizons. These are not incidental features but direct consequences of the WESH structure, understood less as a derivation from Wheeler–DeWitt than as its dissipative Lindbladian completion. Preliminary tests on IBM and Rigetti quantum processors show consistency with the predicted scaling within current hardware limitations; the theory stands or falls on future experimental verdict.

We have deliberately confined this work to the gravitational sector and black hole thermodynamics. Natural extensions, compact astrophysical objects, matter couplings, scalar-tensor formulations, require dedicated studies with distinct observational protocols. At this stage, the priority was establishing the core derivation and its initial empirical contact.

The framework has known limitations. Near singularities, at trans-Planckian scales, or in regimes where the Markov condition $\tau_{\text{corr}} \ll \tau_{\text{Eig}}$ fails, the assumptions underlying WESH break down. We do not claim universality; we claim tractability within a well-defined domain.

Whether this particular formulation survives critical scrutiny is for the community to decide. If it does, the implications extend beyond the specific results derived here. If it does not, we hope it will have at least demonstrated that the functional relations between quantum dissipation, symmetry constraints, and geometric emergence admit richer structures than previously recognized, and that the attempt to derive spacetime rather than assume it remains a viable research direction.

Acknowledgments

Mathematical content, physical arguments, and proofs have been verified by the author and validated by the Lean 4 type-checker using the Mathlib library. The formalization comprises over 6,100 lines of verified code. Axioms are limited to standard textbook results and to QFTT–WESH-specific content derived elsewhere in the Lean corpus.

This work was developed with the assistance of a cross-inferencing multi-AI workflow, primarily involving ChatGPT-5.2 Pro and Claude Opus 4.5 for theoretical development, mathematical derivations, and iterative refinement, but also

Gemini 3 Pro and other models. Aristotle v. 0.6.0 (Harmonic) was also used, in conjunction with ChatGPT-5.2 Pro and Claude Opus 4.5, as a translation tool in the final stages to convert established mathematical content into Lean 4 syntax. The author intends to further document this multi-AI architecture in future work, hoping it may contribute to AI-assisted theoretical physics research. Throughout the process, the research, conceptual framework and its details, workflow orchestration, and verification of every output remained with the author.

I am grateful and dedicate this work to my wife Margie and the little Elvia: thanks for the support, and for giving me the time to understand time. A heartfelt thank you also to Kaïra, the indomitable.

Appendix A: Kernel derivation and the scales ξ and γ_0

Setup. We motivate the causal, L^1 -integrable weight used in the collapse kernel $\gamma(x, y)$ of Eq. (1.20) from a minimal local mediator. Throughout we adopt the Minkowski convention $\eta = \text{diag}(-, +, +, +)$ and $\square = \eta^{\mu\nu}\partial_\mu\partial_\nu$.

A.1 Minimal mediator and retarded propagator. We introduce a scalar mediator $\chi(x)$ with Klein–Gordon dynamics on the pre-chronogenesis sector:

$$S_\chi = \int d^4x \left[\frac{1}{2}(\partial_\mu\chi)(\partial^\mu\chi) - \frac{1}{2}m_T^2\chi^2 \right]. \quad (\text{A.1})$$

The retarded Green function Δ_R solves

$$(\square + m_T^2)\Delta_R(z) = \delta^{(4)}(z), \quad \text{supp } \Delta_R \subseteq \{z^0 \geq 0, z^2 \leq 0\}. \quad (\text{A.2})$$

The correlation length associated with the mediator mass is the Compton scale

$$\xi = \frac{\hbar}{m_T c}. \quad (\text{A.3})$$

A.2 Positive causal envelope and correlation four-volume. The retarded propagator Δ_R fixes the *support* (future light cone) and the range $\xi = \hbar/(m_T c)$, but it is not used directly as a nonnegative L^1 weight. Instead we adopt a coarse-grained, positive causal envelope K_ξ of range ξ , e.g.

$$K_\xi(z) = \exp\left(-\frac{z^0}{\xi}\right)\Theta(z^0)\Theta(-z^2), \quad (\eta = \text{diag}(-, +, +, +)), \quad (\text{A.4})$$

whose L^1 norm defines the correlation four-volume

$$V_\xi := \int d^4z K_\xi(z) = \mathcal{O}(\xi^4). \quad (\text{A.4}')$$

With the normalized measures of Eq. (1.14), this V_ξ is absorbed at the level of the generator. (If desired one may also define the normalized kernel $\bar{K}_\xi := K_\xi/V_\xi$ so that $\int d^4z \bar{K}_\xi = 1$.)

A.3 Collapse kernel and dimensions. The collapse kernel of the main text reads $\gamma(x, y) = \frac{\gamma_0}{N^2} K_\xi(x - y) \Theta[\text{causal}(x, y)]$ (Eq. (1.20)). With K_ξ chosen positive and L^1 -integrable, γ_0 has the dimension of a rate. (If one prefers an explicitly normalized kernel, define $\bar{K}_\xi := K_\xi/V_\xi$ so that $\int d^4z \bar{K}_\xi(z) = 1$.) This choice yields a positive, integrable weight and, when composed with Hermitian jump operators, preserves complete positivity of the dissipative channel.

A.4 WESH–Noether normalization. Coarse-grained consistency imposes a matching condition on the intensity scale:

$$\nu \simeq \gamma_0 \bar{C}_x, \quad \bar{C}_x := \frac{1}{V_\xi} \int d^4y K_\xi(x-y) C(\Psi; x, y), \quad V_\xi = \int d^4z K_\xi(z) \sim \xi^4. \quad (\text{A.5})$$

Here $C(\Psi; x, y)$ is the state-dependent bilocal factor of the WESH channel and V_ξ is the effective correlation 4-volume. With the normalized measures of Eq. (1.14), V_ξ is tracked consistently through the coarse-graining; γ_0 remains the fundamental rate scale, while ν is fixed by self-consistent matching (hence not independently tunable).

A.5 Planck anchoring. With $m_T \sim M_P$ one has $\xi \sim L_P$ by (A.3). Combining this with the matching $\nu \simeq \gamma_0 \bar{C}_x$ (Eq. (A.5)), with $\bar{C}_x = \mathcal{O}(1)$ on correlated domains, the natural anchoring is

$$\gamma_0 = \Theta_0 t_P^{-1}, \quad \Theta_0 = \mathcal{O}(1). \quad (\text{A.6})$$

Here Θ_0 collects normalized cumulants and geometric factors from the time sector, ensuring that the anchoring introduces no additional free parameters or arbitrary scales.

Remarks. (i) The limit $\xi \rightarrow 0$ recovers a local channel; finite ξ implements coarse-grained causality with finite correlation volume. (ii) The static Yukawa form is a spatial illustration only; the operative kernel is the 4D L^1 -integrable K_ξ with causal support. (iii) The construction is minimal and sufficient to support the collapse kernel of Eq. (1.20) and the no-signaling statement Eq. (4.35), while fixing γ_0 via Eq. (A.5).

Appendix B: Parameter s , Emergence of Physical Time, and the Conceptual Limits of a Language Within Time

B.1 The Auxiliary Parameter s and its Role in QFTT–WESH

In QFTT–WESH, an intrinsic parameter s is introduced to write the dynamics of a closed, timeless quantum universe. The universal state $\rho(s)$ is evolved in s but s is *not* an observable: it is a non-physical ordering label used to formulate the GKSL evolution and to state constraints in the WDW sector. “Gauge-like” here means *non-observable scaffolding*; No physical observable depends on the choice of the s -parametrization: one may view s as a gauge-like ordering label (any monotone reparametrization is absorbed by the map $t(s)$). This addresses the *problem of time* in a Wheeler–DeWitt universe.

The s -evolution uses the WESH generator referenced in Eq. (1.15), with \hat{H}_{eff} , $\mathcal{D}[\cdot]$, L_{xy} and γ given in Eqs. (1.17)–(1.20).

Notation. We adopt the operator and kernel conventions of Eqs. (1.17)–(1.20); below we recall only the causal support needed for the rates.

Kernel and causality. We keep the *exponential-causal* dissipative weight (see Eq. (1.20))

$$\gamma(x, y) = \frac{\gamma_0}{N^2} e^{-d(x, y)/\xi} \Theta[\text{causal}(x, y)].$$

Here $d(x, y)$ denotes the invariant causal separation computed from the emergent scalar kernel argument (e.g. via Synge’s world function $\sigma(x, y)$ once $g_{\mu\nu}^{(T)}$ is defined; cf. Box 1).

We reserve ‘Yukawa’ for the *mediator* kernel

$$K(x, y) \propto \frac{e^{-|x-y|/\xi}}{4\pi|x-y|} \Theta[\text{causal}(x, y)].$$

This choice (Eq. (1.20)) avoids a short-distance $1/r$ singularity in the GKSL rates, keeps an L^1 -integrable weight with finite correlation volume $\sim \xi^4$, and—via

$\Theta[\text{causal}]$ —yields exact spacelike no-signaling (Eq. (4.35)).

B.2 Eigentimes and the Emergence of Physical Time t

Eigentime events are the spontaneous collapses that make the arrow of time intrinsic. Physical time t is the coarse-grained monotone of s :

$$\frac{dt}{ds} = \Gamma[\Psi(s)], \quad t(s) = \int_0^s \Gamma[\Psi(s')] ds'$$

The time-production functional is the dimensionless quantity defined in Eq. (1.34) using the normalized measures of Eq. (1.14):

$$\Gamma[\Psi] = \tau_{\text{Eig}} \left[\nu \int_x \text{Tr}[\tilde{T}^2(x) \rho \tilde{T}^2(x)] + \int_{xy} \gamma(x, y) C(\Psi; x, y) \text{Tr}[L_{xy}^\dagger L_{xy} \rho] \right],$$

so that $dt/ds = \Gamma[\rho] \geq 0$, with $\Gamma > 0$ under nondegeneracy (Lemma 1.1), and the local/bilocal matching is set by the coarse-grained consistency condition (Eq. (A.5)). Strict positivity of Γ (monotonicity $dt/ds > 0$) follows under Lemma 1.1; eigentime activation on chronogenetic segments under Lemma 1.2.

Granularity \rightarrow continuum (LLN).

The law of large numbers links event counting to physical time:

$$t(s) \approx \tau_{\text{Eig}} N_{\text{Eig}}(s) \quad (\text{LLN}) \tag{B.1}$$

More precisely:

$$\begin{aligned} N_{\text{Eig}}(s) &= \int_0^s \frac{\Gamma[\Psi(u)]}{\tau_{\text{Eig}}} du + M(s), \\ t(s) &= \int_0^s \Gamma[\Psi(u)] du, \quad \frac{t(s)}{\tau_{\text{Eig}} N_{\text{Eig}}(s)} \xrightarrow{\mathbb{P}} 1. \end{aligned}$$

with martingale $M(s)$ and $\tau_{\text{Eig}} \equiv 1/\nu$. Hence, when $\mathbb{E}[N_{\text{Eig}}] \gg 1$, discrete eigentimes smooth to classical t by the law of large numbers.

Operator-ordering vs. moments (reader guardrail). The intensity functional $\Gamma[\Psi]$ contains the GKSL trace form $\text{Tr}[\hat{T}^2 \rho \hat{T}^2]$, *not* the raw moment $\langle \hat{T}^4 \rangle$; the two coincide only if $[\rho, \hat{T}^2] = 0$. The trace form is required by complete positivity and appears in the definition of $\Gamma[\Psi]$ (Eq. (1.34)).

Example (translation rule $s \rightarrow t$). A temporalized sentence like “collapse occurs *before* the measurement” means: there exist $s_{\text{col}} < s_{\text{meas}}$; mapping by (1.33) gives $t_{\text{col}} < t_{\text{meas}}$. “Before/after” acquires meaning only *after* this mapping.

B.3 Comparison to Other Frameworks and Interpretations

Having established the QFTT–WESH mechanism for time emergence, it is natural to ask how this approach relates to other frameworks addressing the problem of time in quantum gravity. Since this appendix defines the auxiliary parameter s , the eigentime mechanism, and the $s \rightarrow t$ bootstrap, it is the appropriate place to clarify what each approach *assumes* versus what it *derives*.

Existing frameworks can be grouped by their treatment of time:

- (A) *Time as external parameter.* Standard quantum mechanics, GRW (1986), CSL (Pearle, 1989), and Penrose OR (1996) treat t as an assumed external time parameter (not derived from a timeless constraint). Collapse models introduce stochastic, time-asymmetric dynamics but do not address black-hole entropy.
- (B) *Time as relational/frozen.* Page & Wootters (1983) address the Wheeler–DeWitt frozen-time problem by treating time as a conditional correlation within a globally static state. The approach is unitary and does not produce an intrinsic arrow of time or dynamical gravity.
- (C) *Emergent gravity from thermodynamic or holographic postulates.* Jacobson (1995, 2016), Verlinde (2011), and holographic approaches (AdS/CFT, RT, ER=EPR) relate or encode aspects of gravitational dynamics and geometry to entropy or entanglement considerations, assuming either an area/entropy postulate or a microscopic notion of time as input.

Table 4 compares these approaches along four axes: treatment of time, collapse mechanism, arrow of time, and status of the Bekenstein–Hawking entropy.

Framework	Treatment of Time	Collapse Mechanism	Arrow of Time	S_{BH} Status
Page–Wootters (1983)	Relational (timeless global constraint)	None (unitary)	Not intrinsic	Not addressed
GRW (1986); CSL (1989)	External parameter t	Stochastic collapse (phenomenological constants)	Built-in	Not addressed
Penrose OR (1996)	Assumed parameter (not WDW-derived)	Gravity-related objective reduction	Built-in	Not addressed
Jacobson (1995, 2016)	Semiclassical (local horizons/balls)	None (equilibrium condition)	Thermodynamic Input (area/entanglement)	
Verlinde (2011)	Assumes microscopic time	None (entropic-force picture)	Thermodynamic Input (holo-graphic)	
AdS/CFT, ER=EPR	Boundary QFT time	None (unitary boundary)	State-dependent	Computed holographically
QFTT–WESH	Emergent via eigentimes	State-dependent $\Gamma[\Psi]$	Intrinsic	Derived (Sec. 6)

Table 4: Comparison of selected approaches to the problem of time and black-hole entropy. Among the frameworks listed, QFTT–WESH is the only one that starts from a timeless Wheeler–DeWitt constraint and derives both Einstein dynamics and S_{BH} within a single chain, without postulating an area/entropy law or a microscopic time as independent inputs.

With this landscape clarified, Sec. B.4 summarizes the technical status of the $s \rightarrow t$ construction.

B.4 Concluding Remarks

Auxiliary s and emergence of t . The auxiliary parameter s is a scaffold to write the CP–TP WESH evolution (see the master equation). It disappears from observables once physical time is constructed by the bootstrap $dt/ds = \Gamma[\Psi]$ (Eq. (1.33)): after this map, all operational statements are formulated in t .

Finite- N imprint. Residual discreteness at finite N should leave a measurable imprint in the intensity channel: the variance and cross-correlation structure of Γ predicted in Sec. 1.5-1.6 (Eqs. (1.30), (1.34), (1.35)) would provide a direct handle on the granularity of the eigentime mesh and on the causal range ξ .

Bridge to GR. At the stationary fixed point selected by the WESH monotone (App. D, Thm. 5.2), the gradient-alignment condition holds, $\partial_\mu\tau = k \partial_\mu\Phi$ (Eq. (D.13)); with the matching $\frac{k^2}{4\pi G} = \lambda_1 + 3\lambda_2$ (Eq. (4.8)), this enforces the hidden-sector cancellation $T_{\mu\nu}^{(T)} + T_{\mu\nu}^{(nl)} = 0$ (Eq. (4.19)) and yields the emergent Einstein equation with matter (Eq. (4.21)).

Pre-geometric consistency (App. G). The correct foundational constraint at the s -level is WESH–Noether path independence, not thermodynamic detailed balance; the latter emerges only after the $s \rightarrow t$ bootstrap and in the near-horizon KMS regime (Sec. 6.2, Eq. (6.16)). This completes the logical arc from pre-geometric consistency to emergent spacetime and thermodynamics, justifying the use of s as a purely organizational device.

$$T_{\mu\nu}^{(T)} + T_{\mu\nu}^{(nl)} = 0 \quad (N \rightarrow \infty)$$

and the emergent Einstein equation

$$G_{\mu\nu} + \Lambda g_{\mu\nu} = 8\pi G T_{\mu\nu}^{(m)} + O(1/N)$$

are independent of s ; they are statements in the emergent t -theory, confirming that s leaves no footprint in observables (see Eqs. (4.19) and (4.21)).

B.5 Conceptual Limits and the Paradox of Inherited Language

Inevitably, a theory like QFTT–WESH, aiming to position itself upstream of the 4

dimensions, collides with the epistemological problem of using a language within the temporal line. Concepts such as 'before', 'after', 'cause', and 'effect' (but even more implicit assumptions and morphemes) are foundational to our linguistic and logical structures; yet the theory must describe a reality that exists at a more fundamental level than their emergence. At the same time, we identify a taxonomic challenge, implicitly calling for the development of a new mathematical language, perhaps more circular, topological, or inherently atemporal. In the present work, such tension forces a deliberate methodological strategy: to remain communicable, the theory must adopt a temporalized narrative for its exposition, even as its formalism in part describes an atemporal process. The auxiliary parameter s is the controlled semantic scaffold, a *necessary conceptual unit* that dissolves once the formalism is established, essential to navigate this paradox. We could see it in such a way that any temporal sentence admits an s -label version (ordering only), then is translated to a t -statement via Eq. (1.33); Appendix B's LLN line justifies the continuous limit for macroscopic descriptions. This keeps the exposition communicable while ensuring that predictions depend solely on the emergent, measurable t . Here lies the epistemological challenge, but at the same time the beauty of this theory.

Appendix C: WESH conservation law

C.1 Preliminaries: T-neutrality

Lemma (T-neutrality & commutators). If the time field is T-neutral, $[\hat{T}(x), \hat{Q}_{\text{tot}}] = 0$ for all x , then for any conserved charge \hat{Q}_{tot} :

$$[\hat{T}^2(x), \hat{Q}_{\text{tot}}] = 0 \quad \text{and} \quad [L_{xy}, \hat{Q}_{\text{tot}}] = 0, \quad L_{xy} \equiv \hat{T}^2(x) - \hat{T}^2(y).$$

C.2 Generator-level WESH–Noether (atemporal)

Using the standard GKSL identity

$$\text{Tr}(A \mathcal{D}[L] \rho) = \frac{1}{2} \langle L^\dagger [A, L] + [L^\dagger, A] L \rangle,$$

The Hamiltonian contribution is $-i\langle[\hat{Q}_{\text{tot}}, \hat{H}_{\text{eff}}]\rangle$ and vanishes by the commutant condition $[\hat{H}_{\text{eff}}, \hat{Q}_{\text{tot}}] = 0$ (Eq. (1.8)). Setting $A = \hat{Q}_{\text{tot}}$ in the dissipative part, one obtains the decomposition

$$\frac{d}{ds}\langle\hat{Q}_{\text{tot}}\rangle = \int d^4x S_{\text{loc}}(x) + \iint d^4x d^4y S_{\text{bi}}(x, y).$$

Local contribution (anticommutator form).

$$S_{\text{loc}}(x) = \frac{1}{2}\left\langle \hat{T}^2(x) [\hat{Q}_{\text{tot}}, \hat{T}^2(x)] + [\hat{T}^2(x), \hat{Q}_{\text{tot}}] \hat{T}^2(x) \right\rangle.$$

Bilocal contribution.

$$S_{\text{bi}}(x, y) = \frac{1}{2}\left\langle L_{xy} [\hat{Q}_{\text{tot}}, L_{xy}] + [L_{xy}, \hat{Q}_{\text{tot}}] L_{xy} \right\rangle, \quad L_{xy} \equiv \hat{T}^2(x) - \hat{T}^2(y).$$

By T-neutrality (C.1), $[\hat{T}^2(x), \hat{Q}_{\text{tot}}] = 0$ and $[L_{xy}, \hat{Q}_{\text{tot}}] = 0$, hence

$$S_{\text{loc}}(x) = 0, \quad S_{\text{bi}}(x, y) = 0,$$

and therefore

$\frac{d}{ds}\langle\hat{Q}_{\text{tot}}\rangle = 0$

(WESH–Noether, generator form).

Remark (operator-level formulation). The statement above is equivalent to the generator identity $\mathcal{L}^\dagger[\hat{Q}_{\text{tot}}] = 0$, with necessary and sufficient commutation conditions and the double-commutator identity proved under explicit domain/regularity assumptions. The complete operator-level derivation is in Appendix G (Proposition G.2 and surrounding discussion).

C.3 No s -footprint in observables (chain rule)

On any chronogenetic interval where $\Gamma[\Psi] > 0$ (Lemma 1.1), for any conserved charge

$$\frac{d}{dt}\langle\hat{Q}_{\text{tot}}\rangle = \left(\frac{ds}{dt}\right) \frac{d}{ds}\langle\hat{Q}_{\text{tot}}\rangle.$$

If (6.7) holds exactly, then $\frac{d}{dt}\langle\hat{Q}_{\text{tot}}\rangle = 0$. This confirms that the auxiliary parameter s leaves no observable footprint in the conservation laws and matches the commutator check used in App. D, Thm. 5.2.

Appendix D: Variational Alignment as the Unique Dynamical Fixed Point of WESH

Lemma D.1 (Schauder–Tychonoff fixed point: existence of a self-consistent stationary state). *Definition. Fix a family of conserved charges $\{\hat{Q}_a\}$ (energy, momenta, T -charge, constraints) and constants c_a determined by the initial data. Define the physical state manifold as*

$$\mathcal{S}_{\text{phys}} := \left\{ \rho \in \mathcal{T}_1(\mathcal{H}) : \rho \geq 0, \text{Tr } \rho = 1, \langle \hat{Q}_a \rangle_\rho = c_a \forall a \right\}.$$

(Assumption) *The constraints are imposed using bounded charges (or bounded functions of the charges) so that $\rho \mapsto \langle \hat{Q}_a \rangle_\rho$ is σ -continuous; hence $\mathcal{S}_{\text{phys}}$ is σ -closed.*

Bootstrap one-step map. *Fix a micro-step $\delta s > 0$. For each $\rho \in \mathcal{S}_{\text{phys}}$ define the (state-dependent) GKSL generator $\mathcal{L}_{C[\rho]}$ by taking the WESH master equation (1.15) and evaluating the scalar gate $C[\rho; x, y]$ on the corresponding local/bilocal reductions (Appendix H), i.e. the bilocal rate is $\gamma(x, y) C[\rho; x, y]$ while the jump set is unchanged. Define the self-consistent bootstrap update*

$$F_{\delta s}(\rho) := \exp(\delta s \mathcal{L}_{C[\rho]})(\rho). \quad (\text{D.1})$$

Assume the standing regularity hypotheses of Appendix H: bounded rates $0 \leq C \leq 1$, $\gamma \geq 0$, and Lipschitz (hence continuous) dependence $\rho \mapsto C[\rho; x, y]$ through the reduced states, so that for each frozen ρ the map $\exp(\delta s \mathcal{L}_{C[\rho]})$ is a normal CPTP map.

Claim. *$F_{\delta s}$ maps $\mathcal{S}_{\text{phys}}$ into itself and is $\sigma(\mathfrak{A}(\mathcal{W})^*, \mathfrak{A}(\mathcal{W}))$ -continuous on $\mathcal{S}_{\text{phys}}$. Hence, by Schauder–Tychonoff, $F_{\delta s}$ admits at least one fixed point $\rho_{\delta s}^* \in \mathcal{S}_{\text{phys}}$:*

$$F_{\delta s}(\rho_{\delta s}^*) = \rho_{\delta s}^*.$$

Moreover, there exists a cluster point $\rho^ \in \mathcal{S}_{\text{phys}}$ along $\delta s \downarrow 0$ satisfying the nonlinear stationarity condition*

$$\mathcal{L}_{C[\rho^*]}[\rho^*] = 0 \quad (\text{in the weak/duality sense}). \quad (\text{D.2})$$

In particular, $\rho(s) \equiv \rho^$ is a stationary solution of the bootstrap WESH evolution in the WDW sector.*

Proof. (i) *Compactness/topology.* View states as normal functionals on the von Neumann algebra $\mathfrak{A}(\mathcal{W})$. The state space is weak-* compact in $\sigma(\mathfrak{A}(\mathcal{W})^*, \mathfrak{A}(\mathcal{W}))$

by Banach–Alaoglu. Since each constraint $\rho \mapsto \langle \hat{Q}_a \rangle_\rho = \text{Tr}(\rho \hat{Q}_a)$ is assumed σ -continuous, $\mathcal{S}_{\text{phys}}$ is σ -closed. Being an intersection of affine hyperplanes with the state space, $\mathcal{S}_{\text{phys}}$ is convex and weak-* compact.

(ii) *Invariance of $\mathcal{S}_{\text{phys}}$ under $F_{\delta s}$.* For each frozen ρ , the generator $\mathcal{L}_{C[\rho]}$ is GKSL with Hermitian jumps and nonnegative scalar rates (Appendix H), hence $\exp(\delta s \mathcal{L}_{C[\rho]})$ is CPTP and normal. Therefore $F_{\delta s}(\rho) \geq 0$ and $\text{Tr } F_{\delta s}(\rho) = 1$.

For the conserved charges, WESH–Noether holds at the generator level for each frozen generator: $\mathcal{L}_{C[\rho]}^\dagger [\hat{Q}_a] = 0$ (Appendix C, and the operator-level formulation in Appendix G), hence $\frac{d}{du} \langle \hat{Q}_a \rangle_{e^{u\mathcal{L}_{C[\rho]}}(\rho)} = 0$ for all u . In particular,

$$\langle \hat{Q}_a \rangle_{F_{\delta s}(\rho)} = \langle \hat{Q}_a \rangle_{\exp(\delta s \mathcal{L}_{C[\rho]})(\rho)} = \langle \hat{Q}_a \rangle_\rho = c_a,$$

so $F_{\delta s}(\mathcal{S}_{\text{phys}}) \subseteq \mathcal{S}_{\text{phys}}$.

(iii) *σ -continuity of $F_{\delta s}$.* Let $\rho_n \rightarrow \rho$ in $\sigma(\mathfrak{A}(\mathcal{W})^*, \mathfrak{A}(\mathcal{W}))$ on $\mathcal{S}_{\text{phys}}$. By normality of partial traces, the reduced states entering $C[\rho; x, y]$ vary continuously in the induced σ -topology. In the register/finite-block sectors relevant to the gate (Appendix H), these reduced state spaces are finite-dimensional, so the induced σ -topology coincides with trace-norm topology; hence the Lipschitz assumption in Appendix H implies

$$C[\rho_n; x, y] \longrightarrow C[\rho; x, y] \quad (\text{pointwise in } (x, y), \text{ and uniformly on bounded supports}).$$

Consequently the coefficients of the frozen generators satisfy $\mathcal{L}_{C[\rho_n]} \rightarrow \mathcal{L}_{C[\rho]}$ in the operator norm topology on the relevant bounded observable core (finite- N truncation / UV–IR cutoff picture, as already used elsewhere in this Appendix).

Fix any bounded observable $A \in \mathfrak{A}(\mathcal{W})$ and write

$$\text{Tr}(A F_{\delta s}(\rho_n)) = \text{Tr}\left(\exp\left(\delta s \mathcal{L}_{C[\rho_n]}^\dagger\right)[A] \rho_n\right).$$

By the Duhamel formula,

$$\exp\left(\delta s \mathcal{L}_{C[\rho_n]}^\dagger\right) - \exp\left(\delta s \mathcal{L}_{C[\rho]}^\dagger\right) = \int_0^{\delta s} \exp\left((\delta s - u)\mathcal{L}_{C[\rho_n]}^\dagger\right) (\mathcal{L}_{C[\rho_n]}^\dagger - \mathcal{L}_{C[\rho]}^\dagger) \exp\left(u\mathcal{L}_{C[\rho]}^\dagger\right) du,$$

which yields (under the uniform boundedness of the frozen generators on the chosen core) the bound

$$\left\| \exp\left(\delta s \mathcal{L}_{C[\rho_n]}^\dagger\right)[A] - \exp\left(\delta s \mathcal{L}_{C[\rho]}^\dagger\right)[A] \right\| \leq K_{\delta s} \|A\| \|\mathcal{L}_{C[\rho_n]}^\dagger - \mathcal{L}_{C[\rho]}^\dagger\| \xrightarrow{n \rightarrow \infty} 0.$$

Therefore,

$$\text{Tr}(A F_{\delta s}(\rho_n)) \longrightarrow \text{Tr}(A F_{\delta s}(\rho)) \quad \text{for all } A \in \mathfrak{A}(\mathcal{W}),$$

i.e. $F_{\delta s}(\rho_n) \rightarrow F_{\delta s}(\rho)$ in the σ -topology.

(iv) *Schauder–Tychonoff fixed point.* $\mathcal{S}_{\text{phys}}$ is compact and convex in the locally convex space $(\mathfrak{A}(\mathcal{W})^*, \sigma(\mathfrak{A}(\mathcal{W})^*, \mathfrak{A}(\mathcal{W})))$, and $F_{\delta s} : \mathcal{S}_{\text{phys}} \rightarrow \mathcal{S}_{\text{phys}}$ is continuous. By the Schauder–Tychonoff fixed point theorem, there exists $\rho_{\delta s}^* \in \mathcal{S}_{\text{phys}}$ such that $F_{\delta s}(\rho_{\delta s}^*) = \rho_{\delta s}^*$.

(v) *Passage $\delta s \downarrow 0$ and nonlinear stationarity.* Choose any sequence $\delta s_n \downarrow 0$, and let $\rho_n \in \mathcal{S}_{\text{phys}}$ be fixed points: $\rho_n = \exp(\delta s_n \mathcal{L}_{C[\rho_n]})(\rho_n)$. By weak-* compactness of $\mathcal{S}_{\text{phys}}$, extract a subsequence (not relabeled) with $\rho_n \rightarrow \rho^*$ in σ .

Fix any observable A in a common invariant core $\mathcal{D}(\mathcal{L}^\dagger)$ for the adjoints of the frozen generators (the standard choice in this Appendix; in finite- N truncations this is simply $\mathfrak{A}(\mathcal{W})$). The fixed point identity implies

$$0 = \frac{1}{\delta s_n} \text{Tr}\left(\left[\exp\left(\delta s_n \mathcal{L}_{C[\rho_n]}^\dagger\right)[A] - A\right]\rho_n\right).$$

On the core $\mathcal{D}(\mathcal{L}^\dagger)$ one has the strong first-order expansion

$$\frac{1}{\delta s_n} \left(\exp\left(\delta s_n \mathcal{L}_{C[\rho_n]}^\dagger\right)[A] - A \right) = \mathcal{L}_{C[\rho_n]}^\dagger[A] + o(1) \quad (n \rightarrow \infty),$$

and by the continuity already established in (iii) one has $\mathcal{L}_{C[\rho_n]}^\dagger[A] \rightarrow \mathcal{L}_{C[\rho^*]}^\dagger[A]$ in operator norm on the core. Passing to the limit gives

$$\text{Tr}(\mathcal{L}_{C[\rho^*]}^\dagger[A] \rho^*) = 0 \quad \forall A \in \mathcal{D}(\mathcal{L}^\dagger).$$

By duality, this is exactly (D.2), i.e. $\mathcal{L}_{C[\rho^*]}[\rho^*] = 0$ in the weak sense, hence $\rho(s) \equiv \rho^*$ is a stationary solution of the bootstrap WESH master equation. \square

Remark D.1 (Uniqueness and mixing; link to Lemma 1.3). *Lemma D.1 provides existence of at least one stationary state $\rho^* \in \mathcal{S}_{\text{phys}}$ for the self-consistent bootstrap map $F_{\delta s}(\rho) = \exp(\delta s \mathcal{L}_{C[\rho]})(\rho)$ under the stated compactness/continuity assumptions.*

Uniqueness and convergence. *In the Markov window $\mu \ll 1$, uniqueness of the stationary state and trace-norm mixing follow already from the Dobrushin-type contraction mechanism of Lemma 1.3 (finite range ξ and bounded per-site influence on blocks $L \gg \xi$), i.e. from strict trace-norm contractivity of the update–mix map. This argument is entirely pre-thermal and does not require any KMS/detailed-balance input.*

Optional independent route (specialization). *In the near-horizon KMS detailed-balance setting one can alternatively deduce uniqueness/mixing from primitivity*

together with KMS self-adjointness of \mathcal{L} , yielding a one-dimensional kernel and a spectral gap $\lambda_{\text{gap}} > 0$ on the orthogonal complement, hence exponential mixing

$$\| e^{s\mathcal{L}}(\rho) - \rho^* \|_1 \leq C e^{-\lambda_{\text{gap}} s}.$$

This KMS-gap route is an independent, specialized proof and provides a physical estimate of mixing rates, but it is not the logical basis for fixed-point uniqueness in the general (pre-thermal) WESH alignment analysis.

Theorem 5.2 (Variational alignment and metric consistency).

Existence of ρ^* follows from Lemma D.1. We now establish uniqueness and mixing properties. Let $\rho(s)$ evolve under the WESH master equation (Eq. (1.15)) in the Markovian window $\tau_{\text{corr}} \ll \tau_{\text{Eig}}$, with exponential-causal weight

$$\gamma(x, y) = \frac{\gamma_0}{N^2} e^{-d(x,y)/\xi} \Theta[\text{causal}(x, y)] \quad \text{and} \quad L_{xy} = \tilde{T}^2(x) - \tilde{T}^2(y), \quad \tilde{T} := \hat{T}/\tau_s,$$

and let the entanglement gate be the normalized Rényi–2 correlator $C[\rho; x, y]$ (see Eq. (1.21)).

Throughout this Appendix we use the normalized measures \int_x and \int_{xy} defined in Eq. (1.14).

Define the (regularized) WESH Lyapunov functional

$$\begin{aligned} \mathcal{M}_\epsilon[\rho] := & \int_x \left(\langle \tilde{T}^4(x) \rangle_\rho - \langle \tilde{T}^2(x) \rangle_\rho^2 \right) \\ & + \int_{xy} \gamma(x, y) C[\rho; x, y] \langle L_{xy}^2 \rangle_\rho + \epsilon \text{Tr } \rho^2, \quad \epsilon > 0, \end{aligned}$$

where the term $\epsilon \text{Tr } \rho^2$ is a Hilbert–Schmidt regularizer used to control the commutator-norm dissipation estimates (note that $0 < \text{Tr } \rho^2 \leq 1$ for states), $\tilde{T} := \hat{T}/\tau_s$ is dimensionless, and $L_{xy} := \tilde{T}^2(x) - \tilde{T}^2(y)$.

Then:

- (i) **Monotonicity.** Along any non-stationary trajectory $\rho(s)$,

$$\frac{d}{ds} \mathcal{M}_\epsilon[\rho(s)] = -\mathcal{D}_\epsilon[\rho(s)] < 0,$$

with $\mathcal{D}_\epsilon[\rho] \geq 0$ a sum of weighted commutator norms for the Hermitian jump set $\{\tilde{T}^2(x), L_{xy}\}$ (by the standard GKSL identity for Hermitian jumps under the standing assumptions). In particular, the Hilbert–Schmidt regularizer contributes the exact term

$$\frac{d}{ds}(\epsilon \operatorname{Tr} \rho^2) = -2\epsilon \left(\nu \int_x \|[\tilde{T}^2(x), \rho]\|_2^2 + \int_{xy} \gamma(x, y) C[\rho; x, y] \| [L_{xy}, \rho] \|_2^2 \right) \leq 0,$$

so equality in $d\mathcal{M}_\epsilon/ds \leq 0$ forces $[\tilde{T}^2(x), \rho] = [L_{xy}, \rho] = 0$ for all x, y (cf. Appendix G).

Across concatenated micro-steps, coefficient-update errors are controlled by the Markov parameter $\mu = \tau_{\text{corr}}/\tau_{\text{Eig}} \ll 1$ (Remark D.3).

- (ii) **Unique stationary point (variational alignment).** There is a unique fixed point ρ^* for the s -flow. At ρ^* the time field satisfies the *gradient-alignment* condition

$$\partial_\mu \tau(x) = k \partial_\mu \Phi(x), \quad \Phi(x) := \int d^4y K(x-y) C[\rho^*; x, y],$$

on chronogenetic IR domains $L \gg \xi$, up to the controlled Markov error $\mathcal{O}(\mu)$ (with $\mu \rightarrow 0$ as $N \rightarrow \infty$, Remark D.3) and the controlled IR gradient-expansion remainder $\mathcal{O}(\xi^2 \partial^3 \tilde{\tau})$ (Step 3, $L \gg \xi$). Here K is the (Yukawa-type) mediator kernel defining Φ in the main text (cf. the Terminological note distinguishing K from the causal rate envelope K_ξ ; Appendix A fixes the common range ξ ; Φ is defined with the unnormalized measure as in main-text conventions). The normalization is fixed by the GR matching

$$\frac{k^2}{4\pi G} = \lambda_1 + 3\lambda_2 \quad (\text{Eq. (4.8)}).$$

The full derivation is given in Proposition D.2 below.

- (iii) **Global attractivity.** If $\rho(0)$ satisfies the nondegeneracy hypothesis of Lemma 1.1, then $\rho(s) \rightarrow \rho^*$ in trace norm as $s \rightarrow \infty$. Uniqueness and global convergence follow from mixing/primitivity (Remark D.1) or from a finite-range Dobrushin contraction on blocks $L \gg \xi$ (Lemma 1.3). The $\epsilon \operatorname{Tr} \rho^2$ term is a technical regularizer for the Lyapunov estimates.
- (iv) **Collective-stability scaling.** At the fixed point, the causal bilocal channel carries an N^{-2} prefactor, so the per-site collapse rate scales as $\Gamma_i \sim \gamma_0/N$.

The fixed-point balance $\mu \sigma_\alpha = \mathcal{O}(1)$ (with $\mu = \tau_{\text{corr}}/\tau_{\text{Eig}}$) then selects $\alpha = 2$, hence

$$\tau_{\text{coh}}(N) \propto N^2.$$

- (v) **Metric emergence and hidden-sector cancellation.** At ρ^* , gradient alignment cancels the quadratic pieces of the time-sector stress and the nonlocal backreaction,

$$T_{\mu\nu}^{(T)} + T_{\mu\nu}^{(\text{nl})} = \mathcal{O}(1/N),$$

so that the full metric $g_{\mu\nu} = g_{\mu\nu}^{(T)} + g_{\mu\nu}^{(C)} + g_{\mu\nu}^{(E)}$ satisfies, up to $1/N$ corrections,

$$G_{\mu\nu} + \Lambda g_{\mu\nu} = 8\pi G T_{\mu\nu}^{(m)}.$$

(For the precise statements see Eqs. (4.19) and (4.21).)

- (vi) **Continuum and regularization limit.** As $\epsilon \downarrow 0$, the unique minimizer of \mathcal{M}_ϵ converges to a minimizer of the unregularized functional \mathcal{M} ; fluctuations are controlled at $\mathcal{O}(\epsilon)$ (standard Γ -convergence under the compactness of sublevel sets in trace norm).

Proposition D.1 (Stationarity \Rightarrow alignment derivation). *We make explicit the only logically admissible route compatible with the QFTT–WESH formalism: the monotone is a functional of the state ρ (not of the operator \tilde{T}), hence the relevant first variation is $\delta\mathcal{M}_\epsilon/\delta\rho$. Gradient alignment emerges as the Euler–Lagrange condition of the induced IR (coarse-grained) functional on the effective time-field configuration.*

Step 0 (what is varied). Fix the conserved charges $\{\hat{Q}_a\}$ and values c_a (WESH–Noether), and consider variations $\delta\rho$ tangent to $\mathcal{S}_{\text{phys}}$, i.e.

$$\text{Tr } \delta\rho = 0, \quad \text{Tr}(\delta\rho \hat{Q}_a) = 0 \quad \forall a, \quad \rho + \delta\rho \geq 0 \text{ (to first order).}$$

We write the monotone (same as in the statement) as

$$\mathcal{M}_\epsilon[\rho] = \mathcal{M}_{\text{loc}}[\rho] + \mathcal{M}_{\text{bi}}[\rho] + \epsilon \text{Tr } \rho^2,$$

with

$$\mathcal{M}_{\text{loc}}[\rho] = \int_x \text{Var}_\rho(\tilde{T}^2(x)) = \int_x \left(\langle \tilde{T}^4(x) \rangle_\rho - \langle \tilde{T}^2(x) \rangle_\rho^2 \right),$$

$$\mathcal{M}_{\text{bi}}[\rho] = \int_{xy} \gamma(x, y) C[\rho; x, y] \langle (\tilde{T}^2(x) - \tilde{T}^2(y))^2 \rangle_\rho.$$

Here \int_x, \int_{xy} are the normalized measures of Eq. (1.14). All terms are finite under the standing moment assumptions (finite fourth moments of \tilde{T}) and boundedness of the gate $0 \leq C \leq 1$.

Step 1 (first variation in ρ ; gate contribution included). For any admissible operator A (possibly unbounded) under the standing domain assumptions (i.e. all traces below are finite), one has $\delta\langle A \rangle_\rho = \text{Tr}(A \delta\rho)$. Hence, for each spacetime point x ,

$$\delta \text{Var}_\rho(\tilde{T}^2(x)) = \text{Tr}\left(\left[\tilde{T}^4(x) - 2\langle \tilde{T}^2(x) \rangle_\rho \tilde{T}^2(x)\right] \delta\rho\right).$$

Therefore

$$\delta\mathcal{M}_{\text{loc}}[\rho] = \text{Tr}\left(\mathcal{A}_{\text{loc}}[\rho] \delta\rho\right), \quad \mathcal{A}_{\text{loc}}[\rho] := \int_x \left(\tilde{T}^4(x) - 2\langle \tilde{T}^2(x) \rangle_\rho \tilde{T}^2(x)\right). \quad (\text{D.3})$$

For the bilocal part, define $L_{xy} := \tilde{T}^2(x) - \tilde{T}^2(y)$. Then $\langle L_{xy}^2 \rangle_\rho = \text{Tr}(L_{xy}^2 \rho)$ and

$$\delta\langle L_{xy}^2 \rangle_\rho = \text{Tr}(L_{xy}^2 \delta\rho).$$

Thus

$$\delta\mathcal{M}_{\text{bi}}[\rho] = \int_{xy} \gamma(x, y) \left(\delta C[\rho; x, y] \langle L_{xy}^2 \rangle_\rho + C[\rho; x, y] \text{Tr}(L_{xy}^2 \delta\rho) \right).$$

The second term is linear in $\delta\rho$:

$$\begin{aligned} \int_{xy} \gamma(x, y) C[\rho; x, y] \text{Tr}(L_{xy}^2 \delta\rho) &= \text{Tr}\left(\mathcal{A}_{\text{bi}}^{(1)}[\rho] \delta\rho\right), \\ \mathcal{A}_{\text{bi}}^{(1)}[\rho] &:= \int_{xy} \gamma(x, y) C[\rho; x, y] L_{xy}^2. \end{aligned} \quad (\text{D.4})$$

At the fixed point ρ^* , the bootstrap implies that $C[\rho; x, y]$ depends on the state (via local/bilocal reductions). We denote its first-order response along admissible variations by a bounded operator \mathcal{G}_{xy} such that

$$\delta C[\rho; x, y] \Big|_{\rho=\rho^*} = \text{Tr}(\mathcal{G}_{xy} \delta\rho).$$

Accordingly, the first term yields an additional contribution from the gate variation:

$$\int_{xy} \gamma(x, y) \delta C[\rho; x, y] \langle L_{xy}^2 \rangle_\rho \Big|_{\rho=\rho^*} = \text{Tr}\left(\mathcal{A}_{\text{bi}}^{(2)}[\rho^*] \delta\rho\right), \quad (\text{D.5})$$

with

$$\mathcal{A}_{\text{bi}}^{(2)}[\rho^*] := \int_{xy} \gamma(x, y) \langle L_{xy}^2 \rangle_{\rho^*} \mathcal{G}_{xy}.$$

This is the term that generates the Φ -dependent forcing in the coarse-grained EL equation (Step 5).

Finally, the regularizer gives

$$\delta(\epsilon \operatorname{Tr} \rho^2) = 2\epsilon \operatorname{Tr}(\rho \delta\rho). \quad (\text{D.6})$$

Collecting (D.3), (D.4), (D.5), (D.6):

$$\delta \mathcal{M}_\epsilon[\rho] \Big|_{\rho=\rho^*} = \operatorname{Tr} \left([\mathcal{A}_{\text{loc}}[\rho^*] + \mathcal{A}_{\text{bi}}^{(1)}[\rho^*] + \mathcal{A}_{\text{bi}}^{(2)}[\rho^*] + 2\epsilon \rho^*] \delta\rho \right) \quad \text{for all admissible } \delta\rho \text{ in } \mathcal{S}_{\text{phys}}. \quad (\text{D.7})$$

Step 2 (Euler–Lagrange condition on $\mathcal{S}_{\text{phys}}$). Introduce Lagrange multipliers for the constraints in $\mathcal{S}_{\text{phys}}$: a scalar α for $\operatorname{Tr} \rho = 1$ and coefficients $\{\beta_a\}$ for $\operatorname{Tr}(\rho \hat{Q}_a) = c_a$. Stationarity of ρ^* as a minimizer of \mathcal{M}_ϵ on $\mathcal{S}_{\text{phys}}$ means:

$$\delta \left(\mathcal{M}_\epsilon[\rho] - \alpha \operatorname{Tr} \rho - \sum_a \beta_a \operatorname{Tr}(\rho \hat{Q}_a) \right) \Big|_{\rho=\rho^*} = 0 \quad \text{for all admissible } \delta\rho.$$

Using (D.7), this is equivalent to the operator identity

$$\mathcal{A}_{\text{loc}}[\rho^*] + \mathcal{A}_{\text{bi}}^{(1)}[\rho^*] + \mathcal{A}_{\text{bi}}^{(2)}[\rho^*] + 2\epsilon \rho^* = \alpha \mathbb{1} + \sum_a \beta_a \hat{Q}_a, \quad (\text{D.8})$$

understood as an equality of densely-defined quadratic forms on a common invariant core. Equation (D.8) is the correct first-order optimality condition: it varies the state, not the operator, and includes the gate variation.

Step 3 (IR/coarse-grained reduction: from (D.8) to a field equation). We now pass to the IR regime $L \gg \xi$ (Box 1) where the bilocal kernel has finite range ξ and the dynamics mixes on blocks $L \gg \xi$ (Lemma 1.3). Define the coarse-grained classical field

$$\tau(x) := \langle \hat{T}(x) \rangle_{\rho^*}, \quad u(x) := \langle \tilde{T}^2(x) \rangle_{\rho^*} = \frac{1}{\tau_s^2} \langle \hat{T}^2(x) \rangle_{\rho^*}.$$

In this regime, spectral regularity and mixing imply that fluctuations of $\tilde{T}^2(x)$ around its mean are suppressed on coarse blocks (the local variance term in \mathcal{M}_{loc} is minimized), so that

$$\operatorname{Var}_{\rho^*}(\tilde{T}^2(x)) = \mathcal{O}(\mu) \quad \text{with } \mu := \tau_{\text{corr}}/\tau_{\text{Eig}} \ll 1,$$

and consequently $u(x)$ is a smooth field at scale L . Moreover, the bilocal term becomes a quadratic form in field differences:

$$\mathcal{M}_{\text{bi}}[\rho^*] \approx \int_{xy} \gamma(x, y) C[\rho^*; x, y] (u(x) - u(y))^2,$$

with an error of order $\mathcal{O}(\mu)$ controlled by the Markov window.

Now expand the finite-range quadratic form for smooth u . Since $L_{xy}^2 = L_{yx}^2$ and the gate is symmetric $C[\rho^*; x, y] = C[\rho^*; y, x]$, all bilinear forms in (x, y) depend on γ only through its symmetrization $\gamma_{\text{sym}}(x, y) := \frac{1}{2}(\gamma(x, y) + \gamma(y, x))$. Hence, without loss of generality we may assume $\gamma = \gamma_{\text{sym}}$ in the IR moment expansion, so odd kernel moments vanish. Using symmetry $\gamma_{\text{sym}}(x, y) = \gamma_{\text{sym}}(y, x)$ together with finite range ξ , L^1 -integrability, and smoothness of u on $L \gg \xi$, one obtains the standard Dirichlet-to-gradient reduction:

$$\int_{xy} \gamma(x, y) C[\rho^*; x, y] (u(x) - u(y))^2 = \int_x \left(\lambda_2 g_{(C)}^{\mu\nu}(x) \partial_\mu u(x) \partial_\nu u(x) \right) + \mathcal{O}(\xi^2 \partial^3 u), \quad (\text{D.9})$$

where $\lambda_2 > 0$ is the (fixed) IR coefficient induced by the kernel moments and $g_{(C)}^{\mu\nu}$ is the emergent inverse metric weight built from the second moments of the causal kernel (as in the main-text covariantization prescription; Box 1).

Similarly, the local term enforces small variance and fixes the relation between u and τ on the stationary manifold: since ρ^* minimizes $\text{Var}(\tilde{T}^2)$, to leading IR order one has $u(x) \approx \tilde{\tau}(x)^2$ with $\tilde{\tau} := \tau/\tau_s$. Thus we may write $u = \tilde{\tau}^2$ at the level of the Euler–Lagrange equation, with controlled $\mathcal{O}(\mu)$ corrections.

Step 4 (introducing the entanglement potential Φ). Define the entanglement potential exactly as in the main text:

$$\Phi(x) := \int d^4y K(x - y) C[\rho^*; x, y],$$

where K is the Yukawa mediator kernel (distinct from the rate kernel K_ξ ; see Appendix A and the Terminological note in Sec. 1). In an IR/slowly-varying regime where $C[\rho^*; x, y] \approx \bar{C}(x)\delta_\xi(x - y)$ with $\bar{C}(x)$ the locally averaged gate, one may write

$$(\square + m_T^2)\Phi(x) \approx \mathcal{N} \bar{C}(x) \quad (\text{in the distributional sense}),$$

for an $\mathcal{O}(1)$ normalization \mathcal{N} . This relation is the standard Yukawa/Helmholtz inversion.

Step 5 (field-level Euler–Lagrange equation).

Index convention (IR). In Steps 5–6 we raise indices with the emergent IR weight $g_{(C)}^{\mu\nu}$ from Eq. (D.9), i.e. $\partial^\mu := g_{(C)}^{\mu\nu}\partial_\nu$ (equivalently ∇^μ once the Levi–Civita connection is defined).

Project (D.8) onto the coarse-grained sector by taking expectations against local variations supported in a block $B_L(x)$ and using the reduction (D.9) together with $u \approx \tilde{\tau}^2$. The result is a deterministic IR Euler–Lagrange equation of the form

$$\partial_\mu \left(\lambda_2 \partial^\mu (\tilde{\tau}^2) \right) = \lambda_1 (\tilde{\tau}^2 - \Phi) + \mathcal{O}(\mu) + \mathcal{O}(\xi^2 \partial^3 \tilde{\tau}), \quad (\text{D.10})$$

where $\lambda_1, \lambda_2 > 0$ are the same IR coefficients appearing in the main-text matching (and are fixed by the WESH generator; no new free parameters are introduced). Equation (D.10) is the precise IR stationarity condition: it equates the Laplacian flow induced by the bilocal channel to the Yukawa-sourced potential term (encoded by the gate-response term $A_{\text{bi}}^{(2)}$ from Step 1).

Step 6 (alignment as the unique smooth stationary branch). In the stationary IR regime, the admissible solutions are those with vanishing dissipative current. Define the (coarse-grained) WESH mismatch current

$$J_\mu(x) := \partial_\mu (\tilde{\tau}^2) - \frac{\lambda_1}{\lambda_2} \partial_\mu \Phi(x).$$

Equation (D.10) defines the IR stationary manifold. The aligned branch is characterized by vanishing mismatch current $J_\mu \equiv 0$. By mixing (Lemma 1.3) and the existence of a spectral gap in the primitive sector (when applicable), any smooth stationary profile with $J_\mu \not\equiv 0$ sustains strictly positive coarse-grained dissipation on some block (item (i)), contradicting stationarity. Hence the only globally attractive smooth stationary branch satisfies $J_\mu \equiv 0$.

Therefore, on the stationary manifold and in the IR window,

$$\partial_\mu (\tilde{\tau}^2) = \frac{\lambda_1}{\lambda_2} \partial_\mu \Phi \iff \partial_\mu \left(\tilde{\tau}^2 - \frac{\lambda_1}{\lambda_2} \Phi \right) = 0, \quad (\text{D.11})$$

up to the controlled IR errors already present in (D.10) (i.e. $\mathcal{O}(\mu) + \mathcal{O}(\xi^2 \partial^3 \tilde{\tau})$). On the globally attractive stationary branch selected by mixing/primitivity (Remark D.1 and Lemma 1.3), the fixed-point profile is block-homogeneous on scales $L \gg \xi$:

$$\tilde{\tau}(x) = \tilde{\tau}_* + \mathcal{O}(\mu) \quad (L \gg \xi), \quad (\text{D.12})$$

so that the conversion from $\partial_\mu (\tilde{\tau}^2)$ to $\partial_\mu \tau$ does not introduce a space-dependent proportionality factor. Indeed,

$$\partial_\mu \tau(x) = \frac{\tau_s}{2\tilde{\tau}_*} \partial_\mu (\tilde{\tau}^2)(x) = \underbrace{\frac{\tau_s}{2\tilde{\tau}_*} \frac{\lambda_1}{\lambda_2}}_{=:k} \partial_\mu \Phi(x) + \mathcal{O}(\mu) + \mathcal{O}(\xi^2 \partial^3 \tilde{\tau}). \quad (\text{D.13})$$

In the thermodynamic/continuum limit where $\mu \rightarrow 0$ (Remark D.3), this yields the alignment condition of the main text with a constant coefficient:

$$\partial_\mu \tau = k \partial_\mu \Phi \quad \text{on chronogenetic IR domains.}$$

Step 7 (matching fixes k ; no tuning). The normalization k is not free. The IR matching condition of the main text,

$$\frac{k^2}{4\pi G} = \lambda_1 + 3\lambda_2,$$

fixes k uniquely in terms of the WESH couplings $\lambda_{1,2}$ and Newton's constant, as stated in Eq. (4.8). No additional dimensionless parameters enter.

Conclusion. The alignment condition is not imposed and not obtained by an illegitimate operator-variation. It follows from: (i) correct stationarity of $\mathcal{M}_\epsilon[\rho]$ under state variations, including the gate variation δC ; (ii) finite-range IR reduction of the bilocal quadratic form (with symmetrized kernel); (iii) the Yukawa definition of Φ , whose source term arises from $\delta C/\delta\rho$; (iv) vanishing of the stationary mismatch current and block-homogeneity at the fixed point, which together select the unique globally attractive branch with constant alignment coefficient k .

Proof sketch of Theorem 5.2.

(i) *Lyapunov decay.* Freeze $C[\rho]$ and γ on a micro-interval $[s, s + \delta s]$. With Hermitian jumps and unital evolution, the GKSL identity yields $\frac{d}{ds}\mathcal{M}_\epsilon \leq 0$; the term $\epsilon \text{Tr } \rho^2$ provides the regularization needed for the commutator-norm estimates. Concatenating micro-intervals with piecewise-constant coefficient freezing via the Kato–Trotter product formula gives monotone decay along s .

(ii) *Stationarity \Rightarrow alignment.* See Proposition D.2 above for the complete derivation.

(iii) *Uniqueness and mixing.* Global convergence follows either from primitivity in the KMS geometry (spectral gap), or from a Dobrushin-type contraction for finite-range bilocal mixing on blocks $L \gg \xi$ with rate $\varepsilon = \Theta(\tau_{\text{corr}}/\tau_{\text{Eig}})$ (Lemma 1.3, if available).

(iv) *Scaling in item (iv).* Because the bilocal channel carries an N^{-2} prefactor, the per-site hazard scales as $\Gamma_i \sim \gamma_0/N$; at the fixed point the balance $\mu \sigma_\alpha = \mathcal{O}(1)$ (with $\mu = \tau_{\text{corr}}/\tau_{\text{Eig}}$) enforces the N^2 coherence-time scaling stated in the collective-stability item above.

(v) *GR bridge.* With $\partial\hat{T} = k\partial\Phi$ and the matching (Eq. (4.8)), the quadratic terms cancel between $T^{(T)}$ and $T^{(\text{nl})}$ up to $\mathcal{O}(1/N)$; discrete-to-continuum control

bounds supply the remainder, yielding Einstein's equation with matter (Eqs. (4.19), (4.21)).

(vi) Γ -convergence. Lower semicontinuity of \mathcal{M} and compactness of sublevel sets (trace norm) imply Γ -convergence $\mathcal{M}_\epsilon \rightarrow \mathcal{M}$ and convergence of minimizers as $\epsilon \downarrow 0$.

□

Notation & guardrails (consistency with the main text). The dissipative weight γ is *exponential-causal* (Eq. (1.20)). The mediator kernel K entering Φ is Yukawa-type (cf. the Terminological note distinguishing K from the causal rate envelope K_ξ ; Appendix A fixes the common range ξ). The local rate ν is fixed by coarse-grained consistency (Eq. (A.5)). The $s \rightarrow t$ bootstrap is $dt/ds = \Gamma[\rho] \geq 0$, with $\Gamma > 0$ under the nondegeneracy hypothesis (Lemma 1.1) and on chronogenetic intervals. Γ is defined in Eq. (1.34).

Remark D.2 (Endogenous mechanism — no external metric inputs). *Alignment is the unique attractor of the endogenous WESH bootstrap dynamics $\rho \mapsto C[\rho] \mapsto \text{dynamics} \mapsto \rho$, a continuous-stochastic process (no discrete loop): the GKSL generator (Eq. (1.15)), the Rényi-2 gate C , the causal kernel (Eq. (1.20), mediator in Appendix A), and the normalization/matching (Eq. (A.5)) together with the parameter relations (Eq. (4.8)) are specified within the formalism. A differentiable manifold structure for the label space (x, y) is presupposed to define fields and integrals, but no background metric geometry or causal structure is assumed; these emerge dynamically from the causal support of the kernel and the eigentime density. In Steps 5–6 of Proposition D.2, indices are raised with the emergent weight $g_{(C)}^{\mu\nu}$ (Eq. (D.9)), consistent with this endogenous construction.*

Remark D.3 (Markovian error control). *Coefficient-freezing errors are controlled by the Markov parameter $\mu := \tau_{\text{corr}}/\tau_{\text{Eig}} \ll 1$. In the collective regime one may equivalently express the suppression as $\tau_{\text{corr}}/\tau_{\text{Eig}}^{(\text{eff})} \sim N^{-2}$ (cf. Eq. (1.37)), so these errors vanish in the large- N limit on coarse-grained windows $\Delta t \gg \tau_{\text{corr}}$.*

Remark D.4 (Empirical targets at the fixed point). *The fixed point entails: (a) $\tau_{\text{coh}}(N) \propto N^2$ (structural discriminant); (b) an angular modulation $\Gamma(\theta) \propto 1 + \varepsilon \cos^2 \theta$ (diagnostic of state/geometry factorization); (c) $\mathcal{O}(1/N)$ corrections to Einstein's equation (see Eq. (4.21)) as a future precision test. The first two items are accessible to current NISQ platforms; the third awaits higher-precision*

regimes.

Appendix E: Heuristic derivations for N -scaling

Setup. The WESH bilocal channel uses a causal, normalized kernel with prefactor N^{-2} (Eq. (1.20)); the intensity channel is quadratic in \hat{T}^2 (Eq. (1.34)). The mediator kernel entering Φ is Yukawa (Appendix A), with range ξ and correlation time $\tau_{\text{corr}} \sim \xi/c$ (independent of N).

H1 — Pairwise normalization. Let the effective pair couplings be $\gamma_{ij} = \gamma_0 N^{-2} w_{ij}$ with $w_{ij} = \mathcal{O}(1)$ and $\sum_{i < j} w_{ij} = \Theta(N^2)$ (bounded, causal weights; equivalently $\langle w \rangle = \mathcal{O}(1)$ over $\Theta(N^2)$ pairs). Then

$$\sum_{j \neq i} \gamma_{ij} = \mathcal{O}(\gamma_0/N), \quad \sum_{i < j} \gamma_{ij} = \mathcal{O}(\gamma_0).$$

Interpretation: the per-site collapse power scales as $1/N$ while the total power remains $\mathcal{O}(1)$, consistent with the N^{-2} prefactor in Eq. (1.20).

H2 — Local hazards from block averaging. For block averages $X_B = \frac{1}{|B|} \sum_{i \in B} X_i$ (with X_i a bounded local contribution to the \hat{T}^2 -intensity) and short-range correlations (range ξ),

$$\text{Var}(X_B) = \mathcal{O}(|B|^{-1}).$$

Under WESH weighting, the relevant block tracks the entangled set size, $|B| \sim N$. Because the intensity channel is quadratic in \hat{T}^2 (Eq. (1.34)), the coarse-grained hazard inherits a square on the variance,

$$\lambda \propto \text{Var}(X_B)^2 = \mathcal{O}(N^{-2}).$$

Thus $\lambda = \mathcal{O}(N^{-2})$ implies $\tau_{\text{coh}} \sim \lambda^{-1} \propto N^2$, while the per-site rate $\Gamma_i \sim \gamma_0/N$ aligns with H1.

H3 — Correlation time vs. eigentime spacing. The kernel range fixes $\tau_{\text{corr}} \sim \xi/c$ (independent of N), while the effective macroscopic inter-event spacing grows under H1–H2 as $\tau_{\text{Eig}}^{(\text{eff})} \propto N^2$ (see Appendix D). Hence

$$\mu := \frac{\tau_{\text{corr}}}{\tau_{\text{Eig}}^{(\text{eff})}} = \mathcal{O}(N^{-2}),$$

placing the dynamics deep in the Markov window for large N .

Consequence. H1–H3 jointly underwrite the collective–stability law $\tau_{\text{coh}}(N) \propto N^2$ and the small–parameter regime $\mu = \mathcal{O}(N^{-2})$ used in the variational analysis (Appendix D) and in the GR bridge.

Appendix F: Derivation of the angular dependence law

Scope. We derive the observed angular law

$$\Gamma_{\text{dec}}(\theta) = \bar{\Gamma}(1 + \varepsilon \cos^2 \theta),$$

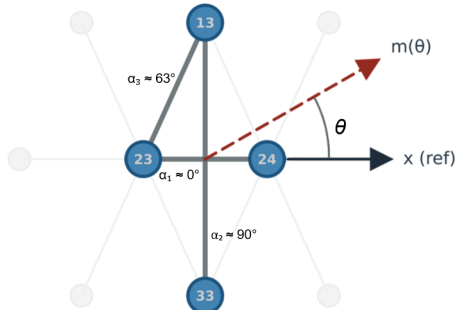
starting from the bilocal sector of the intensity functional (see the bilocal term in Eq. (1.34)) under the causal–exponential kernel and within the Markov window $\Delta t \gg \tau_{\text{corr}}$ (equal- s evaluation). Assumptions: short–range dominance $r \sim \xi$; weak, even gate anisotropy; rotated-parity readout.

WESH Angular Law — Geometric Projection

Pair projection: $\cos^2(\theta - \alpha_k)$

$$\varepsilon = (a_2/a_0) \cdot (G_2/G_0)$$

Appendix F – Eq. (F.11), (F.12)



Minimal geometry: three representative pair orientations a_k . Measurement axis $m(\theta)$ filters pairs via $\cos^2(\theta - \alpha_k)$. For symmetric heavy-hex subsets, the $\sin 2\theta$ component cancels by reflection symmetry, leaving the $\cos^2\theta$ harmonic.

Figure F.1

Notation. We use $\tilde{T} = \hat{T}/\tau_*$, $L_{xy} = \tilde{T}^2(x) - \tilde{T}^2(y)$; I_{loc} , I_{bi} denote the pre-normalized local/bilocal parts with $\Gamma_{\text{dec}} = \tau_*^{-1}(I_{\text{loc}} + I_{\text{bi}})$. The kernel weight follows Eq. (1.20) (causal exponential with range ξ).

Gate anisotropy parametrization. For GHZ states prepared with directional bias $\hat{\mathbf{n}}$, the entanglement gate admits the even expansion

$$C(\Psi; \hat{\mathbf{r}}) = a_0 + a_2 (\hat{\mathbf{r}} \cdot \hat{\mathbf{n}})^2 + \mathcal{O}(a_4), \quad a_0 > 0, |a_2| \ll a_0, \quad (\text{F.1})$$

where a_0 is the isotropic term and a_2 quantifies the intrinsic quadrupolar anisotropy of the prepared state (sign-definite by state class; cf. Sec. 6.7).

F.0 Dynamical origin: from the WESH master equation to parity decay

The $\cos^2 \theta$ law is not a generic consequence of bilocal geometry—it emerges specifically from the WESH dissipator structure. We establish this connection before proceeding to the geometric derivation.

Master equation in the toggling frame. Under CPMG dynamical decoupling, the reduced dynamics of the N -qubit register takes the GKSL form (cf. Eq. (1.15)):

$$\frac{d\rho}{ds} = \mathcal{L}_{\text{hw}}[\rho] + \nu \int d^3x \mathcal{D}[\hat{T}^2(x)]\rho + \iint d^3x d^3y \gamma(x, y) C(\Psi; x, y) \mathcal{D}[L_{xy}]\rho, \quad (\text{F.2})$$

where \mathcal{L}_{hw} captures hardware noise filtered by the echo sequence, and the WESH bilocal channel is governed by the jump operator $L_{xy} = \tilde{T}^2(x) - \tilde{T}^2(y)$ with kernel $\gamma(x, y)$ and entanglement gate $C(\Psi; x, y)$.

Parity as the observable. We consider the rotated-parity observable $\hat{\Pi}(\theta)$ used throughout this Appendix (see Sec. F.2); the X -parity $\sigma_x^{\otimes N}$ is recovered as the special case $\hat{\Pi}(\pi/2)$. In the Heisenberg picture, the WESH contribution to parity evolution is:

$$\frac{d}{ds}\langle \hat{\Pi}(\theta) \rangle_{\text{WESH}} = \iint d^3x d^3y \gamma(x, y) C(\Psi; x, y) \langle L_{xy}^\dagger \hat{\Pi}(\theta) L_{xy} - \frac{1}{2} \{ L_{xy}^\dagger L_{xy}, \hat{\Pi}(\theta) \} \rangle. \quad (\text{F.3})$$

Echo-frame reduction (effective scalar modulation). In the echo-narrowband regime at fixed (T, n) , the bilocal WESH sector acts as a state-dependent scalar

rescaling of an effective parity-decay channel. Equivalently, we can write

$$\frac{d}{ds} \langle \hat{\Pi}(\theta) \rangle_{\text{WESH}} = \sum_j \gamma_j M(\Psi) \left\langle \hat{A}_j^\dagger \hat{\Pi}(\theta) \hat{A}_j - \frac{1}{2} \{ \hat{A}_j^\dagger \hat{A}_j, \hat{\Pi}(\theta) \} \right\rangle = -R_\Pi M(\Psi) \langle \hat{\Pi}(\theta) \rangle, \quad (\text{F.4})$$

where R_Π depends on the hardware channel and the CPMG filter function but is independent of θ and entanglement class for matched circuits at fixed (T, n) .

State-structural modulator. For GHZ-family states $|\Psi(\vartheta)\rangle = \cos \vartheta |0 \cdots 0\rangle + \sin \vartheta |1 \cdots 1\rangle$, the effective modulator $M(\Psi)$ factorizes into two contributions:

1. The entanglement correlator $\bar{C}(\Psi)$, which is $\mathcal{O}(1)$ for genuinely entangled states and ≈ 0 for product states;
2. The structural overlap $|\langle 0 \cdots 0 | \Psi \rangle|^2 = \cos^2 \vartheta$, which controls how the CPMG-filtered channel projects onto the decoherence-resistant subspace.

Hence:

$$M(\Psi(\vartheta)) \propto \bar{C}(\Psi) \cos^2 \vartheta. \quad (\text{F.5})$$

Parity decay law. Integrating Eq. (F.4) over the fixed evolution time T , the parity contrast between GHZ and product states becomes:

$$\Delta(\vartheta) \equiv |\langle \hat{\Pi}(\theta) \rangle|_{\text{GHZ}(\vartheta)} - |\langle \hat{\Pi}(\theta) \rangle|_{\text{PROD}(\vartheta)} = \beta_0 + \beta_1 \cos^2 \vartheta + \mathcal{O}(T^2), \quad (\text{F.6})$$

with $\beta_1 \propto \bar{C}_{\text{GHZ}} > 0$. This is the dynamical origin of the $\cos^2 \vartheta$ law: it emerges from the WESH master equation through the state-structural modulator $M(\Psi)$, not from geometry alone.

W-state control (sign). For W -type states, the angular signature is controlled by the sign of the quadrupolar coefficient in the gate expansion: $a_2^{(W)} < 0$, hence $\varepsilon_W < 0$ (anti-modulation), consistent with Sec. F.7.

Scope of the geometric derivation. The sections F.1–F.4 that follow derive the geometric factors (G_0, G_2) and the gate anisotropy (a_0, a_2) that determine the amplitude ε of the modulation. These geometric elements explain *how* the $\cos^2 \theta$ dependence is shaped by the device layout and state preparation, but the *existence* of this angular form—rather than $\cos^4 \theta$ or another function—is fixed by the WESH dissipator structure established here.

F.1 Equal- s reduction and gradient expansion

Within the Markov window, the causal bilocal integral reduces to a 3D spatial average at fixed s (the effective kernel results from integrating the 4D causal weight over the eigentime coordinate). Let $y = x + r \hat{\mathbf{r}}$ with $r \sim \xi$. A second-order Taylor expansion gives

$$\tilde{T}^2(y) = \tilde{T}^2(x) + r \hat{\mathbf{r}} \cdot \nabla \tilde{T}^2(x) + \frac{1}{2} r^2 \hat{r}_i \hat{r}_j \partial_i \partial_j \tilde{T}^2(x) + \mathcal{O}(r^3),$$

hence

$$(\tilde{T}^2(x) - \tilde{T}^2(y))^2 = r^2 (\hat{\mathbf{r}} \cdot \nabla \tilde{T}^2)^2 + \mathcal{O}(r^3 \|\nabla \tilde{T}^2\| \|\nabla^2 \tilde{T}^2\|). \quad (\text{F.7})$$

The leading r^2 term links scalar differences to a direction-selective form.

F.2 Measurement projection: rotated parity selects $\cos^2 \theta$

With $R_y(\theta) = e^{-i\theta\sigma_y/2}$,

$$\hat{\Pi}(\theta) = R_y(\theta)^{\otimes N} \left(\bigotimes_i \sigma_z^{(i)} \right) R_y(-\theta)^{\otimes N} = (\cos \theta \sigma_z + \sin \theta \sigma_x)^{\otimes N}.$$

Choose the z -axis as angular origin in the x - z plane. Then

$$\hat{\mathbf{m}}(\theta) = \sin \theta \hat{\mathbf{x}} + \cos \theta \hat{\mathbf{z}}, \quad \hat{\mathbf{r}}_{ij} = \sin \alpha_{ij} \hat{\mathbf{x}} + \cos \alpha_{ij} \hat{\mathbf{z}},$$

so that

$$(\hat{\mathbf{m}}(\theta) \cdot \hat{\mathbf{r}}_{ij})^2 = (\sin \theta \sin \alpha_{ij} + \cos \theta \cos \alpha_{ij})^2 = \cos^2(\theta - \alpha_{ij}).$$

Rotated parity thus acts as a geometric projector onto the pair orientation α_{ij} , selecting the $\cos^2 \theta$ harmonic at pair level.

F.3 From microscopic to mesoscopic: lattice-weighted averaging

Bridge. The microscopic average $\langle (\hat{\mathbf{r}} \cdot \nabla \tilde{T}^2)^2 \rangle_{S^2}$ becomes a discrete sum over physical pairs once the causal-exponential kernel collapses the support to $r \sim \xi$ along device edges. Label pairs by k , with orientation α_k and radial weight

$$w_k \equiv r_k^2 \gamma(r_k) \propto r_k^2 e^{-r_k/\xi}.$$

Collecting the gradient factor and the measurement projector from F.1–F.2,

$$\Gamma_{\text{bi}}(\theta) \propto \sum_k w_k C(\Psi; \hat{\mathbf{r}}_k) \cos^2(\theta - \alpha_k). \quad (\text{F.8})$$

Use $\cos^2(\theta - \alpha) = \frac{1}{2}[1 + \cos 2\theta \cos 2\alpha + \sin 2\theta \sin 2\alpha]$ and define

$$G_0 := \sum_k w_k, \quad G_2 := \sum_k w_k \cos 2\alpha_k, \quad G_2^\perp := \sum_k w_k \sin 2\alpha_k. \quad (\text{F.9})$$

For symmetric heavy-hex subsets (Fig. F.1), $G_2^\perp = 0$ by reflections, and

$$\sum_k w_k \cos^2(\theta - \alpha_k) = \frac{1}{2} G_0 + \frac{1}{2} \cos 2\theta G_2.$$

Micro-foundation (for completeness). Standard spherical identities $\int_{S^2} (\hat{\mathbf{r}} \cdot \mathbf{A})^2 d\Omega = \frac{4\pi}{3} \|\mathbf{A}\|^2$, $\int_{S^2} (\hat{\mathbf{r}} \cdot \mathbf{A})^2 (\hat{\mathbf{r}} \cdot \mathbf{B})^2 d\Omega = \frac{4\pi}{15} (\|\mathbf{A}\|^2 \|\mathbf{B}\|^2 + 2(\mathbf{A} \cdot \mathbf{B})^2)$ justify the elimination of the microscopic direction $\hat{\mathbf{r}}$ under angular averaging.

F.4 Radial integral and scaling

With an exponential kernel $K_\xi(r) \propto e^{-r/\xi}$ in 3D,

$$I_\xi = \int_0^\infty r^4 e^{-r/\xi} dr = 24 \xi^5. \quad (\text{F.10})$$

Thus the bilocal contribution scales as ξ^5 in $d = 3$ (in general $I_\xi \propto \xi^{d+2}$).

F.5 Final law and parameterization

Collecting gradient, projection, lattice weights, and radial factor:

$$\Gamma_{\text{dec}}(\theta) = \bar{\Gamma} (1 + \varepsilon \cos^2 \theta), \quad \bar{\Gamma} \propto \gamma_0 \xi^5 a_0 \langle \|\nabla \tilde{T}^2\|^2 \rangle G_0, \quad (\text{F.11})$$

with modulation

$$\varepsilon = \frac{a_2}{a_0} \frac{G_2}{G_0}. \quad (\text{F.12})$$

Equation (F.12) follows by inserting the gate expansion (F.1) into (F.8): a_0 multiplies the isotropic part (G_0), while a_2 multiplies the quadrupolar harmonic (G_2). This factorization completes the bridge from the WESH master equation (F.0) to the observable angular law: Eq. (F.3) and the echo-frame reduction (F.4) show how the bilocal WESH dissipator governs parity decay, while Eqs. (F.8)–(F.12) evaluate its angular projection and yield the robust $\cos^2 \theta$ harmonic with amplitude $\varepsilon = (a_2/a_0)(G_2/G_0)$.

F.6 Device factor and inversion

For any layout,

$$\frac{G_2}{G_0} = \frac{\sum_k w_k \cos 2\alpha_k}{\sum_k w_k}, \quad w_k \propto r_k^2 e^{-r_k/\xi}.$$

IBM Eagle subset. With three representative orientations $(\alpha_h, \alpha_v, \alpha_d) = (90^\circ, 0^\circ, \alpha_3)$,

$$\frac{G_2}{G_0} = \frac{w_v - w_h + w_d \cos 2\alpha_3}{w_h + w_v + w_d}.$$

This exposes the threshold condition for the sign and magnitude of G_2/G_0 in terms of geometric weights (w_h, w_v, w_d) extracted from the device map (Fig. F.1).

Inversion to state anisotropy. From $\varepsilon = (a_2/a_0)(G_2/G_0)$,

$$\frac{a_2}{a_0} = \frac{\varepsilon}{G_2/G_0}.$$

Thus a measurement of ε combined with a device-level G_2/G_0 (computed from the chip layout) yields the intrinsic anisotropy of the prepared state, independently of kernel strength.

F.7 W-state anti-modulation (sign sketch)

For the symmetric single-excitation state $|W_N\rangle$, the rotated-parity correlator is locally concave at $\theta = 0$ in the preparation plane, giving a negative quadrupolar coefficient in the gate expansion:

$$C_W(\Psi; \hat{\mathbf{r}}) = a_0^{(W)} - |a_2^{(W)}| (\hat{\mathbf{r}} \cdot \hat{\mathbf{n}})^2 + \dots,$$

hence $a_2^{(W)} < 0$ and $\varepsilon_W = (a_2^{(W)}/a_0^{(W)})(G_2/G_0) < 0$, in agreement with the observed anti-modulation in the W -state control runs (main text).

F.8 Validity and corrections

Regime. Short-range dominance $r \sim \xi$, weak gate anisotropy $a_2 \ll a_0$, rotated-parity readout.

Corrections. Higher even harmonics in $C(\Psi)$ (e.g. $a_4 \mu^4$) and next order in (F.7) add small $\cos(4\theta)$ admixtures at high precision; environmental channels add an angle-independent baseline.

Scaling. Device dependence enters only via G_2/G_0 ; $\bar{\Gamma}$ inherits the ξ^5 scaling.

Cross-platform outlook. Trapped-ion architectures (linear chains or effectively all-to-all coupling graphs) yield pair-orientation statistics—and thus G_2/G_0 —that differ from heavy-hex superconducting layouts (and may require allowing a phase offset if the layout lacks reflection symmetry, i.e. $G_2^\perp \neq 0$). A dedicated validation on such platforms would test the predicted $\cos^2 \theta$ harmonic independently of superconducting device geometry. This direction was left for future work.

Appendix G — WESH–Noether as Pre-Geometric Path Independence

Context. In the timeless Wheeler–DeWitt sector, the auxiliary parameter s is an *ordinal label* of configurations; no physical time, metric, or thermodynamics exist yet. The foundational constraint is a *pre-geometric* conservation law compatible with the WESH generator (see the master equation, (1.15)). *Terminology.* “Flow” is the shorthand of an *ordinal vector field* in state space; s is not physical time and no temporal structure is assumed prior to the $s \rightarrow t$ bootstrap.

Box G.1: Static vs Dynamic in the Pre-Geometric Regime.

In the timeless WDW sector, there is no external time parameter t to define “flow” in the standard sense. Instead, the auxiliary parameter s labels configurations in a pre-causal ordering structure $(\mathcal{S}, \prec, \mathcal{M})$. This is a *static dynamism*: a frozen landscape of potential transitions, characterized by:

- **Ordinal structure:** States are ordered by the Lyapunov functional $\mathcal{M}[\rho]$;
- **Path independence:** Global charges $\langle \hat{Q}_{\text{tot}} \rangle$ are constant along any WESH flowline in \mathcal{S} ;
- **Gradient architecture:** The vector field $\nabla_\rho \mathcal{M}$ defines potential streamlines.

Physical time emerges when this static configuration is *actualized* via the bootstrap $dt/ds = \Gamma[\Psi] > 0$, converting potential order into temporal flow.

G.1 Operator formulation of pre-geometric Noether

Let \mathcal{L} be the WESH GKSL generator (see (1.15)) and \mathcal{L}^\dagger its adjoint on observables:

$$\mathcal{L}^\dagger[A] = -i[H_{\text{eff}}, A] + \nu \int_x \mathcal{D}_{\hat{T}^2(x)}^\dagger[A] + \int_{xy} \gamma(x, y) C(\Psi; x, y) \mathcal{D}_{L_{xy}}^\dagger[A],$$

with \int_x, \int_{xy} as in Eq. (1.14), $\mathcal{D}_L^\dagger[A] = L^\dagger AL - \frac{1}{2}\{L^\dagger L, A\}$, and $L_{xy} = \hat{T}^2(x) - \hat{T}^2(y)$ (Hermitian).

Definition G.1 (Pre-geometric WESH–Noether). For every global conserved charge \hat{Q}_{tot} ,

$$\mathcal{L}^\dagger[\hat{Q}_{\text{tot}}] = 0. \quad (\text{G.1})$$

This is equivalent to $\frac{d}{ds}\langle\hat{Q}_{\text{tot}}\rangle = 0$ for all $\rho(s)$. The kernel weight is causal–exponential with range ξ (see (1.20)).

Remark G.1 (Self-consistent physical subset). *The “physical subset” is not pre-imposed. Operationally, it is the basin of attraction of the bootstrap fixed point(s) ρ^* that (i) minimize the Lyapunov functional (Appendix D), (ii) satisfy WESH–Noether at the fixed point, and (iii) are reached by iterating the bootstrap from RAQ-physical initial conditions (i.e., they belong to the basin of attraction). WESH–Noether thus acts as a local structural constraint of the (state-dependent) generator throughout the evolution, without a pre/post-bootstrap dichotomy.*

Theorem G.1 (WESH–Noether). *Let \mathcal{L} be a GKSL generator governing evolution in the atemporal ordering parameter s within the Wheeler–DeWitt sector, with Heisenberg adjoint \mathcal{L}^\dagger . Assume Hermitian jump operators $L_\alpha \in \{\hat{T}^2(x), L_{xy} = \hat{T}^2(x) - \hat{T}^2(y)\}$ and the mild spectral regularity of Proposition G.2. Then, for any global charge operator \hat{Q}_a , the following are equivalent:*

$$\mathcal{L}^\dagger[\hat{Q}_a] = 0 \iff [H_{\text{eff}}, \hat{Q}_a] = 0 \text{ and } [L_\alpha, \hat{Q}_a] = 0 \text{ for all } \alpha \text{ with nonzero rate.}$$

No geometric or thermal structure is presupposed.

Corollary G.1 (Path independence / s -conservation). *For all states $\rho(s)$ and all a , $\frac{d}{ds}\langle\hat{Q}_a\rangle = 0$. Equivalently, the charge one-form $\omega_a[\rho] := \text{Tr}(\hat{Q}_a \mathcal{L}[\rho]) ds$ is exact (zero holonomy).*

Remark G.2 (Specialization to the KMS wedge). *In the near-horizon Rindler wedge, the Modular–KMS spectral regularity (Definition 6.2) implies the hypothesis of Prop. G.2 (Lemma 6.3); hence the equivalence holds there verbatim.*

G.2 Necessary & sufficient algebraic conditions (Hermitian Lindblad structure)

In the present framework the Lindblad operators are Hermitian, $L \in \{\hat{T}^2(x), L_{xy}\}$, and the standard GKSL identity

$$\mathrm{Tr}(A \mathcal{D}[L]\rho) = \frac{1}{2} \langle L^\dagger[A, L] + [L^\dagger, A]L \rangle$$

yields, for Hermitian L ,

$$\mathcal{D}_L^\dagger[\hat{Q}] = -\frac{1}{2} [L, [L, \hat{Q}]]. \quad (\text{G.2})$$

Proposition G.2 (Equivalence under mild spectral regularity).

Assume:

- (i) \hat{Q}_{tot} is bounded (or the identities are understood as quadratic forms on a common invariant core);
- (ii) Hermitian jump set $L \in \{\hat{T}^2(x), L_{xy}\}$ in the generator (1.15);
- (iii) (*Mild spectral regularity*) For each such L , the global charge \hat{Q}_{tot} is block-diagonal in the spectral decomposition of L (equivalently: \hat{Q}_{tot} commutes with the spectral projectors of L on the relevant support).

Then the pre-geometric WESH–Noether condition (G.1) holds *iff*

$$[H_{\text{eff}}, \hat{Q}_{\text{tot}}] = 0, \quad [\hat{T}^2(x), \hat{Q}_{\text{tot}}] = 0 \quad \forall x, \quad [L_{xy}, \hat{Q}_{\text{tot}}] = 0 \quad \forall x, y. \quad (\text{G.3})$$

Proof. Sufficiency. If (G.3) holds, each dissipative term in $\mathcal{L}^\dagger[\hat{Q}_{\text{tot}}]$ vanishes by (G.2), and the Hamiltonian part yields $[H_{\text{eff}}, \hat{Q}_{\text{tot}}] = 0$, hence (G.1).

Necessity. Assume $\mathcal{L}^\dagger[\hat{Q}_{\text{tot}}] = 0$ with $\hat{Q}_{\text{tot}} = \hat{Q}_{\text{tot}}^\dagger$. Take the Hilbert–Schmidt pairing with \hat{Q}_{tot} :

$$0 = \mathrm{Tr}(\hat{Q}_{\text{tot}} \mathcal{L}^\dagger[\hat{Q}_{\text{tot}}]).$$

The Hamiltonian contribution vanishes by cyclicity, $\text{Tr}(\hat{Q}_{\text{tot}}[-iH_{\text{eff}}, \hat{Q}_{\text{tot}}]) = 0$. For Hermitian Lindblad operators, one has

$$\text{Tr}(\hat{Q}_{\text{tot}} \mathcal{D}_L^\dagger[\hat{Q}_{\text{tot}}]) = -\frac{1}{2} \text{Tr}([L, \hat{Q}_{\text{tot}}]^\dagger[L, \hat{Q}_{\text{tot}}]) \leq 0.$$

Using $\nu > 0$ and $\gamma(x, y) C(\Psi; x, y) \geq 0$, this yields

$$\int_x \text{Tr}([\hat{T}^2(x), \hat{Q}_{\text{tot}}]^\dagger[\hat{T}^2(x), \hat{Q}_{\text{tot}}]) = 0,$$

$$\int_{xy} \gamma(x, y) C(\Psi; x, y) \text{Tr}([L_{xy}, \hat{Q}_{\text{tot}}]^\dagger[L_{xy}, \hat{Q}_{\text{tot}}]) = 0,$$

hence $[\hat{T}^2(x), \hat{Q}_{\text{tot}}] = 0$ (on the support of \int_x) and $[L_{xy}, \hat{Q}_{\text{tot}}] = 0$ wherever $\gamma(x, y) C(\Psi; x, y) \neq 0$. Plugging back into $\mathcal{L}^\dagger[\hat{Q}_{\text{tot}}] = 0$ leaves $-i[H_{\text{eff}}, \hat{Q}_{\text{tot}}] = 0$, hence $[H_{\text{eff}}, \hat{Q}_{\text{tot}}] = 0$. \square

Remark G.3 (Athermal generality and relation to Section 6). *Proposition G.2 is pre-geometric and athermal: no KMS structure, thermal equilibrium, or wedge geometry is required. The proposition relies solely on mild spectral regularity of the Lindblad operators in the kinematical Hilbert space. Section 6 shows that the near-horizon Rindler wedge, equipped with Modular-KMS spectral regularity (Definition 6.2), provides a concrete regime where the hypothesis of Proposition G.2 is satisfied (Lemma 6.3); the wedge analysis is thus a specialization of the general algebraic framework established here, not an alternative foundation.*

Lemma G.1 (Spectral genericity). *For the time-field operator $\hat{T}(x)$ with continuous spectrum in the WDW sector, the quadratic operator $\hat{T}^2(x)$ has a non-degenerate spectral measure on any bounded interval $[E_{\min}, E_{\max}]$ with probability 1 under generic local perturbations.*

Proof sketch. The spectrum of $\hat{T}^2(x)$ is the image of $\sigma(\hat{T})$ under $\lambda \mapsto \lambda^2$. For continuous $\sigma(\hat{T}) \subset \mathbb{R}$, generic perturbations preserve measure-theoretic nondegeneracy (Kato perturbation theory), which supports the projector-commutation regularity used in Prop. G.2. \square

Remark G.4 (Regularity note). *Commutation with spectral projectors is the minimal operational hypothesis required by the double-commutator identity; it is generic for local polynomials of \hat{T} and stable under local perturbations. Since*

$L_{xy} = \hat{T}^2(x) - \hat{T}^2(y)$, $[L_{xy}, \hat{Q}_{\text{tot}}] = 0$ follows by linearity once $[\hat{T}^2(x), \hat{Q}_{\text{tot}}] = [\hat{T}^2(y), \hat{Q}_{\text{tot}}] = 0$.

The mild spectral regularity is generic for local polynomials of \hat{T} and their differences. It is strictly weaker than assuming any thermal structure and does not presuppose the emergence of t .

Remark G.5 (T-neutrality as a consistency requirement). *If $[\hat{T}, \hat{Q}_{\text{tot}}] \neq 0$, the state-dependent coefficients of the generator induce a charge-dependent intensity; the ordinal speed dt/ds becomes background-dependent, spoiling the universality of physical time. Moreover, along different state-space paths one generically sources \hat{Q}_{tot} , violating path independence. Hence T-neutrality is not an external postulate but the unique choice compatible with path independence, universality of emergent time, and no-signaling.*

Remark G.6 (Operator-level vs expectation-level conservation). *The WESH–Noether condition (G.1) is an operator-level statement, not merely conservation of expectations. Operator-level conservation guarantees zero holonomy of the charge one-form on state space; conserving only $\langle \hat{Q}_{\text{tot}} \rangle$ allows hidden anomalies in the commutant that re-emerge under block decompositions or sub-sector measurements, obstructing the emergence of a unique geometry.*

G.3 From potential order to geometry (bridge to alignment)

Let $\mathcal{M}[\rho]$ be the WESH Lyapunov functional (strictly convex in the regime of interest; see Appendix D). Consider the constrained minimization “minimize \mathcal{M} subject to WESH–Noether”. At a stationary point, the Karush–Kuhn–Tucker optimality conditions require that the state-space gradient $\nabla_\rho \mathcal{M}$ aligns with the gradient of the constraint manifold. For the quadratic structure of \mathcal{M} (in $\|\partial_\mu \tau\|^2$) and the Yukawa-weighted entanglement potential, this forces the field-level relation $\partial_\mu \tau \parallel \partial_\mu \Phi$, i.e.:

$$\partial_\mu \tau = k \partial_\mu \Phi, \quad \Phi(x) = \int K(x - y) C(\rho^*; x, y) d^4y, \quad (\text{G.4})$$

i.e. the pre-geometric consistency crystallizes into an emergent metric relation.

Remark G.7 (Existence vs uniqueness). *WESH–Noether ensures existence of a stationary state (Appendix D, fixed-point lemma via Schauder–Tychonoff) but not uniqueness. Uniqueness follows from additional physical constraints:*

- (i) *Causal support of $\gamma(x, y)$ (no superluminal signaling);*
- (ii) *Finite correlation time $\tau_{\text{corr}} \sim \xi/c$ (Markov window);*
- (iii) *Cross-horizon connectivity (null-plane Markov mixing).*

These are not fine-tunings but consistency requirements for the scaling hypothesis $\xi \simeq L_P$. Together with WESH–Noether, they select the unique fixed point where gradient alignment (G.4) holds.

G.4 Empirical signatures

The pre-geometric constraint yields distinct empirical targets:

1. **Core: collective stability.** The coherence time scales as $\tau_{\text{coh}}(N) \propto N^2$, reflecting causal mixing under the WESH constraint.
2. **Diagnostic: angular dependence.** The decoherence rate obeys $\bar{\Gamma} [1 + \varepsilon \cos^2 \theta]$ with $\varepsilon = (a_2/a_0)(G_2/G_0)$, factorizing state anisotropy and device geometry.
3. **Core: BH thermodynamics/holography.** Near-horizon KMS structure yields the thermodynamic law (area term and logarithmic corrections) without external parameters; the framework establishes WESH validity through a holographic criterion spanning ~ 50 orders of magnitude in radius, from Planck-scale correlations to macroscopic event horizons.

Each item probes a different layer of the construction: collective stability and black-hole thermodynamics test core structural aspects of WESH (including the IR bridge to gravity), while the angular dependence provides a diagnostic check of causal connectivity and state/geometry factorization.

G.5 Physical meaning and scope

Meaning. Eqs. (G.1)–(G.3) formalize the “no-vorticity” intuition without thermodynamic inputs: in the minimal GKSL representation each Hermitian Lindblad channel commutes with the global charges, hence the WESH flow cannot generate spurious global sources. *Scope.* Detailed balance is *derived* at the emergent level (near-horizon KMS), not assumed: see Sec. 6.2, Eq. (6.16).

Laminar-flow analogy. Imagine a stationary laminar fluid where the velocity field is globally time-independent yet locally directed along well-defined streamlines: this captures the pre-geometric WESH structure in state space. "No-vorticity" corresponds to path independence of global charges (zero holonomy of ω_Q); stagnation points correspond to eigentimes where geometric structure crystallizes. Physical time t then emerges as the local flow speed via $dt/ds = \Gamma[\Psi]$, actualizing the potential streamlines into worldlines. This clarifies why classical detailed balance cannot be imposed at this stage: temperature and KMS structure arise only after the flow has crystallized into a geometry.

Operational note n.1 (compatibility with BH sector). The horizon-symmetric (gauge-even) conditional expectation $\mathbb{E}_{\text{even}}(X) = \frac{1}{2}(X + GXG)$ used in the BH discussion is the minimal CP idempotent onto the even subalgebra. It is *compatible* with (G.1)–(G.3) but not required to derive them.

Operational note n.2 (RAQ compatibility). The WESH dynamics preserves the RAQ-physical subspace: T-neutrality and Hermitian jumps ensure that the generator neither sources nor leaks gauge constraints. The global WESH–Noether condition is the observable face of this preservation in the emergent sector.

Appendix H — CP/TP preservation and no-signaling in WESH

Setting. Consider the pre-geometric master equation (1.15) with Hermitian channels

$$L_\alpha \in \{\hat{T}^2(x), L_{xy} = \hat{T}^2(x) - \hat{T}^2(y)\},$$

and scalar rates

$$c_\alpha(s) \in \{ \nu, \gamma(x, y) C(\Psi; x, y) \}, \quad 0 \leq C \leq 1, \gamma \geq 0,$$

assumed bounded and piecewise continuous in s (hence strongly measurable and uniformly bounded on compact intervals). Here $C(\Psi; x, y)$ depends only on *local/bilocal reductions*

$$\rho_x = \text{Tr}_{x^c} \rho, \quad \rho_y = \text{Tr}_{y^c} \rho, \quad \rho_{xy} = \text{Tr}_{(xy)^c} \rho,$$

through bounded, Borel-measurable functionals that are Lipschitz in the trace norm. The effective Hamiltonian H_{eff} is self-adjoint so that $-i[H_{\text{eff}}, \cdot]$ generates

a strongly continuous one-parameter group of trace-norm isometries on the trace class.

Theorem H.1 (CP/TP preservation for the nonlinear WESH evolution). *Under the above assumptions, for any $s \geq 0$ the non-autonomous evolution $E_s : \rho_0 \mapsto \rho(s)$ generated by (1.15) preserves positivity and unit trace; each frozen micro-step is CPTP, and the product-integral limit preserves these properties.*

Proof sketch. Partition $[0, s]$ into $0 = s_0 < \dots < s_N = s$ and *freeze* the rates at the left endpoints:

$$\mathcal{L}_k(\cdot) = -i[H_{\text{eff}}, \cdot] + \nu \int d^4x \mathcal{D}[\hat{T}^2(x)](\cdot) + \iint d^4x d^4y \gamma(x, y) C(\Psi_{s_k}; x, y) \mathcal{D}[L_{xy}](\cdot).$$

Each \mathcal{L}_k is GKSL (Hermitian jumps, nonnegative rates), thus $\Phi_k := \exp(\Delta s_k \mathcal{L}_k)$ is CPTP and $E_s^{(N)} = \Phi_{N-1} \circ \dots \circ \Phi_0$ is CPTP by composition.

Non-autonomous convergence. Assume $s \mapsto c_\alpha(s)$ are strongly measurable and uniformly bounded, and that the map $\rho \mapsto C(\Psi; x, y)$ is Lipschitz in the trace norm via the reduced states. Then the product-integral scheme with frozen coefficients converges strongly to the unique non-autonomous evolution solving (1.15). Strong limits of CPTP maps remain CP and TP, hence E_s is positivity- and trace-preserving (stepwise CPTP). \square

Corollary H.1 (System–ancilla consistency). *For any ancilla A and initial ρ_{SA} , $(E_s \otimes \mathbb{I}_A)(\rho_{SA})$ preserves positivity and unit trace.*

Proposition H.1 (Spacelike no-signaling). *Let Σ be a Cauchy slice and $A \subset \Sigma$ with complement A^c . If (i) $\gamma(x, y) = 0$ for spacelike (x, y) and (ii) $[\hat{T}(x), \hat{T}(y)] = 0$ for spacelike (x, y) , then*

$$\frac{d}{ds} \rho_A(s) = \text{Tr}_{A^c} (\mathcal{L}_{J(A)}[\rho(s)]),$$

i.e. ρ_A depends only on operators supported in the causal domain $J(A)$; spacelike operations on A^c cannot instantaneously affect ρ_A .

Remark H.1 (Nonlinearity vs CP). *Nonlinearity enters only through the scalar rates $c_\alpha(s)$ (via $C(\Psi; x, y)$), not in the operator set $\{L_\alpha\}$. Freezing c_α yields*

GKSL steps; product–integral concatenation preserves CP/TP in the limit, avoiding pathologies such as loss of positivity or violation of complete positivity that can occur in arbitrary nonlinear master equations.

Appendix I — Consistency selection of the quadratic dissipator $\mathcal{D}[\hat{T}^2]$

Setting. Local channels are even, real-analytic functionals of the time field,

$$L_x = F(\hat{T}(x)) = \sum_{m \geq 1} a_{2m} \hat{T}^{2m}(x), \quad L_{xy} = F(\hat{T}(x)) - F(\hat{T}(y)),$$

consistent with CPT–evenness. The operator–level WESH–Noether constraint (App. G, Eq. (G.1)) fixes the commutant structure; here we address the admissible *local* form in the infrared.

I.1 Constraints and selection principle

Constraints.

- (i) **CPT–evenness:** time–reversal on \hat{T} excludes odd powers.
- (ii) **WESH–Noether:** compatibility with (G.1) throughout the flow.
- (iii) **Collective stability (structural requirement):** the bootstrap closure condition $\mu \cdot \sigma_\alpha = \mathcal{O}(1)$ (Sec. 2.6) uniquely fixes $\alpha = 2$, yielding $\tau_{\text{coh}}(N) \propto N^2$ (Sec. 2; cf. Eq. (1.13) in Sec. 1). This is a structural consistency requirement of the fixed-regime, not an empirical postulate.

Proposition I.1 (Quadratic local normal form). *Under (i)–(iii), the admissible local normal form is uniquely quadratic:*

$$F(z) = a_2 z^2, \quad \text{i.e. } \mathcal{D}[\hat{T}^2(x)].$$

Proof. CPT symmetry implies that F is even, hence the leading monomial can be written as $F(z) \sim z^{2n}$ with $n \geq 1$. As shown in Sec. 1 (Eq. (1.13)), under the WESH normalization $\gamma \propto N^{-2}$ one has

$$F(\hat{T}) \sim \hat{T}^{2n} \Rightarrow \tau_{\text{coh}}(N) \propto N^{2n}.$$

Imposing collective stability $\tau_{\text{coh}}(N) \propto N^2$ fixes $n = 1$ uniquely, hence $F(z) = a_2 z^2$ and the local channel is $\mathcal{D}[\hat{T}^2(x)]$. \square

Remark I.1 (Empirical validation). *The N^2 scaling is used in the theory as a fixed-regime consistency condition (collective stability) selecting the quadratic channel. Experimentally, observing $\tau_{\text{coh}} \propto N^2$ acts as a direct validation of this structural requirement and excludes higher even monomials in the collective regime.*

Remark I.2 (Convergence with effective field theory). *The quadratic selection also follows from IR minimality: among CPT-even operators, the lowest-dimension monomial dominates at long wavelengths in the Wilsonian sense. This convergence of two independent arguments—structural (collective stability from bootstrap closure) and effective (Wilsonian IR dominance)—strengthens confidence in the uniqueness of $\mathcal{D}[\hat{T}^2]$.*

Appendix J — Λ as intrinsic shot noise of eigentime production

Scope and claim. This appendix establishes the *natural magnitude* of the infrared cosmological constant in QFTT–WESH as a consequence of the intrinsic fluctuations in eigentime production. The mechanism is dynamical: Λ emerges as the irreducible scalar shot-noise residue of the Lindblad channel generating time. We derive the scaling of the typical fluctuation width $\delta\Lambda_{\text{typ}}$ on a four-volume V_4 , demonstrating that it follows a parameter-free inverse-volume law.

J.0 The Martingale structure of eigentime generation. In QFTT–WESH, eigentime production is a stochastic process governed by the local hazard $\lambda(x)$ (Eq. (1.30)) and the global GKSL intensity functional $\Gamma[\rho]$. The emergent physical time $t(s)$ is bootstrapped via

$$\frac{dt}{ds} = \Gamma[\Psi(s)], \quad t(s) = \int_0^s \Gamma[\Psi(s')] ds', \quad (\text{J.1})$$

generating a counting process $N_{\text{Eig}}(s)$. This process admits the Doob–Meyer decomposition:

$$N_{\text{Eig}}(s) = \underbrace{\int_0^s \frac{\Gamma[\Psi(u)]}{\tau_{\text{Eig}}} du}_{\text{Compensator}} + \underbrace{M(s)}_{\text{Martingale}}. \quad (\text{J.2})$$

The martingale term $M(s)$ represents the irreducible quantum fluctuations of the event count around its compensator.

J.1 Regional counting on the physical manifold. Consider a spacetime region \mathcal{R} of the emergent IR manifold with physical four-volume

$$V_4(\mathcal{R}) := \int_{\mathcal{R}} d^4x \sqrt{-g}. \quad (\text{J.3})$$

We define the *regional eigentime count* $N(\mathcal{R})$ as the cardinality of the set of eigentime events $\{x_i\} \subset \mathcal{R}$. Since eigentime events seed the geometric estimators on scales $L \gg \xi$, they form a quasi-uniform mesh with filling density governed by the hazard. For regions much larger than the correlation length, the expected count is extensive:

$$\mathbb{E}[N(\mathcal{R})] \simeq \bar{\lambda} V_4(\mathcal{R}) \equiv \frac{V_4(\mathcal{R})}{V_\xi}, \quad (\text{J.4})$$

where $V_\xi \sim \xi^4$ is the correlation 4-volume.

J.2 Central Limit scaling from finite-range mixing. The WESH bilocal channel is constructed with an exponential-causal kernel of finite range ξ . This implies a finite correlation time τ_{corr} and a Markov window $\mu \ll 1$. Under the block-mixing hypothesis (Dobrushin-type contractivity for $L \gg \xi$), the event count on large regions obeys the Central Limit Theorem despite local correlations:

$$\text{Var}[N(\mathcal{R})] = \alpha_N \mathbb{E}[N(\mathcal{R})], \quad \delta N(\mathcal{R}) \sim \sqrt{N(\mathcal{R})}, \quad (\text{J.5})$$

where $\alpha_N = \mathcal{O}(1)$ accounts for short-range correlations.

J.3 Derivation of the Λ fluctuation scaling. By IR uniqueness, the cosmological constant couples to the volume element V_4 . We identify Λ_{eff} via the zero-derivative action term:

$$S_\Lambda[g] = -\frac{\Lambda_{\text{eff}}}{8\pi G} V_4(\mathcal{R}). \quad (\text{J.6})$$

Discretizing \mathcal{R} into $N(\mathcal{R})$ correlation cells of volume V_ξ , the total action fluctuates due to the stochastic residue of the GKSL channel in each cell. The action residue obeys random-walk scaling:

$$\delta S_\Lambda(\mathcal{R}) \sim \sigma_\Lambda \sqrt{N(\mathcal{R})}, \quad \sigma_\Lambda = \mathcal{O}(1). \quad (\text{J.7})$$

Solving (J.6) for Λ_{eff} and propagating the uncertainty:

$$\begin{aligned}\delta\Lambda_{\text{typ}}(\mathcal{R}) &\sim \frac{8\pi G}{V_4(\mathcal{R})} \delta S_\Lambda(\mathcal{R}) \sim \frac{8\pi G}{N(\mathcal{R}) V_\xi} \sigma_\Lambda \sqrt{N(\mathcal{R})} \\ &\sim \frac{\alpha_\Lambda G}{V_\xi} \frac{1}{\sqrt{N(\mathcal{R})}}.\end{aligned}\quad (\text{J.8})$$

Imposing the Planck anchoring condition $G \sim \xi^2$ (in natural units) and using $V_\xi \sim \xi^4$, the microscopic scales cancel:

$$\delta\Lambda_{\text{typ}}(\mathcal{R}) \sim \frac{1}{\xi^2 \sqrt{N(\mathcal{R})}}. \quad (\text{J.9})$$

Substituting $N(\mathcal{R}) \simeq V_4(\mathcal{R})/\xi^4$ yields the fundamental scaling:

$$\delta\Lambda_{\text{typ}}(\mathcal{R}) \sim \frac{\alpha_\Lambda}{\sqrt{V_4(\mathcal{R})}}, \quad \alpha_\Lambda = \mathcal{O}(1).$$

(J.10)

This result depends solely on the counting statistics of the underlying process and contains no free parameters beyond the $\mathcal{O}(1)$ coefficient α_Λ .

J.4 Cosmological magnitude: $\delta\Lambda \sim H^2$. Taking the coarse-graining window to be the observable universe at an epoch with Hubble rate H , we have $V_4 \sim H^{-4}$. Equation (J.10) then yields:

$$\delta\Lambda_{\text{typ}} \sim \alpha_\Lambda H^2. \quad (\text{J.11})$$

At the present epoch, this predicts a magnitude $\sim 10^{-122} L_P^{-2}$, consistent with observation. This value is not obtained by fine-tuning the microscopic scale ξ (which is fixed at L_P), but arises dynamically from the large- N suppression factor $1/\sqrt{V_4}$.

Note on interpretation. This derivation predicts the *typical fluctuation amplitude* on a finite volume. The sign and instantaneous value remain stochastic.

J.5 Unified origin of Lorentz emergence and Λ . The tensor and scalar sectors emerge from the same stochastic substrate but scale differently in the continuum limit:

- **Tensor sector (geometry):** Tensorial anisotropies are averaged out by kernel smoothing. Convergence to smooth GR is controlled by the sampling density, with error scaling as $\delta g \sim N^{-1/4}$.

- **Scalar sector (Λ):** The vacuum residue is a global intensive quantity. Local averaging does not cancel it; it persists as a global fluctuation scaling as $\delta\Lambda \sim N^{-1/2}$.

Lorentz symmetry emergence and the cosmological constant are thus dual manifestations of the same eigentime statistics, distinguished only by their symmetry structure under local averaging.

J.6 Relation to Causal Set Theory. The scaling $\delta\Lambda \sim H^2$ is predicted by Causal Set Theory as “everpresent Λ ” (Ahmed et al., 2004; Sorkin, 2007). In QFTT–WESH, discreteness is not postulated axiomatically but derived from the GKSL eigentime production. The agreement in scaling serves as a universality check across discrete-measure quantum gravity approaches.

Scaling hierarchy of the stochastic substrate

Metric reconstruction (tensor): $\delta g_{\mu\nu} \sim N^{-1/4} \rightarrow 0$

Vacuum residue (scalar): $\delta\Lambda \sim \frac{1}{\sqrt{V_4}} \sim H^2$

References

- Adesso, G., Girolami, D., & Serafini, A. (2012). Measuring Gaussian quantum information and correlations using the Rényi entropy of order 2. *Physical Review Letters*, 109(19), 190502. <https://doi.org/10.1103/PhysRevLett.109.190502>
- Ahmed, M., Dodelson, S., Greene, P. B., & Sorkin, R. D. (2004). Everpresent Λ . *Physical Review D*, 69, 103523. <https://doi.org/10.1103/PhysRevD.69.103523>
- Araki, H. (1976). Relative entropy of states of von Neumann algebras. *Publications of the Research Institute for Mathematical Sciences*, 11(3), 809–833. <https://doi.org/10.2977/PRIMS/1195191148>

- Ashtekar, A., Lewandowski, J., Marolf, D., Mourão, J., & Thiemann, T. (1995). Quantization of diffeomorphism invariant theories of connections with local degrees of freedom. *Journal of Mathematical Physics*, 36(11), 6456–6493. <https://doi.org/10.1063/1.531252>
- Blanco, D. D., Casini, H., Hung, L.-Y., & Myers, R. C. (2013). Relative entropy and holography. *Journal of High Energy Physics*, 2013(8), 060. [https://doi.org/10.1007/JHEP08\(2013\)060](https://doi.org/10.1007/JHEP08(2013)060)
- Bousso, R. (1999). A covariant entropy conjecture. *Journal of High Energy Physics*, 1999(07), 004. <https://doi.org/10.1088/1126-6708/1999/07/004>
- Carlen, E. A., & Maas, J. (2017). Gradient flow and entropy inequalities for quantum Markov semigroups with detailed balance. *Journal of Functional Analysis*, 273(5), 1810–1869. <https://doi.org/10.1016/j.jfa.2017.05.003>
- Casini, H., Testé, E., & Torroba, G. (2017). Modular Hamiltonians on the null plane and the Markov property of the vacuum state. *Journal of Physics A: Mathematical and Theoretical*, 50(36), 364001. <https://doi.org/10.1088/1751-8121/aa7eaa>
- Chew, G. F. (1961). *S-matrix theory of strong interactions*. W. A. Benjamin.
- Facchinei, F., & Pang, J. S. (2003). *Finite-dimensional variational inequalities and complementarity problems* (Vols. 1–2). Springer. <https://doi.org/10.1007/b97543>
- Ghirardi, G. C., Rimini, A., & Weber, T. (1986). Unified dynamics for microscopic and macroscopic systems. *Physical Review D*, 34(2), 470–491. <https://doi.org/10.1103/PhysRevD.34.470>
- Gough, J. E., Ratiu, T. S., & Smolyanov, O. G. (2015). Noether's theorem for dissipative quantum dynamical semi-groups. *Journal of Mathematical Physics*, 56(2), 022108. <https://doi.org/10.1063/1.4907985>
- Guerreiro, T. (2025). Entanglement and squeezing of gravitational waves. *Physical Review D*, 112, L101904. <https://doi.org/10.1103/fn5d-mrsj>
- Haag, R. (1996). *Local quantum physics: Fields, particles, algebras* (2nd ed.). Springer. <https://doi.org/10.1007/978-3-642-61458-3>

- Haag, R., Hugenholtz, N. M., & Winnink, M. (1967). On the equilibrium states in quantum statistical mechanics. *Communications in Mathematical Physics*, 5(3), 215–236. <https://doi.org/10.1007/BF01646342>
- Jacobson, T. (1995). Thermodynamics of spacetime: The Einstein equation of state. *Physical Review Letters*, 75(7), 1260–1263. <https://doi.org/10.1103/PhysRevLett.75.1260>
- Jacobson, T. (2016). Entanglement equilibrium and the Einstein equation. *Physical Review Letters*, 116(20), 201101. <https://doi.org/10.1103/PhysRevLett.116.201101>
- Lions, J. L., & Stampacchia, G. (1967). Variational inequalities. *Communications on Pure and Applied Mathematics*, 20(3), 493–519. <https://doi.org/10.1002/cpa.3160200302>
- Maldacena, J. (1999). The large- N limit of superconformal field theories and supergravity. *International Journal of Theoretical Physics*, 38, 1113–1133. <https://doi.org/10.1023/A:1026654312961>
- Maldacena, J., & Susskind, L. (2013). Cool horizons for entangled black holes. *Fortschritte der Physik*, 61(9), 781–811. <https://doi.org/10.1002/prop.201300020>
- McCauley, G., Cruikshank, B., Bondar, D. I., & Jacobs, K. (2020). Accurate Lindblad-form master equation for weakly damped quantum systems across all regimes. *npj Quantum Information*, 6(1), 74. <https://doi.org/10.1038/s41534-020-00299-6>
- Page, D. N., & Wootters, W. K. (1983). Evolution without evolution: Dynamics described by stationary observables. *Physical Review D*, 27(12), 2885–2892. <https://doi.org/10.1103/PhysRevD.27.2885>
- Pearle, P. (1989). Combining stochastic dynamical state-vector reduction with spontaneous localization. *Physical Review A*, 39(5), 2277–2289. <https://doi.org/10.1103/PhysRevA.39.2277>
- Penrose, R. (1996). On gravity's role in quantum state reduction. *General Relativity and Gravitation*, 28(5), 581–600. <https://doi.org/10.1007/BF02105068>
- Petz, D. (1986). Sufficient subalgebras and the relative entropy of states of a von Neumann algebra. *Communications in Mathematical Physics*, 105(1), 123–131. <https://doi.org/10.1007/BF01212345>

- Rattazzi, R., Rychkov, V. S., Tonni, E., & Vichi, A. (2008). Bounding scalar operator dimensions in 4D CFT. *Journal of High Energy Physics*, 2008(12), 031. <https://doi.org/10.1088/1126-6708/2008/12/031>
- Rivas, Á., & Huelga, S. F. (2012). *Open quantum systems: An introduction*. Springer. <https://doi.org/10.1007/978-3-642-23354-8>
- Ryu, S., & Takayanagi, T. (2006). Holographic derivation of entanglement entropy from the anti-de Sitter space/conformal field theory correspondence. *Physical Review Letters*, 96(18), 181602. <https://doi.org/10.1103/PhysRevLett.96.181602>
- Sakharov, A. D. (1967). Vacuum quantum fluctuations in curved space and the theory of gravitation. *Soviet Physics Doklady*, 12, 1040–1041.
- Sorkin, R. D. (2007). Is the cosmological "constant" a nonlocal quantum residue of discreteness of the causal set type? *AIP Conference Proceedings*, 957, 142–153. <https://doi.org/10.1063/1.2823750>
- Spohn, H. (1991). *Large scale dynamics of interacting particles*. Springer. <https://doi.org/10.1007/978-3-642-84371-6>
- Takesaki, M. (1970). *Tomita's theory of modular Hilbert algebras and its applications*. Lecture Notes in Mathematics, Vol. 128. Springer. <https://doi.org/10.1007/BFb0065832>
- Van Raamsdonk, M. (2010). Building up spacetime with quantum entanglement. *General Relativity and Gravitation*, 42(10), 2323–2329. <https://doi.org/10.1007/s10714-010-1034-0>
- Verlinde, E. (2011). On the origin of gravity and the laws of Newton. *Journal of High Energy Physics*, 2011(4), 029. [https://doi.org/10.1007/JHEP04\(2011\)029](https://doi.org/10.1007/JHEP04(2011)029)
- Zeh, H. D. (2007). *The physical basis of the direction of time* (5th ed.). Springer. <https://doi.org/10.1007/978-3-540-68001-7>